UNIVERSITÀ DEGLI STUDI DI PADOVA

UNIVERSITÀ DEGLI STUDI DI PADOVA

Sede Amministrativa: Università degli Studi di Padova

Dipartimento di Ingegneria Industriale - DII

SCUOLA DI DOTTORATO DI RICERCA IN INGEGNERIA INDUSTRIALE

INDIRIZZO: INGEGNERIA CHIMICA, DEI MATERIALI E MECCANICA

CICLO XXVIII

INNOVATIVE FORMING PROCESSES OF ALUMINIUM ALLOYS SHEETS AND TUBES AT ELEVATED TEMPERATURE

Direttore della Scuola: Ch.mo Prof. Paolo Colombo

Coordinatore d'indirizzo: Ch.mo Prof. Enrico Savio

Supervisore: Ch.mo Prof. Stefania Bruschi

Dottorando: Francesco Michieletto

ACKNOWLEDGEMENTS

First of all, I would like to thank Prof. Stefania Bruschi and Prof. Andrea Ghiotti which gave me the possibility to perform my PhD and for their valuable advices, suggestions and teaching.

A particularly thank to Prof. Paolo F. Bariani to whom I express my sincerest gratitude.

A warm thanks to my colleagues for their invalue support during these years and most of all for their solid friendship.

My gratitude goes to my family, for their wonderful support over the years.
This goal could not have been reached without them.

My loving thanks goes to all my friends and all the people who came and crossed my life during these years, who helped and encouraged me to overcome difficulties found every days.

Table of Contents

ABSTRACT:

In the last two decades the international community has been looking for solutions to preserve the environment, and in particular the atmosphere, from the CO_2 emissions through the car exhausts, considered one of the main responsible of the greenhouse effect and, therefore, of the Earth temperature increase. Rules and limits were fixed in the 1997 with the Kyoto Protocol that entered in force in 2005, by which the international community signed the legal responsibility for producing vehicles with CO_2 emission limited to 95g/km to be reached in 2020. The production of cars using lightweight materials can represent an optimal solution because the lower weight means lower energy consumption. Therefore, the automotive companies are now investigating the feasibility of producing parts made of lightweight materials to replace conventional steels for the car chassis and body-in-white components, but without decreasing the passenger safety. High resistance steels and aluminium alloys have demonstrated to be the best solution thanks to their low density, high corrosion resistance and excellent stiffness-to-weight ratio. In case of use of aluminium alloy sheets and tubes, it is possible to reduce the car weight of about 15–20 % with also a consequent weight reduction of all the connected vehicle parts and therefore a substantial reduction of the pollutant exhausts.

The main limit of light alloys is the poor formability and the high springback exhibited during room temperature deformation. Temperature assisted processes have proven to increase material formability: Superplastic and Quick Plastic Forming, already used for shaping aluminium sheets, have shown a relevant increase in the material formability allowing to form very complex parts but are extremely expensive due to the very long process times, therefore not applicable for mass production. On the other hand, cold and warm hydroforming processes, nowadays at the state-of-the-art for shaping hollow components, exhibit very high initial investment cost due to the high pressure of the fluid used as deformable mean and to the high tons presses needed for keeping the dies closed during the process. Moreover, a strict forming temperature limit is fixed by the fluid boil and burst temperatures, which may limit the material formability.

In this research work, innovative forming processes were investigated to prove the feasibility of shaping aluminium sheets and tubes at high temperature, exceeding the limits of the already available process technologies. In particular, the Hot Stamping (HS) technology was applied to form 5xxx and 6xxx series aluminium alloys proving the capability of stamping an automotive component on a hot stamping industrial plant, and thus validating the laboratory tests results. An experimental apparatus able to work with the innovative technology of the Hot Metal Gas Forming (HMGF) process was designed and developed to form aluminium alloy tubes. In doing so, resistance heating was used as heating system and cold air in pressure was used to bulge-up the tubes during the process. The formability of different 6xxx series aluminium alloys tubes was investigated by means of free bulging tests and,

afterwards, shaping component inside a die, evaluating the influence of the most important process parameters. Finally, in collaboration with an industrial company, the shaping of an aesthetic component with also the evaluation of the surface appearance was carried out demonstrating the applicability of the new process to form an industrial part.

SOMMARIO:

Negli ultimi decenni, la comunità internazionale è alla continua ricerca di provvedimenti per salvaguardare l'atmosfera e l'ambiente terrestre. In campo automobilistico e dei trasporti la produzione di biossido di carbonio dai gas di scarico delle autovetture, meglio conosciuto come CO_2, è ritenuto tra i maggiori responsabili del rafforzamento dell'effetto serra e dunque dell'innalzamento del clima terrestre. Per porre un concreto rimedio e regolamentare l'efficienza sul consumo medio di un autoveicolo, con il protocollo di Kyoto stipulato nel 1997 ed entrato in vigore nel 2005, la comunità internazionale si è impegnata legalmente alla produzioni di veicoli in grado di rispettare il limite di emissione di 95 g di CO_2 per kilometro entro l'anno 2020. L'alleggerimento complessivo di un automobile è sicuramente tra le soluzioni più immediate per la riduzione delle particelle inquinanti, in quanto veicoli più leggeri richiedono minore forza motrice e di conseguenza minore consumo di energia. Per questo motivo le compagnie automobilistiche negli ultimi anni sono alla ricerca di materiali innovativi per sostituire l'acciaio che comunemente è impiegato per la realizzazione di telai e parti di carrozzeria, senza pregiudicare la sicurezza dei passeggieri.

Gli acciai alto resistenziali ma soprattutto le leghe leggere, hanno dimostrato essere delle ottime alternative grazie alle loro proprietà di bassa densità, resistenza alla corrosione, ed ottimo rapporto rigidezza-peso. Con l'utilizzo di parti stampate ma anche di elementi tubolari in lega di alluminio il peso medio della sola scocca di una vettura può essere ridotto del 15 – 20 %, portando ad un conseguente ridimensionamento di tutte gli organi connessi ed ad una sostanziale riduzione delle emissioni dannose.

La principale limitazione nella lavorazione delle leghe di alluminio è la loro scarsa attitudine a subire deformazione plastica a temperatura ambiente collegata oltretutto ad un elevato ritorno elastico. Per far fronte a questa problematica, numerosi processi innovativi utilizzanti alta temperatura sono stati o sono tuttora in fase di studio con l'obiettivo principale di incrementare la formabilità del materiale. I confermati processi di deformazione di lamiera di alluminio quali Superplastic Forming e Quick Plastic Forming, hanno dimostrato sicuramente un vantaggio in termini di formabilità riuscendo oltretutto a generare parti complesse, ma sono d'altro canto estremamente costosi e soggetti a tempi molto lunghi di processo, per cui non applicabili per produzioni in larga scala. L'idroformatura a freddo e a tiepido, invece, che rappresenta l'attuale tecnologia all'avanguardia per la sagomatura di parti cave, oltre a necessitare di elevati costi iniziali connessi alle elevate pressioni del fluido necessarie per la deformazione e alle presse ad alto tonnellaggio richieste per la chiusura degli stampi durante l'iniezione del liquido stesso, presenta severi limiti nella temperatura massima di processo. Infatti le emulsioni acqua olio generalmente impiegate come mezzo deformante risultano infiammabili al di sopra del campo tiepido per l'alluminio, limitando dunque il range termico utilizzabile per il processo e di conseguenza la formabilità del materiale.

In questo lavoro di ricerca sono stati studiati processi innovativi per la produzione di componenti di alluminio in lamiera e tubolari che superassero i limiti di processo delle attuali tecnologie produttive. In particolare la tecnologia dello stampaggio a caldo (Hot Stamping), oggigiorno applicata agli acciai alto resistenziali, è stata applicata con successo su lamiere di alluminio serie 5xxx e 6xxx, e validata con test industriali eseguiti su una vera linea di stampaggio producendo un componente automobilistico. Inoltre è stato realizzato e sviluppato un prototipo in grado di operare con la tecnologia innovativa del Hot Metal Gas Forming, che utilizza gas in pressione invece di fluidi per deformare componenti tubolari al alta temperatura. Prove di formabilità su tubi di alluminio serie 6xxx, ma anche la realizzazione di componenti in stampo, hanno permesso inoltre lo studio di numerosi aspetti critici per il processo. In fine, la sagomatura di un componente industriale in collaborazione con una azienda, curando oltretutto la qualità estetica del formato, ha permesso di verificare l'applicabilità e l'efficacia di questo processo anche a livello industriale.

Chapter 1

Introduction

1.1. The industrial problem

The last decade has seen a continuous demand of increased structural performances in automotive in order to improve the dynamic behaviour of cars, the chassis stiffness-to-weight ratio, passenger safety as well as reducing fuel consumption and, consequently, the emission of pollutants in order to counter negative effects on the global environment. Such trends have been strengthened by new regulations established by EU and US commissions after the Kyoto protocol came into force in 2005 [1], with challenging targets in term of the control of fuel emissions. Specifically, a target of 95 g/km by the 2020s was set, as shown in Figure 1.1. With such goals, the automotive industry is continuously working towards new innovations in both the engines and the structural parts of the car-body-in-white: the former towards the integration of more efficient and electricity-driven technologies, the latter characterised by the optimisation of materials and structures, and even through the introduction of new concepts and designs.

Figure 1.1: CO_2 emission target fixed with Kyoto protocol [2].

One possibility is represented by the hot stamping process, nowadays applied to high strength steels, during which the blank is heated at elevated temperature and simultaneously formed and quenched inside cooled dies. Thus, the increase in strength due to the material quenchability allows blank thickness reduction and, therefore, mass saving.

One of the most recent trends is the use of light alloys, especially 5xxx and 6xxx series which have proved to be among the best candidates to replace steels due to their low weight, good strength, corrosion resistance, weldability and paintability [3]. The use of lightweight materials such as aluminium and magnesium can reduce the weight of passenger vehicles up to 40–75 % by replacing ferrous auto body structures and body panels. It was reported that a 10 % weight reduction in an average automotive body could improve the fuel efficiency by 6–8 % [4]. By using aluminium alloys a cost increase of up to 30–100 % is expected, while it is forecast to be around 50–150 % for the magnesium alloys [5]. On the other hand, since 80 % of the total energy consumption throughout the life cycle of an automobile occurs during the utilisation (driving) period, the use of lightweight parts is still seen as a prominent, long-term and cost effective response to fuel efficiency and emission reduction demands [6].

As these alloys are usually characterised by reduced formability when formed at room temperature, a number of scientific studies are now focusing on different means to enhance their formability limits. A substantial increase of the formability and, at the same time, a drastic reduction of springback can be achieved if the sheet metal undergoes plastic deformation at elevated temperatures, as shown by the application to the AA5xxx series of the Superplastic Forming (SPF) and the Quick Plastic Forming (QPF) technologies. However, the high costs of the grain refining treatment before deformation required by SPF and the low production rates of both SPF and QPF, where the average values of the strain rate must be less than 10^{-3} s^{-1} and between 10^{-3} and 10^{-1} s^{-1} respectively, make these two new technologies unsuited to the high-volume production of economically competitive parts. The same trend is observed in the processes for tubular shaping. Hollow parts, are among the most interesting components of the car, truck and motorcycle chassis, allowing a significant increase of the stiffness compared to sheet metal components together with the reduction of the total car weight. In tubular frames, these components, usually obtained from direct or indirect hot extrusion, are required in non-uniform sizes and shapes. Therefore, in the past few years, the only material processing methods that allowed producing these sections were conventional stamping procedures combined with spot welding operations.

More recently hollow components tend to be shaped through a hydroforming process at room or warm temperature to take advantage of the increase of formability allowed by the hydrostatic pressure and warm temperatures. In fact, many studies have shown that the quality of the hydroformed parts is greater than the value of the old conventional stamped and welded components. Quality is established in terms of (i) how well the hydroformed designed component replaces the function of the currently designed component, (ii) how well the new component assembles into the structure, (iii) weight to performance ratio and (iv) total cost of the part. However, the process setup is often characterised by a longer process time compared to stamping processes, mostly due to the time required for the fluid to fill and empty the dies, and presents temperature limitations due to the forming media, which may be water- or oil-based, used to shape components. Moreover, the high pressure needed for shaping complex parts at room temperature requires elevated tons presses to clamp the two half matrix during

the fluid injection, and leads to high investment costs associated with both the hydraulic press, intensifier pump equipment and tooling.

In the scientific environment, what has become of interest is the development and evaluation of new processes to manufacture lighter and even more complex components with increased stiffness-to-weight ratio, with the aim of reducing the vehicle weight and therefore CO_2 emissions, Figure 1.2.

Figure 1.2: Aston martin Vanquish [7] and Fisker Karma aluminium space frame [8].

High production volumes and economic competitiveness, thanks to lower material costs due to the absence of expensive pre-treatments, means that there is interest in investigating the applicability of the Hot Stamping (HS) technology to the aluminium alloys sheets. Furthermore, the overcoming of any hydroforming problems, especially those connected to temperature and formability, can be achieved by the recently developed Hot Metal Gas Forming (HMGF), in which pressurised gas is used instead of fluids to deform a metal blank that is preliminarily heated in furnace.

Both of these innovative technologies are currently in a preliminary stage. Hot stamping of aluminium alloys is tested only on a AA6xxx, and neglects several aspects concerning the stamping process parameters, material heat treatments, surface quality and stamped parts mechanical properties. Moreover, the behaviour of other aluminium alloys series under Hot Stamping condition are still unexplored such as, for example, the automotive AA5083 alloy usually used in the superplastic delivered condition. The HMGF process, thanks to the first promising results in laboratory applications, is gaining more interest and seems ready to be implemented in industrial applications. Even so, several aspects have been neglected or have not been investigated in depth. Only a few research groups are focused on this novel forming process and, especially on aluminium alloys, only studies of cylindrical short components were performed. Process properties connected to tube heating system, such as the electrical insulation are unknown and, moreover, many researches are focused on part feasibility, without investigating post-forming mechanical properties or aesthetics surface appearance.

1.2. Objective and work organisation

The aim of this research is to study the formability of aluminium alloys sheets and tubes at high temperatures and high strain rates, applying innovative forming technologies to overcome the limits of the current industrial processes. To fulfil the purpose, two main fields of research have been pursued:

1. The evaluation of the rheological behaviour and the formability of aluminium alloys sheets, currently used in the automotive industry, at elevated temperatures and high strain rates by means of innovative formability tests.
2. The design and development of new forming process at elevated temperatures, called Hot Metal Gas Forming, carried out on tubular preforms of aluminium alloys.

Regarding the formability of aluminium alloys sheets, the main activities performed can be summarised as:

- ✓ Complete rheological characterisation at varying process parameters, namely temperature and strain rate, of two aluminium alloys: AA5083 (aluminium-magnesium alloy) in commercial condition and with superplastic characteristics, and AA6016 (aluminium-magnesium-silicon alloy), all used in the automotive sector. Each characterisation includes: microstructural analysis on the as-delivered material and after being thermally cycled, true stress-true strain curve determination through hot tensile tests, micro-hardness, true strain at fracture and microstructural features and fracture area morphology in order to define the best formability window for each metal sheet as a function of the temperature and strain rate.
- ✓ Determination of the Forming Limit Diagrams (FLDs) through Nakajima tests carried out at elevated temperatures to confirm the formability data obtained from the hot tensile tests.
- ✓ Validation of the formability data through industrial trials conducted on an industrial hot stamping plant for the production of an automotive component.

Whereas, considering the research activity on the innovative Hot Metal Gas Forming process, starting from a literature review on the existent experimental apparatus, the principal activities were focused in:

- ✓ Design and develop of an experimental apparatus able to evaluate the formability of aluminium tubes and to perform the innovative Hot Metal Gas Forming process, that allows shaping hollow parts heated at high temperature through electric current.
- ✓ Formability tests performed on two different series of aluminium alloys hot extruded tubes (AA6060 and AA6082) obtained with different process parameters.
- ✓ Feasibility study on shaping tubes inside a die to create square components, investigating also the effects of different die materials with different electrical insulation properties and surface roughness, and evaluating the influence of different process parameters as temperature and time cycle.
- ✓ Design of a measurement software in LabVIEW® environment, able to measure radius and thickness of deformed tubes.
- ✓ Industrial case of study in collaboration with an Italian company, trying to create a complex aesthetic hollow component starting from AA6060-T5 aluminium alloy tubes with different thickness, specifically 1.5 mm, 2 mm and 3 mm, and an fixed external diameter of 20 mm. In doing so, the activities were focused on (i) the design of the die and die-support structure, (ii) the investigation of the best forming process parameters,

with the purpose to obtain the desired component without defect with the lowest process time and (iii) the post-forming evaluation of the aesthetic properties of the part, mainly connected to the anodisation chemical treatment.

This thesis is divided into five chapters. The first presents the introduction of the work with a brief description of the industrial request on light alloys formability especially in automotive sector. The second chapter present a literature review on the metal sheets stamping processes development, and on tube shaping processes, focusing principally on aluminium alloys as raw material. Afterwards, two main chapters explain the experimental activities and the results, respectively on aluminium metal sheet forming where the technologies of Hot Stamping were applied, and on the Hot Metal Gas Forming process with the conceptual design of an experimental apparatus and the subsequent formability tests on aluminium tubes. The final chapter summarises and concludes the result of this research work.

Chapter 2

Literature review

In the last two decades, increasingly stringent regulations on fuel consumption, gas emissions and product recyclability have been focused the automotive industry's attention on the use of high-strength aluminium alloys for the manufacture of lightweight structural sheet parts in the car body and the body-in-white. Moreover, one of the most recent trends is represented by the use of light alloy complex shaped hollow parts in the manufacturing of the car chassis, which allows a significant increase of the stiffness compared to sheet metal components together with the reduction of the total car weight.

The AA5xxx and AA6xxx series proved to be the best candidates for their engineering properties, due to, for example, their low density and good strength, corrosion resistance and weldability, and, not least of all, for the lower cost compared with the aluminium alloys for aeronautical applications. However, when they are formed at room temperature as in conventional sheet and tube metal forming processes, the AA5xxx and AA6xxx series, exhibit too low formability and marked springback for stamping and shaping accurate parts with a complex geometry.

A substantial increase of the formability and, at the same time, a drastic reduction of springback can be achieved if the sheet metal undergoes plastic deformation at elevated temperatures [9,10].

Anyway, the innovative categories of forming processes introduced in the last decades for the aluminium alloys are characterised by too low production rates, make these technologies unsuited to the high-volume production of economically competitive parts. Thus, high production volumes and economic competitiveness suggest investigating the applicability of the Hot Stamping (HS) technology nowadays used on high strength steels to shape sheets of aluminium automotive series. Furthermore, innovative processes need to be found also for

tubes shaping, where the Hydroforming process is the main technology used, with severe restrictions due to limited process temperature and long setup time.

Therefore, coupling lightweight material and innovative process technologies, it is possible to obtain, referring to the automotive industries:

- Weight savings of 40% on a typical mid-sized automobile, Figure 2.1, which reduces greenhouse gas emissions and increases fuel economy;
- No fit issues on the auto assembly line where two pieces construction could become one piece;
- Simplification of the assembly process.

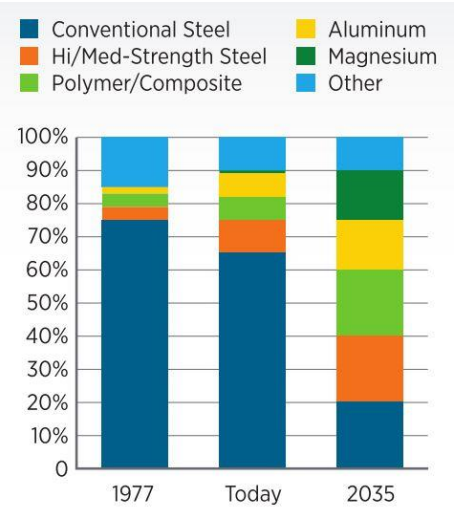

	Weight (lb)	
Component	Standard materials	Advanced lightweight materials
Body-in-white	1,630	860
Body panels	986	540
Bumpers	137	97
Engine cradle	77	31
Corner suspension	104	57
Wheels	157	130

Figure 2.1: Typical composition of past and present cars versus a future lightweight vehicle, and weight comparison of components built with standard versus advanced lightweight materials [11].

This chapter presents a literature review concerning the industrial process and academic researches on metal sheets and tubes shaping, especially focused on aluminium alloys. Starting with an introduction on aluminium alloys, in paragraph one, especially focused on the two series investigated in this research work, namely AA5xxx and AA6xxx, the second paragraph describes sheet metal forming processes of aluminium alloys and high strength steels at high temperature highlighting research improvements on process cycle and energy consumption reduction. In detail, the Hot Stamping process, the Super Plastic Forming, the Quick Plastic Forming and innovative deformation processes were considered. Finally, the third paragraph presents the evolution in processes for shaping hollow components, focusing especially on the innovative Hot Metal Gas Forming process, previously introduced by the Hydroforming process that represents the foundation of this new technology.

2.1. Aluminium alloys

Steel car bodies and frames, have been traditionally fabricated from stamped sheet parts joined by spot welding. Recently developments, have included innovative process technologies as hot stamping process, superplastic process, quick plastic process or hydroforming technique. Moreover, with the market introduction of new high strength steel grades and the

increase in the use of aluminium alloys, it has been possible to improve the stiffness and reduce the weight of vehicles.

Similar design and manufacturing principles as those used for steel body structures can be applied to realize an all-aluminium car body, obviously with concepts and properly adapted fabrication technologies. As an example, a Porsche 928 sports car with an all-aluminium body was exhibited in 1981, the weight of the aluminium body was 161 kg, representing a weight reduction of 106 kg compared to the steel body. Therefore, aluminium alloys have been started to be used for various automotive parts for its low specific weight, around 1/3 of steel. Their uses is not limited to conventional castings such as engine blocks, but extends to hoods, trunk lids, outer panels such as doors and protection covers including heat insulators.

The properties of aluminium that make this metal and its alloys the most economical and attractive for a wide variety of uses are appearance, light weight, fabricability, physical properties, mechanical properties, and corrosion resistance. Especially for its density of 2.7 g/cm3 and its high excellent corrosion resistance in most environments, including atmosphere, water (including saltwater), petrochemicals, and many chemical systems, this material is very attractive for the automotive and aerospace field. Moreover, some aluminium alloys exceed structural steel in strength. Aluminium is non-ferromagnetic, a property of importance in the electrical and electronics application, is non-pyrophoric that is an important characteristic in applications involving flammable liquids or explosive materials. Finally, aluminium is non-toxic and has an attractive appearance in its natural finish, which can be bright and shiny.

Considering the aerospace industries, is used in virtually all segments of the aircraft, missile, and spacecraft airframes, engines, accessories, and tankage for liquid fuel. Aluminium is widely used because of its high strength-to-density ratio, corrosion resistance, and weight efficiency. In the automotive sector, instead, standard usage of approximately 70 kg for vehicle in early 80's years, as expected, is increased drastically with the average fuel economy mandates and emphasis on material recycling [12]. Aluminium sheets are nowadays used for hoods, trunk decks, bright finish trim, air intakes, and bumpers, while extruded shapes, pipes and bars are used for frame structure.

It is convenient to divide aluminium alloys into two major categories, based on phase solubility: non-heat treatable and heat treatable. These heat treatments include solution heat treatment, quenching, and precipitation or age hardening. Therefore, aluminium alloys are divided in nine series based principally on the chemical composition. In detail:

- 1xxx Controlled unalloyed (pure) compositions;
- 2xxx Alloys in which copper is the principal alloying element, though other elements, notably magnesium, may be specified;
- 3xxx Alloys in which manganese is the principal alloying element;
- 4xxx Alloys in which silicon is the principal alloying element;
- 5xxx Alloys in which magnesium is the principal alloying element;
- 6xxx Alloys in which magnesium and silicon are principal alloying elements;
- 7xxx Alloys in which zinc is the principal alloying element, but other elements such as copper, magnesium, chromium, and zirconium may be specified;
- 8xxx Alloys including tin and some lithium compositions characterizing miscellaneous compositions;

- 9xxx Reserved for future use.

The temper designation follows the alloy designation. Basic temper designations, consist of individual capital letters, while major subdivisions of basic tempers, if required, are indicated by one or more digits following the letter.

- F – as-fabricated: applied to products shaped by cold working, hot working, or casting processes in which no special control over thermal conditions or strain hardening is employed;
- O – Annealed: applied to wrought products that are annealed to obtain lowest-strength temper and to cast products that are annealed to improve ductility and dimensional stability;
- H – Strain hardened, for products that have been strengthened by strain hardening, with or without supplementary thermal treatment to produce some reduction in strength. The H is always followed by two or more digits indicating the operation used to hardening material;
- W - Solution Heat-Treated: referred to an unstable temper, applicable only to alloys whose strength naturally changes at room temperature over a duration of months or even years after solution heat treatment;
- T - Solution Heat-Treated: This applies to alloys whose strength is stable within a few weeks of solution heat treatment. The T is always followed by one or more digits indicating the operation performed for solution heat treatment.

Regarding, the main mechanical and physical properties, aluminium alloys exhibit high thermal conductivity four time as fast as steel, around 200-300 W/mK, relevant thermal expansion twice that for steel. Therefore, combination of high coefficient of thermal expansion and high thermal conductivity can cause considerable distortion on aluminium components during hot processes. In addition, regarding the electrical properties, aluminium exhibits higher conductivity than steel, which means that much higher currents are required to produce the same heating effect. Consequently, resistance heating apparatus (through Joule effect) employed on aluminium alloys, need higher electric current capabilities than those normally used for steel. Taking into account the most used aluminium alloys series in automotive sectors, 5xxx and 6xxx, studied in this research work, they differ mainly for characteristic of to be non-heat treatable (AA5xxx) and to be heat-treatable (AA6xxx).

The major alloying element in 5xxx alloys series is magnesium that confers, when it is used as the major alloying element or with manganese, a moderate high-strength work and hardening. Even if manganese inside aluminium matrix, increases strength either in solid solution or as a finely precipitated intermetallic phase, magnesium is considerably more effective than manganese as a hardener, indeed about 0.8 % Mg being equal to 1.25 % Mn, and it can be added in considerably higher quantities. Alloys in this series possess good welding characteristics and good resistance to corrosion in marine atmospheres. However, 5xxx alloys exhibits limitations on the amount of cold formability and on safe operating temperatures permissible, especially for the higher-magnesium alloys (over about 3.5 %) and operating temperatures above about 65 °C susceptible to stress-corrosion cracking [12].

Alloys in the 6xxx series contain silicon and magnesium approximately in the proportions required for formation of magnesium silicide (Mg_2Si), thus making them heat treatable. Although not as strong as most 2xxx and 7xxx alloys, 6xxx series alloys have good formability, weldability, machinability, and corrosion resistance, with medium strength. Alloys in this heat-treatable group may be formed in the T4 temper (solution heat treated but not precipitation heat treated) and strengthened after forming to T6 condition by precipitation heat treatment [12]. The mechanism of strengthening by age hardening involves the formation of coherent clusters of solute atoms. This causes a great deal of strain because of mismatch in size between the solvent and solute atoms. The cluster stabilizes dislocations, so, when dislocations are anchored or trapped by coherent solute clusters, the alloy is considerably strengthened and hardened [12]. Heat treatment for precipitation strengthening includes a solution heat treatment at a high temperature to maximize solubility, followed by rapid cooling or quenching to a low temperature to obtain a solid solution supersaturated with both solute elements and vacancies. This behaviour is most effective near the solidus or eutectic temperature, where maximum solubility exists and diffusion rates are quick. However, care must be taken to avoid incipient melting of low-temperature eutectics and grain boundary phases. Such melting evolves in quench cracks and loss in ductility. A temperature of 550 °C for a time dependent from the component mass, is the requisite to complete the dissolution of the Mg_2Si precipitates within the aluminium matrix [13]. The high strength is produced by the finely dispersed precipitates that form during natural or artificial aging heat treatments. This final step must be accomplished not only below the equilibrium solidus temperature, but below a metastable miscibility gap called the Guinier-Preston (GP) zone.

In the precipitation process, the saturated solid solution firstly develops solute clusters, which then become involved in the formation of transitional precipitates (non-equilibrium). Successively, the final structure consists of equilibrium precipitates, which do not contribute to age hardening (precipitation strengthening). Natural aging refers to the spontaneous formation of a G-P zone structure during exposure at room temperature, while artificial aging includes exposure at temperatures above room temperature so as to produce the transitional forms of the equilibrium precipitate of a particular alloy system as showed in Figure 2.2 for an AA6061 alloys [14].

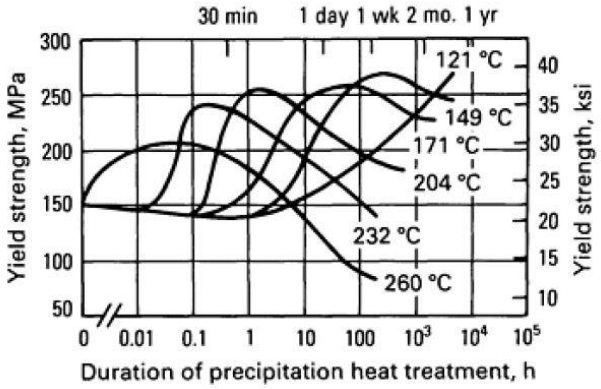

Figure 2.2: Precipitation heat treatment or artificial aging curves for solution heat-treated aluminium alloy 6061.

2.2. High temperature forming processes

A substantial increase of the formability and, at the same time, a drastic reduction of springback can be achieved if the sheet metal undergoes plastic deformation at elevated temperatures [1]. Sheet metal working operations at elevated temperatures have gained in the last few years even more importance due to the possibility of producing components characterized by high strength-to-mass ratio. The main process used to produce automotive stamped parts, is represented by the Hot Stamping (HS) applied on high strength steels, while aluminium alloys are nowadays produced through Superplastic (SPF) and Quick Plastic Forming (QPF) processes which require time cycle two or three order of magnitude higher than HS.

2.2.1 Hot stamping process (HS)

Hot stamping of ultra high strength quenchable steels (HHS) is nowadays widely utilized in the automotive industry to produce components like bumpers and pillars with enhanced crash resistance characteristic and geometrical accuracy due to reduced springback. This process, was used for the manufacturing of a structural component in a standard mass production vehicle in the 1984 [15]. Since that year, the hot stamping process was used to produce high millions of structural parts each year, which different geometries and function abilities.

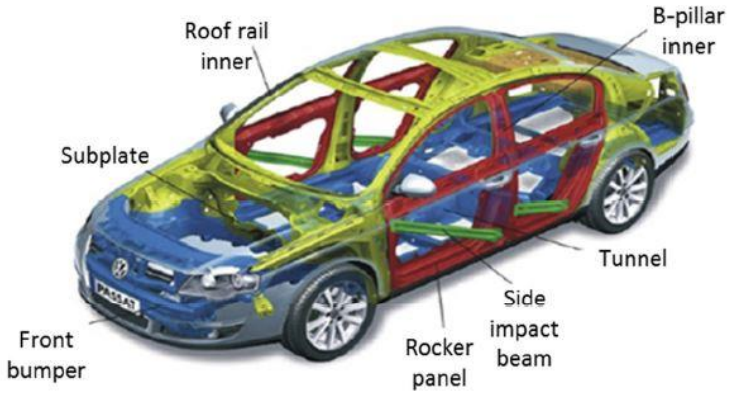

Figure 2.3: Hot stamped parts in a typical middle class car [16].

This technology uses steel blanks heated up above austenitization temperature and successively transferred into the press where deformation and quenching take place simultaneously in order to achieve a fully martensitic microstructure in the formed component at room temperature [17]. The advantages are due to the low material strength during the stamping operation in austenization condition, and the very high component resistant obtained after quenching caused to the martensitic transformation. Moreover the quench operation performed into stamping dies, allows an optimal final part geometry preventing the possibility of relevant springback. The materials subjected to this process technology, utilized due their capabilities to reach the martensitic structure without severe cooling rate, are the 22MnB5, with chemical composition reported in Table 2.1, the 27MnCrB5 and the 37MnB4.

Table 2.1: Chemical composition of 22MnB5 material.

C	Mn	Si	Ti	Cr	B
0.25	1.40	0.35	0.05	0.3	0.005

Indeed, using these materials, the quenching cooling rate necessary to avoid the bainitic transformation vary from 30 °C/s to 14 °C/s respectively with martensite start temperature from 450 °C for the 22MnB5 to 350 °C for the 37MnB4. All of these HHS reach after quenching an increment of around 200 % of yield stress as shown in Figure 2.4, for different austenitization temperatures.

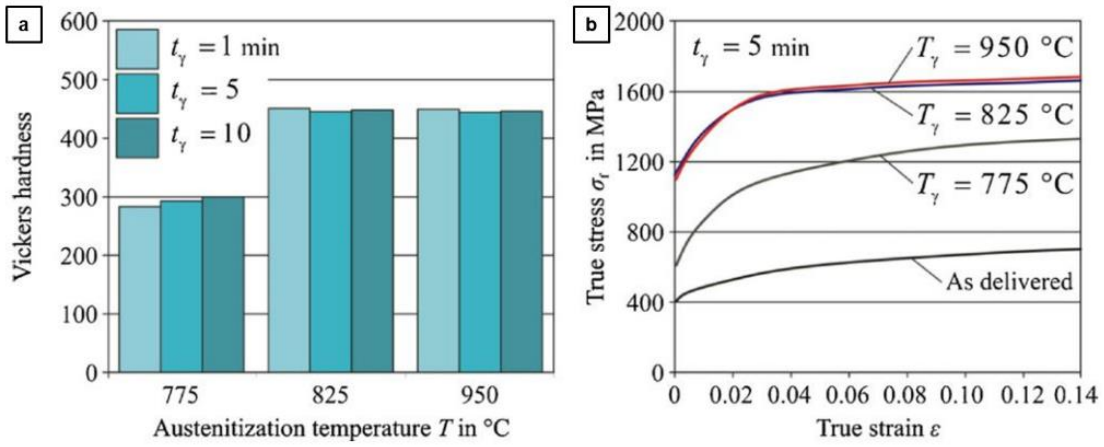

Figure 2.4: Mechanical properties at different austenitization temperatures, Vickers hardness (a) and true stress (b) [18].

It is worth noticing that process parameters are focused principally on temperature, austenitization time and cooling rate. These three parameters, indeed, have a strong influence on the material behaviour in terms of flow curves and hardness. Thus, in the last years, the focus of different research activities in the field of hot stamping is moving on the reduction of the cycle time which directly depends on the cooling performance of the tools. Moreover, the reduction of energy costs are leading to the necessity to look for less energy consuming heating methods. Several researches were performed to develop new concepts of cooled tools[19], investigating also new tool materials [20], and testing different heating technologies applied to the process [21,22]. Regarding this last innovation field, Merklein et al. found that using induction heating system applied to the uncoated material, is possible reaching similar mechanical properties on the material compared with the common convective heating. The study proved that a tremendous reduction of heating time can be obtained which results in lower investment cost and reduced floor space for the heating device [23]. Moreover, many studies were focused on reducing the austenitization temperature, trying also to reduce the austenitization time. At now, results proved that 180 seconds are necessary to obtain a fully austenitic microstructure and consequently a fully martensitic structure in the final part considering an initial blank thickness of 1.75 mm [24]. Furthermore, as known, austenitization time increase with austenitization temperature decreases, as shown in Figure 2.5.

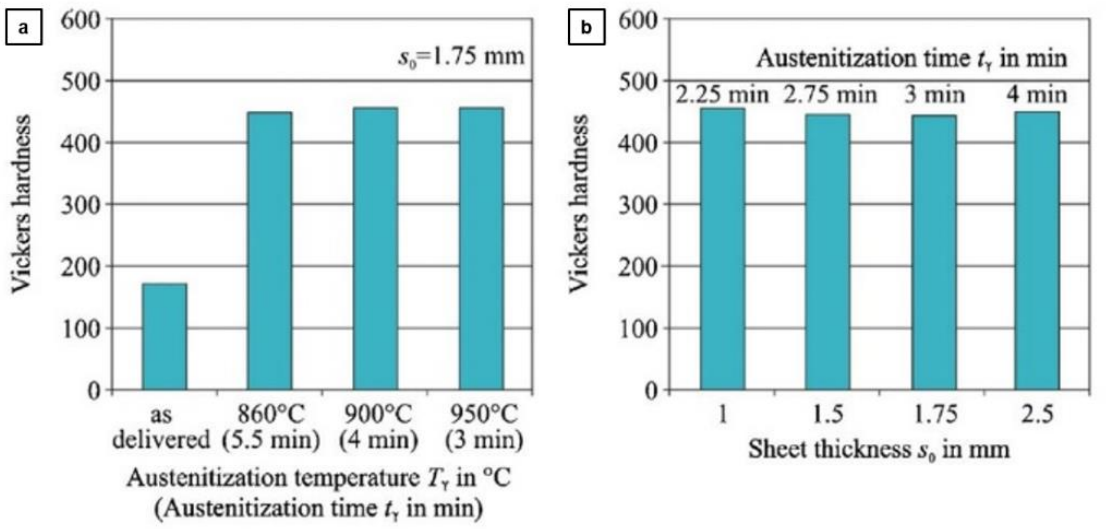

Figure 2.5: Influence of austenitization temperature, time (a), and sheet thickness (b) on the minimum austenitization time to achieve the maximum hardness of 470 HV [25].

Time cycle are due also to the slow heating rates used on blank and indirectly connected to the material coating used to avoid steel oxidation. In fact, Al-Si coating developed by Arcelor-Mittal for the most used hot stamping material: 22MnB5, needs a substantial time interval to assure a good diffusion of the iron atoms from the steel to the coating, and so puts a strickt limit to the heating rate. In industrial process, this problem is resolved using roller gas heat furnaces but these structures need to have a very large volumes around 30 - 50 m. Therefore, this issue remains open for hot stamping implants with compact dimension or in specific research laboratories where the process is replicated for analyse the material behaviour. Indeed, the M. Merklein at al. study on induction heating applied on Al-Si coated boron steel, proved, that a heating rate of about 12 K/s is recommended in order to avoid melting of the coated layer and to improve the diffusion of Fe into Al-Si-layer [23]. Recently, through an European project has been investigated the possibility to create new high strength steels suitable for the hot stamping application [26]. The main purpose, was to obtain a reduction of both process energy consumption and process time cycle, hence the abatement of environmental impact and of economical costs of the hot stamping process. In doing so, the optimization of the austenitizing parameter combined with a reduction of the cooling rate required, were the main work issues investigated, Figure 2.6.

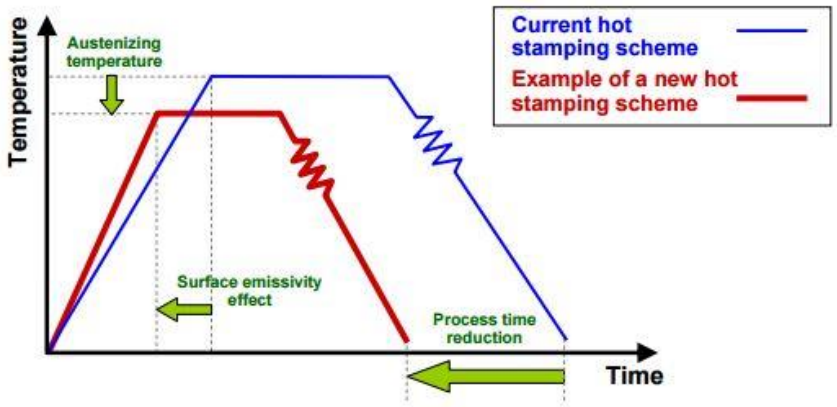

Figure 2.6: Target Hot Stamping cycle time using new high strength steels [26].

This research work developed two new steel grades with low Ac3 temperature (785 °C and 810 °C), providing a significant reduction of produced CO_2 emissions during heating in the furnace stage (over 20 %), with relevant reduction in the gas consumption, also in the furnace operation (over 20 %). Moreover, both high strength steels created, shown acceptable and comparable final mechanical properties, as compared to the 22MnB5, Figure 2.7, and an adequate weldability and spot weld resistance [26]. Anyway, several future post-mechanical characterizations, especially concerning the coating behaviour at high temperature, need to be performed before their application on mass production.

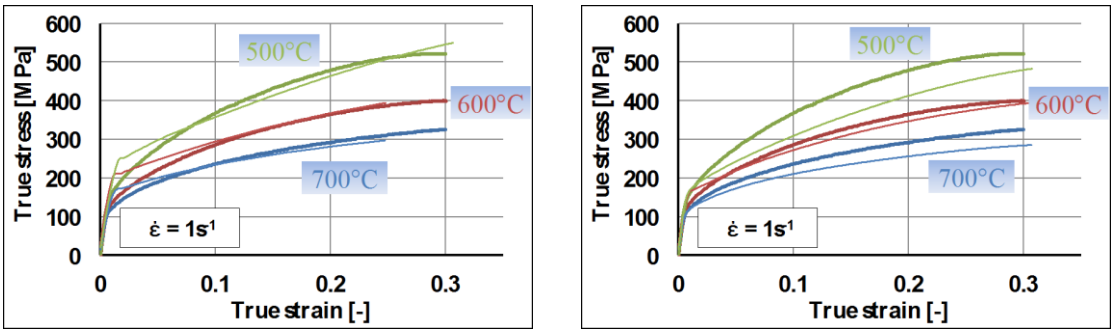

Figure 2.7: True stress-True strain behaviour of the two innovative high strength steels created, putting in evidence their influence to the temperature [26].

In the last years, in order to achieve a further body-in-white weight reduction and exploit the potential for lightweight construction, studies on process chain for the production of thin hot stamped component were carried out. The behaviour of blank thickness between 1.5 mm and 0.5 mm were investigated considering several critical process aspects as the heat losses during the blank transfer from furnace to die [27]. Figure 2.8, shows how blank foil of 0.5 mm in thickness cools down quicker due to the smaller mass-surface ratio, presenting the possibility to perform the martensite start transformation before stamping operation started during a long lasting air cooling or when the blank comes in contact with press tools. Therefore, innovative process-forming tool concepts require to be designed to apply the Hot Stamping process on very thin high strength steel blanks for a further reduction of vehicle weight and, as consequence, of CO_2 emissions.

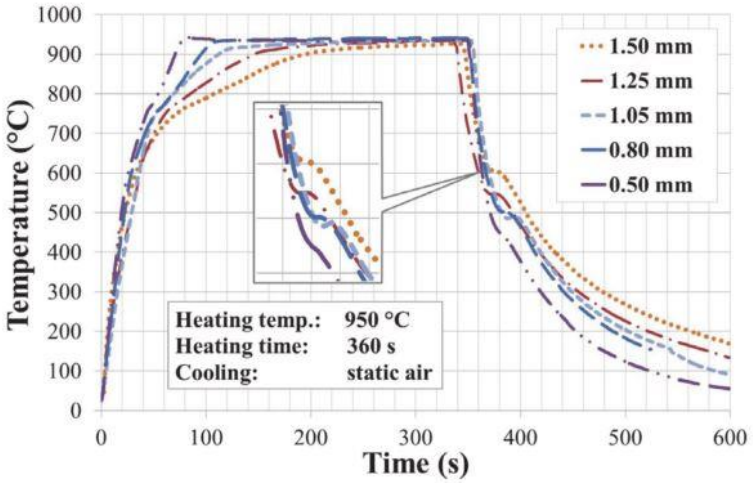

Figure 2.8: Temperature profile for different 22MnB5 sheet thicknesses [27].

Therefore, excluding the blank heating operation, nowadays the time cycle needed to a completely stamped part in hot stamping process, is around 15 – 25 seconds, including transfer, forming and die quenching, Figure 2.9. Final part temperature of 150 °C is usually necessary because, an early take-off from die clamping, can implement thermal distortions on the geometry or a not completed martensite transformation. Moreover, blank thickness lower than 1 mm, need new tools concept to avoid the martensitic transformation of the component before completing the shaping.

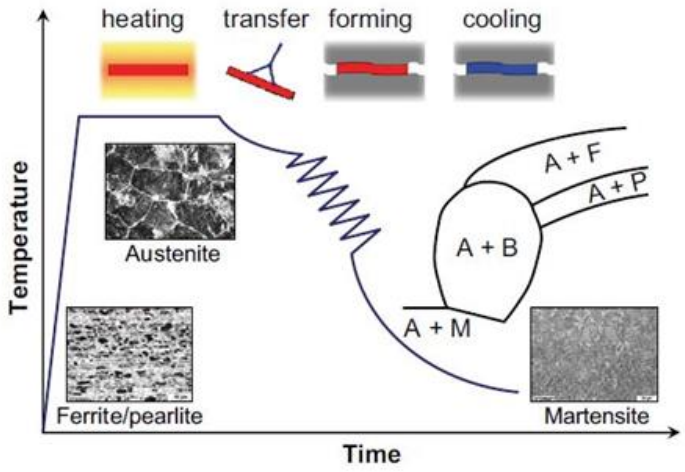

Figure 2.9: Hot stamping process cycle [28].

2.2.2 Super Plastic Forming (SPF)

The superplastic forming (SPF) operation is based on the fact that some alloys can be slowly stretched well beyond their normal limitations at elevated temperatures. Isothermal low strain rate conditions in superplastic forming, result in low workpiece flow stress. Moreover, the higher temperatures mean that the flow stress of the sheet material is much lower than that at normal temperature. The process consist on placing the sheet to be formed in an appropriate SPF die, which can have a simple or a complex geometry, representative of the final part to be produced. Sheet and tooling are heated and then a gas in pressure, rather than a hard punch, is applied, plastically deforms the sheet into the shape of the die cavity, Figure 2.10.

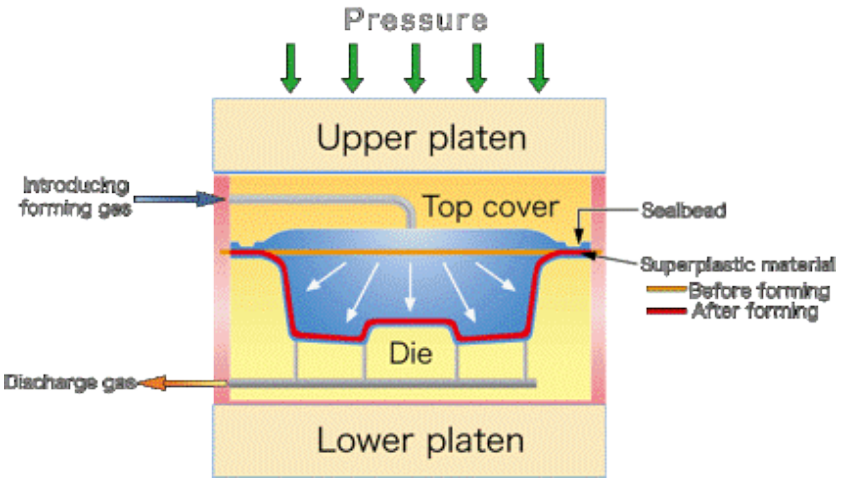

Figure 2.10: Super Plastic Forming processes.

Although cycle times for superplastic forming are relatively long, of the order of 20 min per part, economies of manufacture are realized primarily through reduced machining and assembly costs. The latter savings is a result of the fact that individual superplastically formed parts are usually used as replacements for assemblies of many separate component parts. In general, lower strain rates and increased dwell time, increase the potential degree of shape complexity and shape sophistication of the component, but on the other hand, can influence microstructure due to exposure to high temperatures for long periods. Superplastic behaviour on metal sheets, has been demonstrated in titanium alloys, especially Ti-6Al-4V, Supral alloys, and aluminium alloys confined especially in 2xxx, 7xxx, and some 5xxx series as the AA5083.

The main material requirement for the process is a very fine and stable grain size that for the aluminium alloy stays in the range from 7 μm to 10 μm. Usually, microstructure with superplastic characteristics, is achieved by static or dynamic recrystallization. In static recrystallization, a deformed microstructure is allowed to undergo discontinuous recrystallization during static annealing, while in dynamic recrystallization, a deformed microstructure undergoes gradual, continuous recrystallization and grain refinement. Because of the stable grain size requirement for a superplastic metal, not all commercially available alloys are superplastic. The titanium alloys are superplastic as conventionally produced, and not need to develop alloy modifications nor special mill-processing methods to make them superplastic. Instead, the aluminium alloys require special processing or particular alloy development to become superplastic. Often several consecutive cold rolling operations with high thickness reduction are used to create the superplastic grains size.

Moreover, superplastic process needs a relatively high temperature (greater than about one-half the absolute melting point), and a strictly controlled strain rate, usually in the range from 10^{-5} to 10^{-3} s^{-1}. Therefore, this technology is limited to niche sectors as the aeronautical and aerospace industries but also extended to the luxury automotive sectors where the very long process times are compensated with expensive products. Regarding the deformation mechanism during the superplastic deformation, there is a good relation between the m value (strain rate sensitivity), and the superplastic ductility. Moreover, process temperature has an important role because temperature variation in the forming die was proved to be the primary source of localised thinning, thus, strain localisation and necking represent the dominant modes of failure. Indeed, Superplastic materials exhibit in fracture location, cavitation near inclusions, triple points, and second-phase particles, generally generated by the interlinking and nucleation of growing cavities [29].

The deformation mechanism generally accepted as responsible for fine-grain superplasticity in aluminium alloys is grain-boundary-sliding (GBS) creep, which supplies a high strain-rate sensitivity (m = 0.5) while producing the low flow stress typically necessary for successful commercial superplastic forming operations [30]. During this deformation mechanism, crystals slide past one another without changing it shape, Figure 2.11. The movement of one grain past another, in pure material may be accomplished by dislocation or diffusive mechanisms [31].

Elongated and aligned grains, make the GBS mechanism easier, moreover, similarly elongated grains have a mechanical coupling that tends to rotate them with respect to the applied stress, while, spherical grains obstruct the rotational mechanism. In addition, grain boundary orientations allow easier GBS mechanism, in fact, during the deformation process

micro-voids that are caused by material movement, allow grains translation generating the stretching.

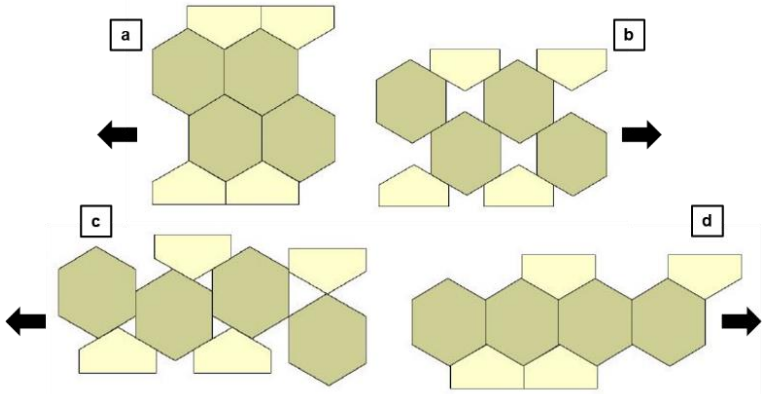

Figure 2.11: Representation of the GBS deformation mechanism.

So, in this mechanism, intergranular slip plays and important role. Alloying additions can decrease the tendency to grain sliding, in fact, adding intergranular particles, creates an increase in friction between boundaries, thus this mechanism of strengthening is used on high temperature alloys to provide safe use when creep deformation become a problem. Instead, a reassessment of grains orientation focused on grain boundary can increase the sliding process [32].

Failure mechanism connected of GBS, is due to cavitation, thus the material fracture takes place by nucleation, growth and coalescence of creep cavities on the grain boundaries, predominantly perpendicularly oriented to the applied stress. During creep process, an increase in the number of cavitated boundaries supports the mechanism of continuous cavity nucleation and growth. Sometime pre-existing cavities, voids or pores, previously introduced by the forming operations, become direct points for voids nucleation during the process. In aluminium-magnesium alloys sheets subjected to tensile test at temperatures between 250 °C and 550 °C under GBS deformation mechanism, separated fracture surfaces were found to exhibit fibrous structures [33,34]. These fibres were very thin (about 0.1 μm in diameter) and extended up to 100 μm before fracture. Thus, a superplastic behaviour is connected to the appearance of the fibres. This type of localized superplasticity at the fracture surfaces leading to formation of fibrous structures is referred to as micro superplasticity, and should not be confused with the superplasticity that occurs in the bulk alloys. Presence of a liquid or quasi-liquid phase along the grain boundaries of the Al–Mg alloys, which is formed as the result of solute atom segregation was suggested as a possible reason for fibres generation on the fracture surfaces [33].

S. Das et al. analysed on an aluminium alloy AA5083 the behaviour of the aluminium MgO and $MgAl_2O_4$ oxides tribo-layers that covers aluminium surface, from 200 μm to 3 μm thick, at different process temperatures. The analysis was done by means of TEM images, on layers subjected at low strain rate deformation [35], as shown in Figure 2.12. Tensile tests at a temperature of 420 °C and 545 °C under strain rate respectively of $4 \cdot 10^{-1}$ and $4 \cdot 10^{-2}$ s^{-1}, were performed finding that only at highest temperature and lowest strain rate, fibres are also in the oxide tribo-layer suggesting a superplastic behaviour of the oxide. Figure 2.12 shows the surface morphology of a sample deformed at elevated temperature (545 °C and $4 \cdot 10^{-2}$ s^{-1}). The

Al–Mg grains appear subjected to sliding, while the tribo-layer on the top shows cracks that were bridged by the fibrous structures

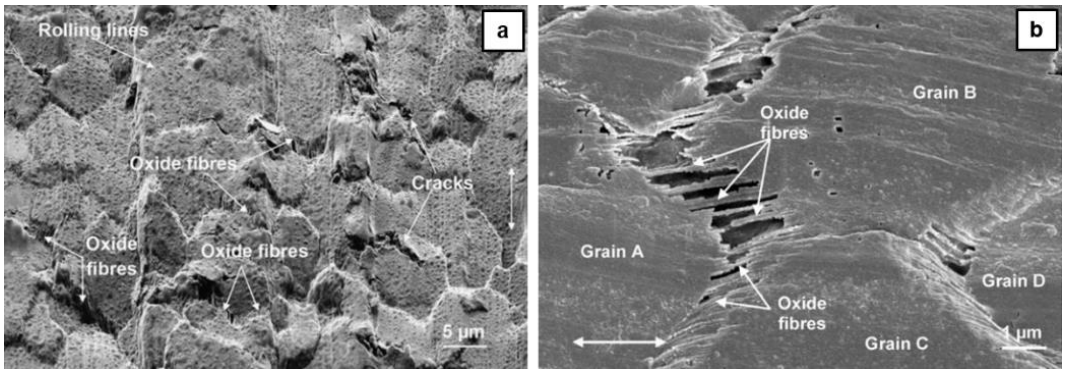

Figure 2.12: Secondary electron image (a) and higher magnification view of the surface of a sample deformed. The two-sided arrow show the tensile direction. (b) [35].

2.2.3 Quick Plastic Forming (QPF)

As described prior, SPF forming process is not suitable for the high production rate, and the raw materials, that require a particular small and oriented grains microstructure, are too expensive, around three times the cost of standard aluminium sheets. Therefore, the needs of the automotive industry, which plays with products volume higher than the aerospace and aeronautical industries where SPF is nowadays one of the principal productive processes, require developing low-cost and faster forming cycle productive process. So, General Motors (GM) and the U.S. Department of Energy (DOE) have sponsored several research works in collaboration with Kaiser Aluminum and with the Pacific Northwest National Laboratory (PNNL) to develop innovative aluminium forming processes.

Based on these studies, quick plastic forming (QPF), which takes place at higher forming rates, was developed. The result is a cost-effective, higher-volume manufacturing technology for producing automotive lightweight components. The QPF process made its debut on the industrial field when GM utilized the QPF technology to create the entire outer panel of the Malibu Maxx's liftgate as one piece instead of two pieces [11]. In this process, a sheet of AA5083 aluminium alloy having grain size of approximately of 30 µm was heated at a temperature of around 400 °C to 500 °C. The sheet was stretched under the pressure of a working gas into conformance with the surface of a forming tool. The sheet forming pressure was increased gradually up to a final pressure of about 250 to 500 psi. Strain rates of the order from 10^{-3} s^{-1} to 10^{-2} s^{-1}, were used and forming operation was performed within 12 minutes. Since the end of 2005, over 300000 panels were produced through QPF reducing the process cycle at around 2 - 3 minutes per part [36].

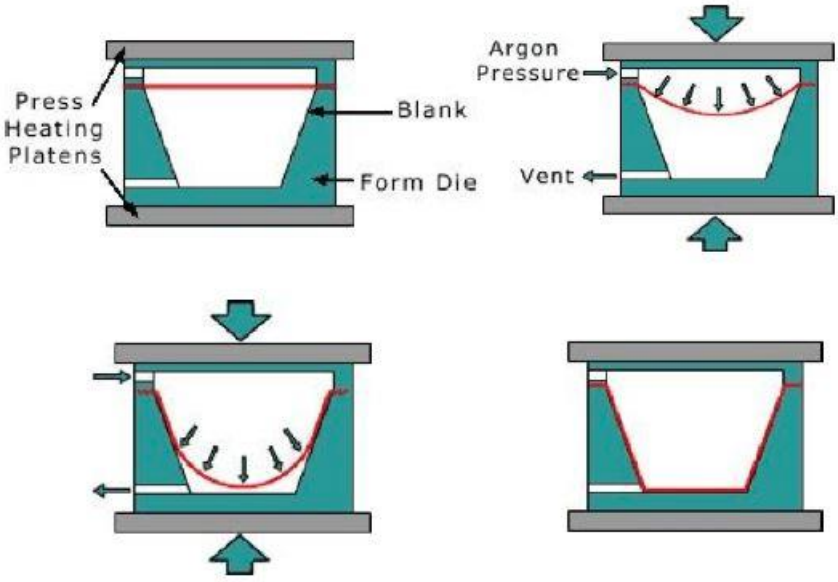

Figure 2.13: Quick Plastic Forming process

Using QPF, the material deformation mechanism is due to the Solute Drag (SD) creep. Indeed, no specific grain dimension is needed, so larger grain-sizes-microstructure materials can be used. SD is a dislocation glide-control mechanism, which can occur in aluminium alloys, especially in Al-Mg aggregation. Weeterman [37] introduced the first widely accepted mechanism for SD creep based on the idea that creep rate is controlled by iteration between dislocation and solute atoms. In this case, the dislocation glide motion becomes the rate-limiting step of creep deformation. The average dislocation velocity is controlled by drag force from the solute atmosphere. This mechanism appears when solute atoms have a significant volumetric size differenced with the matrix atoms, causing strain fields that interact with dislocations in motion. If the diffusion becomes through the lattice, it is called Nabarro-Herring creep. The diffusional flux between the boundaries parallel and perpendicular to the stress axis is proportional to the stress and to the lattice diffusivity, and it is inversely proportional to the diffusion distance between the diffusion source and diffusion sink. Therefore, the velocity which the diffusion source and the diffusion sink move apart is proportional to the diffusional flux, Figure 2.14 (a). On the other hand, if creep occurs by diffusion along the grain boundaries, it is called Coble creep, Figure 2.14 (b). The driving force for Coble creep is the same as for Nabarro-Herring creep. The total number of grain boundary diffusion paths is inversely proportional to the grain size [38].

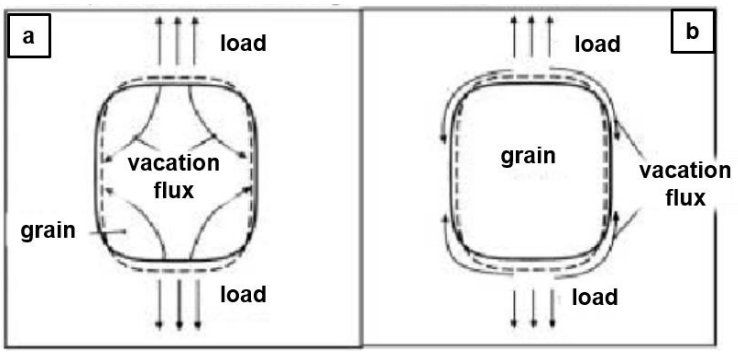

Figure 2.14: Creep mechanism, Nabarro (a) and Coble (b).

Deformation under SD creep has received less attention compared to the GBS creep mechanism. This is due to the fact that tensile elongation obtained under SD creep condition is generally lower than under GBS but not always true. However, SD mechanism has the advantages to need lower temperatures and faster strain rates, and to be independent of grain size and grain morphology. Another important aspect is due to the fracture morphological behaviour, that especially for the aluminium alloys lead the GBS deformation mechanism to obtain a lower final deformation than the SD creep mechanism. Cavitation development with strain under Solute Drag creep is slower than under GBS creep. So, QPF process becomes more suitable for high mass production, using lower temperatures, higher strain rates and showing independent behaviour to grain structure and dimension with a slower cavitation development than the SPF. Concluding, GBS and SD creep are known to govern the plastic deformation of aluminium alloys sheet, as the AA5083, where GBS creep dominates deformation at slow strain rates and high temperatures, and SD creep dominates deformation at relative fast strain rates and relative low temperatures. M. Taleff et al. [30], investigated a wide range of high temperatures from 375 °C to 500 °C with strain rate from $3{\cdot}10^{-4}$ s^{-1} to $3{\cdot}10^{-2}$ s^{-1}, evaluating quantitatively the stress transients followed with rate changes from GBS to SD. Results exhibited a clearly differentiates between GBS and SD creep and offered conclusive proof that SD creep dominates deformation at fast strain rates and low temperatures. Moreover, the authors observed that in the AA5083 material for deformation in the SD creep regime, pronounced stress transients followed the strain-rate changes, Figure 2.15 and that the relative transient measure was independent by temperature.

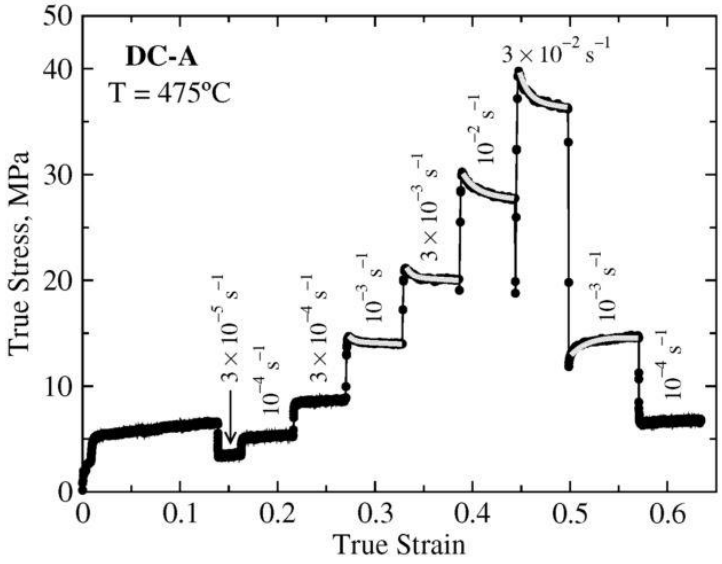

Figure 2.15: Transients characteristic of SD creep for AA5083 strain rate change test at 475 °C [30].

In addition, investigation of the transition from GBS to SD of a modified AA5083 aluminium sheet material containing a Cu addition of 0.61% in weight was investigated. Thus, tensile tests were performed at temperatures from 425 °C to 500 °C and at initial true strain rates ranging from $3{\cdot}10^{-5}$ s^{-1} to $6{\cdot}10^{-2}$ s^{-1}, evaluating also the fracture morphologies through SEM images [39]. Results revealed a change in failure morphology upon the transition from necking-controlled failure under SD creep, to cavitation-controlled failure under GBS creep, as shown in Figure 2.16.

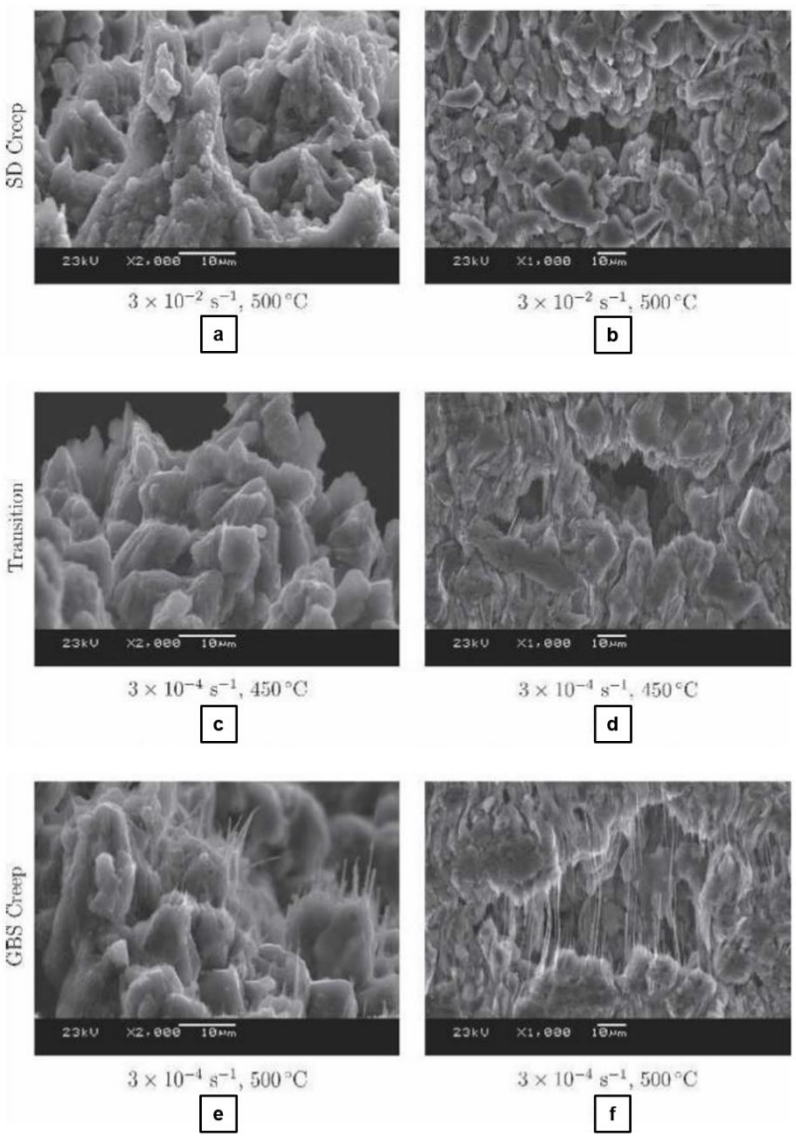

Figure 2.16: SEM images illustrating the transition from SD creep to GBS creep with a tensile axis approximately vertical for each images. The left column shows fracture surfaces formed under (a) SD creep, (c) the transition from GBS to SD creep, and (e) GBS creep conditions. The right column shows surface cavity openings formed under (b) SD creep, (d) the transition from GBS to SD creep, and (f) GBS creep conditions [39].

Under SD creep, failure surfaces exhibited large local plasticity and deformation structure elongated along the tensile axis. On the other hand, under GBS creep, failure surfaces exhibited sub-micrometers diameter fibres along the tensile axis, which is characteristic of failure at grain boundaries by local grain-boundary plasticity. At the transition between these two mechanisms, the failure surfaces exhibited a mix of both feature types, with fewer sub-micrometers fibres. The transition from GBS to SD in grain-refined AA5083 materials was evaluated also in [29], where four SPF AA5083 grades were examined studying the evolution of microstructure and microtexture from the as-received condition through deformation transition from GBS to SD creep. From the previous studies [30,41] where it was proved that a temperature of 450 °C was sufficient to activate both deformation mechanisms only applying different strain rates, the quantitative determination of cavity fractions, and grains orientation through orientation

imaging microscopy (OIM) were investigated. Therefore, temperature was kept constant at 450 °C and strain rates of $3 \cdot 10^{-4}$ s^{-1}, to produce deformation dominated by GBS creep, and $3 \cdot 10^{-2}$ s^{-1}, to produce deformation dominated by SD creep, were chosen. Results proved that the cavitation growth rate was higher when GBS controls deformation. Furthermore, results reported in Figure 2.17, showed that the disorientation distributions are not presented during GBS condition, while a dynamic grain grown appeared. In addition, an increased population of low angle boundaries was apparent in the sample deformed through GBS, instead, development of low angle boundaries and grains elongation appeared when SD contributes to deformation [40].

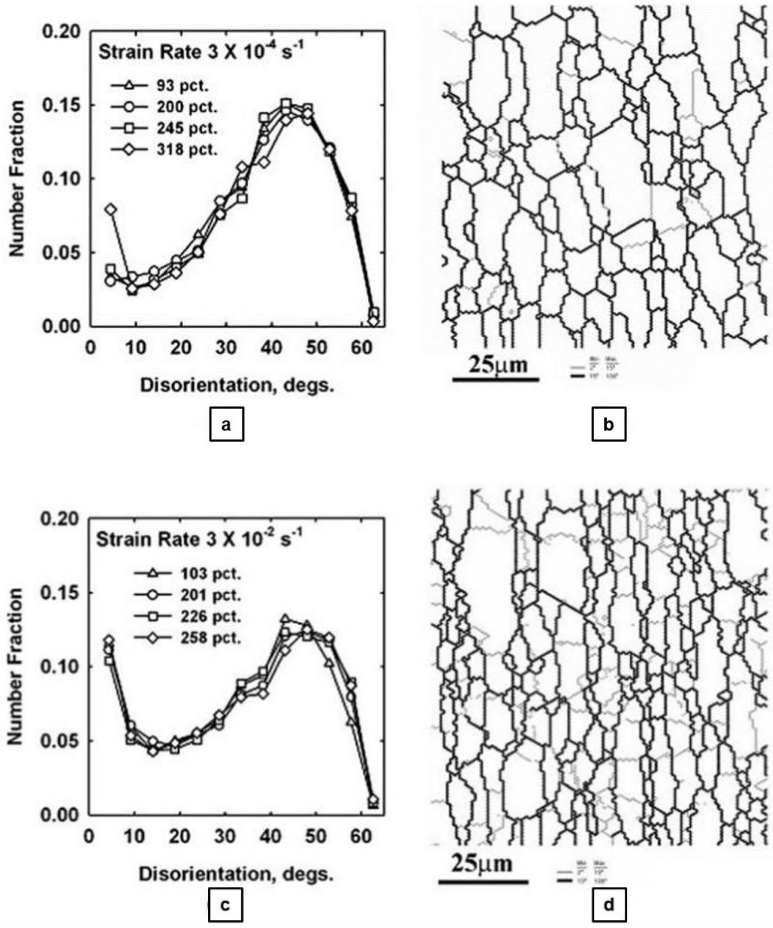

Figure 2.17: OIM disorientation distributions and grain maps for AA5083 alloys sheet showing the persistence of random grain to grain disorientation distributions and limited grain growth during straining under GBS conditions (a) ad (b), while (c) and (d) shown the development of low angle boundaries and grain elongation taking place with SD contribute deformation [40].

An additional prove of lower formability of AA5083 alloy during the deformation mechanism of GBS, was found performing mechanical test in tension, in plane-strain bulging and in balanced biaxial bulging at temperatures and strain rates characteristic of QPF and SPF processes [42]. Figure 2.18 shows the FLD created with three points, calculated at temperatures of 450 °C and 500 °C and with the strain rates typical of SD deformation mechanism, $3 \cdot 10^{-2}$ s^{-1}, and of GBS deformation mechanism, $3 \cdot 10^{-4}$ s^{-1}. Results, confirmed that limits for deformation under SD creep were higher compared of those for deformation under GBS creep associated with more rapid cavitation evolution.

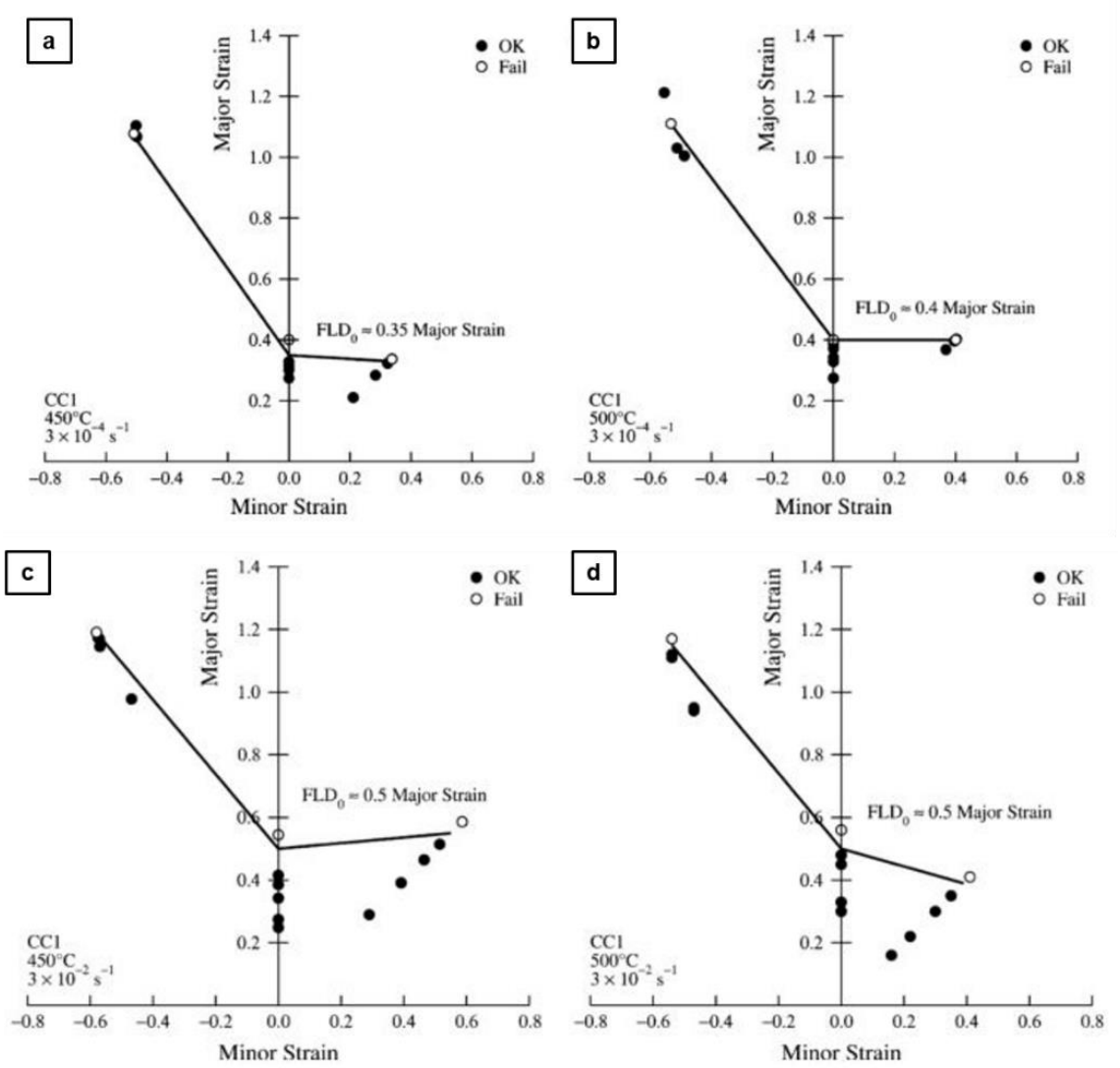

Figure 2.18: Rupture-based forming limit diagrams are shown for AA5083 material at a strain rate of $3{\cdot}10^{-4}$ s^{-1} and temperatures of (a) 450 °C and (b) 500 °C, and at a strain rate of $3{\cdot}10^{-2}$ s^{-1} and temperatures of (c) 450 °C and (d) 500 °C [42].

2.2.4 Innovative aluminium sheet forming process

In the last years innovative process solutions have been investigated in order to increase the forming productivity and reduce some of the drawbacks, such as the high percentage metal sheet thinning and the high process time cycle, of SPF and QPF. One of the applications was the combination of hot drawing with conventional SPF, in forming of a vehicle dash panel [43,44]. The process called hot draw mechanical pre-forming (HDMP) is represented in Figure 2.19 and showed interesting results in terms of increase of strain rate reducing on ten time compared to the SPF cycle process, moreover proved to preserve a good thickness distribution on the shaped part and its applicability to materials without superplastic characteristics.

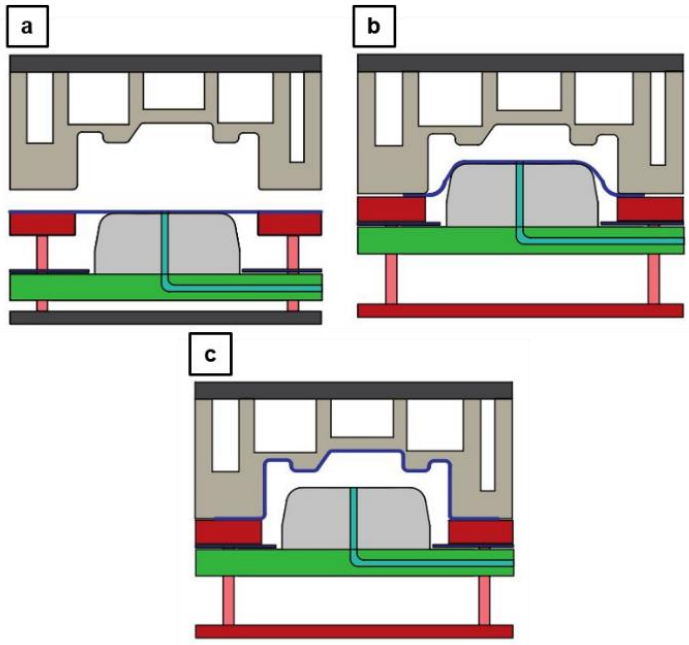

Figure 2.19: Schematic of the hot draw mechanical pre-forming process where (a) the sheet is first loaded into the die set, (b) a drawing stage pre-forms the panel and (c) a gas forming stage completes the forming operation [43].

In this type of process, where a punch is adopted, an important role is due to the friction behaviour between punch and metal sheet. For this reason, the influence of friction coefficient on microstructure and stress distribution on the final parts, were investigated [45], as also the influence of punch geometry on material formability [46]. Moreover, studies on process parameter referring to temperature and strain rate have proved that for a typical superplastic aluminium alloy AA5083, but without superplastic characteristics, a temperature of 400 °C was sufficient to shape completely a complex part in 8 minutes, with 92 % of material deformation and only 54 % as maximum thickness reduction [47].

Another innovative forming process on aluminium alloys sheets was introduced by J. Lin et al. which tried to shape 6xxx series using the hot stamping technology [48,49]. As described in section 2.1, Al-Si-Mg is a heat treatable aluminium alloy series, which exhibits an increase of ductility from the solution heat treatment (SHT), so in T4 condition, while the strength is obtained from the aging process (T6 condition) [40]. he idea was to take advantage from the SHT, which guarantees on the material a uniform distribution of alloying elements through the dissolution of Mg2Si precipitates, for a stamping force reduction and material ductility increment [51]. Successively, to perform the stamping operation using cooled dies for quenching directly the aluminium stamped part, avoiding thermal distortions (very relevant in aluminium), avoiding the formation of coarse β phase. Thus, a possible process cycle of the Hot Stamping of aluminium alloys is shown in Figure 2.20 [52].

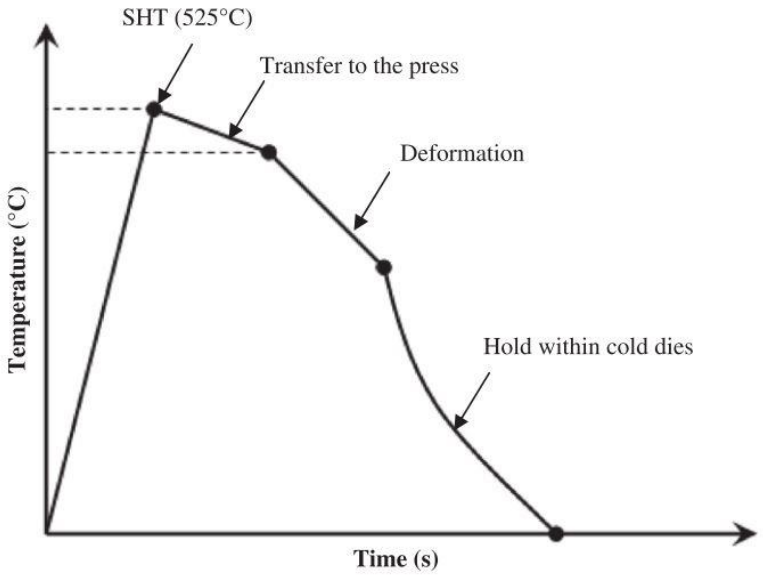

Figure 2.20: Possible hot stamping process for an AA6xxx aluminium alloy.

Deeper considerations on this innovative process concept are needed, due to the high process temperature and the high thermal conductivity of the aluminium that generates sheet temperature dropping during contact with cold dies [53]. Studies were conducted on the influence of different die temperatures on the final part strengthening, evaluating the possibility to use warm die at 350 °C [54] avoiding water cooling. Results exhibited that the higher the temperature, the lower the final part hardness, especially over 250 °C, Figure 2.21.

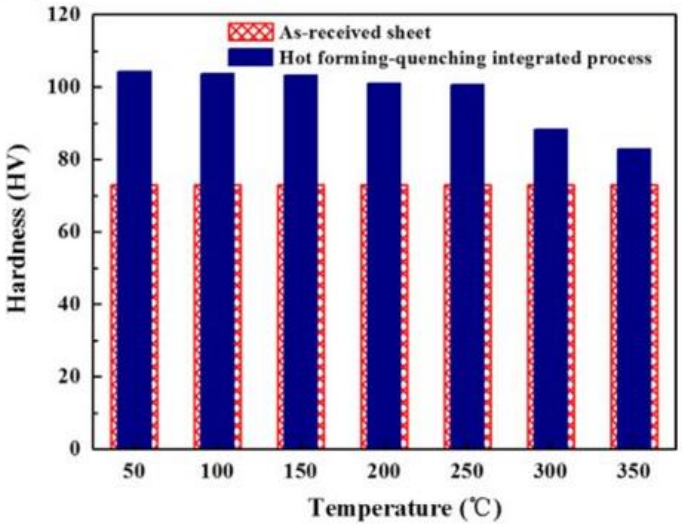

Figure 2.21: Dependence of Vickers hardness on forming-dies temperature in: during an hot forming-quenching integrated process [54].

So, with this technology, the quenching sensitivity shows to be a critical aspect, as for Hot Stamping of boron steel, in fact the cooling ability of cold-dies was proved to be crucial to determine final strengthening.

One of the recent research works were focused on measuring of the heat transfer coefficient during HS with an innovative equipment able to consider also the effect of contact

pressure between the forming tool and the aluminium alloy used as material for prototype validation [55].

Moreover also the solution time, solution temperature and final aging parameter, have exhibited a key role on the final mechanical properties as strength and hardness [56]. Using this new approach, the Hot Stamping process on aluminium alloys sheets, a new evaluation of fracture morphology, void nucleation and microstructure evolution, need to be performed considering the high strain rate characteristic of HS application [56]. In doing so only two complete studies were conducted on aluminium alloy formability subjected to the Forming and cold-die Quenching (HFQ) process, in detail a research work on AA2024 series [57] and another on a AA6082 series [58], finding the best forming parameters related to temperature, punch velocity and evaluating also the microstructure characteristics after forming operation and the fracture morphology.

2.3. Tube forming processes at high temperature

Not only metal sheets, but also hollow components can be shaped in forming operations to create simple or complex shapes using die cavities. In this section the technology of Hydroforming process and its development over the years are described focusing principally on the recent warm hydroforming. Successively, the literature review on the innovative Hot Metal Gas Forming process was analysed in detail from the preliminary studies until the recent process evolutions.

2.3.1 Hydroforming process

Nowadays the main industrial process to form closed sections is the tube hydroforming, which uses internal hydraulic pressure to bulge-up tube closed inside a matrix. This technology is not so recently in fact, already before World War II liquid was used as soft punch to create complex geometries, thanks to the hydrostatic pressure benefits on material formability, becoming very used especially for automotive components and aerospace industry.

Hydroforming can be divided in three branches: Shell hydroforming, Sheet hydroforming (SHF) and Tube hydroforming (THF), [59]. The first one developed by Prof. Z.R. Wang in 1985 at Harbin Institute of Technology in China, used water in pressure to create from cylindrical shell, water tanks, LPG tanks or building decorations [60], Figure 2.22 (a). The second one, that reached the research peak from the beginning of the 1990s, uses liquid instead of or coupled with a punch, to improve sheet formability increasing the limit draw ratio (LDR) and enhancing the surface quality [61], Figure 2.22 (b). Shell hydroforming, is usable on all of materials used for cold forming as stainless steel, carbon steel, high strength steel but also on light alloys like aluminium or magnesium, obviously reducing pressure used from 200 MPa usually applied on steel sheets, to 30 MPa for aluminium foils [62].

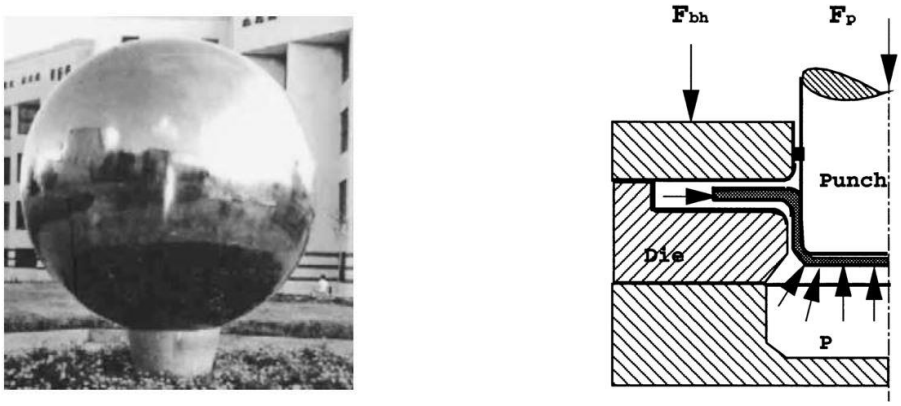

Figure 2.22: Image of a spherical vessel produced through shell hydroforming (a) [60] and schematic representation of a sheet hydroforming process (b) [61].

Tube Hydroforming, instead, used seamless or welded tube, to give to the final part, many advantages as part consolidation, weight reduction, improved strength and stiffness, highly accurate dimensions and less springback [63,64].

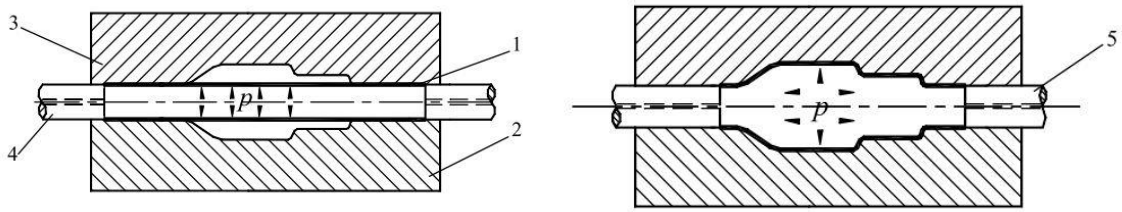

Figure 2.23: Representation of a tube hydroforming process, 1-tube, 2-lower die, 3-upper die, 4-5-axial punch [59] .

Compared to the SHF, the THF uses higher internal pressure in the range from 400 MPa to 600 MPa with peaks of 1000 MPa for high strength materials as Inconel. Thus, a THF implant needs elevated tons presses to clamp the dies during the fluid injection. Normally, the ability of the industrial equipment used in the hydroforming production line ranges from 20000 kN to 120000 kN. Figure 2.24, shows a schematic representation of a hydroforming press. To save energy as much as possible and to shorten the cycle time of the whole process, many development techniques were studied and applied in hydroforming equipment design [65].

As example, one group led by Wang et al. studied and developed an innovative high pressure forming apparatus, based on a double-action press. Maximum clamping force reached of 10000 kN, with supported internal pressure of 400 MPa, was designed. Moreover, a pressure control able to operate using range from 0–150 MPa or 150–400 MPa was developed in order to meet the needs of forming different materials [66].

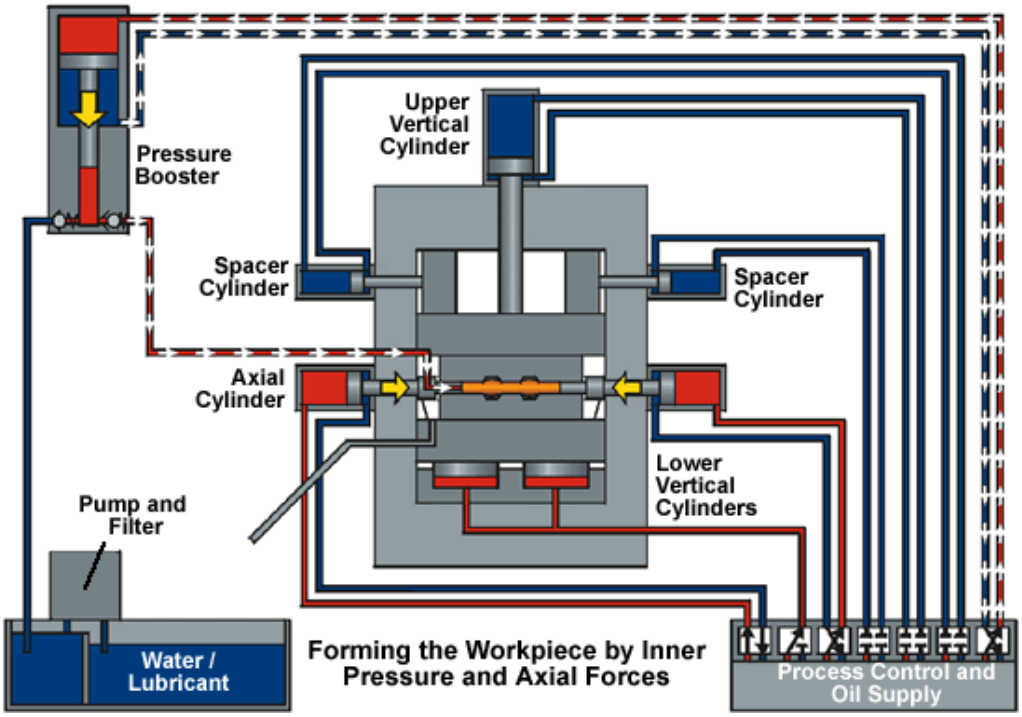

Figure 2.24: Schematic representation of an industrial tube hydroforming implant of the 35000 kN clamping device installed at the Institute for Metal Forming Technology (IFU) of the University of Stuttgart [67].

Regarding the automotive sector that represents one of the main application field of tube hydroforming, process advantages are connected to the considerable mass saving. In fact, lightweight components can be obtained not only using light materials but also through the elimination of the support flanges required for welding, or using thinner steel. In spite of that, the component stiffness is still maintained while the discontinuous spot-welded joints can be eliminated [68–70]. For example, the tubes hydroformed can be used to produce bumper supports that have the purpose to collapse and transmit the impact force to the front frames. Indeed, nowadays, many conventional bumper structures are assembled from several parts, Figure 2.25 (a), thus, several manufacturing processing steps are needed, with the result of somewhat complex [71,72]. Hydroformed bumper supports, as shown in Figure 2.25 (b), are rather simple in the shape but their ability to absorb energy through plastic deformation is relatively high, Figure 2.25 (c) [73].

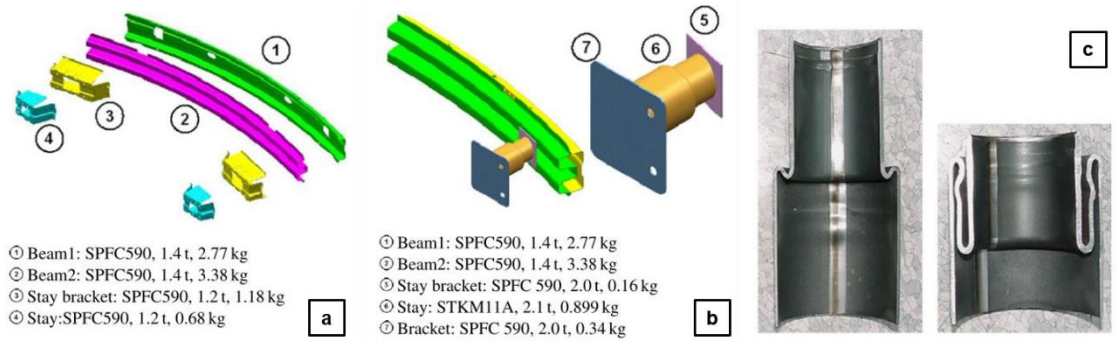

Figure 2.25: Bumper support structure produced through commonly assembled process (a) and through hydroforming process (b); bumper support functionality during crash test (c) [73].

Due its potentiality, many studies were conducted on tube hydroforming technology with the aim to improve the process stability and to reduce the process cycle. Shirayori [74], studied the deformation behaviour of aluminium and copper tubes with thickness deviation in the circumferential direction, in order to obtain the effect of the initial blank errors on the final forming results. Therefore, free hydraulic bulging test were conducted giving the conclusion that the cross sectional shape of the bulged tube maintained its circular shape until just before tube bursting. Tendency that was found independently of the amount of the initial thickness deviation. Instead, tubes behaviour during the unconstrained expansion, depended strongly on the plastic flow, on the hardening properties, as well as on the local wall thickness. Thus, Shirayori found that the maximum expansion appears at where the initial thickness is the smallest, therefore, the minimum expansion appears at where the initial thickness is the greatest. Moreover, he proved that the degree of thickness deviation, increases as the tube expansion, as shown in Figure 2.26, and that the bursting position is near to the thinnest point along the axial centre of the bulged tube.

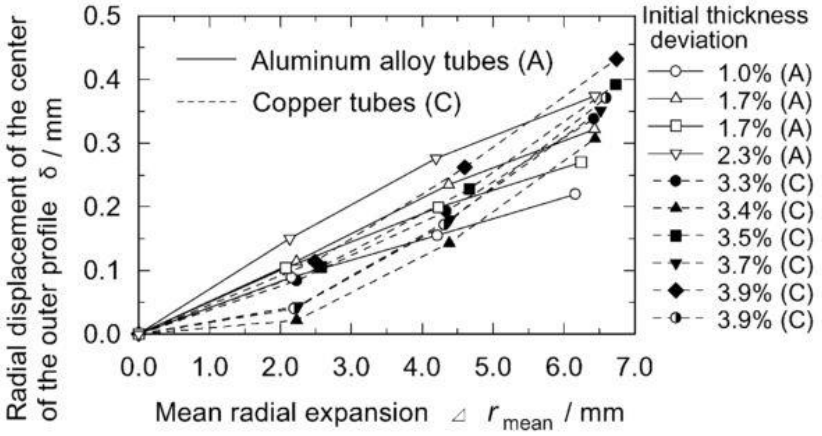

Figure 2.26: Radial displacement of the centre of the outer profile at the axial centre of aluminium and copper tubes [74].

Successively evaluating the material behaviour during free hydraulic bulging tests, S. Fuchizawa et al. studied the influence of strain hardening exponent on the deformation of thin walled tube subjected to hydrostatic external pressure [75]. The relation of strain hardening exponent on the tube deformation, has proved that when the n-value increases, the internal pressure needed for a certain dome height has to be increased. Later on, in another research work, he evaluated the influence of plastic anisotropy on deformation of thin-walled tubes in bulging forming [76], proving that the r-value in the longitudinal direction affects the maximum expansion ratio, while in the hoop direction affects the maximum internal pressure supported. Both researches were performed on an experimental apparatus in which one tube extremities was fixed while the other can moved freely along the longitudinal axis. Anyway, an axial feeding during the deformation step, has demonstrated to be necessary for process shaping using hollow matrix due to the presence of friction that has a key role on the parts realization. With this purpose, Schmoeckel et al. [77,78] designed a device to identify the different friction zones on a typical tube hydroforming process. Moreover, Vollertsen, developed a new measuring principle of the friction coefficient, COF, in the plastic forming location, based on tube upsetting. The author investigated also different tube materials, in

detail low carbon steel, high alloyed steel and aluminium alloy, bulged inside hardened tool steel covered with plasma nitriding or with a hard coating from combining PVD and CVD coatings [79]. Figure 2.27, highlights the problem concerning friction using aluminium tubes instead of steel materials tubes, but show also that COF can be reduced, and so comparable to that of steel, using nitride tools. An innovative tube hydroforming approach to reduce the friction effect, was proposed by Mori et al. in [80] which used an oscillating internal hydraulic pressure coupled with axial feeding, to deform aluminium tubes inside a die as shown in Figure 2.28.

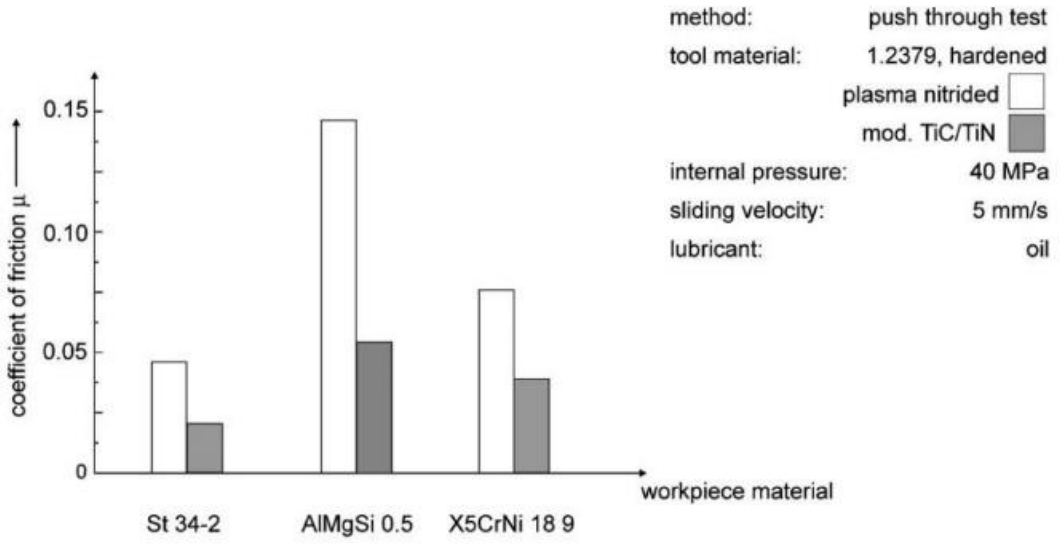

Figure 2.27: Results of COF for different tool coatings and tubes material [79].

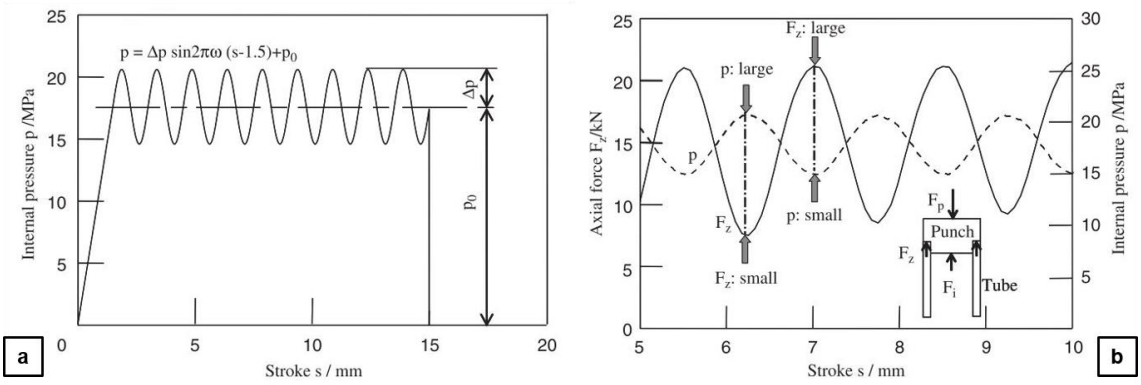

Figure 2.28: Oscillation of internal pressure in pulsating hydroforming of tube (a) and oscillation of axial force and internal pressure during pulsating hydroforming (b) [80].

Using this approach, at the moment of low internal pressure, the material is pushed in the deformed zone by axial feeding and wrinkling are induced. Subsequently at the moment of high internal pressure, the tube is bulged and the wrinkles become smoothed. Therefore, the author demonstrated that the defects of local thinning and so bursting of the tube can be prevented by oscillating pressure and axial feeding thanks to the sequential appearance and disappearance of small wrinkling. Figure 2.29 illustrates three specimens of a bulge test, conducted with oscillating pressure, as well as high and low constant pressure respectively. The image highlights the uniform expansion appearing in the pulsating hydroforming process that

is completely different from the round bulge in the conventional hydroforming processes where local thinning becomes with deformation.

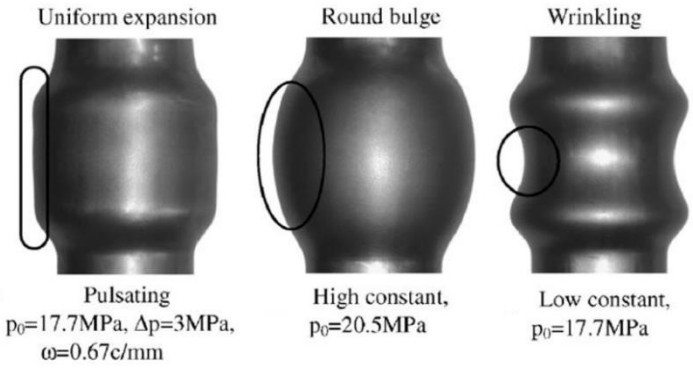

Figure 2.29. Hydroformed tubes obtained through experiment in three pressure paths.

Although the elevated advantages of this technology, hydroforming processes have shown several limitations with lightweight alloys, suffering their reduced formability. Therefore, to improve the formability of light alloys, warm media forming method was proposed in [81] proving that formability can increase using elevated temperatures. In [82] a drawing ration of 3.0 was reached for a metal sheet of AlMg0.4Si1.2 alloy in one pass at 250 °C, compared to room temperature test which reached LDR of 2.4. Results were obtained by heating die and blank holder during the process, and by cooling punch and die entrance radius to increase the transmittable drawing force. Moreover, in a study of Novotny [83] two different automotive aluminium alloy series, namely AA5182 and AA6016, were subjected to warm hydroforming, using a hot pressure fluid and rather cold tools. Results, proved that using 240 °C process temperature for the 6xxx series and 300 °C for the 5xxx series, both material exhibit a significant drop in flow stress and at the same time a rising fracture strain especially for the AA5182. Successively many other authors investigated the formability increment with temperature coupled with hydrostatic pressure, studying in detail their influence on aluminium alloys tube hydroforming. In the Keigler and Harrison study [84], a cycle time around 2 min was used to shape completely a component of AA5182 with the limit on strain rate fixed to avoid a material formability decrement. Therefore, a pressure of 55 bar was used to bulge up aluminium tube inside the die kept closed with a required load of 25 tons. On the contrary, using cold hydroforming, not subjected to strain rate influence, cycle times of 30 seconds are usually used nowadays to shape hollow component using liquid pressure up to 1500 bar depending on tube material.

With the years, the innovative technologies, have also allowed a better monitoring of raw tube and of the final part, aiding to understand better the material behaviour during the process. As example, through an optical measure system is now possible to evaluate the geometric properties and the quality of the tubular semi-finished product before and after the deformation. Indeed, often, supplied tubes, differ from each other [85] and need to be controlled before starting the deformation. On the other hand, during the process, optical measure system, can provide information such as the maximum attainable circumferential expansion and the initial yield stress of tubes and can also be used to identify the effect of parameters such as wall thickness or hardening distribution into the tube's expansion behaviour. In addition, optical measurements can be used to compare results outcome from

different process parameters in terms of temperature and pressure, as done by S. Yuan [86]. His study has proved that to evaluate the tube formability in a better way than the conventional testing methods usually used to investigate the state of stress and strain, (tensile tests or forming limit diagrams), the anisotropy of the tube, the stress state and the non-uniform distribution of thickness should be taken into account together. So optical measure systems coupled with bulged test in free air can be the correct solution for obtaining more realistic formability results.

Anyway, warm hydroforming has a restriction. Nowadays the maximum temperature usable on aluminium and magnesium alloys (tubes and sheets) is about 300 °C, due to the absence of appropriate fluid media which can work effectively at higher temperature. Therefore, one of the main disadvantages of this process is the limited temperature usable. Indeed, emulsion based on water and oil mixture can reached boil or burn temperature with possible critical condition for the operator. Furthermore, tube hydroforming, is generally slow, 30 to 50 sec/part, without considering setup operations, mostly due to the time required to the fluid to fill in and empty the dies. The technology presents also high investment costs associated with: (i) hydraulic press, (ii) pumping implant for the fluids and (iii) high resistance tools. Moreover, with complex parts, can generate undesirable strain in the material at uncontrolled locations, thus achievable shapes are restrictive especially for light alloys as aluminium and limited with the material behaviour at low temperatures. Even with these restrictions, in industrial field, especially in original-equipment-manufacturer (OEM), have been found many applications for the hydroformed tubular sections and especially during the last ten years, have been designed several components thinking to the Hydroforming as the best tubular manufacturing shaping process [87].

2.3.2 Hot Metal Gas Forming process

The overcoming of Hydroforming problems can be represented by the recently developed Hot Metal Gas Forming process, in which pressurized gas is used instead of fluids to deform a metal blank that is preliminarily heated in furnace. Fukuchi at al. carried out several studies concerning the concept and the equipment design of hot gas forming [88]. It is worth noticing that HMGF was not designed to replace Hydroforming, but was originally conceived as a low cost alternative. Therefore, the main technology knowledges were derived directly from hydroforming previous studies. Afterward the Fukuchi studies, Y. Liu et al. investigated the deformation behaviour of tubes subjected to the gas forming process proving that the steady-state creep equation commonly used in the analysis of superplastic forming or other elevated temperature forming processes, can not be applied to the Hot Metal Gas Forming of tubes. In fact, during the process, the effective stress increases as tube diameter expands and wall thickness decreases so, a steady-state creep condition does not exist [89]. In this research work, the author presented some experimental results on transient creep behaviour of a magnesium alloy, and provided an analysis on transient creep behaviour and its application in tube forming mechanics verifying that non-steady-state creep plays important role in the gas tube forming process at elevated temperatures, especially when the strain rate is high.
Successively, the author developed a new experimental set-up for tube gas forming process at elevated temperature [90]. In this research work, as-received magnesium alloy tubes with

42.4 mm in diameter and 2 mm in wall thickness, were bulged up using a tube biaxial formability test described in [91]. During the test, the tube specimen was rapidly heated to the desired temperature in about 100 s using an induction-heating unit. The maximum temperature reached at centre of the tube, location (A) in Figure 2.30, was 410 °C and was measured through a K-thermocouple. The specimen true strain was evaluated measuring the pre-etched circles grid on the tube before and after deformation, finding a maximum as 0.35 in location A. The average strain rate was calculated as 0.005/s by dividing the total effective strain by the total forming time. The effective true strain in location B was measured as 0.14 in the same way as sample A at about 200 °C, while location C represents the non-deformed state of the Mg alloy tube.

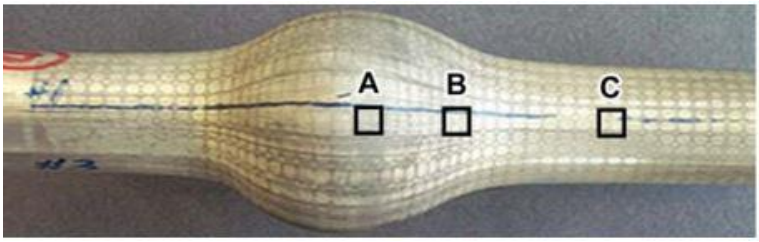

Figure 2.30: AZ31 Magnesium alloy tube after hot metal gas forming [90].

In 2009, Mori's research group developed a hot gas bulging process of an aluminium alloy tubes using resistance heating [92]. In the experimental apparatus the tube was rapidly heated by the electric current to increase the formability and to decrease its flow stress. Tube extremities were distance 150 mm in length and were clamped with copper electrodes split in half. The air inside the tube was sealed before starting the resistance heating using a constant and direct current power supply. Moreover an axial feeding on both the extremities was applied during the heating. A schematic representation of the designed apparatus is reported in Figure 2.31.

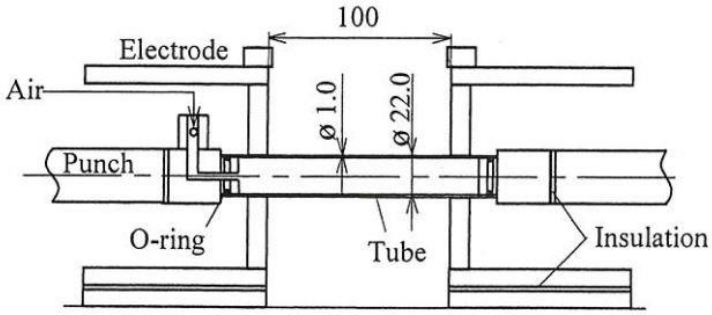

Figure 2.31: Hot gas bulging process of aluminium alloy tube using resistance heating [92].

Electric current in the range from 2500 A to 6000 A was applied for heating sealed tube with initial pressure in the range from 2 bar to 8 bar, while an axial feeding rate from 0 to 40 mm/s and for 30 % of tube length was varied in order to understand the influences of process parameters on tube formability. During test, temperature was measured through a termocamera after covering tube surface with graphite. Therefore, tube was expanded without a control of internal pressure observing that tube continues to expand even after stopping both axial feeding and resistance heating, due to the decrease in flow stress. Results obtained for different initial pressure values and current of 2500 A are shown in Figure 2.32.

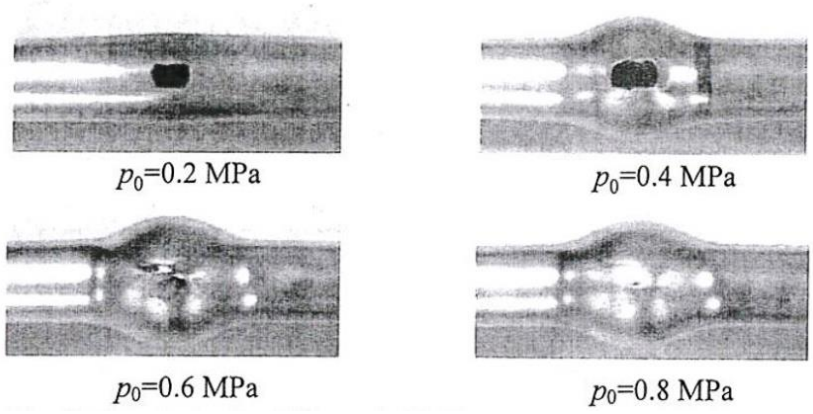

Figure 2.32: Burst tube for different initial internal pressures and electric current of 2500 A [92].

Moreover in this study it was measured the relation between pressure applied and forming time until tube bursting for fixed value of current as reported in diagram of Figure 2.33 (a). In addition, the tube thermal distributions during heating phases, due to the heat transfer from the tube centre to the copper electrodes was evaluated, proving that a ring inserted between tube and electrode created in stainless steel material, that presents a low thermal conductivity and a high electrical resistance, prevents an high temperature drop near tube extremities, as shown in Figure 2.33 (b).

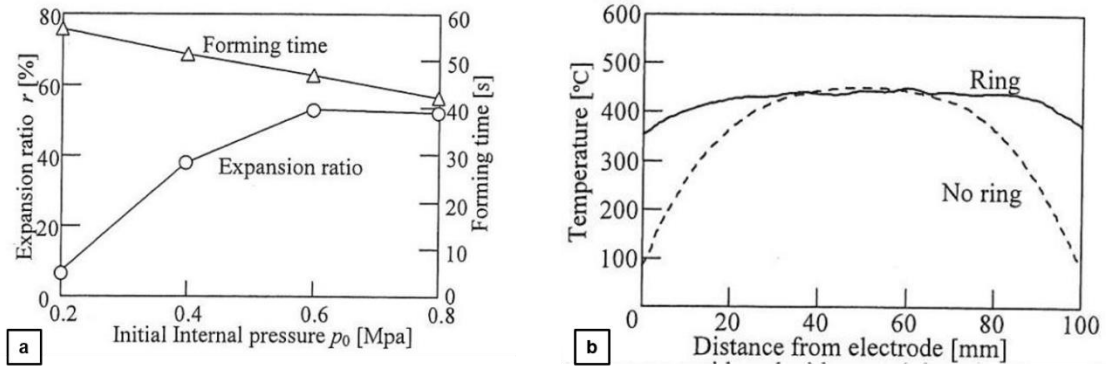

Figure 2.33: Relation between expansion ratio and electric current applied for an initial internal pressure of 0.8 bar (a), and temperature distribution along tube with and without stainless ring (b) [92].

Through this machine setup, crack appeared larger near the central region than using only copper material, increasing the aluminium formability so, tube expansion ratio, Figure 2.1. Due to this result, an equipped and process improvement was proposed from the same authors in [93].

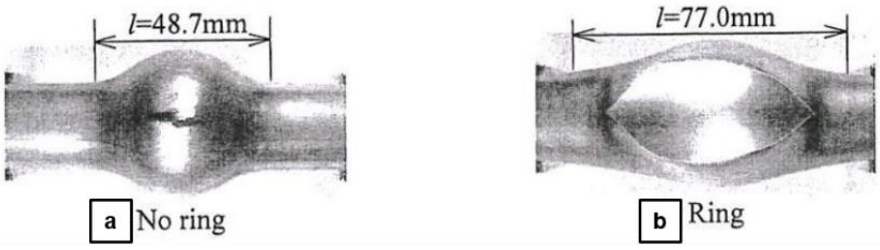

Figure 2.34: Burst tube with (a) and without (b) stainless ring using an electric current of 5000 A and an internal sealed pressure of 0.8 MPa [92].

Successively, the author investigated the possibility of bulging an aluminium AA6063 alloy tube with and without an axial feeding inside a die at room temperature [93]. In this case, process temperature was controlled applying a constant value of current intensity for a prearranged time, and measured with a thermocamera through a heatproof glass. Early, tube mechanical properties were measured using hot tube tensile test, finding the high influence of temperature and strain rate on material strength, as reported in Figure 2.35.

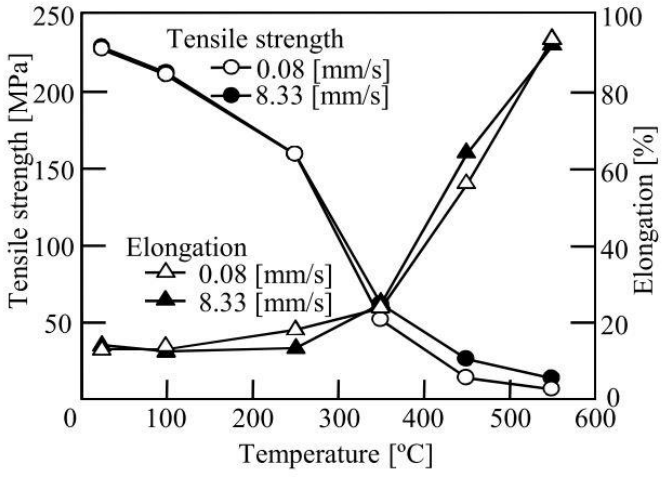

Figure 2.35: Variation in tensile strength and elongation with heating temperature obtained from tensile test of AA6063 tube [93].

In hot gas bulging test inside a die the process adopted from Mori, was reported in Figure 2.36 (b), while the apparatus scheme modified compared to that presented in Figure 2.31, is reported in Figure 2.36 (a).

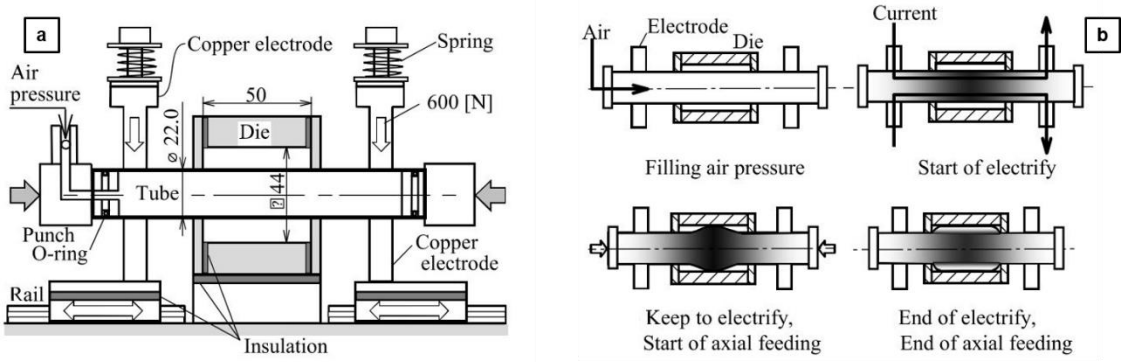

Figure 2.36: Experimental apparatus for hot gas bulging aluminium alloy tube (a), and sequence of HMGF process using pressure sealed air and resistance heating (b) [94].

During bulge operation, the electric current was kept along the tube section and the expansion was assisted through axial feeding. Copper electrodes were closed with two spring applying a 600 N in load, while the internal die diameter was 44 mm with a length of 50 mm. Therefore, an increase on diameter of 100% was required for a complete die filling. Owing to the heating, the tube was expanded by decreasing the flow stress of the tube and by increasing the internal pressure due to the thermal expansion of air sealed in the tube. In doing so, a sealed air pressure variable from 10 bar to 20 bar was applied on tube with thickness of 1 mm using process parameters reported in Table 2.2.

Table 2.2: Process parameter used for the HMGF operation [93].

Wall thickness [mm]	1.0
Pressure of sealed air [MPa]	1.0 – 2.0
Current density [A/mm^2]	61 - 121
Velocity of axial feeding [mm/s]	0 – 30
Amount of axial feeding [mm]	0 – 20

Tests results of the hot gas bulging operation without axial feeding are shown in Figure 2.37 highlighting the quality of the bulged tubes.

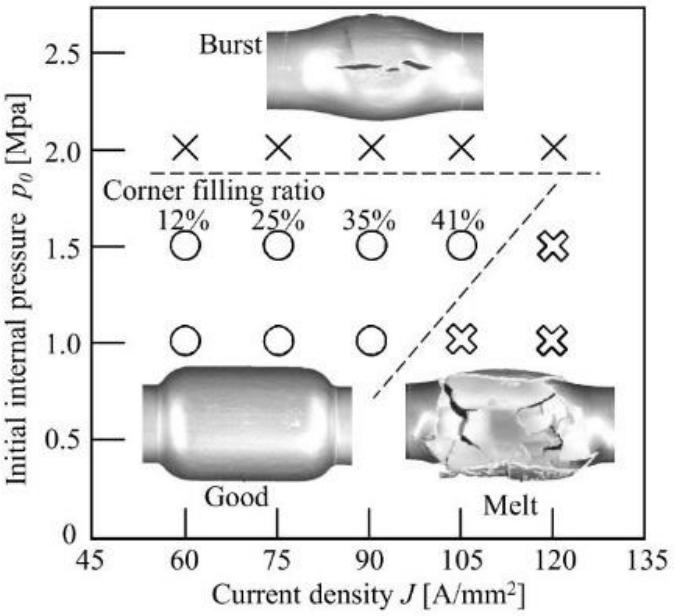

Figure 2.37: Forming range and corner filling ratio in hot gas die bulging without axial feeding for different current densities and initial internal pressures [93].

Therefore, when the initial internal pressure was too large, the bursting occurred, and the tubes become melted by excessive current density.

The best corner filling ratio was found using 106 A/mm2 and an initial sealed pressure of 1.5 MPa. Thus, these parameters were applied for successive forming operations used to investigate the influence of the axial feeding and the feeding rate. Results, demonstrated that more the amount of axial feeding and the feeding velocity are large, more the wrinkling occurred, while folding, occurred for large amount of axial feeding and small feeding velocity. An axial feeding of 20 mm/s was proved to be the optimum, Figure 2.38.

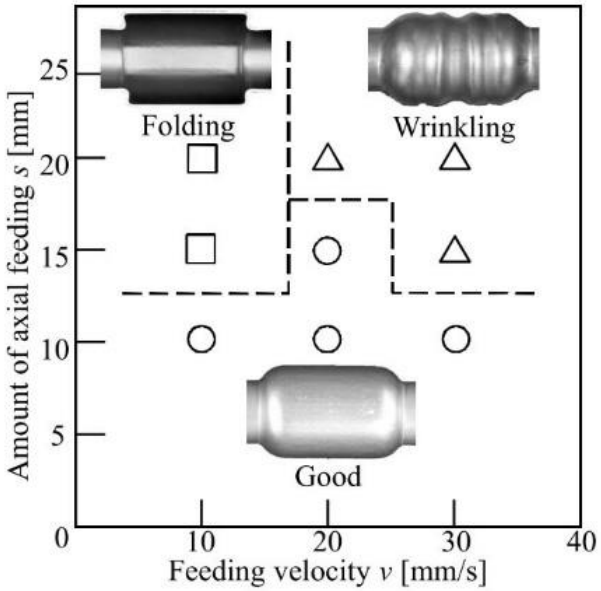

Figure 2.38: Effects of amount of axial feeding and feeding velocity on forming shape of tube [93].

Further optimizations of the same process were then evaluated from the same Authors in [94], where the effect of the initial wall tubes thickness on bulging AA6063 aluminium alloy tubes inside a die at room temperature was investigated. In this case, process parameters used are reported in Table 2.3 respectively for tube with thickness of 1 mm and 2 mm:

Table 2.3: Process parameter used for the HMGF operation [94].

Wall thickness [mm]	1.0	2.0
Pressure of sealed air [MPa]	1.0	2.0
Current density [A/mm^2]	80	80
Heating time [s]	4.5 - 7.0	4.5 - 7.0
Velocity of axial feeding [mm/s]	0 – 40	0 – 40
Amount of axial feeding [mm]	0 – 20	0 - 20

In this research work, the measurement of the relation between the maximum expansion ratio and the initial wall thickness deviation, with and without the axial feeding, confirmed that as the initial deviation increases, the maximum expansion ratio decreases, in good relation with the experimental and theoretical works of Shirayori et al. and Groche et al. in hydroforming field [74,85].

Moreover the results in terms of axial feeding and axial feeding rate on the formed components, are reported in Figure 2.39 (a) and in Figure 2.39 (b), where was observed that small amount in axial feeding and velocity have brought tube bursting inside but also outside the die especially at lowest amount of feeding or for thicker tubes.

In addition, results obtained from tube with 2 mm in thickness showed the best die filling thanks to the lower temperature decrement exhibited when tube surface comes in contact with the die.

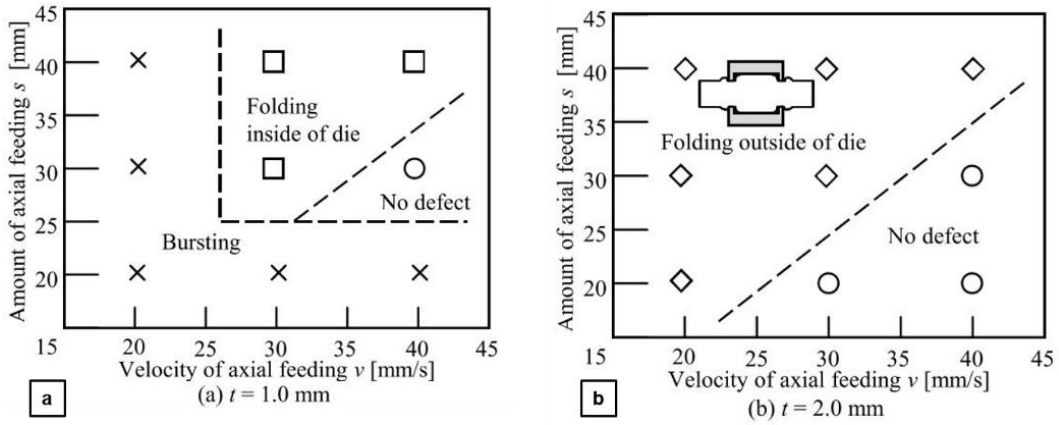

Figure 2.39: Effects of velocity of axial feeding and amount of axial feeding, on forming shape of tube with thickness of 1 mm (a) and 2 mm (b) [94].

To prevent, this phenomenon of temperature drop and consequent formability reduction, in [95] the authors, have proposed different dies with low thermal conductivity values as shown in Table 2.4.

Table 2.4: Thermal conductivity of die and used heating conditions [95].

Die material	Thermal conductivity of die [W/mK]	Heating condition	
		Current density [A/mm2]	Resistance heating time [s]
Mild steel: AA400	51.6	106	8.0
Stainless steel: SUS304 16.3	16.3	106	7.5
Ceramic: Photoveel	1.7	76	8.0

From the thermal and electrical properties of Table 2.4, stainless steel showed the lowest thermal conductivity while, using the ceramic dies, the amount of current density was reduced to prevent tube melting. The main results are reported in Figure 2.40 (a) that shows the increase in temperature with steel dies and ceramic die, and the achieved form filling accuracy respectively, Figure 2.40 (b). The study, demonstrated the remarkable increment of corner filling for the ceramic die compared to steels die due to the prevention of temperature drop. Anyway, although the formability was increased by using ceramic die, authors proved that is complicated to use ceramic dies on gas forming operation, due to their low toughness.

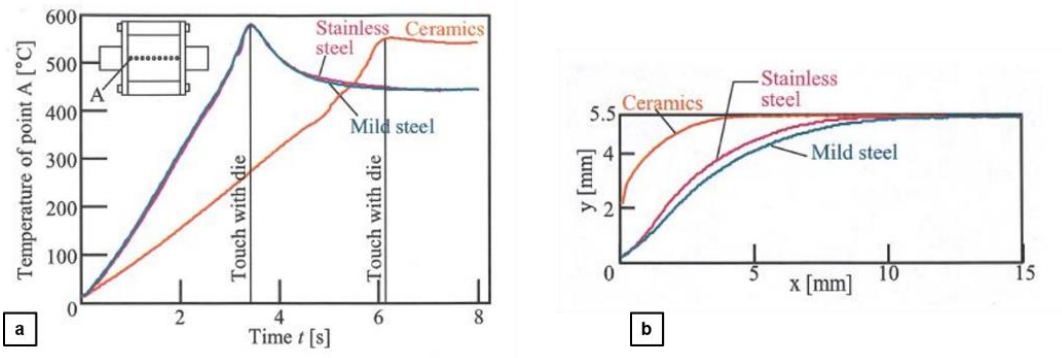

Figure 2.40: Variations of temperature of die corner using mild steel, stainless steel and ceramic dies (a) and corner filling using the three die materials [95].

For this reason, another possibility to avoid the fast reduction of the temperature was developed even in the stainless steel die, where, experiments showed that an increase in current density immediately after the first contact has a strong influence on the form filling. Figure 2.41 and Figure 2.41 show the current density path and the temperature distribution with and without current density rise immediately after the contact.

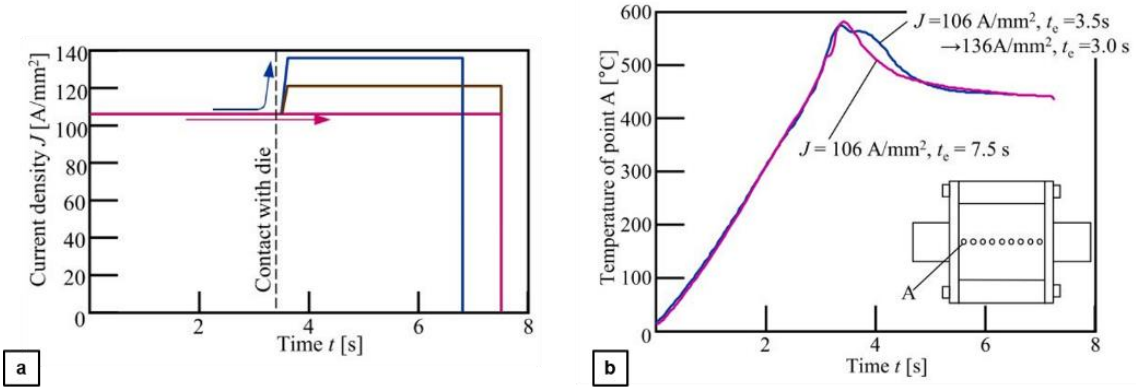

Figure 2.41: Path of current density and relative temperatures with and without increase after touch with die [95].

By the comparison of these temperature distributions, only a small difference was found. Indeed, the temperature drop occurred anyway, but, a small postponement of the application instant of the current increment, implicated a great impact on the flow stress and on the forming capabilities as illustrated in Figure 2.42.

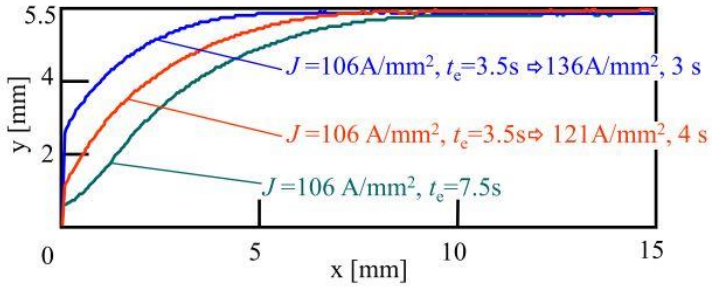

Figure 2.42: Effect of increase in current density after touch with die on deforming shape of tube using stainless steel die [95].

Therefore, Mori et al. research work proved that the filling ratios for the ceramic die and the stainless steel die are the same when the current density for the stainless steel die is doubled. The filling ratios of the die corner and the electrical energy used for resistance heating are shown in Figure 2.43. However, the stainless steel die was found to be the best for bulging operation, due to the low toughness of the ceramic die.

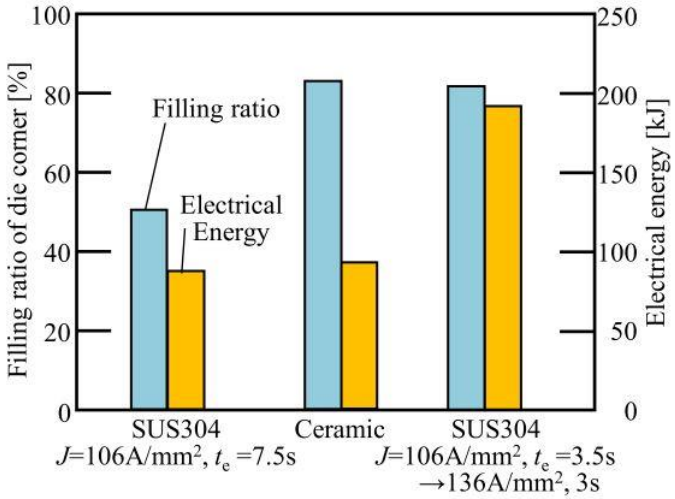

Figure 2.43: Filling ratios of die corner and electrical energy [95].

Another experimental apparatus for the HMGF process was proposed in He Zhu-Bin et al. research [96], where free bulging test were carried out at different temperatures ranging from 350 °C to 500 °C to evaluate the formability of AA6061 extruded tubes. In fact, hot tensile tests performed with samples obtained from tube components along the axial direction, can not reflect the real tube formability overcome through bulging deformation. Thus, bulging equipment was improved, Figure 2.44, in comparison to that of the first Mori et al. research work, including: warm die, heating rate control during the process, and moreover, applying the air in pressure successively to tube heating. Indeed, during the process, tube was placed in the dies and sealed by punches. The upper and lower dies were heated by resistance heating, which acted as heat maintainers to heat indirectly the tube. At the same time, the tube was heated directly by induction heating at the position where the deformation was needed. The temperature was controlled by PID regulator with accuracy of ±1.0 °C. Finally ,when the tube was heated to the target temperature, high pressure gas was introduced into the tube until bursting.

Figure 2.44: Experimental setup for hot metal gas forming of He Zhu-Bin et al. research [96].

In this study, the initial tube geometry presented 27.8 mm in external diameter and 1.8 mm in thickness while the length of free bulging zone was two times the external diameter of the tube. As expected, it was found that the amount of bursting pressure, decrease with the

temperature increase, as show in Figure 2.45 (a) qualitatively and in Figure 2.45 (b) for trend distribution.

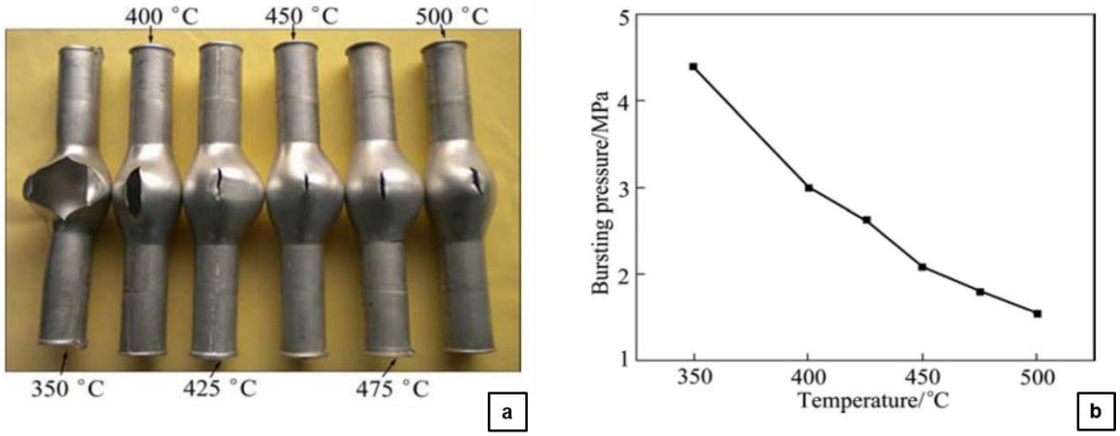

Figure 2.45: Workpieces obtained at different temperatures (a) and effect of temperature on bursting pressure (b) [96].

Moreover, even if the amount of expansion ratio increased with the temperature, this research work found that for aluminium alloy tested, an expansion ratio peak (of 86 %) was reached at around 425 °C. Indeed, a decreasing trend was found moving from 450 °C to 500 °C with a final value of 65 %, as reported in Figure 2.46

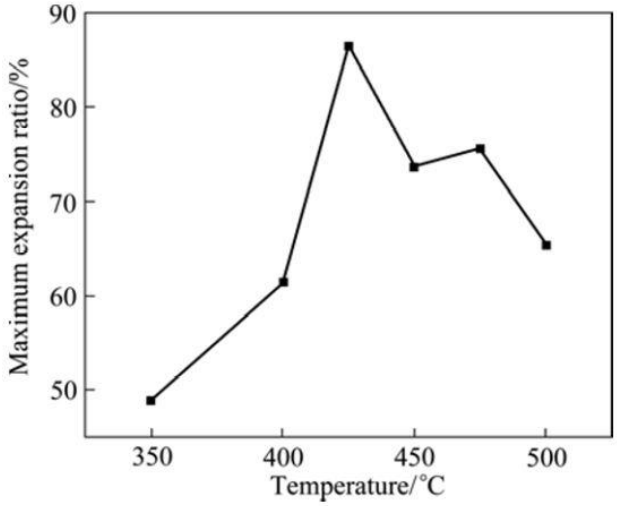

Figure 2.46: Effect of temperature on maximum expansion ratio [96].

Measures of post-forming properties exhibited hardness value highest in the location characterized of maximum deformation with value of 42.5 Vickers on test performed at 425 °C. Moreover, in this research the fracture morphology and microstructure after forming operation were also analysed. The fracture mechanism found was still the micro void aggregation typical of aluminium at elevated temperature, while regarding the microstructure, original equiaxed grain was found stretched in the deformation direction and grown obviously with increasing the temperature. Abnormal grain growing was also measured at 500 °C, with size more than 200 μm compared to the 30 μm grain size for the as-delivered tube condition.

The same author in [97] has performed free bulged tests through the HMGF process, to evaluate the formability of titanium alloy TA2 in annealed condition with 2 mm in thickness and external diameter of 30 mm. So, induction heating was used to bring the tube rapidly at target temperature in the location where free bulging happened, while infrared thermometer was used to measure the temperature. Figure 2.47, shows the sealing structure used, designed using inner set drawbar with polyurethane rings at tube extremities, screws at tube end, compression ring and nuts.

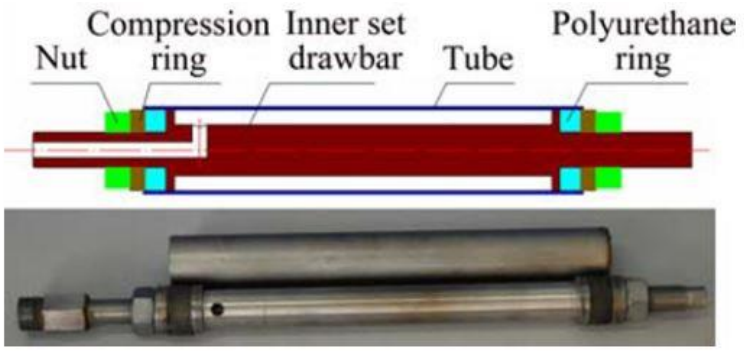

Figure 2.47: Sealing structure using inner set drawbar of tube end [97].

Tests results on titanium TA2 bulged tubes are shown in Figure 2.48 (a) comparing qualitatively workpieces achieved at different temperatures, while in Figure 2.48 (b) are shown the bursting pressures at different temperatures.

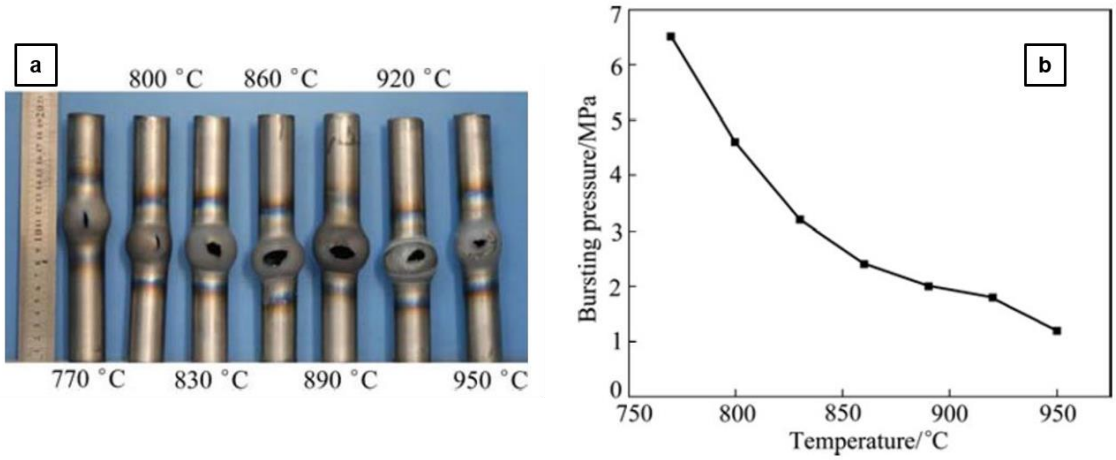

Figure 2.48: Workpieces obtained at different temperatures (a) and effect of temperature on bursting pressure (b) [97].

A comparison among all performed tests proved that the maximum expansion ratio increased with the temperature and reached the maximum value of about 70% at 890 °C, verifying that, the ideal temperature range for forming TA2 tubes through gas in pressure is from 860 °C to 920 °C. Another evaluation exhibited from this research was the difficult on using an induction heating system during bulging process. First, the induction coil needs to be accurately shaped so with the same distance among the spirals. Moreover, a spiral shape using equal diameter coil has proved to be a wrong choice considering the increment of tube diameter during the process, as shown in Figure 2.49. Thus, tube expansion resulted always

limited by coil diameter indeed, the lower the distance between generator (induction coil) and load (tube), the higher the temperature increment.

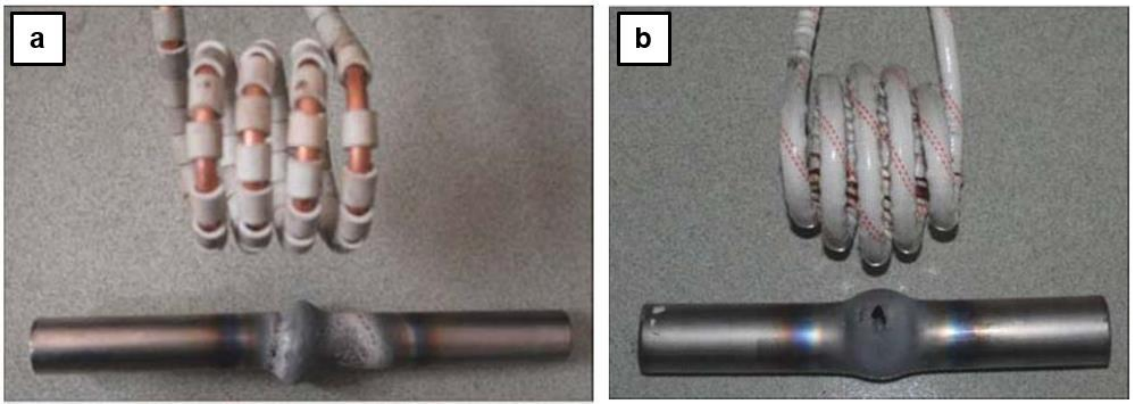

Figure 2.49: Heating effect of two different induction coils: (a) equal diameter coil; (b) variable diameter coil [97].

Recently, a different material was investigated in [98], where Mori et al. developed a new gas forming process of an ultra-high strength steel hollow parts. In this process concept, the tube was bulged by internal pressure of air with the decrease in flow stress of the heated tube without control of internal pressure during forming operation. Higher pressures and higher temperatures, were needed using ultra-high strength steel tubes instead of lightweight tubes as found in Zhou-Bin et al. research work on TA2 tubes. [97] and Vadillo et. Al. in [99,100]. Moreover, steel tubes processed at high temperature can generate oxidation mechanisms. Thus, this research work describes as V-shaped hollow parts were successfully formed by a shaped punch and successively quenched by pressurized air, avoiding the oxidation of the tubes outer surface forming the parts in a case filled with CO_2 gas. Table 2.5, reported the main process characteristics, while the scheme of the experimental apparatus is shown in Figure 2.50 (a) with also a particular of the cross-section of die in Figure 2.50 (b). As the other experimental apparatus used by the authors, tube was clamped between two copper electrodes under a load of 640 N generated by springs. Moreover, to preserve the electric heating of the tool, during heating phases punch and die were not in contact with tube.

Finally, as the previous experiments of the author, pressure was initially sealed inside tube and was not controlled during the forming operation.

Table 2.5: Process parameter used for gas forming of V-shaped hollow part [98].

Current density [A/mm^2]	33
Heating temperature of tube [°C] (Heating time [s])	800 (6.3) – 950 (7.5)
Initial internal air pressure [MPa]	0.0 – 2.5
Punch speed [mm/s]	80
Punch stroke [mm]	27
Reduction in internal volume of tube	20 % ; 60 %
Holding time at bottom dead centre [s]	0.1 - 60

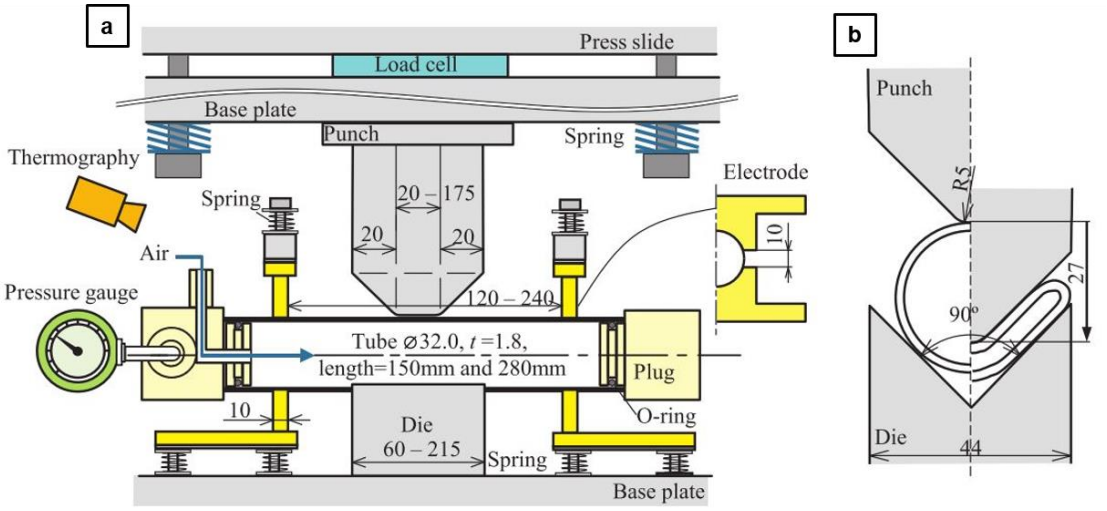

Figure 2.50: Representation of the experimental apparatus (a) and representation of the cross-section of die for HMGF of ultra-high strength steel hollow part using sealed tube and resistance heating [98].

Figure 2.51 shows the shaped tubes performed applying a tube internal volume reduction of 20% and a forming punch application of 60 seconds. In detail: Figure 2.51 (a) shows the case where heating temperature of 950 °C and initial internal air pressure of 0 MPa is not sufficient to put in contact the tube with the inclined portion of the punch; Figure 2.51 (b) represents test with heating temperature of 950 °C and initial internal air pressure of 1.5 MPa, while in Figure 2.51 (c) is possible to observe the result of an excessive internal pressure of 2.5 MPa. Finally Figure 2.51 (d) and Figure 2.51 (e) show the results for cold forming and furnace heating of a non-sealed tube reported as comparison.

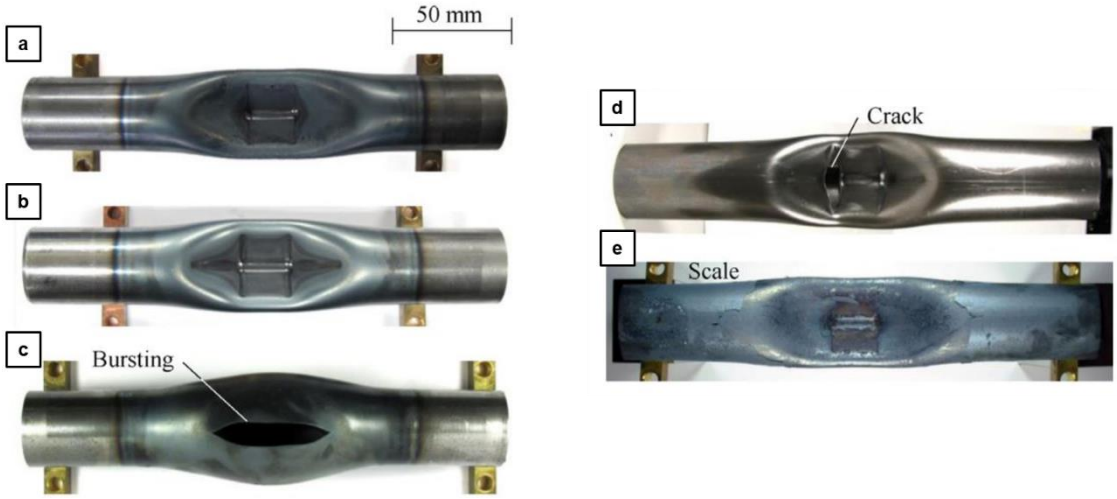

Figure 2.51: Formed v-tubes with different process parameters: temperature and internal pressure [98].

As found in the He Zhu-Bin et al. research [97], due to the high temperature of the process, the sealing o-rings reach melting temperature during the furnace heating causing a reduction of the internal pressure during the process and confirming that innovative sealing technologies need to be investigated for processes at very high temperatures. In forming operation through the punch, two important relations were found by the author. In detail (i) the higher the tube

temperature the lower the radius of die corner, as shown in Figure 2.52 (a) and (ii) the higher the holding time of punch the lower the cross-sectional shape as shown in Figure 2.52 (b).

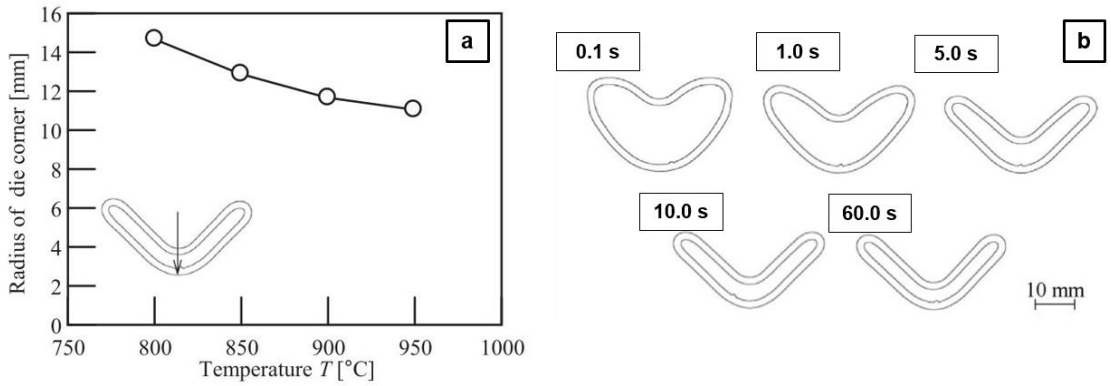

Figure 2.52: Relationship between radius of die corner at centre of formed tube and heating temperature for an internal pressure of 1.5 MPa a volume reduction of 20% and a holding time of punch of 60 seconds (a). Effect of holding time at bottom dead centre on cross-sectional shape for a temperature of 950 °C, an internal pressure of 1.5 MPa and a volume reduction of 20% (b) [98].

Moreover, due to the tube material characteristics, the increasing of strength of the formed tube was performed through cold blowing air during the holding time. As expected, the component hardness increased especially using longest cooling time. Considering instead the component appearance after quenching operation, the surface quality was not enough for painting. For this reason, in this study an oxidation prevention of the part was proposed by forming the component in a case filled with CO2 gas, as represented in Figure 2.53.

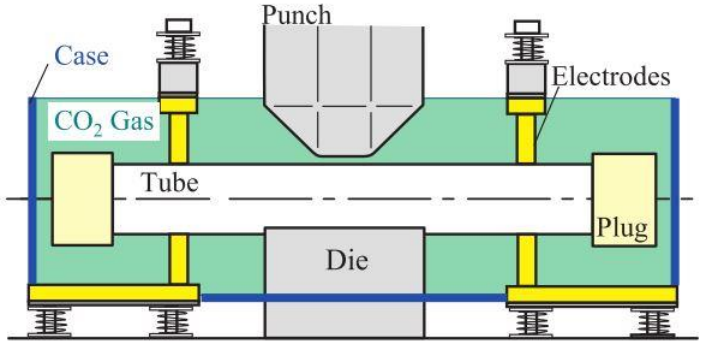

Figure 2.53: Prevention oxidation in gas forming of high strength steel by CO_2 gas [98].

Therefore, Hot Metal Gas Forming (HMGF), thanks to the first promising results in laboratory applications, is gaining larger interest and seems ready to be implemented in industrial applications.

2.4. Conclusions

Aluminium alloys are usually characterized by reduced formability at room temperature, so a number of scientific studies are nowadays focused on different means to enhance their formability limits. Temperature assisted processes have proved to increase aluminium formability, so innovative deformation techniques have been developed specifically for shaping aluminium at high temperature.

The process currently utilized in the automotive industry to produce small series parts dedicated to sports cars is the Superplastic Forming. However, it is conducted at temperatures higher than 450 °C and is too slow to be applied to mass production, since it involves strain rates lower than 10^{-3} s^{-1}. Moreover, the sheets must be provided in the so-called superplastic state: the grain size must be smaller than 10 μm, which further increases the production costs. Nevertheless, superplastic forming allows a drastic increase of the material formability and therefore the production of much more complicated shapes compared to the room temperature forming process. To overcome the drawbacks of the superplastic forming, in the last years, several investigations have explored the feasibility of deforming sheets at elevated temperature, but at higher strain rates compared to those typical of superplastic forming. Thus, Quick Plastic Forming, patented by General Motors, investigates range of strain rate between 10^{-3} s^{-1} and 10^{-1} s^{-1} and is based on a gas forming technology. The quick plastic forming can be conducted either on superplastic-type sheets or on conventional sheets and has proved to be effective in enhancing the material formability and can therefore represent a suitable alternative to superplastic forming. Another process variant that is now under investigation is represented by the hot stamping process, during which the blank is heated at elevated temperature and simultaneously formed and quenched inside cooled dies. Unlike the extensive literature existing on the HS technology applied to steel sheets (especially boron steel), at the time of these study, only a pioneering work on AA6082 material was published. Therefore, the applicability of the HS technology on the main aluminium alloys used in automotive sector needs to be deeply investigated to understand its real applicability of HS process for shaping quickly aluminium automotive components. With this purpose, a complete investigation aimed to obtain the best formability process parameters in terms of temperatures and strain rates applied on both heat treatable and non-heat treatable aluminium alloys, is needed. Moreover, nowadays, aluminium rheological characteristics at hot temperatures are confined to one-dimensional stress test without considering different strain paths that are indeed very important in sheet deformation. In addition, the validation of laboratory test results from studies on HS of aluminium alloys, on a full scale industrial blank subjected to different strain paths deformation during a stamping operation, is currently missing but is of primary importance to understand if really HS technology is suitable for aluminium sheets.

Considering aluminium alloys tubes formability, hydroforming is one of the most popular processes to obtain complex parts by using liquids as active part of the dies. In cold process very high pressures are required for shaping parts from hollow components and, moreover high tons presses are necessary to keep close dies during the forming operation. Considering also the poor formability that aluminium alloys exhibit at room temperature, warm hydroforming is nowadays the advanced process solution for shaping aluminium tube. Although attractive, the most relevant problems are related to the limited heating temperatures that the used fluids, namely water- or oil-based emulsions, can reach during the process. Furthermore, traditional hydroforming set-up are often characterized by a longer process-time compared to stamping processes, mostly due to the time required to the fluid to fill in and empty the dies. An innovative solution, could be replace liquid with gas in pressure, in the so-called Hot Metal Gas Forming process (HMGF), avoiding temperature limits, decreasing pressure needed for shaping parts and increasing the formability especially on lightweight alloys. Anyway, this technology is only under preliminary studies, and several aspects need to

be investigated before it reaches an industrial applicability. The tube heating technology of electrical resistance, seems to be the suitable choice for the process, but no investigation on electrical insulators in the tube-die interfaces, has been evaluated yet. A coupled control among current, temperature and inflation pressure during the deformation, is needed. Furthermore, the applicability of the process using only gas in pressure was applied only to rounded short components without investigating the feasibility on shaping sharp components, or creating parts starting from long tubes. Finally, the technology still needs to be tested in applications where different geometries have to be created simultaneously on the same component. In fact, nowadays using only gas in pressure without any other mechanical component, only simple round geometries were created.

Chapter 3

Approach

The main objective of this research is to study the formability of metal sheets and tubes made of aluminium alloys when shaped at high temperatures and high strain rates. Aluminium presents a limited deformability at room temperature that can be efficiently improved when heated at higher temperatures. Even though in recent years new forming processes have been developed to enhance aluminium workability, they are still affected by long process times. Moreover, forming processes as Super Plastic Forming and Quick Plastic Forming, require an accurate control of process parameters. In particular, they are very temperature sensitive and a stable deformation rate is not easy to achieve using high temperature gases acting as a soft punch. On the other hand, tube shaping performed through hydroforming or warm-hydroforming processes, presents restricted ranges of working temperature due to their use of water or oil-based liquids as forming media to shape components. For this reason, costly equipment designed for operating at high pressure are needed.

The work developed in this PhD thesis, aims to contribute at the innovation of Hot Stamping processes for the automotive industry towards their implementation on aluminium alloys sheets made of AA5083 and AA6016 alloys, rather than common high strength steels, by focusing on cycle time reduction. To deeply understand the deformation mechanism at high temperature and strain rate, a complete rheological characterization under different process parameters was performed, investigating also the influence of the as delivered condition for the AA5083 alloy (commercial annealed and with superplastic characteristics) and the influence of the applied solubilisation heat treatment on the AA6016 alloy. These characterizations were achieved by means of several analysis: microstructural analysis of the as-delivered and heat treated material, determination of the true stress-true strain curve through tensile testing, micro-hardness measurements, evaluation of the true strain at fracture, observation of microstructural features and of the fracture area. In this manner, an accurate definition of the

best formability window for each tested aluminium sheet, as a function of the forming temperature and the applied strain rate, was possible. Successively, different strain paths, typically employed in stamping process deformations, were investigated with an experimental apparatus capable to replicate the stamping conditions through the Nakajima test performed at high temperatures. In doing so, the Forming Limit Diagrams (FLDs) were carried out at elevated temperatures, measuring the deformation through a 3D optical measuring system, to confirm the formability data obtained from the hot tensile tests.

Finally, this comprehensive analysis on the workability of the investigated aluminium alloys allowed applying the laboratory test results on a real hot stamping plant. Thanks to a collaboration with an Italian company operating in the automotive field, under-cover-engine components made by the same aluminium alloys, were stamped just in one step by setting the forming parameters that manifested the best material workability.

With regard to the aluminium tube formability, the use of gas at elevated temperature in the recently so-called Hot Metal Gas Forming process (HMGF) has shown promising capabilities thanks to an enhanced formability of the material due to the high process temperatures, allowing the possibility to form parts with low pressures applied. Accordingly, after a literature review to analyse the existing experimental apparatus developed for implementing this technology, an experimental apparatus to evaluate the aluminium tubes formability and to perform the innovative Hot Metal Gas Forming process was designed. The mechanical parts and sub-systems composing the apparatus were designed according to the heating system chosen and the gas selected to deform the tube, improving the best features of the two already existing prototypes described in literature (Mori et al. and He et al.).

Electric current was used to heat up the aluminium tube rapidly, while cold air released with a pressure ranging from 1 to 20 bar, was exploited to inflate the hollow component. After the equipment assembling, a software was developed in LabVIEW® environment, for controlling and measuring the temperature and other important parameters during the process. The first tests on the prototype, were performed to understand the effects of the innovative heating technology applied to the process, afterwards the formability of aluminium alloy tubes AA6060 and AA6082 supplied with different extrusion parameters was analysed by using also an optical measuring system to evaluate their expansion in free air.

After these experimental attempts to acquire a knowhow on the technology, further tests were accomplished to shape hollow components with desired form by constraining the tubes to expand inside a die. The feasibility of HMGF process was evaluated performing the tests under different process parameters and by analysing the influence of different die materials on material formability, electrical insulation, surface quality and friction. Throughout all the tests, a particular attention was paid to the process time cycle concerning its industrial applicability, in order to reduce the part forming cycle as much as possible without compromising the final component.

Furthermore, the applicability of the developed HMGF experimental apparatus for shaping aluminium tubes was validated creating a complex aesthetic hollow geometry in collaboration with "Anodica Industries" company. Different tubes made of AA 6060-T5 aluminium alloy presenting different initial thickness equal to 1.5, 2 and 3 mm and a fixed external diameter equal to 20 mm, were bulged inside a die, evaluating the difficulties in creating wide and narrow convex and concave curves, and investigating the influence of

process parameters as temperature and pressure. The industrial case evidenced the capability of the experimental apparatus and the process potentiality, not only to satisfy the part feasibility, but even to guarantee an excellent aesthetic appearance after submitting the shaped tubes to an anodization chemical treatment.

Chapter 4

Hot stamping of aluminium alloy sheets

This chapter describes the experimental apparatus, the procedures and the results, of the investigation into the rheological behaviour of different aluminium alloys, namely commercial grade AA5083-O, AA5083 with superplastic characteristics and AA6016-T4. The aim is to identify which are the best forming parameters in order to deform these aluminium alloys at high temperature, increasing the formability, and with high strain rate decreasing the process cycle for a possible mass production.

Firstly, after a description of the main properties and characteristics of the investigated materials, the procedure used to analyse their microstructure is presented. A description of the laboratory equipment is given, followed by a description of the procedures used to investigate the rheological behaviour of the aluminium alloys. In this case, several tests were performed with different temperatures and strain rates for obtaining the true stress-true strain curves and the anisotropy.

After, all equipment for post-deformation investigations are presented, in detail: micro-hardness instrument and S.E.M. microscope used for the fracture surface observation and to measure the fracture area of each sample stretched in order to obtain the formability window of the materials studied. In addition, the Nakajima experimental apparatus is described, in addition to the procedure used to simulate mechanically an industrial stamping cycle on the commercial grade AA5083, in order to evaluate whether the best formability parameters, found through the mono-dimensional stress tests, can be employed to the three-dimensional stress tests.

Finally, industrial trials conducted on a real industrial hot stamping plant are reported, with the aim to verify the laboratory results; in particularly the temperature and the strain rate that guarantee the maximum formability for each aluminium alloy that is investigated.

4.1. Investigated materials

The two aluminium alloys series studied in this section are AA5083 supplied in annealed (commercial) condition and in superplastic condition so after a high grain refinement through cold rolling operations, and AA6016 in T4 condition (solution heat treated but not precipitation heat treated).

The chemical composition of AA5083 is reported in Table 4.1.

Table 4.1: Chemical composition of AA5083 used in this research work.

Si	Fe	Cu	Mn	Cr	Mg	Zn	Ti	Al
0.4	0.4	0.1	0.4-1.0	0.25	4.0-4.9	0.25	0.15	balance

Moreover, in annealed condition and superplastic condition, the materials exhibit mechanical characteristics as reported in Table 4.2, where is possible to appreciate the higher value of strength and hardness of the superplastic grade compared to the commercial one.

Table 4.2: Mechanical properties of AA5083 in different supplied condition used in this research work.

	AA5083-COM.	AA5083-SPF
Property	Value	
Yield stress [MPa]	163	378
Rupture stress [MPa]	338	462
A% (rupture)	23	7
Vickers hardness [HV]	85.22	130.60

The chemical composition of the AA6016-T4, is reported in Table 4.3, with mechanical properties showed in Table 4.4

Table 4.3: Chemical composition of AA6016-T4 used in this research work.

Si	Fe	Cu	Mn	Cr	Mg	Zn	Ti	Al
1.10	0.16	0.2	0.06	0.1	0.69	0.2	0.15	balance

Table 4.4: Mechanical properties of AA6016-T4, used in this research work.

Property	Value
Yield stress [MPa]	90
Rupture stress [MPa]	160

A% (rupture)	21
Vickers hardness [HV]	50

It worth noting that the lower values of strength in the 6xxx aluminium series compared to the 5xxx series, which have better formability characteristics for this material, at room temperature.

4.2. Thermal tests

Each aluminium alloy object in this investigation was previously analysed in its microstructure through optical observation of the grains size and conformation. The as-delivered condition was compared with samples subjected to several thermal cycles, in order to understand the microstructure behaviour of each aluminium alloy with the high temperature. In doing so, a piece of material with a dimension of 10 x 10 mm^2, was cut from each metal sheet, and prepared for the thermal cycle. Using a laboratory furnace, aluminium samples were heated up to the target temperature and held for 5 minutes for temperature homogenization. Subsequently, the sheet samples were water-quenched to preserve their microstructure for the optical observation. In Table 4.5, the different heating temperatures for each aluminium alloy are reported. Considering the heat treatable AA6016 alloy, an additional heating cycle was inserted, to investigate the temperature of the solubilisation thermal treatment, typical of this aluminium series. Specifically, a target heating temperature of 550 °C was reached and maintained for 5 minutes, which represents the time required to dissolve the Mg_2Si precipitates within the aluminium matrix.

Table 4.5: Thermal cycles of the aluminium alloys investigated.

Aluminium series	Target temperature [°C]	Soaking time [s]	Quench type
AA5083-O	20 ; 300 ; 400 ; 450 ; 500	300	water
AA5083-SPF	20 ; 300 ; 400 ; 450 ; 500	300	water
AA6016-T4	20 ; 300 ; 400 ; 450 ; 500 ; 550	300	water

After quenching, the specimens were prepared for metallographic analysis through mechanical polishing and finally, chemically etched using a solution of 15.5 ml HNO_3, 0.5 ml HF and 84 ml H_2O, namely Graff & Sargent solution, for 120 seconds. Moreover, to put in evidence the grain boundary, all the aluminium samples were kept in a controlled air hoven at a temperature of 120 °C for 24 hours, in order to oxidise the grain edge. It is worth noting that a temperature of 120 °C is not enough to generate any kind of material grains alteration, but it is very useful for the grain size observation on materials with high resistance corrosion property such as aluminium alloys. Figure 4.1 shows the differences among the three aluminium alloys in the as-delivered condition, while, Figure 4.2 shows the microstructural analysis performed after the thermal cycles application considering temperatures and time reported in Table 4.5.

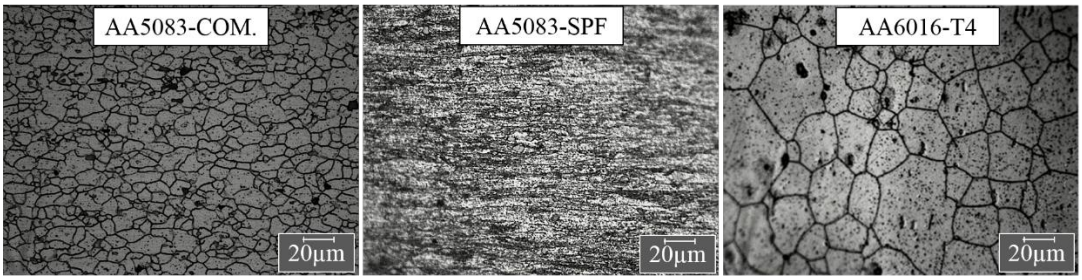

Figure 4.1: Microstructure of the aluminium alloys studied in the as-delivered condition.

In Figure 4.1, the AA5083-SPF exhibits a very thin grain structure, with a strong texture in the rolling direction, with an average dimension calculated in ≈ 4 μm. On the other hand, the AA5083-COM. shows an equiaxed, homogeneous microstructure with an average grain size of 15 μm, confirming that the material underwent complete recrystallization during the annealing after cold rolling. Finally the AA6016-T4 presents an average grain size of 50 μm with globular grain geometry and a homogeneous grain distribution.

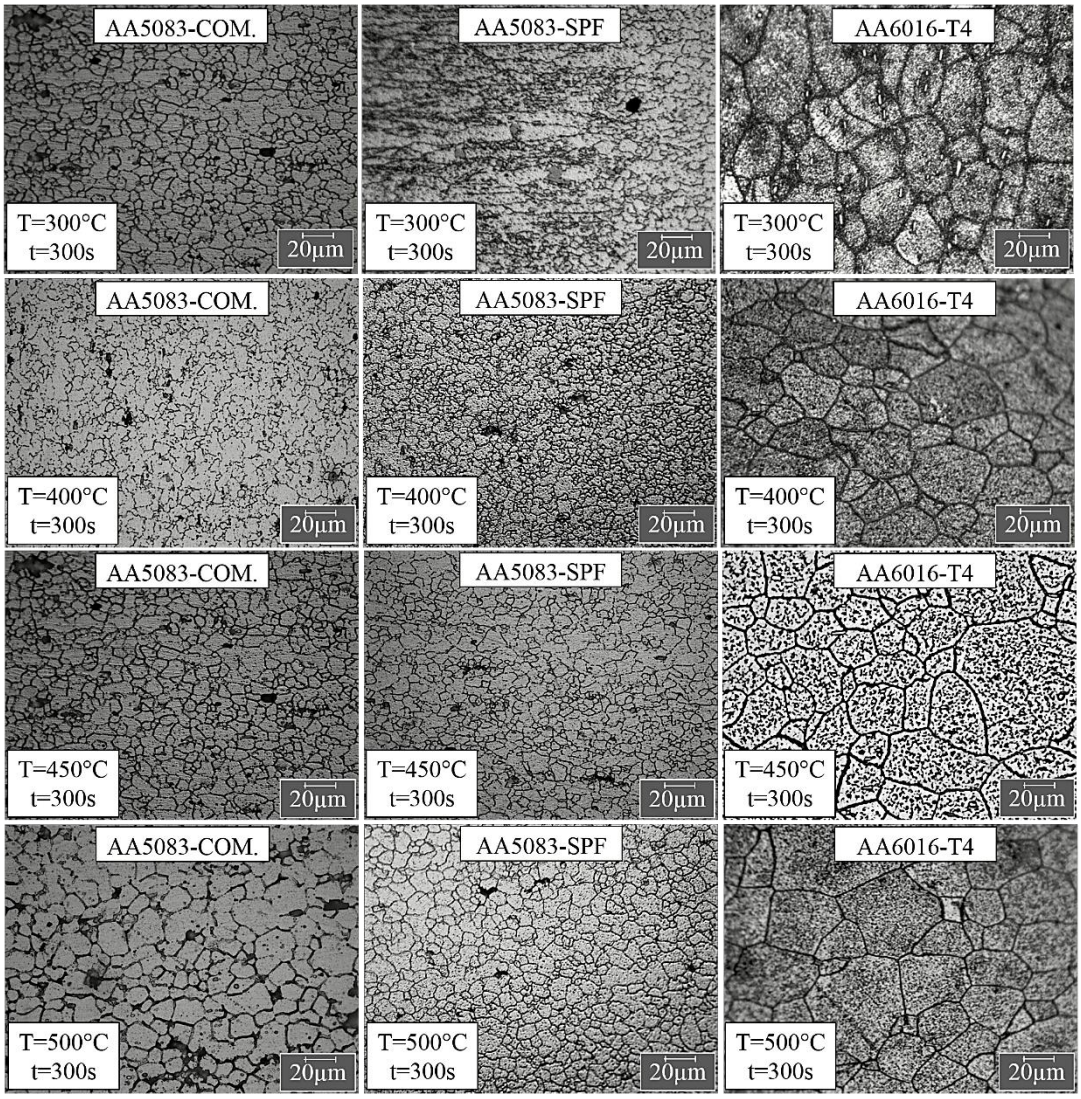

Figure 4.2: Microstructure of the aluminium alloys studied after thermal cycles reported in Table 4.5.

Considering microstructure pictures of commercial grade AA5083 in Figure 4.2, it is possible to observe that no appreciable differences in grain shape and dimension take place with temperature increments. Instead, the recrystallization phenomenon, which for the aluminium alloys begins at around 350 °C, is appreciable in the superplastic grade AA5083 by observing the microstructure picture at 400 °C. Indeed, the high grade of energy stoked in the lattice of the AA5083 with superplastic characterization, due to the high cold rolling thickness reduction, facilitates the recrystallization phenomenon that starts at 300 °C, which completely changes the grain size and shape. Therefore, at 450 °C and 500 °C, grain size and structure of the AA5083-SPF are comparable of that of the commercial grade.

Regarding the microstructural behaviour of AA6016 with temperature, it is worth noting that no appreciable differences can be seen between the microstructure of the as-delivered condition and the microstructure of all the heat-treated samples both in the size and in morphology of the grains. Finally, one has to give particular consideration for the solubilisation temperature of the thermal treatable aluminium alloy AA6016, namely 550 °C

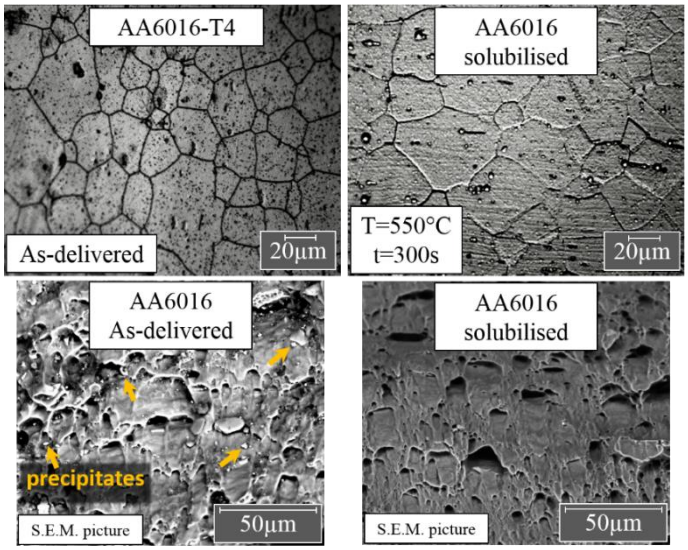

Figure 4.3: Microstructure of the AA6016 aluminium alloy before and after solubilisation heating treatable, optical microscope picture and S.E.M. back scattered electron picture.

Figure 4.3, shows a comparison between the AA6016 in the as-delivered condition and after the solubilisation heating treatment, performed by keeping the material sample at 550 °C for 300 seconds and finally water quenched to preserve the microstructure. In both cases, the average grain size is in the range from 50 µm to 55 µm, without any appreciable grain coarsening due to the thermal cycle. Regardless, the SEM images shown in Figure 4.3, confirm that the thermal cycle was effective in dissolving the Mg_2Si precipitates on the aluminium matrix.

4.3. Hot tensile tests

To investigate the aluminium alloys formability, uniaxial tensile tests were performed considering different temperatures and strain rates in order to analyse material behaviour in the warm and hot field of temperature and in a wide range of deformation speeds, relative to

the SPF, QPF and Hot Stamping processes. The twofold objective of this study are (i) to determine the material response to deformation (in terms of flow stress, plastic anisotropy, and strain at fracture), and (ii) to evaluate the post-deformation material characteristics (in terms of micro-hardness and microstructure).

4.3.1 Experimental apparatus

The uniaxial tensile tests at elevated temperatures were carried out on a universal 5 t MTS™ testing machine adapted for high temperature testing, shown in Figure 4.4.

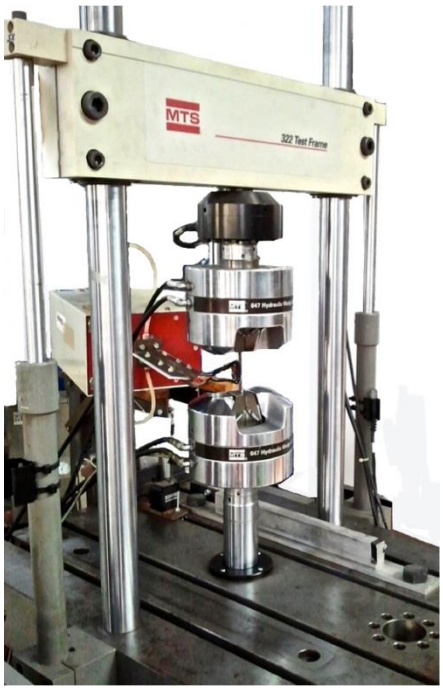

Figure 4.4: MTS 5kN hydraulic press used to perform tensile test with different strain rate, equipped with a frontal inductor heater.

A high frequency inductor system represented by a flat head, allows the aluminium sample to be quickly heated, while the temperature was controlled through a K-type thermocouple spot-welded in the central zone of the specimen, which was machined according to the ISO 10130 standard. Each tensile sample presented a geometry reported in Figure 4.5, with a gauge length of 65 mm, a width of 12 mm and a thickness depending the initial aluminium metal sheet thickness. Specifically the thicknesses were: AA5083-COM. 1 mm, AA5083-SPF and AA6016 1.5 mm. Before performing the hot tensile tests, a thermal calibration through a Flir Thermocamera, was done in order to find the uniform temperature length, in relation with the induction head geometry used. From measurement, a uniform thermal length of 15 mm was found using a temperature range from 200 °C to 500 °C. This value was used as initial sample length in true stress-true strain calculation for tensile test at temperature higher than room temperature.

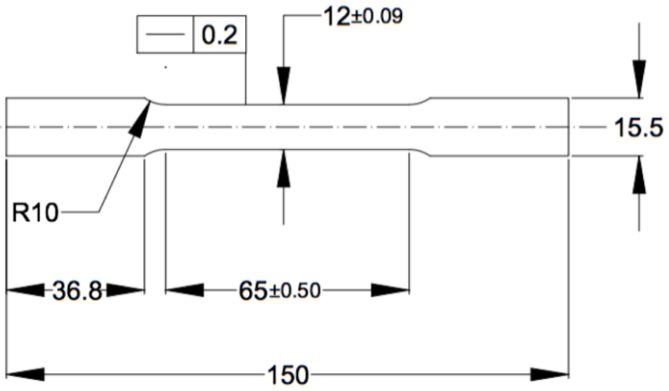

Figure 4.5: Tensile test sample geometry in according to ISO 10130.

To measure the true strain directly, even after non-uniform deformation, the hot tensile test machine was equipped with the Aramis™ system from GOM to detect in-line the specimen surface strain field. As shown in Figure 4.4, the inductor head was placed behind the specimen heating its central zone; it was moved by a brushless motor in order to account for the specimen elongation during the test and thus to keep the temperature field in the central part of the specimen uniform especially during test with low strain rate. The temperature recordings provide the feedback both to the inductor for keeping the temperature with an accuracy of ± 2 °C and to the brushless motor to follow the specimen deformation. The Aramis™ is a non-contact optical deformation measuring system. It records the evolution of the displacement of a stochastic pattern at high contrast sprayed on the specimen. The system uses a high resolution and high frames camera to produce a photographic history of the specimen deformation, and allocates coordinates to the image pixels. During a tensile test, the first image taken represents the un-deformed state of the specimen and this is considered to be the reference condition. Finally, the software compares consecutive sequential photographs captured with the reference photograph, and evaluates each single pixel deformation and displacement, calculating the complete specimen true strain, as shown, Figure 4.6. Finally, through the Aramis™ system, it is possible to obtain the anisotropy value, measuring the amount of minor strain and, from the volume constancy, the thickness reduction, (eq. 4.1), based on the visible surface geometry modification.

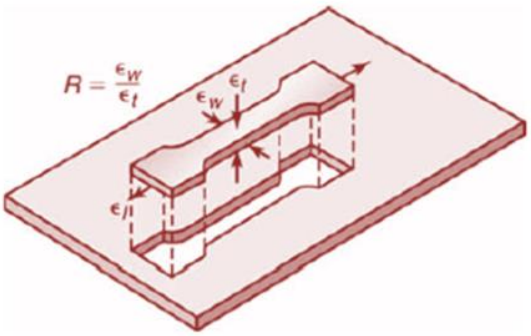

$$R = \frac{\varepsilon_w}{\varepsilon_t} = \frac{\ln\frac{w_0}{w_t}}{\ln\frac{t_0}{t_t}} \qquad \text{(eq. 4.1)}$$

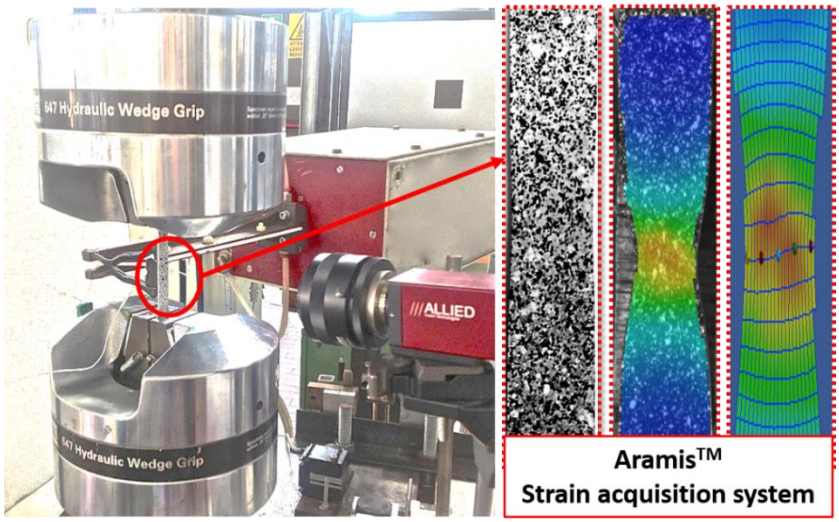

Figure 4.6: Example of a hot tensile test elaborated through the Aramis™ strain acquisition system.

To utilise the frames rate of the camera that was used (an IEEE Allied Pike CCD sensor), a software was developed in the LabVIEW® environment, shown in Figure 4.7, was developed in order to arrive (after software image setting) at a maximum recording speed of 450 fps with a resolution of 640 pixel along the specimen length direction.

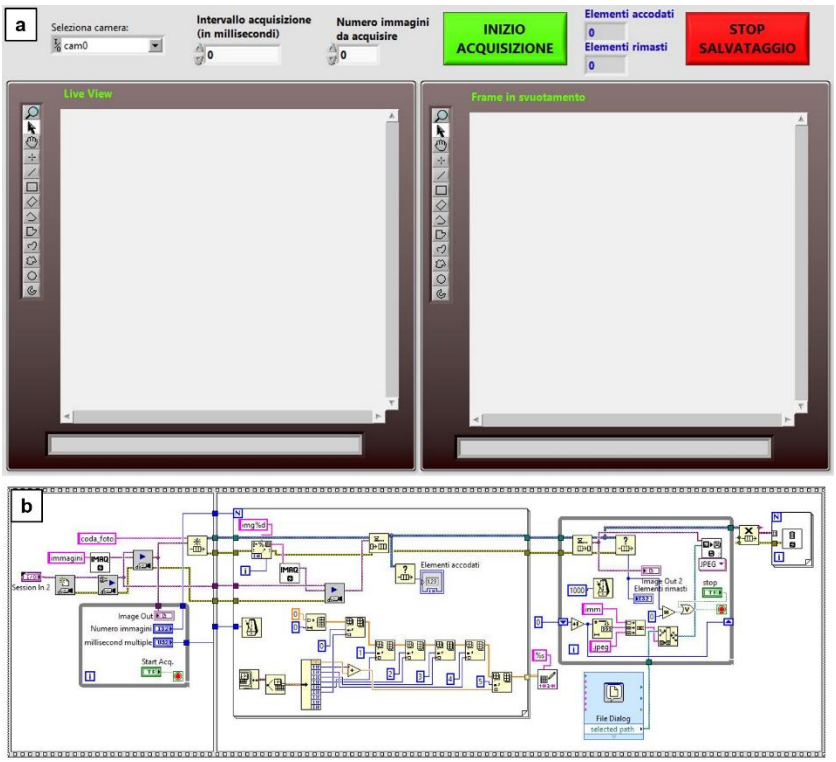

Figure 4.7: High frame rate and resolution acquisition software developed in LabVIEW® environment, Front panel (a) and block diagram (b).

4.3.2 Experimental plan

The complete experimental plan, used for all of the aluminium alloys tested, is shown Table 4.6.

Table 4.6: Experimental plan for hot tensile testing.

$\dot{e}$ [s-1]	T [°C]				
10^{-2}	-	300	400	450	500
10^{-1}	20	300	400	450	500
10^{0}	-	300	400	450	500

Each testing condition was repeated twice in order to assure the repeatability of the results. Furthermore, each testing condition was repeated on samples machined at 0°, 45° and 90° with respect to the rolling direction, in order to evaluate the average normal and planar anisotropy coefficients as a function of the temperature and strain rate. The room temperature test was also conducted on samples machined at 0°, 45° and 90° with respect to the rolling direction. The anisotropy value for each testing condition was evaluated at a fixed amount of strain, equal to 0.25. Finally, only in the case of the thermally treatable aluminium alloy AA6016, tests with conditions reported in Table 4.2, were performed on solubilised material condition after solubilisation of tensile samples in a furnace at 550 °C for 300 seconds and consecutive water quenching.

4.3.3 Experimental procedure

During testing, the specimen was heated up to the testing temperature, held at this temperature for a certain time to homogenise both the temperature and microstructure, and then strained until fracture. When the fracture starts, the test was stopped and the specimen was water quenched in order to retain the material microstructure. The heating rate was fixed at 10 °C/s and the soaking time was 90 s. The choice of the soaking time was made after microstructural observations on aluminium samples heated at different temperature and soaked for different time. Figure 4.8 shows the temperature vs. time diagram of the tensile tests.

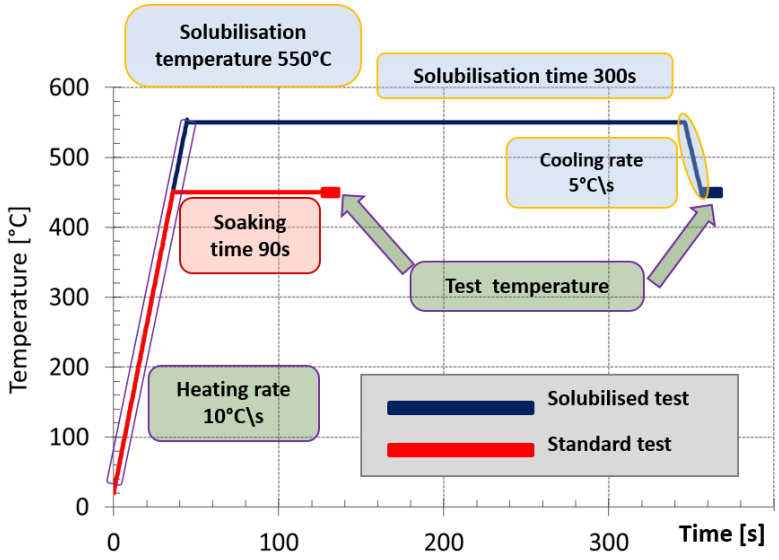

Figure 4.8: Temperature vs. time diagram of the hot tensile tests. The red line refers to the standard tensile test and the blue line to the tensile test after solubilisation.

The red line refers to a test without solubilisation, so in the case of the AA5083 in commercial and superplastic grade and for the AA6016-T4 condition. In this test type the sample was heated up to the target temperature (always lower than the solubilisation temperature) with a heating rate of 10 °C/s, than a soaking time of 90 s was applied for homogeneatization, and finally the material was tensile tested until fracture at constant temperature and strain rate. The blue line refers only to a test where the AA6016 sample was previously subjected to solubilisation at 550 °C for 5 minutes, then cooled down at 5 °C/s to the target temperature where it was strained until fracture, without any further soaking time.

After material braking, the true strain at fracture ε_f, considered as a measure of the material formability, was evaluated on the basis of the sample initial area by measuring its area at fracture according to (eq. 4.2):

$$\varepsilon_f = \ln \frac{A_{initial}}{A_{fracture}} \qquad \text{(eq. 4.2)}$$

The true strain at fracture was not directly calculated from the Aramis measurements, since the specimen pattern at elevated temperature and very close to the fracture point had deteriorated too much in order to provide reliable results. Consequently, a micrometer was used to calculate the fracture width, while measurements provided through electron microscope S.E.M. were used to calculate an average value of fracture thickness, in order to obtain an accurate value of fracture area for each specimen stretched, as showed in Figure 4.9.

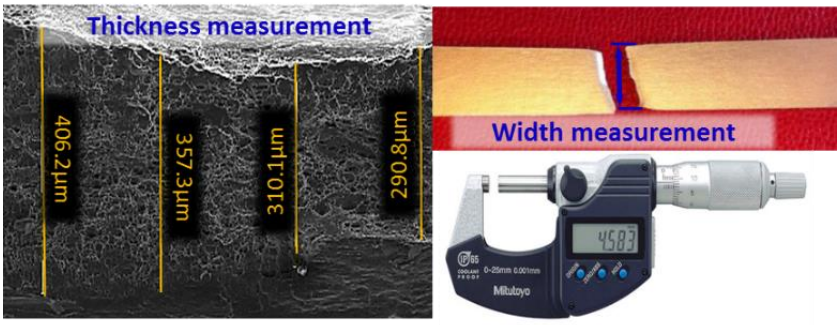

Figure 4.9: Measurement approach for calculating the sample area at fracture.

4.3.4 Results

In this section, the results of the hot tensile tests are presented, considering in detail the influence of the two main parameters: temperature and strain rate. Therefore, for all the diagrams reported, one of these two parameters is kept constant, whilst detailing the material behaviour changes as a function of the strain rate or the temperature. Initially, a comparison was made between the two studied grades of the aluminium alloy AA5083, namely the commercial and the superplastic, and between the two conditions treated for the aluminium alloy AA6016, namely the not solubilised and the solubilised one. Subsequently another two important parameters for the metal sheet deformation, that are the normal anisotropy and the planar anisotropy, were analysed. Finally, through the strain at fracture parameter, a three-dimensional diagram for the formability, in terms of temperature and strain rate, was proposed for each aluminium alloy tested.

Room temperature

Figure 4.10 shows the difference among the aluminium alloys tested without any thermal cycle and stretched at room temperature. The AA6016 solubilised specimen was thermally treated before testing, with the procedure reported in 4.3.3 and, after water quenching, stretched at room temperature as the others.

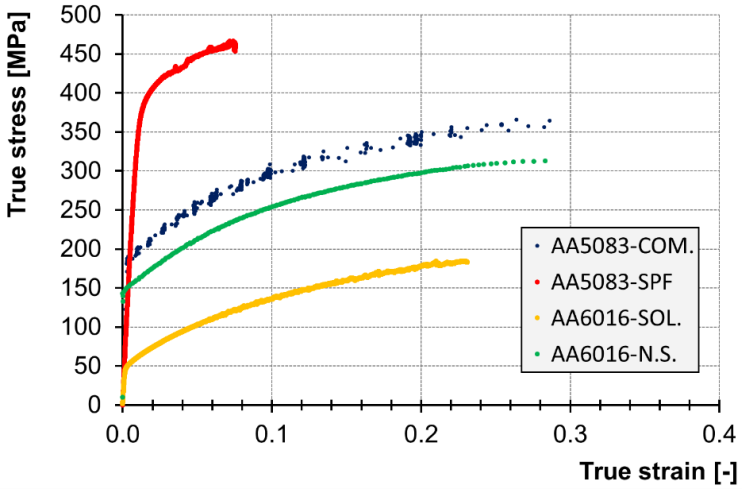

Figure 4.10: Difference among the aluminium alloys tested at room temperature.

The aluminium 5000 series demonstrates the highest value of true stress, especially in the superplastic grade, which presents a strength which is approximately 25 % higher than the commercial grade, and a very short strain before fracture. This is explained by considering the different grains size and morphology between the two AA5083 grades, as shown in Figure 4.1. In fact, for the Petch-Hall equation (eq. 4.3), there is a relation between the amount of the grain boundary, and therefore the grain dimension, and the yield stress of the material. Grain boundaries obstruct dislocations movement, meaning that increasing large grains have a relatively low material strength.

$$\sigma_y = \sigma_i + \frac{k_y}{\sqrt{D}} \qquad \text{(eq. 4.3)}$$

σ_y = yield stress

σ_i = material constant of dislocations movement start

k_y = Peth parameter, *unpinning constant.*

D = average grain diameter

Regarding the AA6016, the solubilised condition shows low values of true stress parameter, which are around 50 % compared to the T4 condition. Even if the grain dimension and geometry not appear different between the two material conditions, as shown in Figure 4.1, the reason for this behaviour can be attributed to the dissolution of the hardest Mg_2Si precipitates on aluminium matrix after the thermal treatment as shown in Figure 4.3.

Temperature and strain rate influence

To highlight the influence of temperature and strain rate on the aluminium flow stress, the results of both 5000 aluminium grades are considered together. The same procedure was followed for the 6000 aluminium series for the heat-treatable and non-heat-treatable material.

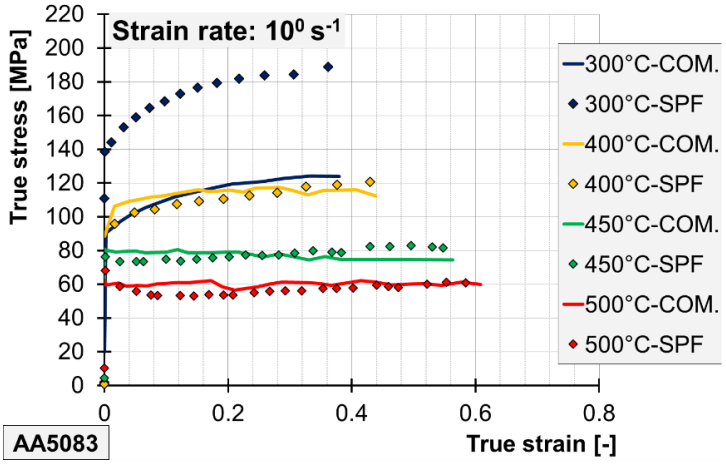

Figure 4.11: Temperature sensitivity and comparison between AA5083 commercial grade (solid line) and superplastic grade (dotted line) at a constant strain rate of 10^0 s^{-1}.

Figure 4.11 shows the strong influence of the temperature for the AA5083 series stretched with constant strain rate of 10^0 s^{-1}. In the test performed at a temperature of 300 °C that stays below the 0.5 Tm (homologous temperature), the superplastic grade AA5083 shows a higher flow stress compared to the one sample at the commercial grade. This difference in behaviour can be attributed to the different microstructural features exhibited by the two grades at 300 °C, being the microstructural homogenization of the superplastic grade due to the thermal cycle not fully completed happened, Figure 4.2. By increasing test temperature from 300 °C to 500 °C, the material behaviour of the two aluminium grades becomes comparable. At 400 °C the strain hardening behaviour is still present, however at 450 °C and 500 °C, both aluminium grades show a completely plastic behaviour until fracture. Moreover, in the highest range of temperatures, flow stress values become very close as confirmed from the images of material microstructure after hot thermal cycles, shown in Figure 4.2.

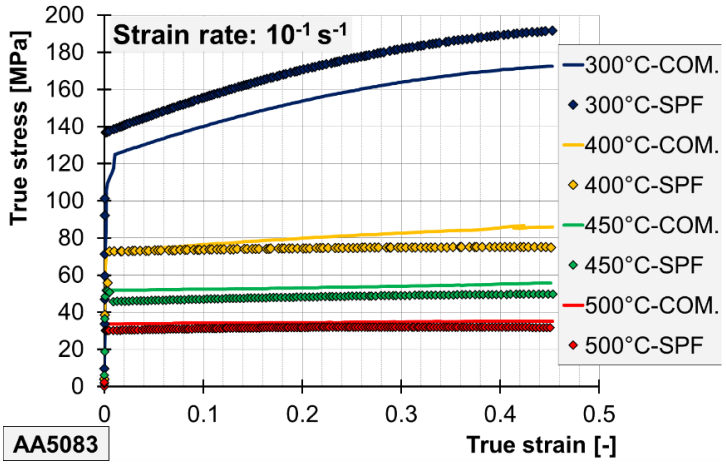

Figure 4.12: Temperature sensitivity and comparison between AA5083 commercial grade (solid line) and superplastic grade (dotted line) at a constant strain rate of 10^{-1} s^{-1}.

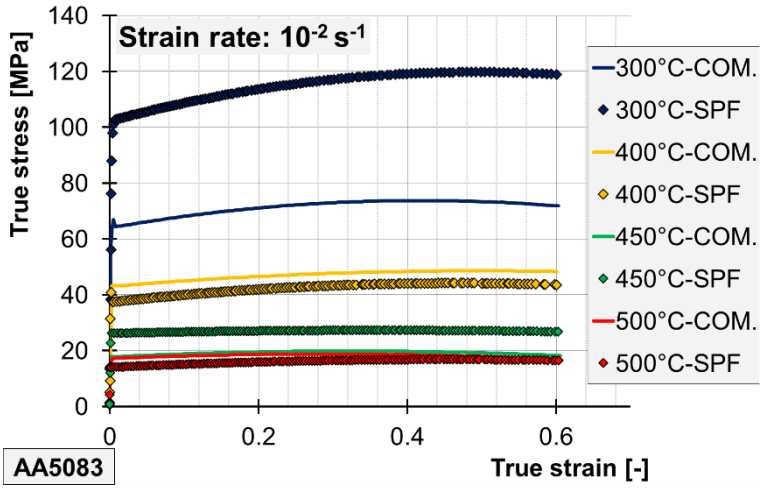

Figure 4.13: Temperature sensitivity and comparison between AA5083 commercial grade (solid line) and superplastic grade (dotted line) at a constant strain rate of 10^{-2} s^{-1}.

Figure 4.12 and Figure 4.13, show the influence of temperature on material flow stress for lower strain rate (10^{-1} and 10^{-2} s^{-1}). The trend is comparable with the highest strain rate. A little variation in strain hardening contribution affects the test at 300 °C and 400 °C where the phenomenon is reduced and completely absent at 450 °C and 500 °C. It is also observed that, regardless of the strain rate, the material response to deformation does not depend on the grade as-received condition, as shown in Figure 4.14 for a test with a temperature of 450 °C. It is possible to conclude that for this aluminium series, the material flow stress is highly sensitive to both strain rate and temperature for both the grades.

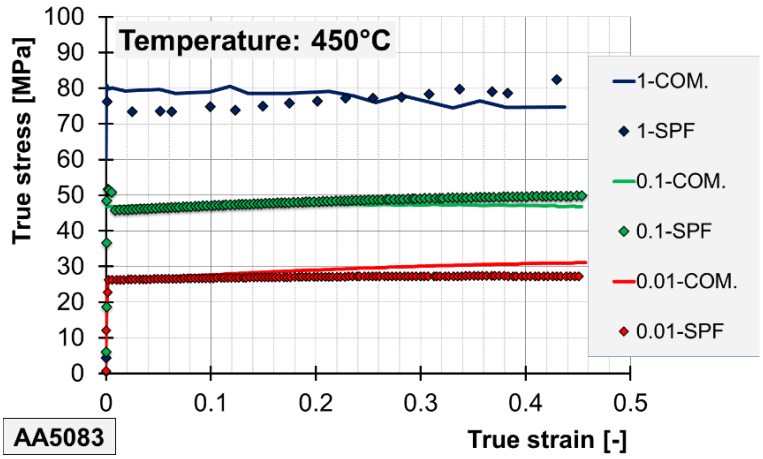

Figure 4.14: True stress-true strain curves at varying strain rate and temperature equal to 450 °C. AA5083 commercial grade (solid line) and superplastic grade (dotted line).

Figure 4.11, Figure 4.12 and Figure 4.13 show the flow stress sensitivity to temperature at a strain rate respectively at 10^{0}, 10^{-1} and 10^{-2} s^{-1}, for both the solubilised and non-solubilised material condition.

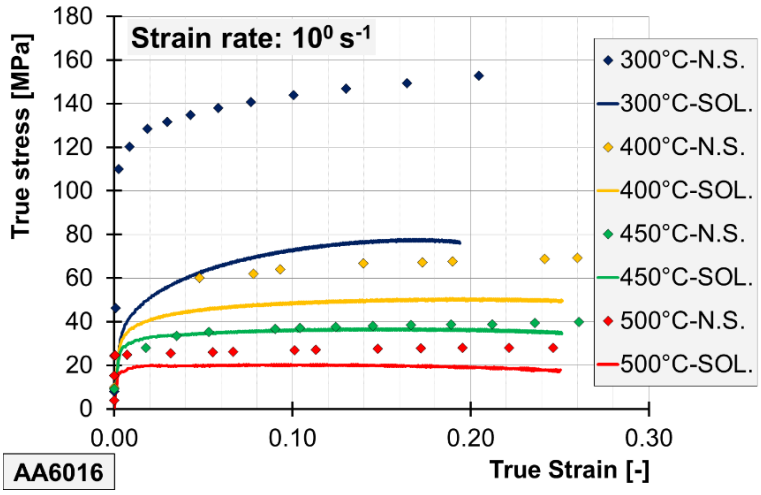

Figure 4.15: Temperature sensitivity and comparison between AA6016 solubilised condition (solid line) and non-solubilised condition (dotted line) at a constant strain rate of 10^{0} s^{-1}.

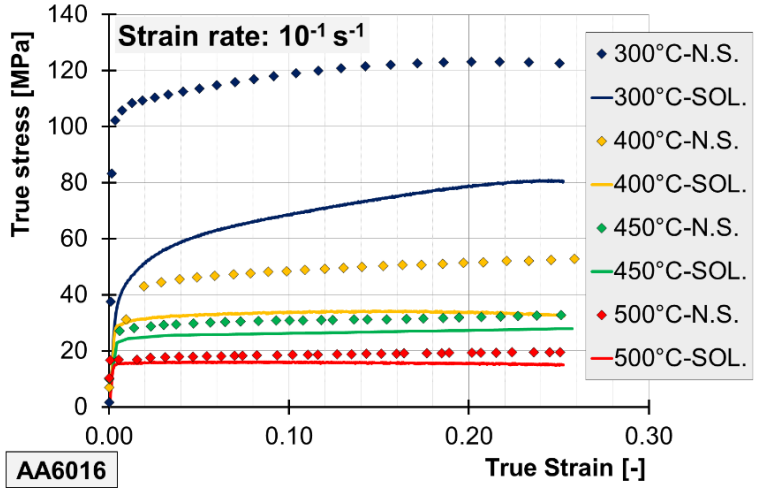

Figure 4.16: Temperature sensitivity and comparison between AA6016 solubilised condition (solid line) and non-solubilised condition (dotted line) at a constant strain rate of 10^{-1} s^{-1}.

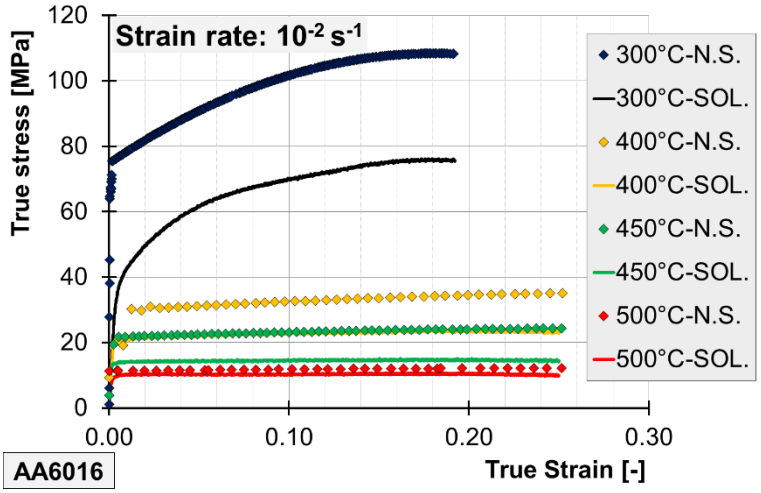

Figure 4.17: Temperature sensitivity and comparison between AA6016 solubilised condition (solid line) and non-solubilised condition (dotted line) at a constant strain rate of 10^{-2} s^{-1}.

Independently from its microstructural condition, the material exhibits a significant sensitivity to temperature and a reduced strain hardening at increasing temperature. Moreover, the solubilised material shows a lower flow stress compared to the non-solubilised one for each testing condition, the difference being more significant at decreasing temperature.

The material flow stress sensitivity to strain rate is instead shown in Figure 4.18 at a temperature equal to 450 °C: as expected, the material is strongly influenced by the strain rate.

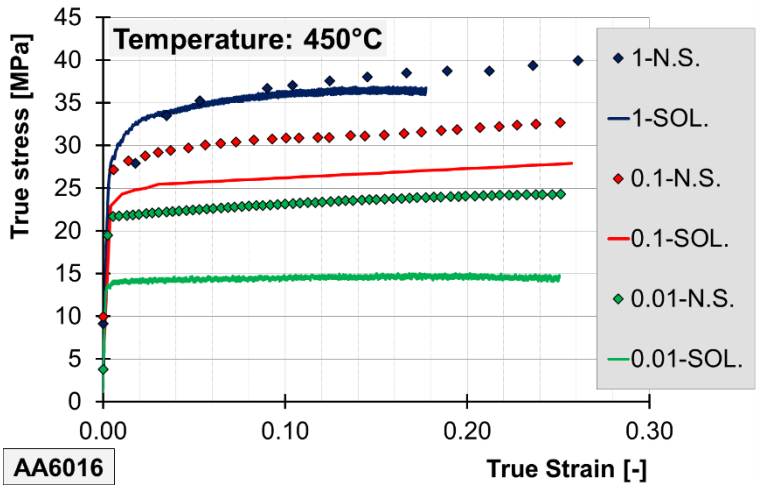

Figure 4.18: True stress-true strain curves at varying strain rate and temperature equal to 450 °C. Solubilised condition (solid line) and non-solubilised condition (dotted line).

Furthermore, for the two lowest values of the strain rate, the flow stress of the non-solubilised material is higher than the solubilised one, whereas at 1 s^{-1} the two are comparable. The same happens at 400 °C and 500 °C, whereas at 300 °C, Figure 4.19, the flow stress of the solubilised material is not influenced by the strain rate.

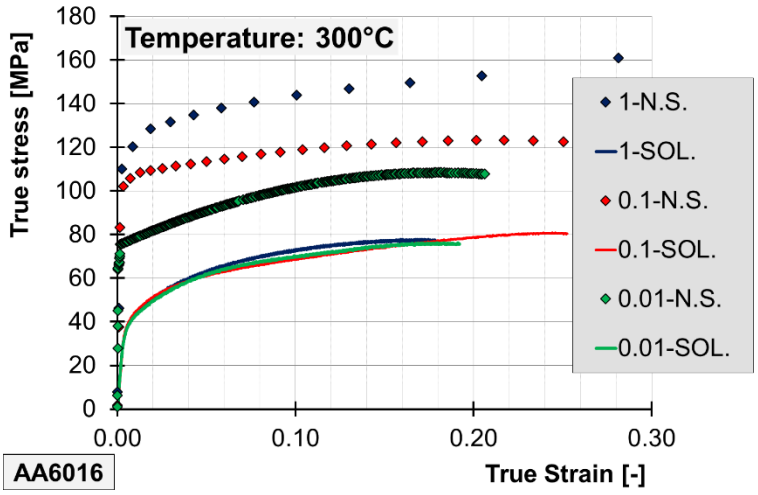

Figure 4.19: True stress-true strain curves at varying strain rate and temperature equal to 300 °C. Solubilised condition (solid line) and non-solubilised condition (dotted line).

It is worth noting that all of the flow stress curves shown in the graphs were cut at a value of strain equal dependence by the strain rate, since the deterioration of the Aramis™ pattern at high temperature does not allow a reliable measurement of the strain until fracture.

Formability window

In this section, 3D-curves are shown that qualitatively represent the formability windows for aluminium alloy tested in their each condition and based on the strain at fracture parameter calculated as described in 4.3.3. These diagrams are useful to understand which are the best process parameters, in terms of temperature and strain rate, to deform the material.

TEST TEMPERATURE [°C]	STRAIN RATE [s^{-1}]	ε_r
T room		0.632
300°C	0.01	1.330
400°C	0.01	1.927
450°C	0.01	1.690
500°C	0.01	1.163
100°C	0.1	0.704
200°C	0.1	0.965
300°C	0.1	1.176
400°C	0.1	2.085
450°C	0.1	2.102
500°C	0.1	1.553
300°C	1	0.982
400°C	1	1.231
450°C	1	1.899
500°C	1	1.837

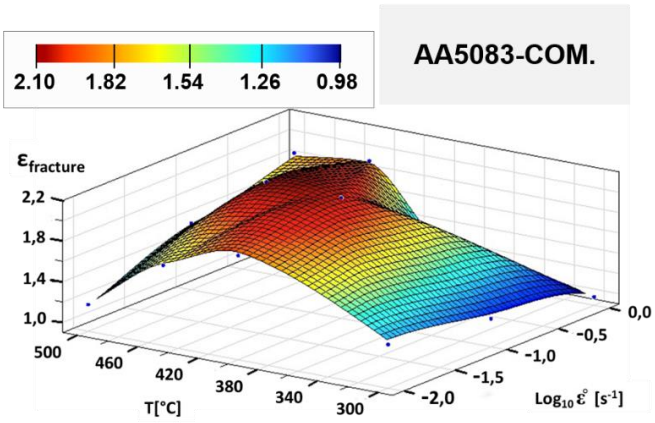

Figure 4.20: True strain at fracture at different testing temperatures and strain rates for the AA5083 alloy in commercial grade.

Figure 4.20 shows the true strain at fracture as a function of temperature and strain rate for the commercial grade AA5083. From the graph three zones can be distinguished with respect to the testing temperature: in the high temperatures zone, the formability is quite good, especially for high strain rates; the intermediate temperature zone has the highest formability peak, and, finally, the lowest temperatures zone presents the lowest values of ductility. At the lowest strain rates, the material exhibits the lowest ductility, regardless of the high testing temperature. This behaviour is exactly the same as the one exhibited during SPF by a superplastic AA5083 grade, in Figure 4.21. The ductility peak is reached at 450 °C for strain rates of 10^{-1} s^{-1} and 1 s^{-1}, which is the typical range of the hot stamping process. In particular, in the case of the superplastic grade, the highest value of the material true strain at fracture is assured at testing temperatures equal to 400 °C and 450 °C and strain rate equal to 10^{-1} s^{-1}. Therefore, in the range of the investigated strain rates, for both the grades it appears to be convenient to deform at a rate of 10^{-1} s^{-1} at an intermediate temperature range.

TEST TEMPERATURE [°C]	STRAIN RATE [s^{-1}]	ε_r
T room		0.164
300°C	0.01	1.404
400°C	0.01	1.659
450°C	0.01	1.506
500°C	0.01	1.228
100°C	0.1	0.146
200°C	0.1	0.330
300°C	0.1	1.340
400°C	0.1	2.181
450°C	0.1	2.272
500°C	0.1	1.624
300°C	1	0.929
400°C	1	1.625
450°C	1	2.016
500°C	1	1.678

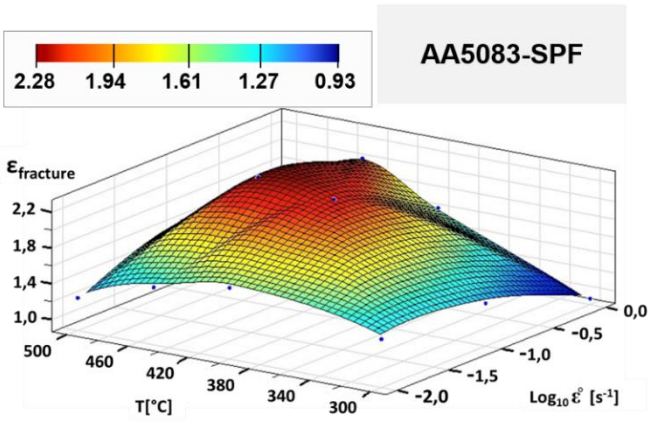

Figure 4.21: True strain at fracture at different testing temperatures and strain rates for the AA5083 alloy in superplastic grade.

The formability maps in terms of true strain at fracture as a function of the temperature and strain rate for the solubilised and the non-solubilised material are shown in Figure 4.22 and Figure 4.23 respectively. The solubilised material shows a higher sensitivity to the strain rate, especially in the intermediate temperature range, with a wider formability window and highest values of formability shown for the temperatures of 450 °C and 500 °C. On the other hand, the not-solubilised material presents in general lower values of the true strain at fracture, with a formability peak between 450 °C and 500 °C for the lowest and highest values of the strain rate.

TEST TEMPERATURE [°C]	STRAIN RATE [s^{-1}]	ε_r
T room		0.913
300°C	0.01	0.918
400°C	0.01	2.416
450°C	0.01	3.392
500°C	0.01	5.255
100°C	0.1	0.656
200°C	0.1	1.172
300°C	0.1	2.258
400°C	0.1	2.623
450°C	0.1	3.901
500°C	0.1	4.005
300°C	1	1.681
400°C	1	2.841
450°C	1	3.545
500°C	1	4.653

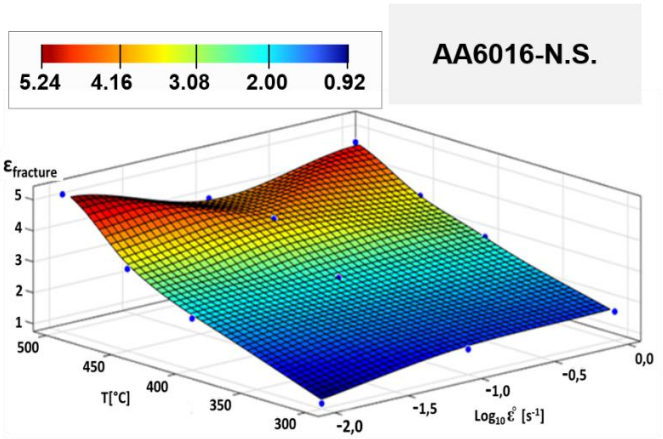

Figure 4.22: True strain at fracture at different testing temperatures and strain rates for the AA6016 alloy in T4 condition.

TEST TEMPERATURE [°C]	STRAIN RATE [s^{-1}]	ε_r
T room		0.700
300°C	0.01	1.645
400°C	0.01	1.831
450°C	0.01	3.463
500°C	0.01	5.214
100°C	0.1	1.616
200°C	0.1	1.447
300°C	0.1	2.885
400°C	0.1	4.916
450°C	0.1	5.511
500°C	0.1	5.915
300°C	1	1.717
400°C	1	3.473
450°C	1	3.941
500°C	1	5.203

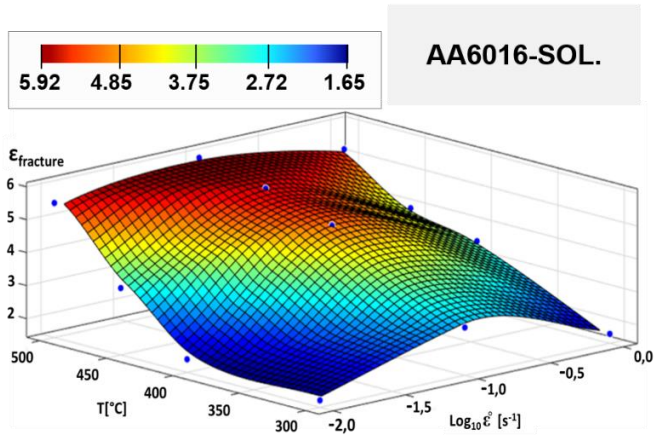

Figure 4.23: True strain at fracture at different testing temperatures and strain rates for the AA6016 alloy after solubilisation heating treatment.

It is possible to conclude that a temperature range from 450 °C to 500 °C, with a strain rate from 0.1 s^{-1} to 1 s^{-1}, represent the best process parameters to obtain the formability peak for the aluminium alloys studied and also that the AA6016 exhibits higher values of strain at fracture compared to the AA5083.

Anisotropy

Another important parameter to understand the metal sheet formability is the normal and the planar anisotropy. The two aluminium alloys were tested on samples machined at 0°, 45°

and 90° with respect to the rolling direction. The anisotropy value for each testing condition was evaluated at the fixed amount of strain equal to 0.25, using the relations in (eq. 4.4), (eq. 4.5) e (eq. 4.6).

$$R = \frac{\varepsilon_w}{\varepsilon_t} = \frac{\ln \frac{w_0}{w_t}}{\ln \frac{t_0}{t_t}} \quad \text{(eq. 4.4)}$$

$$\bar{R} = \frac{R_0 + 2R_{45} + R_{90}}{4} \quad \text{(eq. 4.5)}$$

$$\Delta R = \frac{R_0 - 2R_{45} + R_{90}}{2} \quad \text{(eq. 4.6)}$$

Regarding the aluminium alloys 5000 series, the diversity in grains geometry between the commercial and the superplastic grade increases the value of the average normal anisotropy calculated at room temperature, as shown in Figure 4.24 (a-b). In the warm and hot work field, it is possible to see that the average normal anisotropy of the superplastic and commercial grades is slightly influenced by the strain rate, being, on average, higher (or rather, closer to 1) at higher temperature and lower strain rate. With respect to the temperature, it is observed that higher values lead to an increased average normal anisotropy, with the exception of the testing temperature of 500°C, at which the material tends to be more anisotropic.

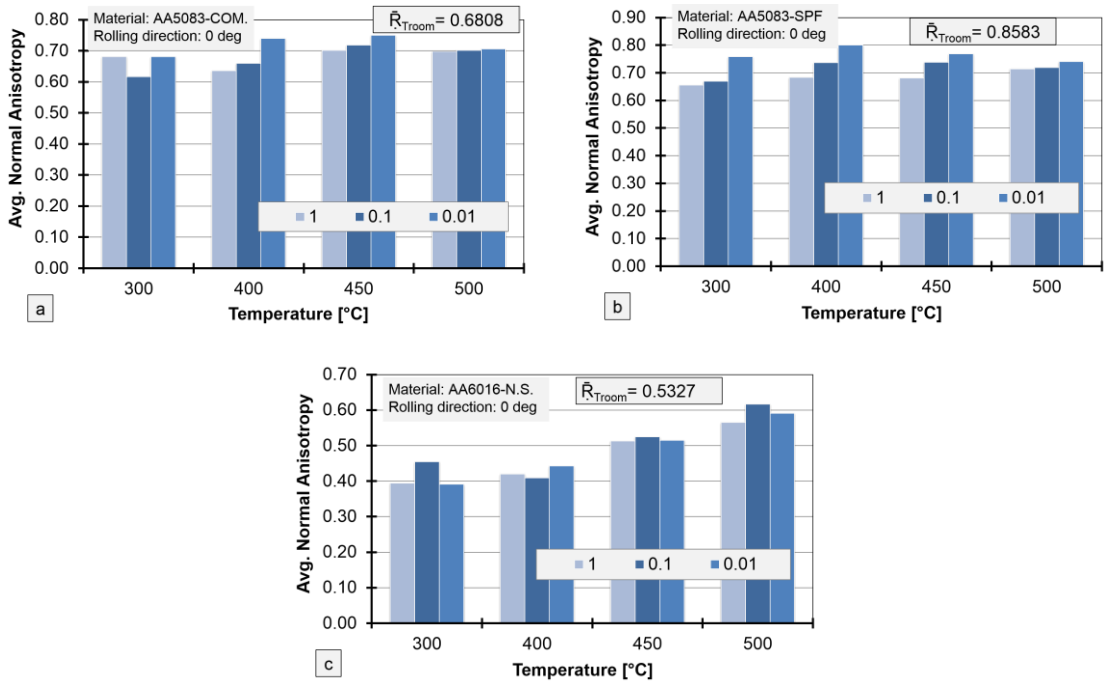

Figure 4.24: Average normal anisotropy at different testing temperatures and strain rates for the AA5083-COM. (a), AA5083-SPF (b) and AA6016-N.S. (c).

For the AA6016 sample, the anisotropy analysis was performed only for the not solubilised material because the solubilisation heat treatment does not affect the material grains morphology. Figure 4.24 (c), shows how high temperatures influence the average normal

anisotropy, while the strain rate does not affect the isotropic behaviour. In comparison with the AA5083 aluminium alloy, the normal anisotropy values found were always lower both for cold and high temperature test. In conclusion, considering that a value around 0.6 represents an isotropic aluminium alloys, all tests performed exhibit, except for AA5083 in superplastic condition stretched at room temperature, an isotropic behaviour as expected from the microstructure analysis, Figure 4.1.

The same trend was found in the planar anisotropy, Figure 4.25, where coefficients are close to zero at all testing conditions for both AA5083 grades, except for the superplastic grade at room temperature, as expected from its microstructure, and the AA6016 at room temperature and 500 °C stretched with a strain rate of 10^{-1} s^{-1}.

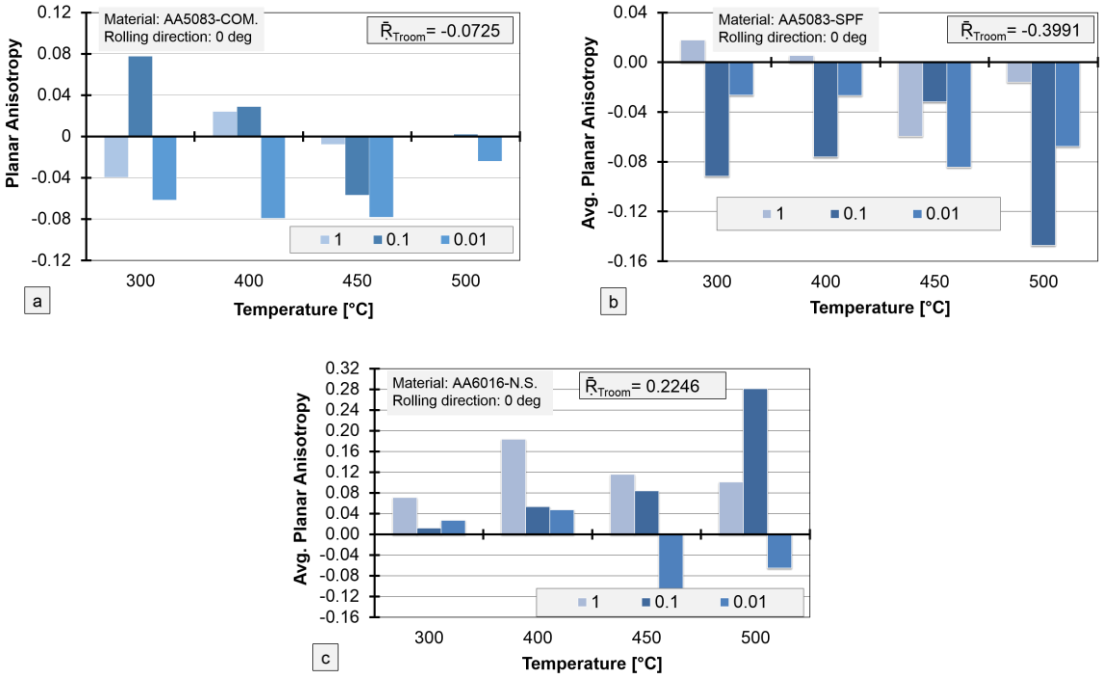

Figure 4.25: Average planar anisotropy at different testing temperatures and strain rates for the AA5083-COM. (a), AA5083-SPF (b) and AA6016-N.S. (c).

4.4. Post deformation analysis

The material properties after deformation shown in this section consider the micro-hardness measurement, the microstructure optical observation after deformation and the study of the fracture morphology through an S.E.M. analysis.

4.4.1 Micro hardness measurement

After stretching, mechanical material properties were evaluated using a micro hardness Vickers instrument which is able to localise the hardness measure within a single grain. Considering the aluminium alloy series studied, the amount of hardness on each stretched sample can be calculated using equation (eq. 4.7) with a load parameter of 50 grams. For each

stretched condition, five measures were taken nearby the sample fracture zone, and an average value was calculated considering its standard deviation.

$$\mu HV = 1{,}854 \cdot \frac{P}{\left(d/_{1000}\right)^2} \qquad \text{(eq. 4.7)}$$

P = load in grams;

d = average footprint pyramidal diagonal.

Figure 4.26, shows the superplastic and commercial AA5083 micro-hardness after testing as a function of temperature and strain rate. As expected at room temperature, the superplastic grade exhibits a significantly higher hardness compared to the commercial grade, thanks to its very fine-grained microstructure. At increasing temperatures, the superplastic grade hardness tends to decrease, showing values comparable to that at room temperature at 300 °C and high strain rate, where the material microstructure is still fine. On the contrary, the micro-hardness of specimens strained at higher temperatures is lower, being equal to 90 HV on an average. At the optimal forming conditions identified in the previous paragraph, the superplastic grade exhibits a lower micro-hardness than that at room temperature, but comparable to the commercial grade one. The commercial grade exhibits a linear trend: at increasing testing temperatures, the material micro-hardness decreases, being the predominant effect at the highest temperature; whilst the strain rate trend is opposite, since the higher the strain rate the lower the micro-hardness. At the optimal forming conditions, identified in the previous paragraph, the commercial grade micro-hardness is comparable to that of the material in the as-delivered condition.

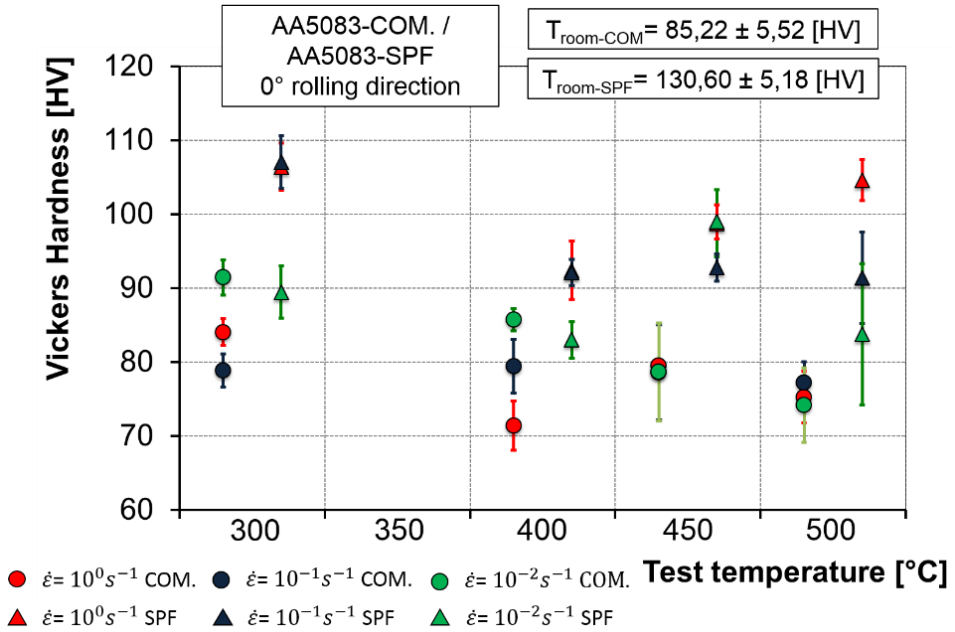

Figure 4.26: Vickers micro-hardness after tensile testing as a function of the temperature and strain rate for AA5083 series. Commercial grade (circle) and superplastic grade (triangle).

Regarding the AA6016, in Figure 4.27, micro-hardness measurements are shown as a function of the tensile testing temperature and strain rate for the solubilised and the non-

solubilised material providing evidence for the opposite trend of the two conditions with the temperature.

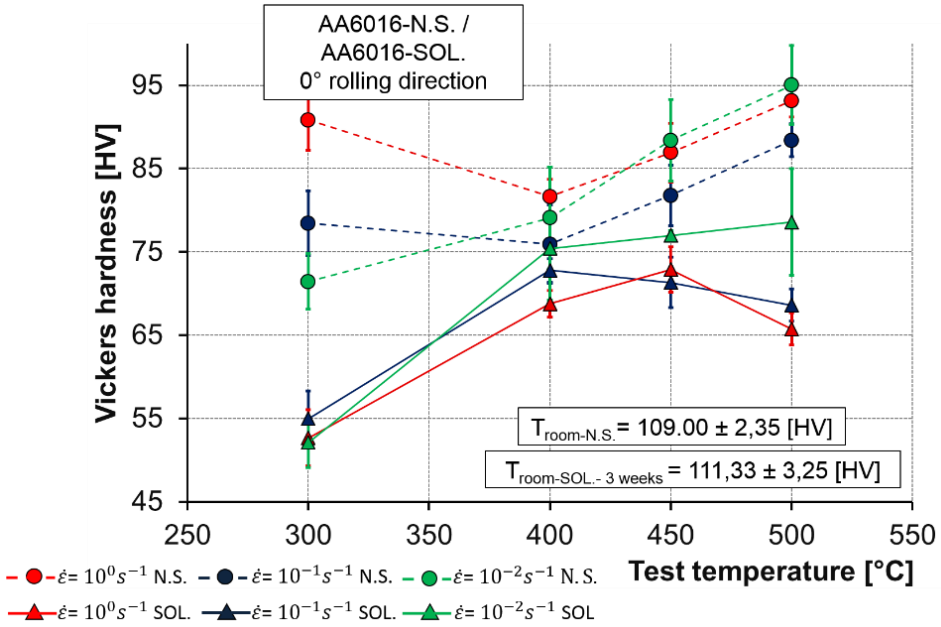

Figure 4.27: Vickers micro-hardness after tensile testing as a function of the temperature and strain rate. Solubilised condition (solid line) and not-solubilised condition (dotted line).

As expected, the non-solubilised material exhibits higher hardness values, regardless of the testing condition, even if it is in general lower than the as-delivered material. In the temperature range of maximum formability, the not-solubilised material shows hardness values which are on average 20 % less than the one of the as-delivered blanks, however they are still acceptable. On the contrary, the hardness values of the solubilised material are drastically reduced, especially at 300 °C. An interesting result is the hardness value of the solubilised material stretched at room temperature and measured after three weeks, which it shows to be comparable with that in the as delivered material condition. This result is due to the natural ageing of the material which leads to new precipitations of the hardest particles on aluminium matrix.

4.4.2 Fracture morphology

The observation of the fracture surfaces of the deformed specimens can represent an effective way to identify the predominant deformation mechanisms, and hence support the results from mechanical testing. The analysis was focused on the fracture surfaces both parallel and perpendicular to the tensile loading direction of specimens.

Regardless of the room temperature, the failure features at strain rates equal to 10^{-1} s^{-1} are characteristic of a conventional ductile shear fracture, as shown in, Figure 4.28. In fact, except for the superplastic grade AA5083, where fragile fracture behaviour confirms the result obtained from the tensile test, all images show the presence of more or less deeper dimples. The softest material condition of the AA6016 after solubilisation, indeed, has shown the deepest dimples and, considering the images in longitudinal direction, many sliding planes near fracture location.

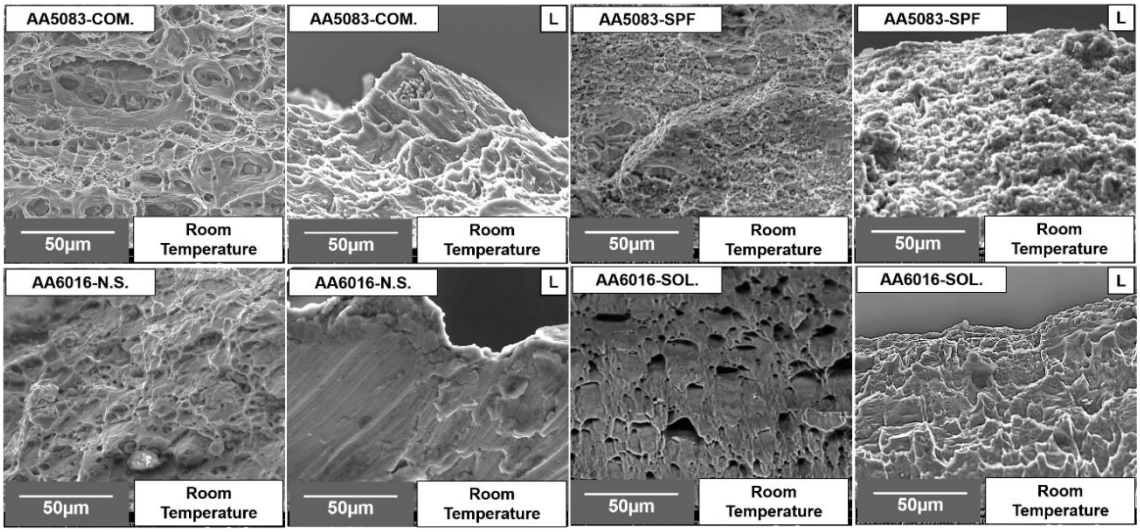

Figure 4.28: Fracture surfaces at room temperature in perpendicular direction and in parallel direction (L), for all aluminium studied.

All of the test conditions are analysed for the commercial grade AA5083 (Figure 4.29, last column identified with an "L"), in both of the perpendicular and longitudinal directions, the fracture surfaces regardless to temperature and strain rate appear elongated with large plastic zones, which is a feature typical of ductile fracture. At lower strain rates, from the analysis of the fracture surfaces parallel to the tensile loading direction, a change of the fracture morphology from failure only due to SD creep controlled by necking, to the one due to both SD and GBS controlled by cavitation is evident as found in [39] and described in section 2.2.3.

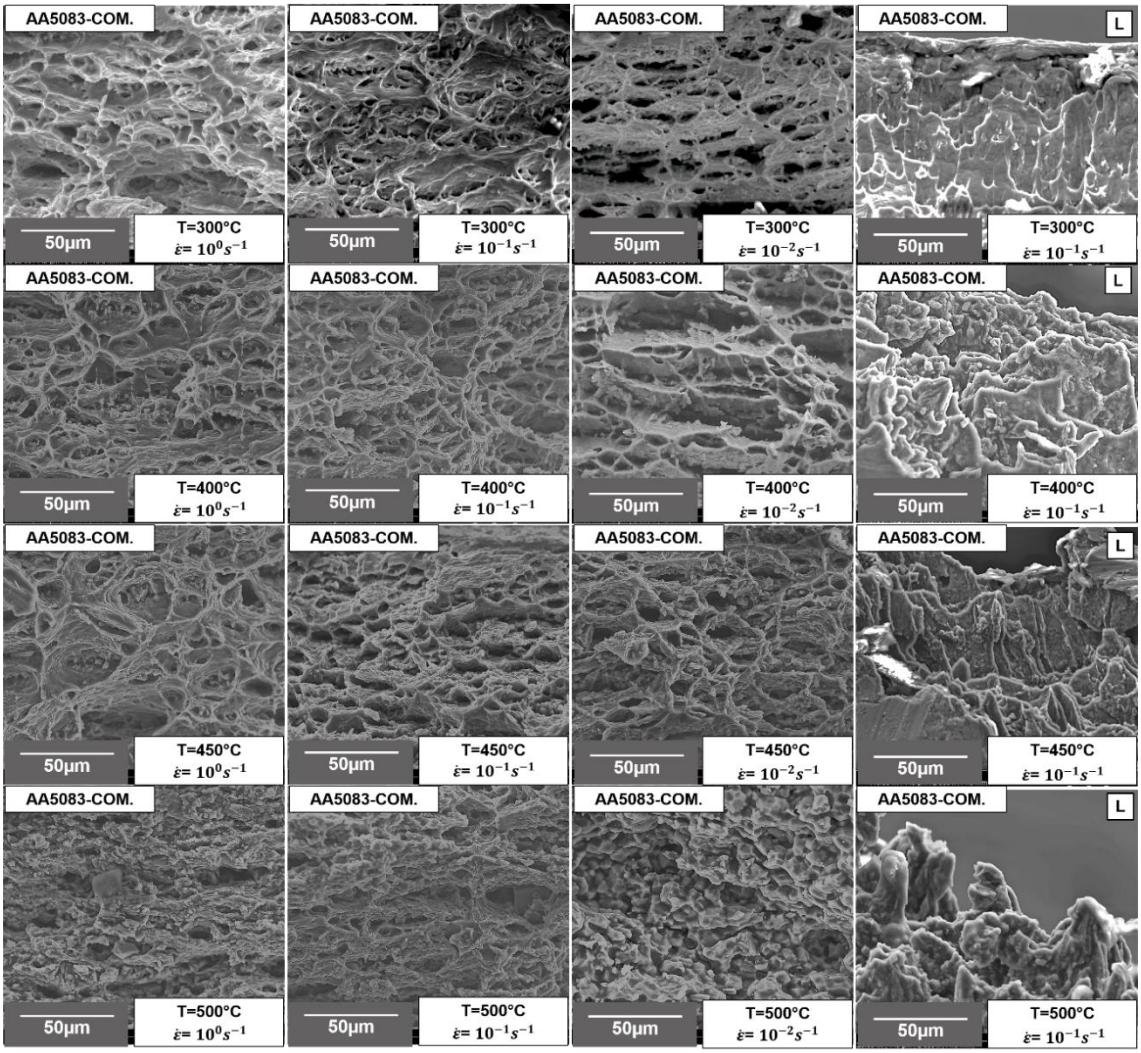

Figure 4.29: Images of the fracture surface of AA5083-COM. stretched at different strain rates and temperatures, in perpendicular direction and in longitudinal direction (L).

However, at 500°C for the lowest strain rates performed, some sub-micrometer filaments along the tensile loading direction appear together with some large cavities opening between the grains. This phenomenon is due to a material deformation mechanism that decreases the strain rate and is typical of the superplastic deformation process. To validate this result an AA5083 commercial sample was stretched at a strain rate which was one and two orders of magnitude lower than the strain rate used in this research, namely 10^{-3} s^{-1}, and 10^{-4} s^{-1}. As shown Figure 4.30, the amount of the sub-micrometer filaments increases significantly.

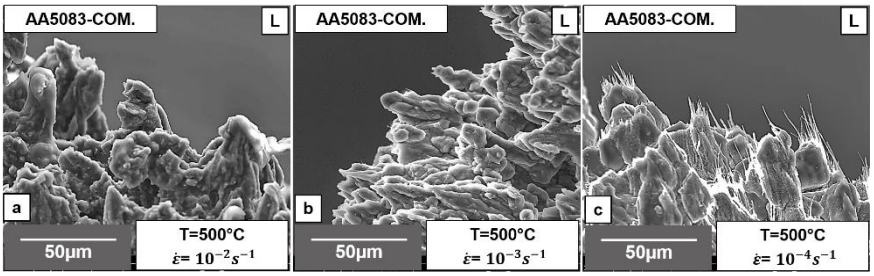

Figure 4.30: Comparison with AA5083-COM. parallel fracture morphology, stretched at a constant temperature of 500 °C and a strain rate respectively of 10^{-2} (a), 10^{-3} (b) and 10^{-4} s^{-1} (c).

The same behaviour has been exhibited in the superplastic AA5083, except for the room temperature test (shown previously in Figure 4.28) as proven with the microstructure analysis in 4.3. A comparison among the strain rate was performed, as shown in Figure 4.31 for the test temperature of 450 °C where it is worth noting that at the lowest strain rate, cavities appear more rounded and regularly shaped, as a result of the cavitation mechanism due to Grain Boundary Sliding.

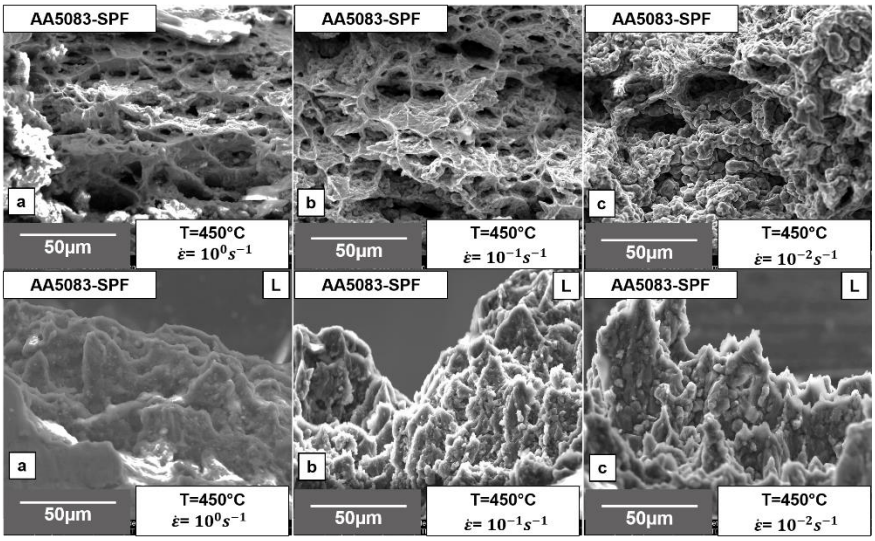

Figure 4.31: Comparison with AA5083-SPF perpendicular and parallel (L) fracture morphology, stretched at a constant temperature of 450 °C and a strain rate respectively of 10^{0} (a), 10^{-1} (b) and 10^{-2} s^{-1} (c).

Regarding the 6016 aluminium alloy, Figure 4.31 shows the fracture surfaces, in the perpendicular direction, for all testing conditions, which demonstrates the occurrence of ductile shear fractures and the enhancement of the material ductility at increasing testing temperatures in terms of increasing number and dimensions of dimples until 400 °C. The only exception is represented by the testing temperature of 500 °C, where the fracture surface appears almost free of dimples with a very thin fracture thickness. The final column shows the fracture morphology for the solubilised material, which demonstrates that there are no appreciable differences in the fracture mechanism.

Comparing also the fracture morphology of the two different aluminium alloys, the AA6016 shows more plastic behaviour. In fact, the classic ductile fracture with dimples appearance, characteristic of AA5083, is present only at warm temperatures and it is replaced at higher temperature with a complete material sliding behaviour without the presence of any cavities inside the specimen section.

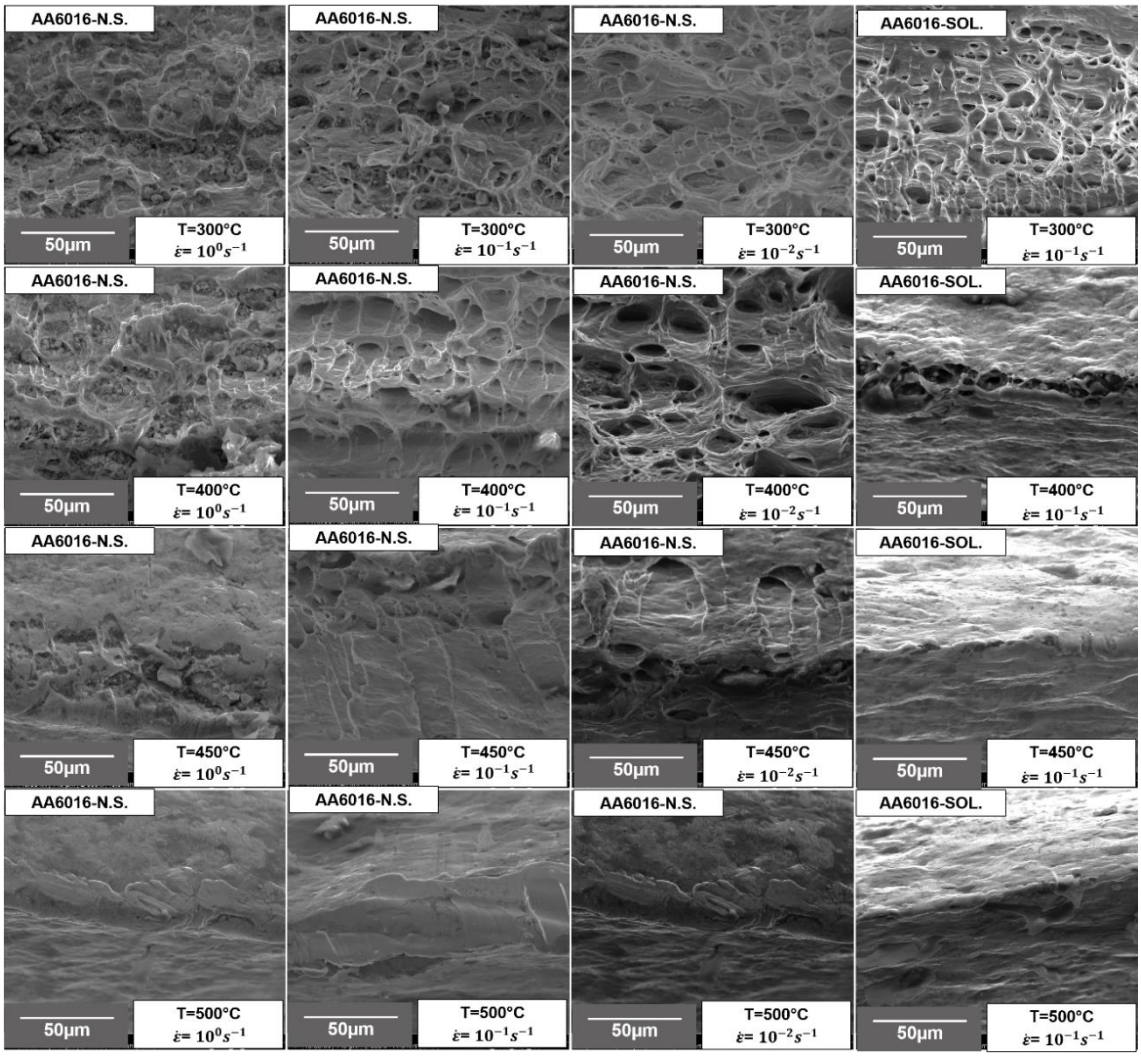

Figure 4.32: Images of the fracture surface of AA6016 in perpendicular direction stretched at different strain rates and temperatures. Material in not solubilise condition and after solubilisation heat treatment in the four column for strain rate equal to 10^{-1} s^{-1}.

4.4.3 Surface topography

Considering the results obtained from the hot tensile test in terms of surface quality, an interesting result was found in the case of AA6016. Specifically, a significant aesthetic surface changing manifests after stretched material in solubilised condition. To better explain this phenomenon, the surface topography of solubilised and not-solubilised samples after deformation were measured by means of a Sensofar Plu-Neox™ digital profilometer. Figure 4.33 shows the results in the case of samples processed at 500 °C and 0.1 s^{-1}: it is evident that the solubilisation treatment greatly affects the surface appearance and roughness. Whereas the not-solubilised sample presents a surface topography comparable to that of the as-delivered material, the solubilised sample has a surface that cannot be considered acceptable for the subsequent finishing operations. The AA5083 instead, in both commercial and superplastic conditions, was not aesthetically affected by the temperature and deformation at high temperature and the surface topography was equal of that of the material in the as-delivered condition.

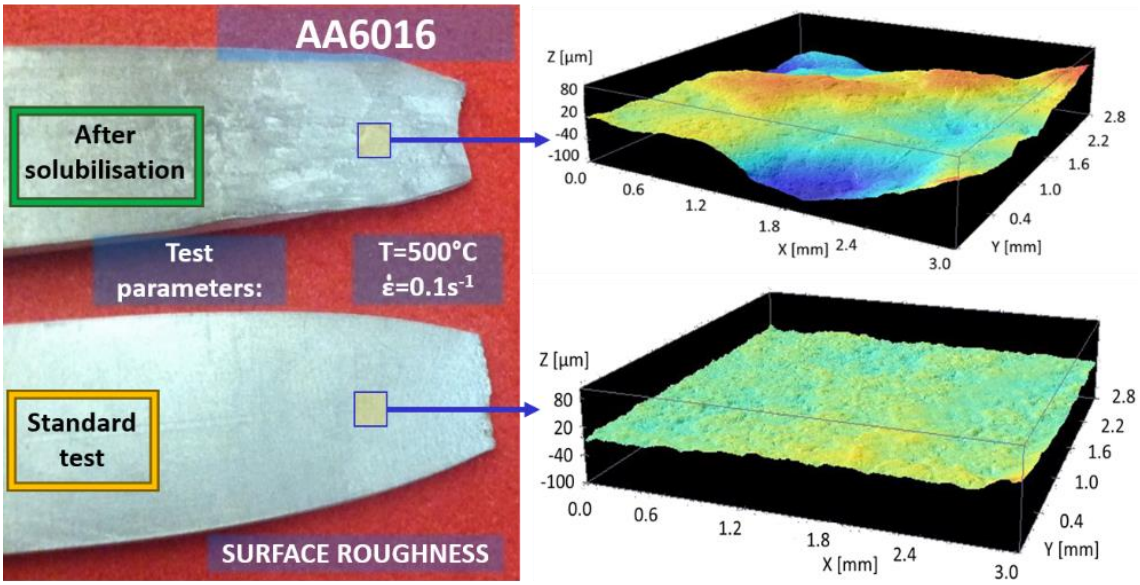

Figure 4.33: Surface topography of AA6016 solubilised and not-solubilised samples after deformation.

4.4.4 Microstructure evaluation after deformation

To investigate the influence of the temperature coupled with the deformation on the material properties, the microstructure evaluation on stretched specimens was performed to highlight grains size and dimension.

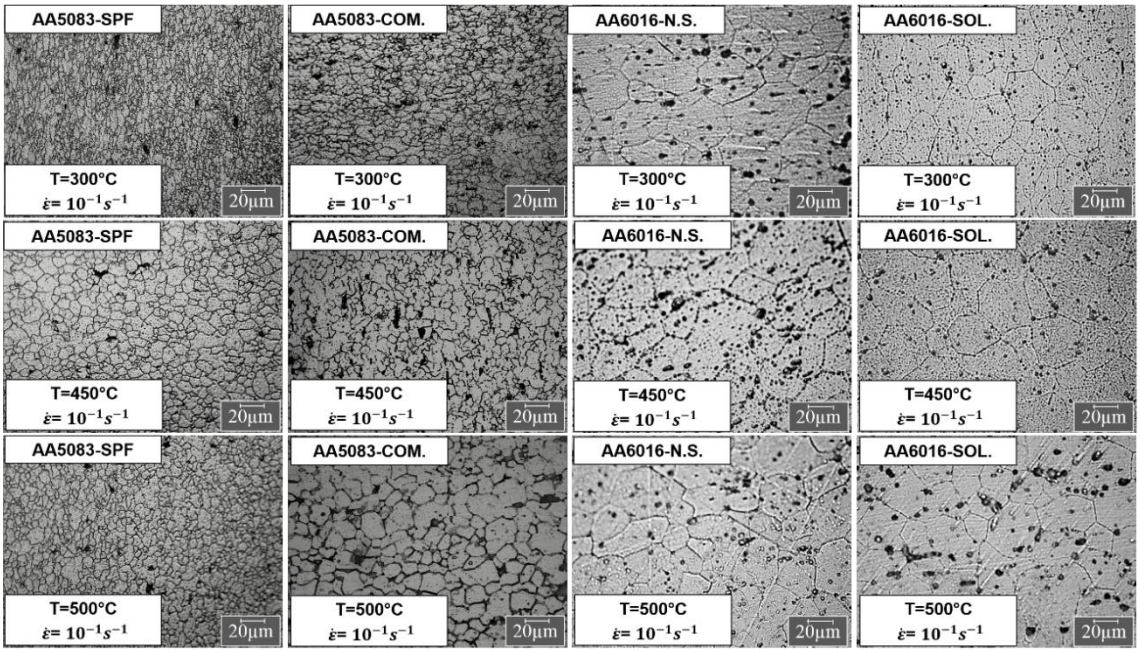

Figure 4.34: Microstructures after tensile deformation (indication of the deformation conditions and material is shown in the micrographs).

All of the micrographs presented in Figure 4.34, are relative to a strain rate equal to 10^{-1} s^{-1}. Regarding the AA50083 it can be seen that the commercial grade exhibits grain coarsening at 500 °C, whereas at lower temperatures the microstructure is similar to that at

room temperature, as shown in Figure 4.1. On the other hand, the superplastic grade shows a fine-grained structure at 300 °C, at which the mechanism of static recrystallization is not effective during the specimen heating, whereas at 450 °C the microstructure is fully recrystallized and an incipient grain coarsening is appreciable at 500 °C. When observed at 450 °C and 500 °C, the microstructure of the superplastic grade is finer than that of the commercial grade, as a proof of the higher values exhibited in the micro-hardness measurements. Again, the microstructural observations confirm the quality of the optimal forming conditions, previously identified for the two alloys.

In the case of AA6016, no appreciable differences in the grain size and morphology can be seen in either of the solubilised material or in T4 condition, proving that the applied thermo-mechanical cycle does not change the initial material microstructure.

4.5. Validation of laboratory test results

In this section, two methods are presented which are used to verify the results obtained from the rheological characterization of the two aluminium alloys in terms of one-directional stress path through the hot tensile test. In the stamping operation it is known that the material is subject to different strain paths and stress conditions, so a validation test was performed in order to confirm the applicability of the best formability windows found in terms of temperature and strain rate to different strain paths.

In the case of 5xxx aluminium alloy, considering the comparable results in terms of true stress - true strain diagrams and post deformation analysis between the superplastic and the commercial grades, and also avoiding the extra-costs of the specific microstructure of the superplastic grade, the validation results were confined only to the commonly available alloy grade. Therefore, the aluminium alloy AA5083 in commercial grade was tested through the Nakajima test with an experimental apparatus designed in the laboratory. The temperature influences on formability were investigated, with the strain rate kept constant at 0.1 s^{-1} at which the hot tensile tests gave the highest values of strain at fracture.

Finally, all of the aluminium alloys and grades were subject to hot stamping trials to form an automotive component in a real hot stamping industrial plant using the best formability parameters, obtained through the laboratory tests. Industrial trials, are an important challenge aimed at providing a complete validation of the applicability of the Hot Stamping technology to form, under industrial process conditions, sound and accurate parts with microstructural and mechanical properties comparable with those of the as-received material.

4.5.1 FLD

The Forming Limit Diagram represents the deformation limit of a material taking in to account the major and the minor strain of a metal sheet stretched until break. During the so-called Nakajima test, the blank was fixed between a cylindrical die and a blank holder, and stretched over a punch while a draw bead prevents the sheet from being drawn into the die. To measure the strain values, an optical measure system Aramis™ by GOM, was used, as described in 4.3.1, in stereoscopic mode taking a photographic history of the deformation test

through two high definition CCD cameras. In order to vary the deformation strain path, metal sheet specimens were prepared with seven different geometry ratios, from 200 x 200 mm^2 to 200 x 30 mm^2. Thus, the centre of the square specimen produced equal biaxial stretching under the punch, whereas the specimen with a high geometry ratio approached a state of uniaxial stretching.

The testing apparatus according to ISO12004 [101], is shown in Figure 4.35, and allows one to heat the specimens to the testing temperature, and to deform at a constant temperature until failure. The set-up consists of a hemispherical punch of 100 mm in diameter and a blank holder mounted on a 200 kN hydraulic testing device with a controlled ram speed ranging between 0.01 and 150 mm/s. Cartridge heaters were inserted in both the hemispherical punch and the blank holder, in order to maintain the temperature of the blank constant during the experiments. A high frequency induction heating head was used to heat up the blank to the target temperature. The shape and the size of the induction head were designed for the control of the heating rate and the temperature uniformity with different blank geometries.

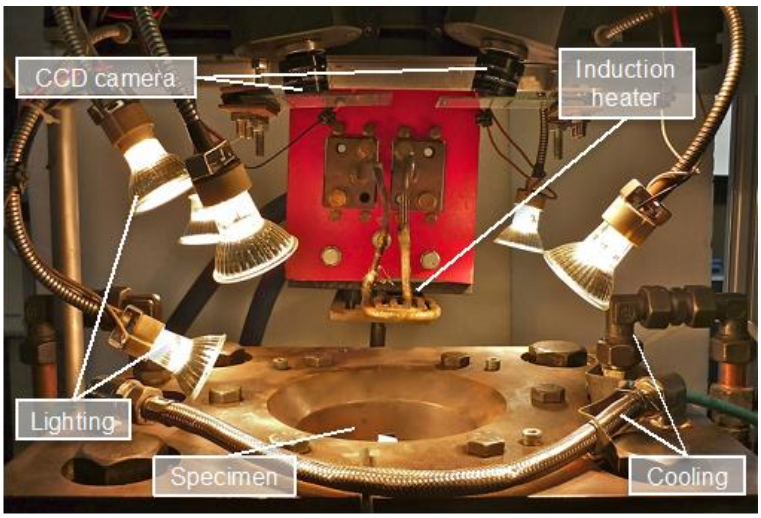

Figure 4.35: Experimental set-up for the Nakajima tests at elevated temperatures with details of the heating and the lighting devices.

The blank temperature was continuously monitored through three K-type thermocouples spot-welded, respectively on the centre, on the intermediate and the outer diameter of the blank surface deformed by the punch. During the test, the maximum difference among the temperatures at the three thermocouples was maintained under 5 °C. A 0.5 mm thick graphite foil between the sheet metal specimen and the punch was used as a lubricant. Further details on the experimental apparatus are reported in [24].

Each blank was heated at 10 °C/s to the testing temperature, and subsequently held at this temperature for 90 s for homogenization. Before straining, the inductor head was rapidly removed (within two seconds) by a pneumatic actuator, allowing the strain to be measured by the Aramis™ system, Figure 4.36.

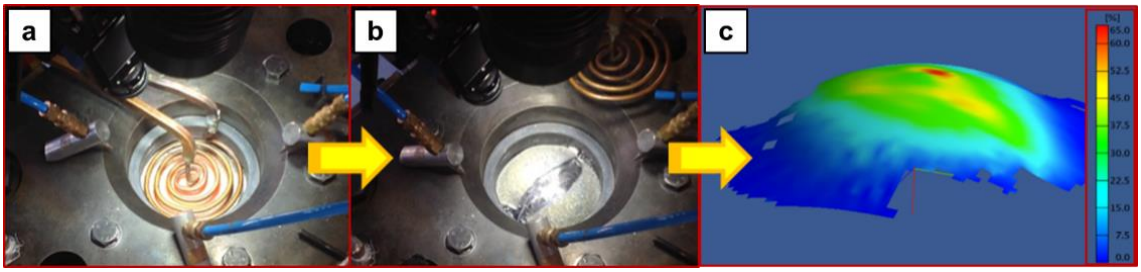

Figure 4.36: Nakajima test process sequence: specimen heating (a), specimen deformation (b), strain elaboration (c).

The testing conditions of the Nakajima test are shown in Table 4.7. The values were determined according to the results of the maximum formability window reported in 4.3.4 found through hot tensile tests.

Table 4.7: Experimental plan for Nakajima tests at elevated temperatures.

$\dot{e}$ [s^{-1}]	T [°C]			
10^{-1}	20	400	450	500

Figure 4.37 shows the AA5083 FLD sensitivity to temperature at a strain rate equal to 10^{-1} s^{-1}. It is possible to observe that the material formability increases significantly compared to room temperature, with the highest formability limits at 450 °C, in agreement with the results of the hot tensile test. In fact, at 500 °C (green line) stays below the red one line (450 °C) especially in region with negative minor strain. It is also worth noting the translation of the plain strain point in the right direction as the temperature increases. This phenomenon is due to the specimen thermal distortion during the heating phase, where blank holder and draw bead fix the metal sheet.

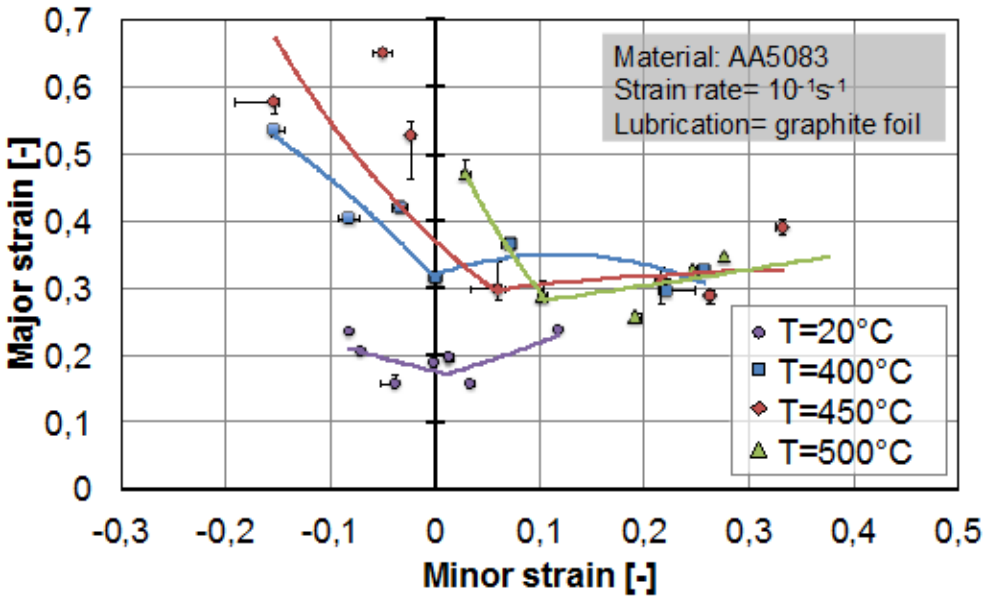

Figure 4.37: Forming Limit Diagrams of the AA5083 alloy at different temperatures for a strain rate of 10^{-1} s^{-1}.

4.5.2 Industrial trials

In the industrial trials, an under engine cover was hot stamped on an industrial hot stamping plant, consisting in a double effect hydraulic press and an external gas furnace for the blank heating. The forming dies were cooled through water channels to ensure part rapid cooling after forming. After heating, the blank was manually transferred to the press and its surface temperature monitored through an infrared thermo-camera. A surface temperature decay of approximately 30 °C was measured. The hot stamping trials were conducted at a temperature of 400 °C, 450 °C and 500 °C on blanks that were heated in the furnace at 430 °C, 480 °C, and 530 °C respectively. This compensates for the temperature decay during the manual transfer. In the case of AA6016 solubilised material, the initial blanks were kept in the furnace for 30 minutes at a temperature of 550 °C to ensure the complete dissolution of the precipitates. The average strain rate of the trials was in the range $10^{-1}s^{-1}$ to $1s^{-1}$.

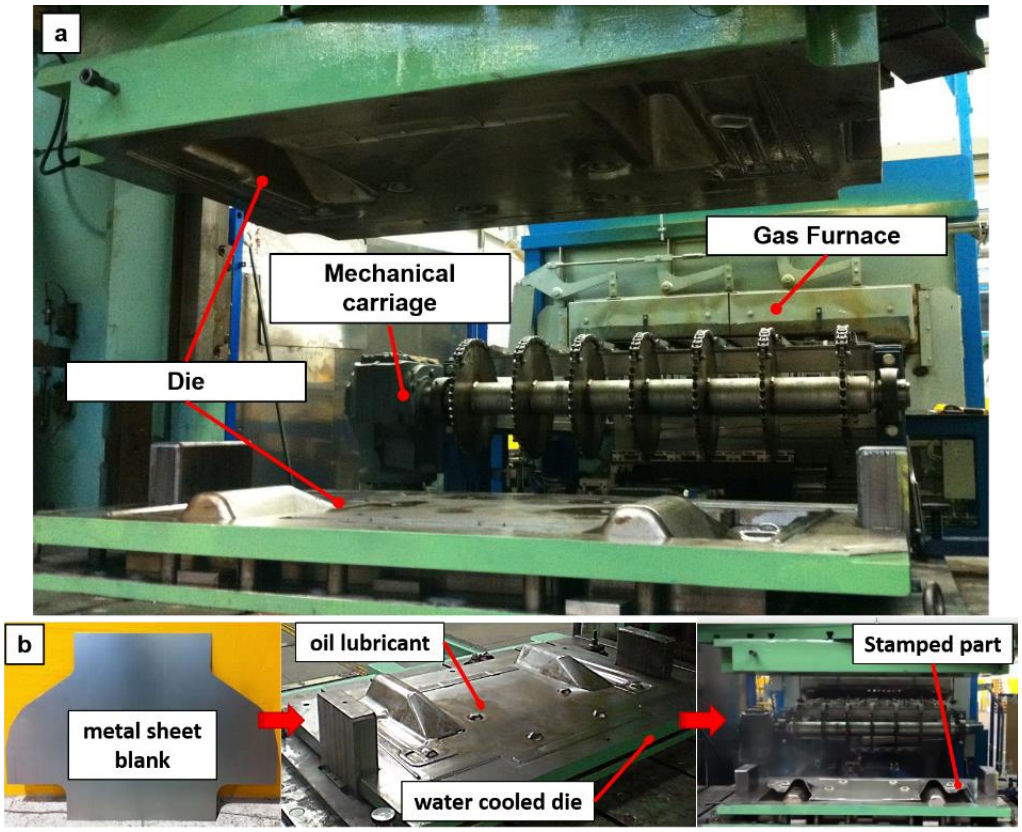

Figure 4.38: Industrial Hot Stamping press with gas furnace and mechanical carriage (a) and Hot Stamping sequence (b).

Regarding the AA5083 stamped parts, as expected comparable results were found between the commercial and the superplastic grade, as found with hot tensile test and the post forming analysis. Figure 4.39 shows the microstructure and the Vickers hardness evaluated at the three testing temperatures in two areas of the AA5083 commercial component where the material was most heavily deformed. At both the forming temperatures of 400 °C and 500 °C failures were detected in the component. Moreover, at 500 °C, the component microstructure is much coarser, with a decay of the mechanical characteristics. However, at the forming temperature of 450 °C the component was sound, with microstructural and mechanical characteristics comparable with those of the as-delivered blank material.

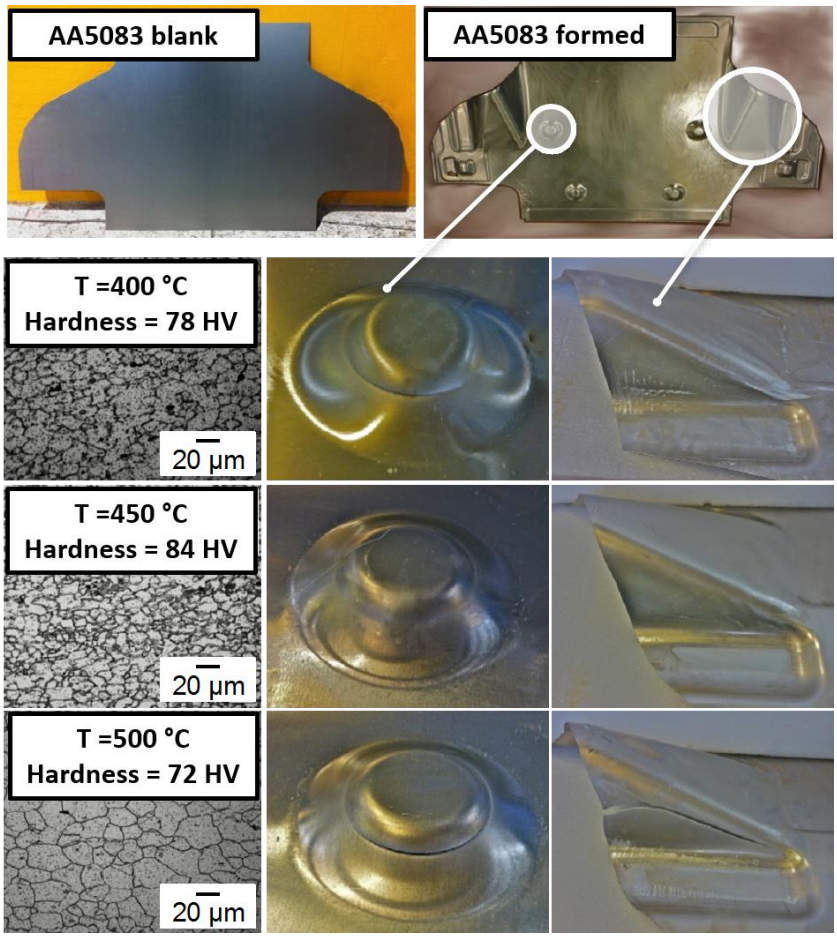

Figure 4.39: The AA5083 commercial industrial component before and after the deformation, with details of the microstructures, the Vickers hardness and the most critical areas at different forming temperatures.

Considering the other aluminium alloy series studied, sheets subjected to both the heat treatments previously considered, namely solubilised and non-solubilised, were tested. Figure 4.40, shows the different results obtained for the two heat-treated blanks: not-solubilised (a) and solubilised (b). As predicted by the laboratory tests, no failures were appreciable in the stamped parts, but a completely different surface appearance was shown to be visible to the eye. Figure 4.40, shows also that in both cases the stamped part microstructures are not affected by grain coarsening.

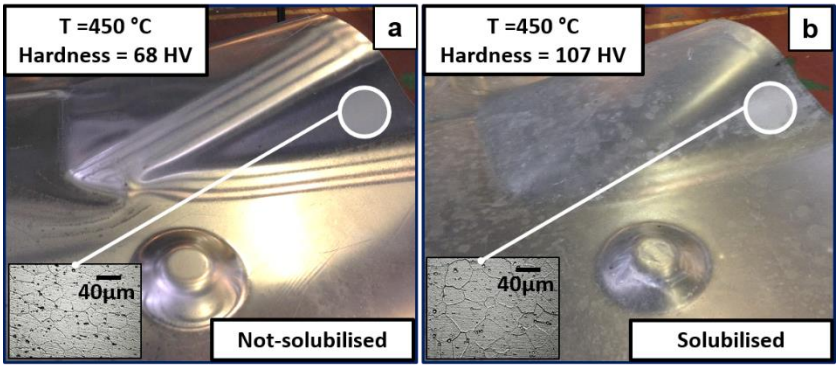

Figure 4.40: Hot stamped part: not-solubilised condition (a), and solubilised condition (b).

It is worth noting the outstanding increment of the hardness parameter for the solubilised condition. This behaviour is due to the natural ageing of the material after precipitates dissolution during the solubilisation heat treatment. In fact, hardness measurements and microstructure observation were performed four weeks after the hot stamping trials.

4.6. Conclusions

This section will summarise the main results regarding the study of formability of two different aluminium alloys automotive series, AA5083 and AA6016, in two different grades: superplastic and commercial for the first one and T4 and solubilised for the second one, deformed applying the Hot Stamping process on aluminium alloy.

An evaluation of as-delivered material was performed in order to verify the microstructure through optical observation and to understand its variation when subjected to different thermal cycles. These analyses have provided evidence for how the superplastic grade of the AA5083 disappears at process temperature of 400 °C with relative low heating time, changing its microstructure as the AA5083 in annealing and commercial condition. Moreover solution heat treatment performed at 550 °C on AA6016 has proved that the complete dissolution of the Mg_2Si precipitates on aluminium matrix.

From these results, hot tensile test were performed on both alloys in both grades, using temperature and strain rate typical of the Hot Stamping process. Deformation measurement was realised through an optical measure system allowing the calculation of the true stress-true strain diagram, while the accurate measuring of the fracture surface, by means of electronic microscope, has facilitated the creation of a three-dimensional formability diagram for each material. Indeed, strain at fracture, used as formability parameter, was plotted together with temperatures and strain rates used during the hot tensile tests. Subsequently, post-forming material properties were investigated in terms of micro-hardness measurement, microstructure evolution after forming and surface fracture morphology. Higher values of strain at fracture were found in the AA6016 compared to the AA5083, proving that 6xxx aluminium series is more suitable for hot stamping operations, while interesting behaviour has been revealed comparing the AA5083-SPF with the AA5083-O where no relevant differences in terms of formability were uncovered. Indeed, true stress-true strain differences were highlight only at room temperature, as expected, and at 300 °C warm temperature at highest (10^0 s^{-1}) and lowest (10^{-2} s^{-1}) strain rates, where the superplastic alloy has displayed a very high stress value compared to the commercial grade. At the best forming condition of 450 °C and 10^{-1} s^{-1}, materials behaviour (considering also the post-forming analysis) are comparable which suggests an industrial choice of the cheaper material condition, namely the commercial condition. Concerning instead the Al-Mg-Si alloy, results have shown that after a solubilisation heat treatment, the material appeared more ductile especially at low temperature. At best the forming condition found for this alloy at 450 °C - 500 °C and strain rate 10^{-1} s^{-1}, strain at fracture values were comparable. An important aspect has emerged by observing the surface morphology after heat treatment, which is too rough to be suitable for aesthetic parts characteristic of automotive industries.

The validation of laboratory tensile test was performed for the AA5083-commercial alloy by investigating the behaviour at different strain paths through a prototype Nakajima test

apparatus at the University of Padua engineering laboratory. A fixed strain rate of 10^{-1} s^{-1} and different temperatures test have allowed the production of a FLC diagram for the studied material, confirming a best formability temperature of 450 °C. Fracture surface analysis on both aluminium series have proved that at lowest strain rate and highest temperature the fracture mechanism of cavitation, typical of the GBS deformation mechanism, brings the material to an early rupture compared with that found at higher strain rate where a ductile fracture, with dimples and connected to the SD deformation mechanism, appeared.

A final evaluation was performed stamping a real automotive component (under engine cover) in collaboration with an Italian automotive industrial partner, in a hot stamping industrial implant. AA5083 and AA6016 sheets in both conditions were stamped using the best forming parameters obtained from laboratory test. With regards to the AA6016 in solubilisation condition, a rough surface quality was confirmed. Optimal surface quality was instead obtained by stamping the part at 450 °C without thermal treatment and using strain rate in the range from 10^{0} s^{-1} and 10^{-1} s^{-1}. AA5083, even though it exhibited lower formability, was successfully stamped using a temperature of 450 °C and the same ram speed applied for the AA6016. However, stamping temperatures of 500 °C and 400 °C coincided with part failure especially in locations where high deformation was requested.

In conclusion, it is possible to use cold dies to shape aluminium alloy parts at elevated temperature and high strain rate, under hot stamping process conditions. Hot Stamping technology applied on aluminium alloy sheets can decrease drastically the time cycle to produce an aesthetic automotive component in only one stamping operation, conserving also the initial mechanical properties in terms of hardness and microstructure. The cheaper AA5083 commercial grade can be used for hot stamping operation instead of the expensive superplastic grade obtaining the same component results. For a heat treatable aluminium alloy such as the AA6016, high deformation at high strain rate performed immediately after a solubilisation heat treatment involved in rough surface quality, not usable for an aesthetic component. On the other hand, the non-solubilised hot stamped parts present an optimal surface quality and respect very well the final shape without defects. Therefore, results obtained through mono-tensile test are correlated with an accurate analysis of the material behaviour in terms of process parameter, namely the temperature and strain rate, and microstructure evolution before and after deformation, can be extended as process parameters for realising a real industrial aluminium component through Hot Stamping.

Chapter 5

Hot gas forming of aluminium alloy tubes

This chapter describes the design of an experimental apparatus developed to reproduce the innovative Hot Metal Gas Forming process (HMGF), able to bulge aluminium alloys tubes at high temperature through cold gas under pressure. The aim is to evaluate in depth the potential of the process in terms of the forming capability of hollow components at high temperature, reducing the deformation time cycle compared to the common hydroforming process. The mechanical description of the prototype will be described, followed by an explanation of the thermal tests aimed at building an understanding of how the chosen heating system operates in relation to heating the tube specimen. Afterward an explanation of the process control software developed in the LabVIEW® environment will be described. Subsequently, there is a description of the tests performed on two different aluminium alloy 6xxx series tubes, namely AA6082 and AA6060, carried out to evaluate the possibility of studying the tubes' formability, through bulging-up operation in free air. Tubes of aluminium 6xxx series were chosen for their higher formability characteristic, which was proven in the rheological studies presented in the Chapter 4, compared with other automotive aluminium alloys series such as the 5xxx. Moreover, these formability tests were used to validate the functionality of the experimental apparatus design. Lastly, some studies are presented which evaluate the possibility to bulge-up tubes inside a die, creating components with a desired shape. The first one uses a square die, which allows the investigation of the influence of process parameters such as temperature, pressure and die material on the obtained part. The second one is shaping a complex industrial component, created in advance by machining, in

collaboration with Anodica Industries™ which works in creation of aluminium anodised handles.

5.1. The experimental apparatus

This paragraph explains in depth the design of the Hot Metal Gas Forming experimental apparatus. The main aim was to design a simple apparatus in order to guarantee the functionality of the process and so satisfying some necessary characteristics:

- High tube temperature;
- Load pressure inside the tube;
- Capability of testing different tube lengths and diameters;
- Operator safety.

For this reason, a description is given of the heating system choice to increase tube temperature, as well as a description of the design of each mechanical component and their functionality inside the assembled apparatus. Finally, the results of preliminary heating tests are shown, which were performed to verify the experimental apparatus functionality.

5.1.1 Heating system

In choosing the technology for heating the tubes, one consideration was the requirement to quickly heat up a hollow component in non-ferromagnetic material (aluminium). Even if the induction technology was capable of quickly and locally heating with high accuracy magnetic and also non-magnetic material (especially using very high working frequencies 200 - 400 kHz), it presents the problem of needing a solid fixed induction head, located near the component to be heated. Also, for the process dynamicity, the increase of external tube diameter should be followed by an induction head modification for keeping the distance constant between the tube surface and the inductive coil. Indeed as is well known, this distance is a key factor for the amount of current flowing in the material and so for the heating generated on the component, as shown in, Figure 5.1. Moreover, heating the tube with an induction system complicates the possibility of using a die because requires the induction coil removing, before applying the die matrix.

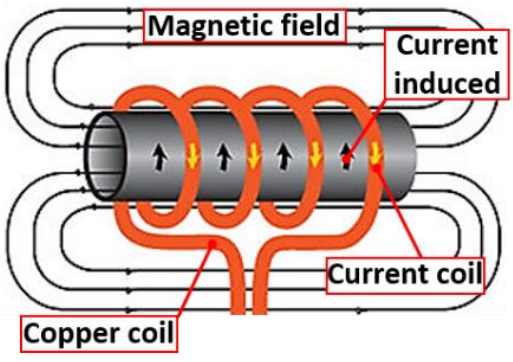

Figure 5.1: Scheme of the induction system functionality on a tube component.

For all of these reasons, the heating technology used in this experimental apparatus uses the electric current flow, exploiting the Joule effect. In fact, in this case, the two electric poles placed on tube extremities allow the electric current flow along all tube length through its cross-section. Therefore, all the space around the specimen is free and usable for a die structure.

The electrical power needed to generate the tube heating is given through an external current generator, composed of six modules that provide a maximum power of 60 kW, with a low voltage of 10 V and a high continuous current of 6000 A, as shown in, Figure 5.2.

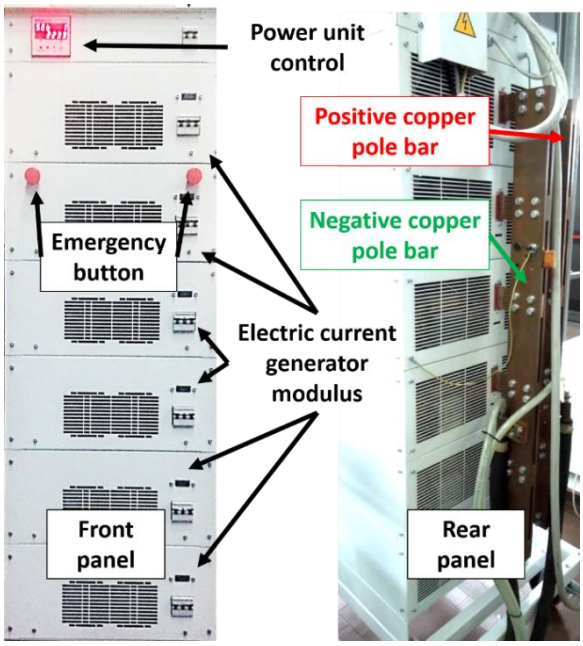

Figure 5.2: Electric current generator with a total power of 60 kW.

The same generator allows for an in line current intensity control with an accuracy of 1 A that can work in a local mode operation in which one can vary the current intensity manually, or in a remote control in which one can regulate the amount of current using an analogical signal in a range from 0 to 10 V. All of the power produced from the electric source it is passed from the generator to the tube through two flexible electric cables. An internal water-cooled canal for keeping the temperature in the usable range characterises the internal structure, as shown in Figure 5.3. This design solution allows one to test different tube lengths, because one copper jaw electrode is fixed while the other can get in position with tube length.

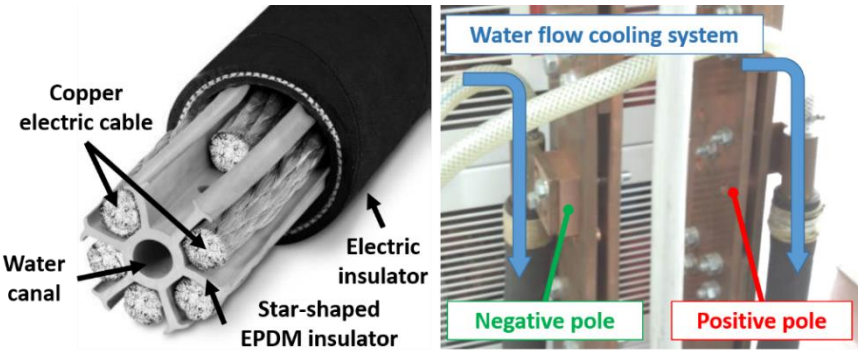

Figure 5.3: Structure of the water cooled electric cables used to handed on electric current from the electric generator to the tube.

The cooling system is composed by water re-flow with a heat exchanger used to maintain the demineralised water at a temperature of approximately 24 °C.

The connection between the tube extremities and each electric cable is performed using two copper jaw half components with thickness of 35 mm and internal hemispheric section depending on tube external diameter, as shown in Figure 5.4.

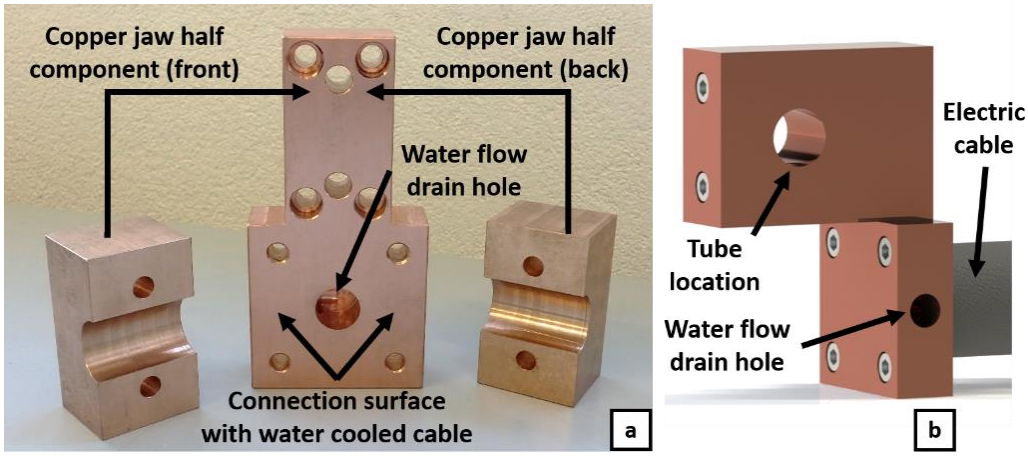

Figure 5.4: Copper jaw components (a) and assembled jaw (b).

5.1.2 Mechanical design

A steel frame composes the main body of the experimental equipment. A plate, with a length of 960 mm, a width of 360 mm and a thickness of 20 mm, represents the base to where all the other frame parts are fixed. To guarantee the possibility of testing different tube lengths, two parts of the steel frame are fixed, whilst a third part is situated in the middle and is able to move along two quenched chromed linear rails with a diameter of 20 mm, as shown in, Figure 5.5. Therefore, one extremity of the tube is fixed while the other is localised on the mobile plate, which allows the use of different tube lengths.

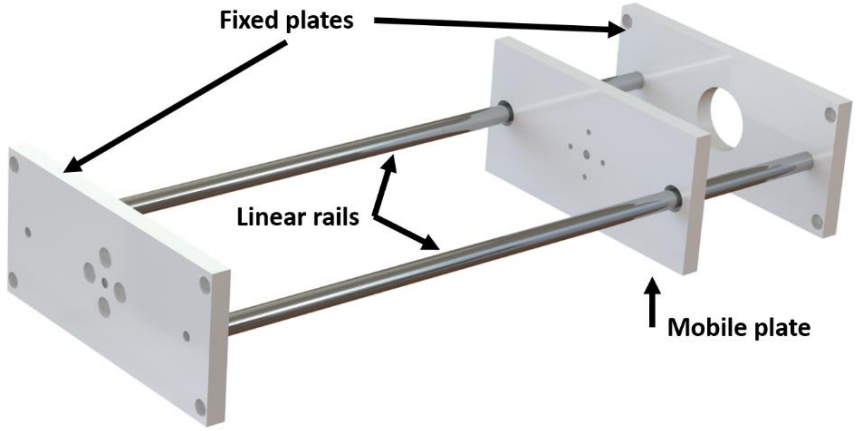

Figure 5.5: Steel frame principal structure used to test tubes with different length.

The frame dimension allows one to load tubes with a maximum length of 500 mm and an external diameter of 40 mm, taking into account a maximum tube diameter expansion during the heating process of 150%. Moreover, the apparatus exhibits an inter-axle distance of 240 mm between the two linear rails to allow the possibility of using a die during the process. The

fluency of the mobile plate is assured by two linear ball bearings (model KH2030-PP), which have the properties reported in Table 5.1.

Table 5.1: Mechanical and geometrical characteristics of the linear ball bearings model KH2030-PP.

Model	n° balls	D int. [mm]	D ext. [mm]	L [mm]	Load din. [N]	Load stat. [N]	Weight [kg]
KH2030-PP	6	20	28	30	990	815	0.034

One of the fixed plates is characterised by a central hole with a diameter of 70 mm, as shown in Figure 5.5, created for a future possible implementation of an axial actuator for assisting the material flow during tube expansion, so helping the maintenance of the initial tube thickness whilst avoiding material stretching during the bulging process. Therefore, without an actuator, two manual brakes are implemented on the mobile plate in order to fix its position along the rails based on the length of the tube.

During the operation, the two linear ball bearings, are subjected to the two linear rails inflection, with the worst condition represented in Figure 5.6. Thus, their mechanical verification was evaluated using the representation of a bar fixed at the extremities and subjected to a local load in the middle point.

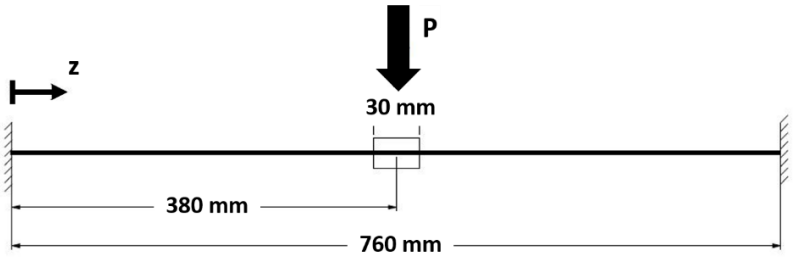

Figure 5.6: Structure representation of linear rail solicitation.

The total inflection quota and angle was calculated using the (eq. 5.1 and (eq. 5.2 considering the total weight supported by the two linear rails, due to the mass of the mobile plate inclusive of the two brakes and of one copper jaw, as reported in Table 5.2, and the mechanical and geometrical properties of one of the two linear rails, as shown in Table 5.3.

Table 5.2: Load supported by the two linear rails.

Component	Mass [kg]	Load [N]
Mobile plate	6.9	67.8
2 x brake	0.6	6
Copper jaw	3.8	37
Total load (+20%)	13.6	133

Table 5.3: Mechanical and geometrical properties of linear rails.

Component	I [mm^4]	E [MPa]	l [mm]	D [mm]
2 x linear rail	7850	210000	760	20

$$f = -\frac{\frac{P \cdot z^3}{12} - \frac{P \cdot l \cdot z^2}{6}}{E \cdot I} \quad \text{(eq. 5.1)}$$

$$\varphi = -\frac{dv}{dz} = \frac{\frac{P \cdot z^2}{4} - \frac{P \cdot l \cdot z}{8}}{E \cdot I} \quad \text{(eq. 5.2)}$$

$$C_0 = s_0 \cdot P \quad \text{(eq. 5.3)}$$

P = total load (+20%) [N]

z = quote of mobile plate location [mm]

l = total linear rail length [mm]

E = Young modulus [MPa]

I = moment of inertia [mm4]

C0 = static load coefficient [N]

s0 = factor of safety

An inflection angle of $6.34 \cdot 10^{-3}$ °/min, which was obtained by taking in to account a safety factor of 4 from the linear ball bearings data sheet, and a static load coefficient C_0 [N] obtained through the eq. 5.3, allowed the static load factor K_{F0} to be identified from Figure 5.7..

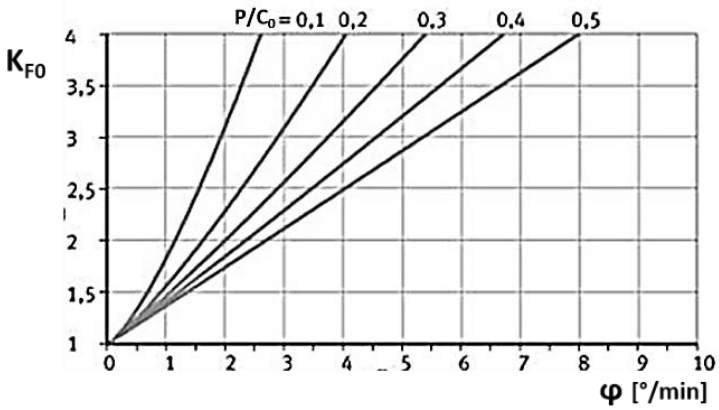

Figure 5.7: Static load factor diagram.

A static load result of 173 N during the process operation was calculated by multiplying K_{F0} with the total load (+20%). Compared the maximum static load supported, shown in Table 5.1 this verifies the linear ball bearings resistance and therefore the satisfactory mobility of the middle plate.

The primary structure is connected to the main plate through triangular supports, which, if required, can be rotated for increasing the space between the fixed and the mobile plate, allowing tests on tubes longer than 500 mm. The entire assembled structure of the prototype frame is shown in Figure 5.8, where the principal dimensions are also reported.

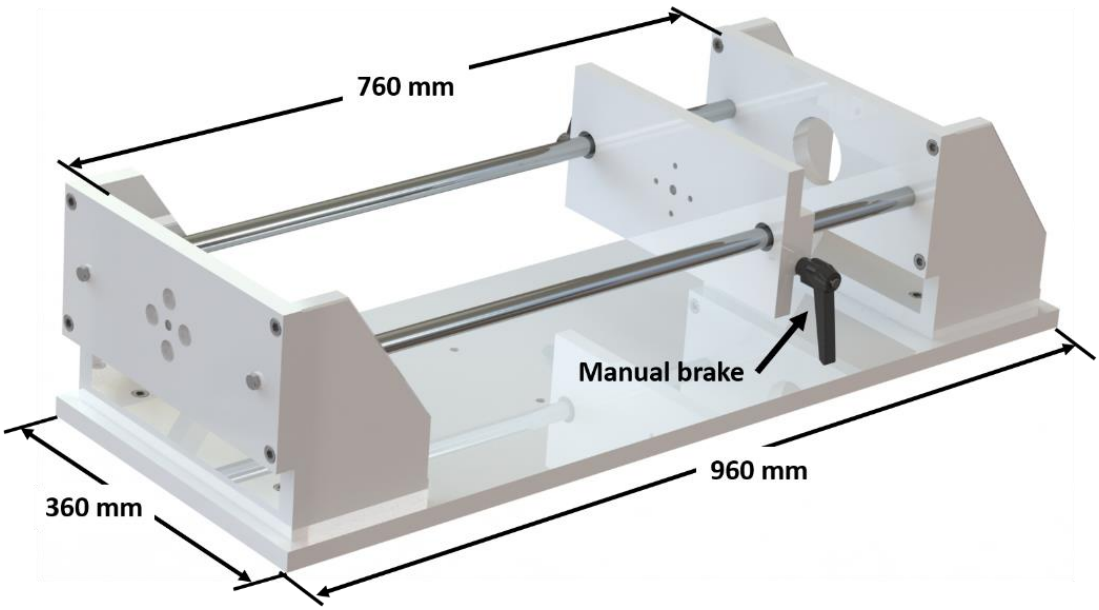

Figure 5.8: Experimental apparatus mechanical structure.

Adequate support for the tubes during the test is guaranteed by two cylindrical bushings made from the AISI 310 material, one for each tube extremity, each with an external diameter equal to the internal tube diameter. Two o-ring grooves on each cylindrical bushing, which are required to guarantee the tube sealing, are also machined.

The electrical insulation between the steel frame and the two cylindrical bushings directly in contact with the tube, heated through high electric current, is provided by polyether-ether-ketone (PEEK) cylindrical elements with a diameter of 80 mm, as shown Figure 5.9.

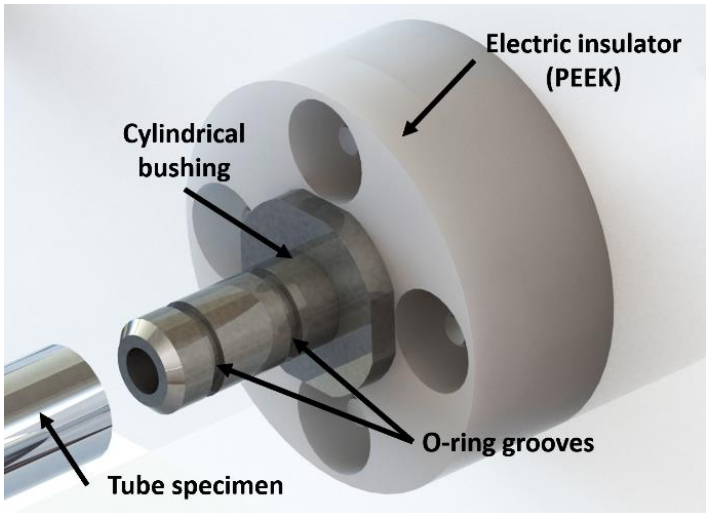

Figure 5.9: Detail of cylindrical bushing and of electrical insulator.

Finally, cold pressurised gas, with an output maximum pressure of 20 bar, is used to bulge the heated tube during the test. An external compressor is used to arrive at the target pressure, as shown in Figure 5.10 (a), while a manual pressure regulator allows the air pressure to be controlled in the range 1 to 20 bar. For an accurate pressure measurement, a digital pressure measurement is integrated allowing an accuracy of 0.01 bar, as shown in Figure 5.10 (b).

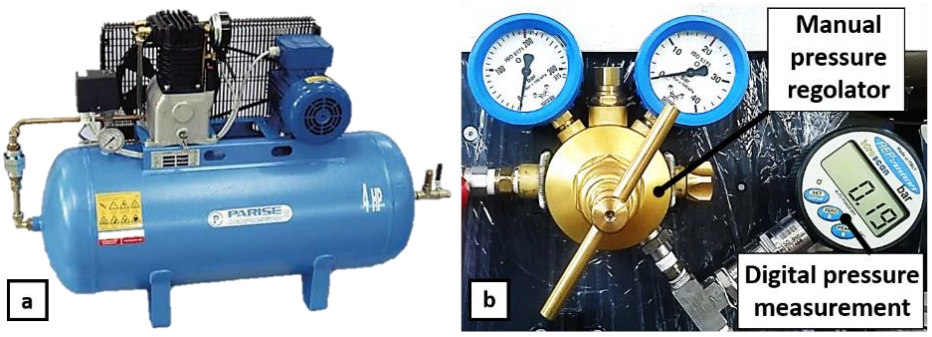

Figure 5.10: Air compressor system: 20 bar compressor apparatus (a) and manual pressure regulator and digital measurement (b).

The complete prototype is presented in Figure 5.11, showing each of the components which have been detailed in this section.

.

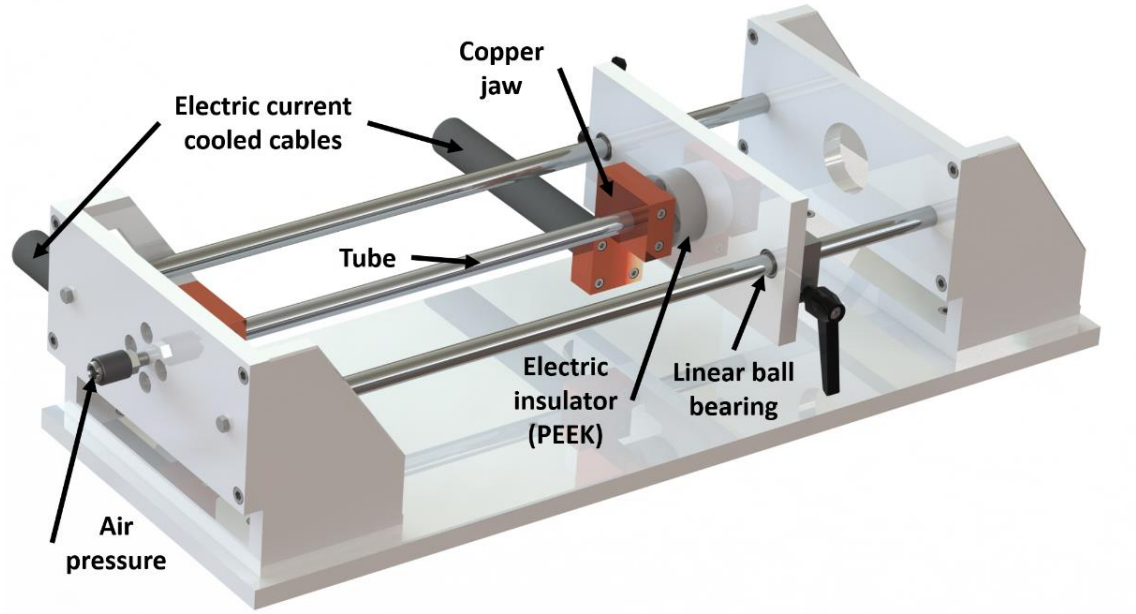

Figure 5.11: Hot Metal Gas Forming prototype.

5.1.3 Preliminary heating tests

To evaluate the working of the prototype, especially in tube heating stage, some heating trials were performed on AA6060 tubes, which were obtained through direct hot extrusion and with chemical composition reported in Table 5.4.

Table 5.4: Chemical composition of AA6060 tube used for preliminary heating test.

Si	Fe	Cu	Mn	Cr	Mg	Zn	Ti	Al
0.41	0.19	0.15	0.016	0.012	0.42	0.016	0.00	balance

Each specimen was cut at the required dimension from 6 m extruded tubes. For the experiments, each specimen exhibited an outer diameter of 30 mm and an average thickness

of 1.5 mm. Four different tube lengths were studied; 203 mm, 265 mm, 327 mm and 390 mm respectively. Figure 5.12 shows the drawing of the specimen. The experiments were focused on the assessment of electric current intensity effects on tube temperatures distribution, with and without pressurised gas application.

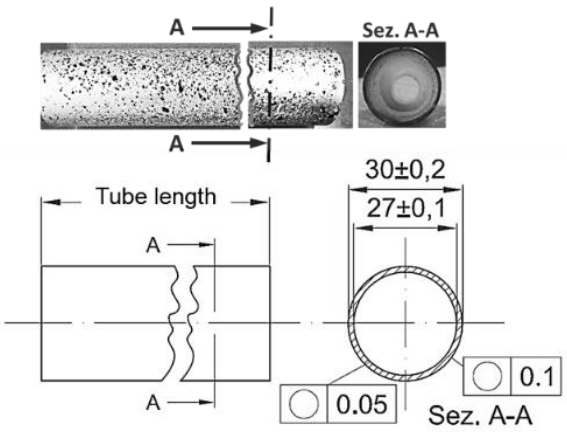

Figure 5.12: Tube dimension used for heating test.

During the tests, the temperature distribution caused by the electric current intensity on the outer surface of the tube was monitored through a thermo-camera measurement system. Theoretically, a constant thickness on a component permits a homogeneous current density flux and so, a uniform temperature. Instead, the electric connection on the tube extremities, operates as two cool sources, generating an inverse parabola temperature profile.

As illustrated in Figure 5.13, during thermal tests, the temperature gradually becomes non-uniform along the tube length at higher temperature. The highest temperature values show a uniform thermal length from 40 mm to 50 mm in the middle zone of the specimen, depending on the tube length. To guarantee an optimal temperature control during the heating phase, a pyrometer, with an accuracy of ±0.01 °C, was pointed at the outer surface of the tube during the heating and the bulging of the specimen, allowing a localized temperature measurement..

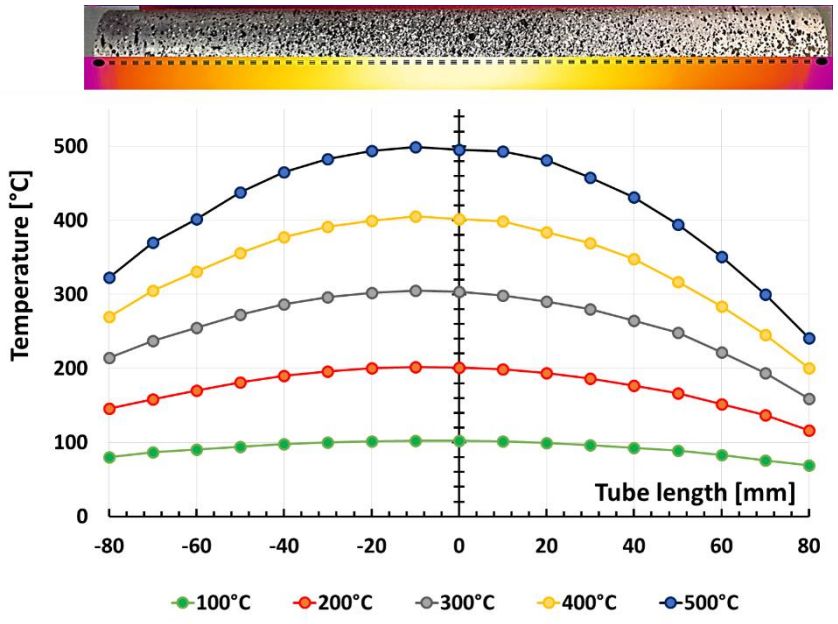

Figure 5.13: Temperature distribution measured through Flir™ Thermo-Camera.

To evaluate the real correlation between the electric current emitted through the power generator and the temperature reached on the tube surface, several thermal tests were done at different current intensity values. In doing so, at the beginning the current value was imposed and applied until tube temperature was stable. Table 5.5 shows the results of thermal tests where, as expected, the correlation between the temperature and the current is given by an exponential law as the material electrical resistivity increases with the temperature, as shown Figure 5.14 for a tube length of 390 mm. In this type of test, the time necessary to arrive at the target temperature using a constant current value was approximately 300 seconds.

The preliminary heating tests provided evidence of limitations of the methodology described above to heat the tube, in particular: (i) inaccurate control of heating rate, (ii) long process time required to calibrate the heating parameter and (iii) the temperature-electric current correlation law changes with the tube length and material. For this reason, a real-time closed-loop control, based on the measured temperature, was implemented allowing one to control the heating rate and to keep the target temperature constant in the bulged area.

Table 5.5: Correlation between thermal and electrical parameters.

Tube length = 203 mm					
Temperature [°C]	100	200	300	400	500
Current Intensity [A]	1350	2000	2350	2610	2820
Voltage generated [V]	1.48	2.23	2.65	3.00	3.30
Voltage to copper electrodes [V]	0.12	0.19	0.25	0.30	0.37
Tube length = 265 mm					
Temperature [°C]	100	200	300	400	500
Current Intensity [A]	1000	1400	1650	1860	2040
Voltage generated [V]	1.28	1.75	1.98	2.23	2.74
Voltage to copper electrodes [V]	0.17	0.23	0.26	0.29	0.36
Tube length = 327 mm					
Temperature [°C]	100	200	300	400	500
Current Intensity [A]	900	1300	1510	1720	1910
Voltage generated [V]	1.14	1.58	1.85	2.13	2.50
Voltage to copper electrodes [V]	0.23	0.29	0.34	0.40	0.47
Tube length = 390 mm					
Temperature [°C]	100	200	300	400	500
Current Intensity [A]	800	1200	1400	1600	1770
Voltage generated [V]	1.05	1.50	1.82	2.07	2.35
Voltage to copper electrodes [V]	0.25	0.31	0.40	0.48	0.57

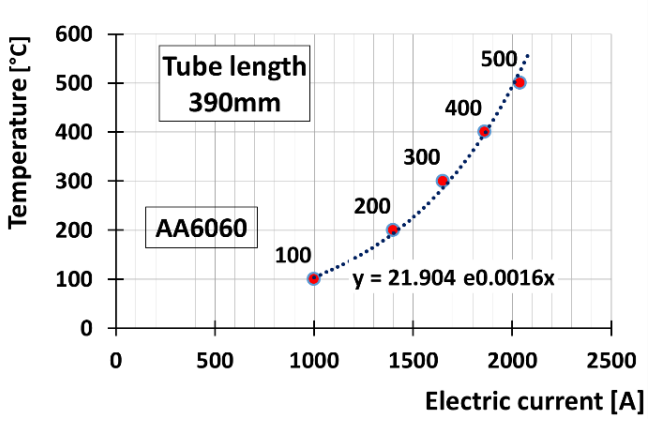

Figure 5.14: Exponential law correlating temperature and electric current parameters for tube length of 390 mm.

In doing this, it was possible to use all 6000 A available to heat the aluminium tubes to the target temperature; reducing drastically the heating time cycle to 11 seconds to reach 550 °C. Through this control the electric generator automatically reduces the supplied current in order to keep the specimen temperature constant. Moreover, an additional temperature measurement was implemented for monitoring the air temperature inside the tube through a sealed K-thermocouple fixed in the middle tube location without touching the inner surface. The evaluation of internal tube temperature dropping during the air inflating can be monitored.

Furthermore, in case of using a close die, internal air temperature becomes a reliable measurement while the optical pyrometer becomes unusable. Figure 5.15, shows the temperature trend measured by the pyrometer and by the sealed thermocouple respectively for the external tube surface and for the internal tube air, using an electric current of 6000 A. As expected, the air temperature trend appears completely different compared to the tube surface because it needs more time to heat up.

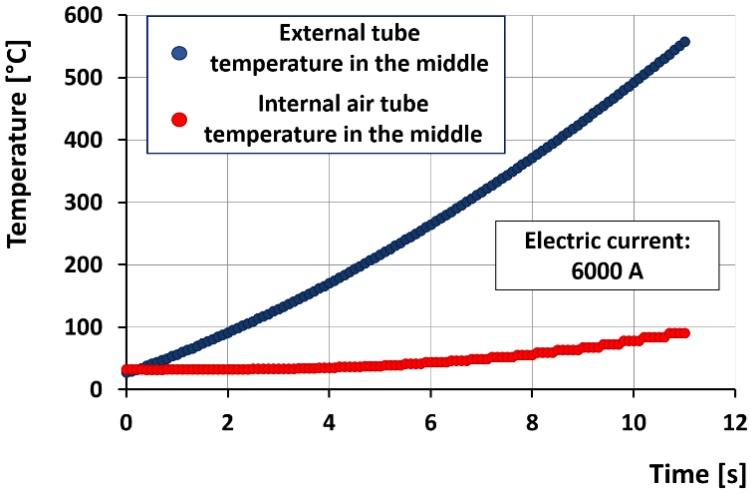

Figure 5.15: Time necessary to heat up tube at 550 °C using 6000 A.

Finally, the evaluation of electric tension dispersion was analysed by measuring the voltage with a multimeter at the tube extremities on the copper jaws. The comparison between these measurements and the voltage supplied by the current generator demonstrated a power loss

of 75%, as shown in Table 5.5. This behavior is due to the long water-cooled cables used to provide the electric power from electric generator to the tube.

The observation of the thermal distribution also demonstrates the importance of having a tube constant section distributed along its length. In fact, Figure 5.16 highlights the temperature distribution applying an inverse current flow on the same tube, inverting the electric current poles. The temperature trend appears unsymmetrical due to the heating technology used, as different tube sections support different electric current densities increasing or decreasing the temperature locally.

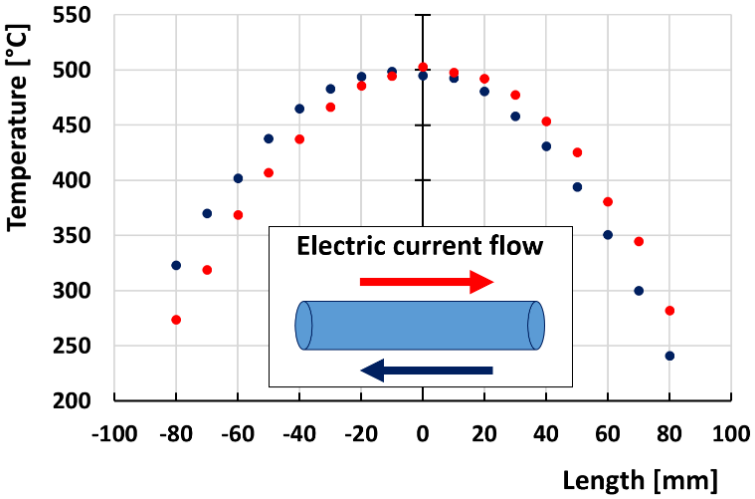

Figure 5.16: Temperature distribution evaluated changing the electric current flow direction.

5.1.4 Process control software

A process control software was developed in the LabVIEW® environment in order to: (i) regulate the real-time closed-loop control based on tube temperature, (ii) guarantee the repeatability of a process cycle in terms of tube temperature, time of heating, inflating time, and (iii) monitor and record all the temperature sensors.

In doing so, a cRIO-9022 was equipped with:

- NI AI 9205 analogic input module, used to capture voltage signal from the pyrometer in a range from 0 to 10 Volt;
- NI TC 9213 temperature input module, able to read 16 separated thermocouple channel with a shield signal;
- 2 x NI DO 9474 digital output module, used to send a signal to the electric generator for starting and stopping operation and to open and to close pneumatic circuits;
- NI AO 9263 analogic output module, used to regulate the electric current generator output in a real-time closed-loop control, based on the measured temperature.

The software was based on a machine state structure, as shown in Figure 5.17, split in five sequences:

- Data parameter input;
- Die heating stage;
- Tube heating stage;
- Tube temperature homogenisation and air inflating;
- Data saving.

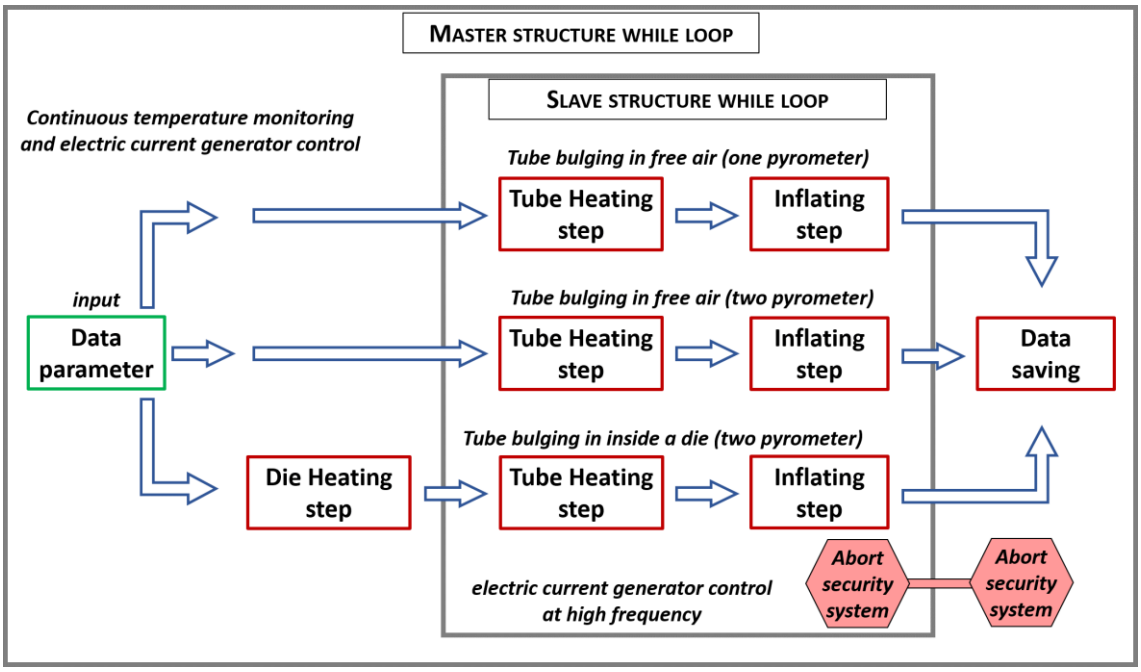

Figure 5.17: Block diagram of the state machine structure created for the HMGF control software.

The first step, as shown in Figure 5.18, is choosing the principal process parameters as the tube target temperature and the time heating. Moreover, an activation button is implemented for the die heating, for the bulge test inside a die, and the switch for using one or two pyrometers.

Furthermore, two auxiliary controls are dedicated to enable or disable the automatic inflation start and the security control on temperature threshold, based on the internal air temperature.

Regarding formability test using die, temperature control is included, with the possibility to regulate the heating time and the initial die temperature, useful in case of tests in series where the die is kept at warm temperature.

Finally the values of the P.I.D. control are implemented, which are used to regulate the electric current power generation using the real-time closed-loop control.

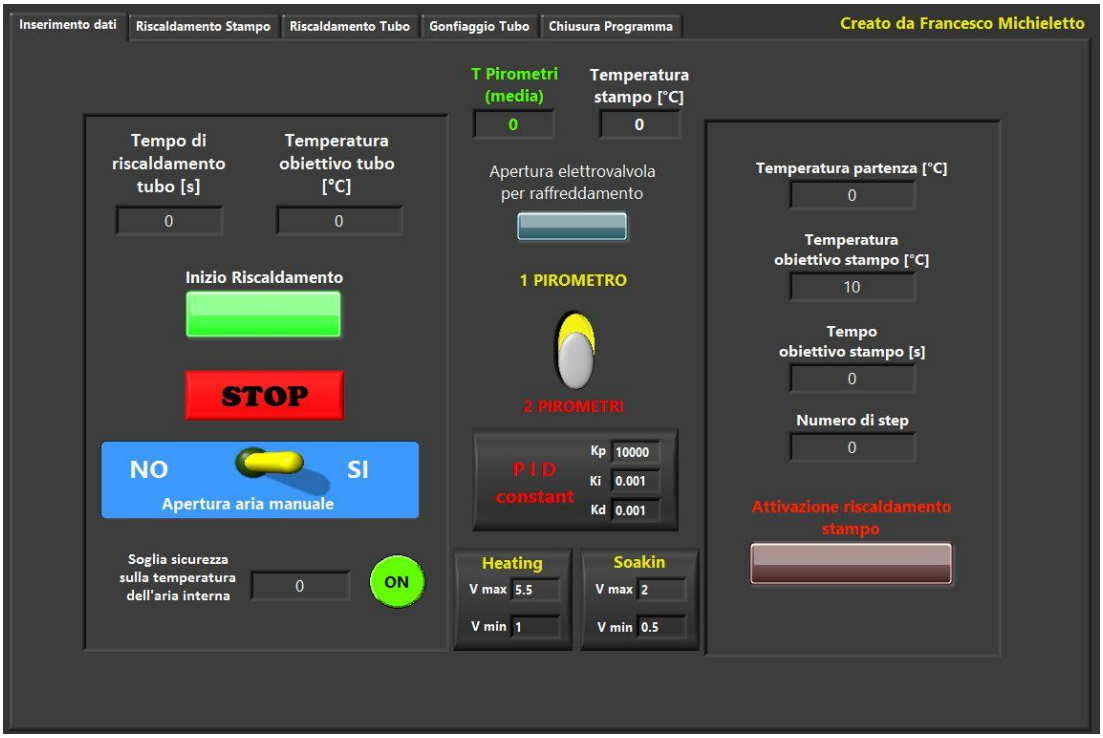

Figure 5.18: Front panel of process parameters input step of the HMGF control software.

The function of the second step, as shown in Figure 5.19, is to monitor the die heating and appears if activated in the first step. Die heating is performed by electric heaters activated through relays excitation, while the temperature measurement is performed using three K-thermocouples. In this panel, as shown in Figure 5.19, the possibility of enabling and disabling the automatic control is implemented.

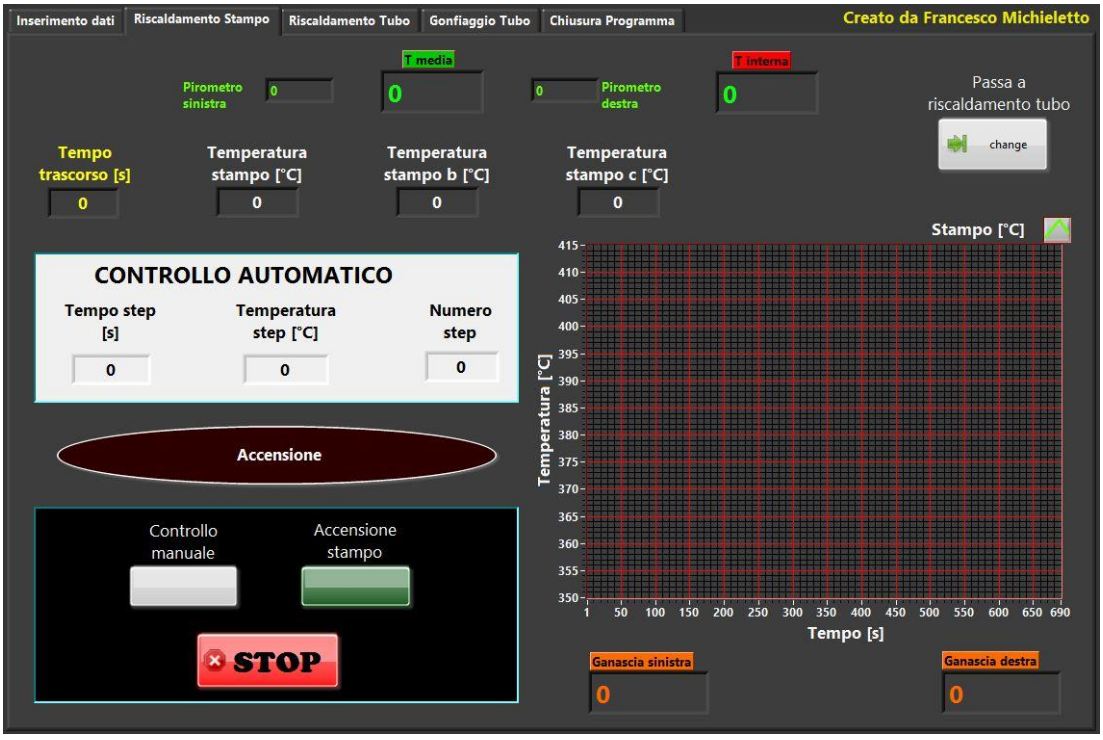

Figure 5.19: Front panel of die heating step of the HMGF control software.

Regarding the tube heating, the third panel shows the temperature trend of the external tube surface measured through one or two pyrometers. In addition the air temperature is monitored inside the tube with a sealed K-thermocouple. Die temperatures and copper jaws temperatures, used to understand possible asymmetrical temperature distributions, are also shown. The amount of current provide by the electric generator is reported inclusive of a blue led indicating when it is working.

The same graphic appears during the inflating step, combined with the possibility to manually enable the air pressure and an additional pneumatic circuit, which could be used for cooling operations, as shown in, Figure 5.20.

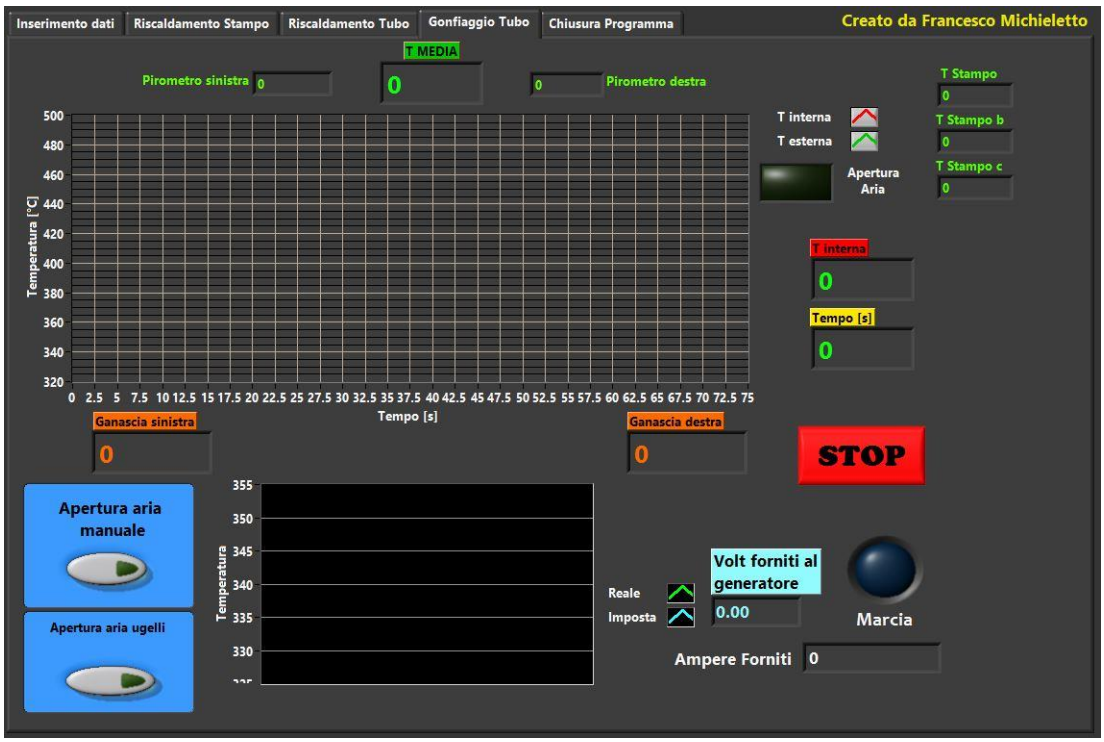

Figure 5.20: Front panel of the inflating step of the HMGF control software.

The final panel is only use to close the program and save the results monitored from the first instance of the process. Data are summarised in an excel file with parameters reported in Table 5.6.

Table 5.6: Data recorded by the process control software.

Time [s]	Die temperature 1 [°C]	Die temperature 2 [°C]	Die temperature 3 [°C]	
Time [s]	Tube surface temperature 1 [°C]	Tube surface temperature 2 [°C]	Tube surface average temperature [°C]	Tube internal air temperature [°C]

Time [s]	Copper jaw right [°C]	Copper jaw left [°C]

5.2. Tube formability evaluation

This paragraph described the procedures and the results of tests performed through the Hot Metal Gas Forming prototype, which is used to evaluate aluminium tubes formability bulged-up in free air until breakage. In doing so, two different aluminium alloys 6xxx series hot extruded tubes produced with different process parameters, in detail AA6082 and AA6060, are investigated. Moreover, different tube lengths of the same extrusion condition are tested as mean of repeatability, and to investigate a possible relation between tube length and its formability. With this aim, an optical measured system applied to a CCD-camera is used to capture images during the hot tube expansion in free air and to calculate the major radial deformation as tube formability parameter. During the test, tube temperature and air pressure are kept constant until breakage. Finally, the post-forming properties of each bulged tube are evaluated in terms of microstructure analyses and micro-hardness measurements.

These tests are performed to understand the potentiality of the HMGF apparatus designed, and the influence, on tube formability, of the main process parameters, such as the bulging temperature, the heating time and the bulging pressure. Moreover, formability results were used to highlight the best AA6xxx alloy, from the two, for use in the HMGF technology.

5.2.1 Material

The materials that were investigated were aluminium alloys AA6060 and an AA6082 that present silicon and magnesium as the highest percent in weight in aluminium matrix as shown in Table 5.8. The presence of this element inside the aluminium matrix increases the strength either in solid solution or as a finely precipitated intermetallic phase. The effect of manganese is to increase the recrystallisation temperature and to increase the quench sensitivity in heating treatment.

Table 5.7: Chemical composition of aluminium alloys AA6060 and AA6082.

AA6060								
Al	Mg	Si	Fe	Mn	Zn	Cr	V	Ti
98.9	0.42	0.41	0.19	0.016	0.016	0.012	0.013	0.011
AA6082								
Al	Mg	Si	Fe	Mn	Zn	Cr	V	Ti
97.6	0.61	0.98	0.19	0.51	0.053	0.0005	0.006	0.008

Table 5.8: Mechanical properties of AA6016, AA6082 and AA6060 used in this research work.

	AA6082-T5	AA6060-T5
Property	Value	
Yield stress [MPa]	180	135
Rupture stress [MPa]	250	175
A% (rupture)	10	11
Vickers hardness [HV]	95	55

Finally, both alloys present an electrical resistivity of $0.32 \cdot 10^{-6}$ Ω·m and different melting point temperature of 655 °C for the AA6060 and of 555 °C for the AA6082.

Semi-finished tubes were obtained through direct hot extrusion with five different process parameters, respectively: two different homogenisation temperatures, measured through a thermocouple inside the extrusion die and with a pyrometer on the exit of extrusion chamber, two different feed rates process and finally, two different quenching types: air and water. The tubes were extruded with a thickness of 1.5 mm, an outer diameter of 30 (±0.2) mm and an inner diameter of 27 (±0.2) mm. Table 5.9 described all process condition for each tube and alloy.

Table 5.9: Description of different tube extrusion parameters.

AA6060			
Tube Denomination	Homogenisation range temperature [°C]	Quenching	Feed Rate process [m/min]
II	430 - 480	Air	8
III	460 - 510	Air	8
V	460 - 510	Air	24
VI	460 - 510	Water	8
VII	430 – 480	Water	8
AA6082			
Tube Denomination	Homogenisation range temperature [°C]	Quenching	Feed Rate process [m/min]
II	460 - 510	Air	3
III	490 – 540	Air	3
V	490 - 540	Air	9
VI	490 - 540	Water	3
VII	460 - 510	Water	3

The material response to the deformation was investigated by torsion tests carried out at elevated temperatures, on the raw material before extrusion. Figure 5.21 shows the results of the experiments in terms of true stress–true strain curves for the AA6060 while the flow curves for the AA6082 presented the same trend, with an increase of true stress value for each condition of around 8%.

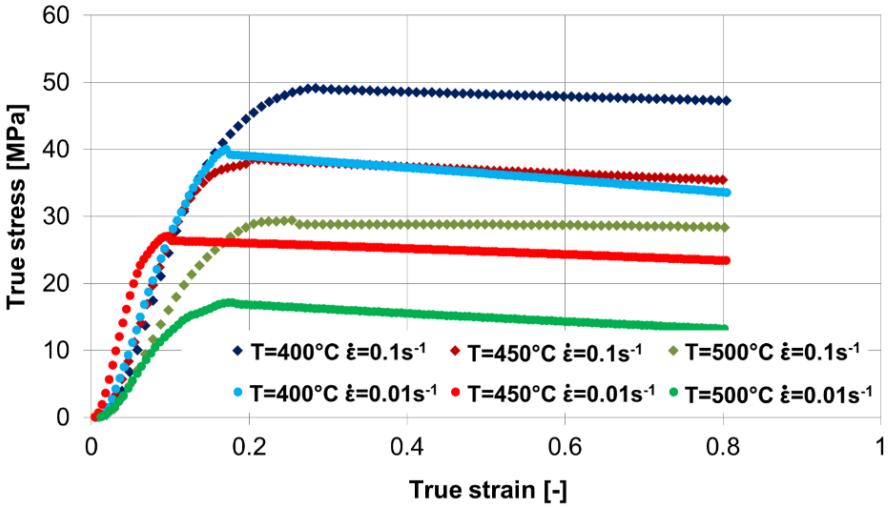

Figure 5.21: True stress – true strain response of AA6060.

Three tests were performed for each pair of temperature and strain rate, and the representative flow-curves trends are shown in the figure highlighting the influence of temperature and strain rate. Based on these results, and in order to reduce as much as possible the air pressure (for the safety of the operator), the best process parameters were found. A tube temperature of 520 °C was identified as the minimum requirement to bulge-up the aluminium tube with air at low pressure (8 bar), allowing a good strain control and good formability.

Before starting the formability evaluation, the thickness of each tube was measured to assess the thickness uniformity. In fact, this parameter was shown in section 5.1.3 to be important for the temperature distribution along the tube due to the heating system used. Figure 5.22 shows the four measurement points on the tube circumference that were measured at an angle of 90 deg. No appreciable thickness deviation was found from the nominal tube thickness of 1.5 mm.

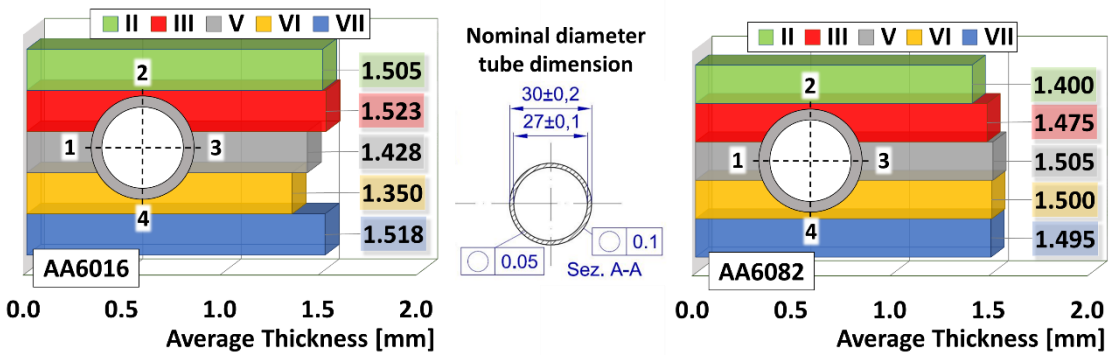

Figure 5.22: Nominal and real diameter tube dimension for each tube analysed.

For each extrusion condition four different tube lengths, nominally, 203 mm, 265 mm, 327 mm and 390 mm, (the same that were used during the preliminary heating tests described in section 5.1.3), were investigated to study the relation between hollow component length and its formability.

5.2.2 Experimental set-up

During the formability test, the temperature of the bulged area was measured and kept constant by a pyrometer pointed at the outer surface of the tube during the heating and the bulging of the specimen with an accuracy of ±1 °C. Cold air under pressure was automatically blown inside tube specimen after reaching the target temperature of 520 (±3) °C with a pressure of 8 bar imposed through the manual pressure regulator. All tests were done within a heating time of 200 seconds in order to homogenise heat distribution and a target temperature of 520 (±3) °C. The thermal cycle used for each deformation test is shown in Figure 5.23.

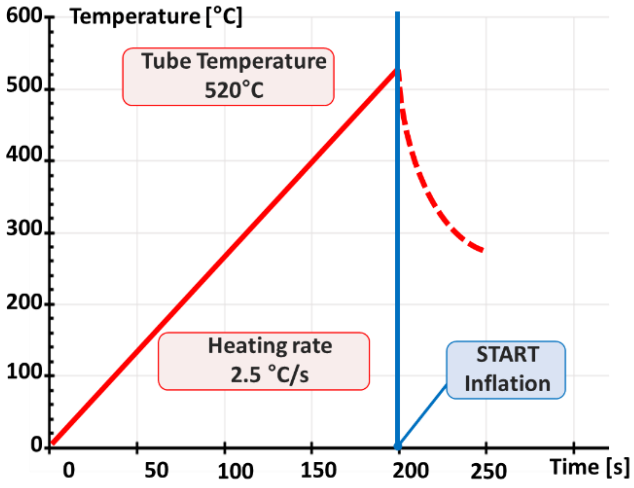

Figure 5.23: Thermal cycle used for deformation test.

To measure the real strain due to bulge expansion, a CCD-camera measurement system was adopted. Each tube sample was prepared spraying a high temperature resistance stochastic pattern on the outer surface whose deformation was captured by a CCD-camera during the test. Images were then post-processed using the software Aramis by Gom™ in order to calculate, in each surface point, the major true strain at fracture and to measure the radial displacement in each image captured, using the same procedure explained in section 4.3.1, , as shown in Figure 5.24.

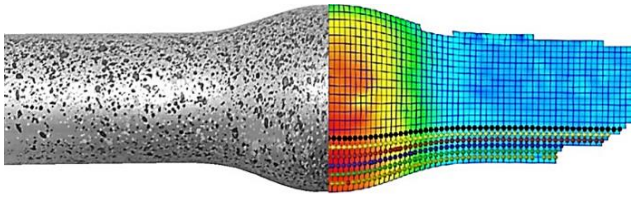

Figure 5.24: Bulged tube post-processes using the software Aramis by Gom™.

Figure 5.25 (a) shows the experimental equipment and the measurement configuration. After fracture occurred, cold air in pressure continuous to flow inside tube, cooling down the

specimen at room temperature in few seconds and allowing the maintenance of microstructure for future analyses. In Figure 5.25 (b) shows the images sequence of the tube bulging test, taken at a temperature of 520 °C and a strain rate of $0.1s^{-1}$, with a time step of 2 s. To complete the tube deformation up to rupture, a time around 10 seconds is required, increasing the external diameter from 30 mm to 43.80 mm at the bulge peak before the fracture appearance.

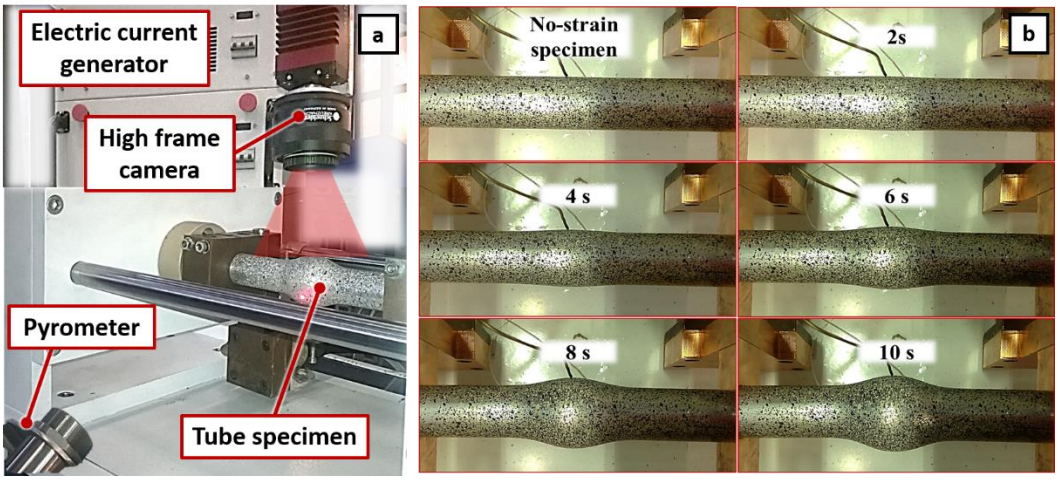

Figure 5.25: Experimental set-up to evaluate tube formability (a) and tube deformation picture story at 520 °C and an air pressure of 8 bar (b).

5.2.3 Formability results

The first analysis can be done considering the true strain before fracture of each extruded tube condition of both aluminium 6xxx alloys, as shown Figure 5.26 and Figure 5.27.

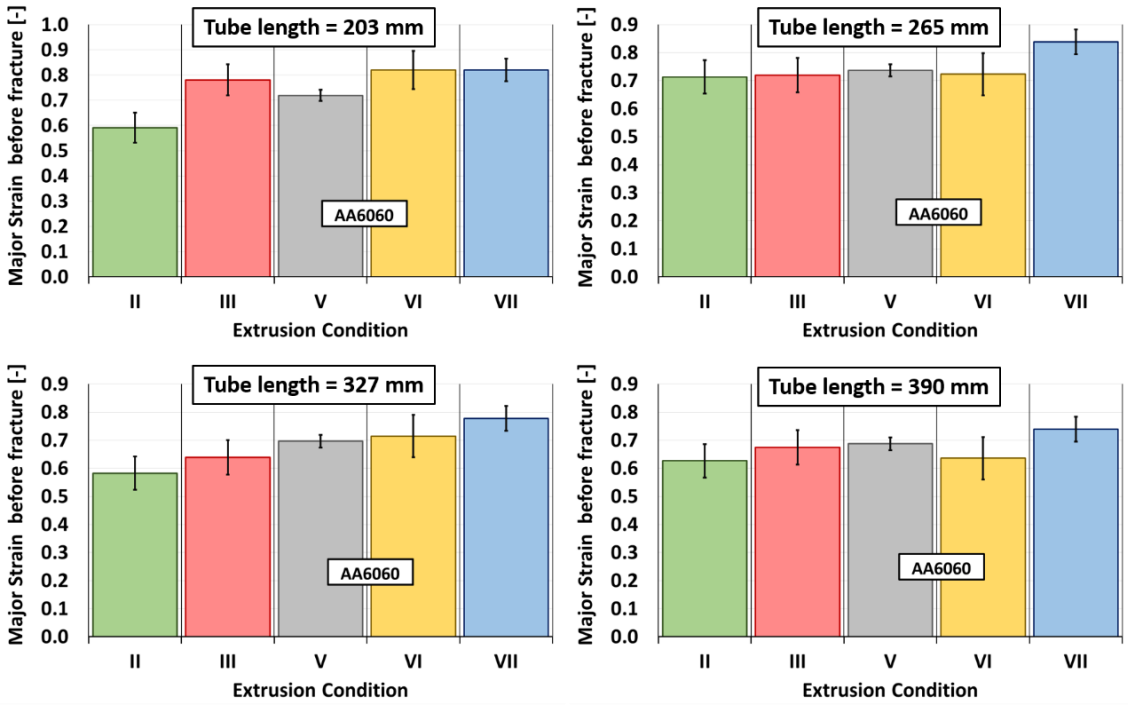

Figure 5.26: Major strain before fracture of AA6060 tubes extruded with different extrusion parameters and tested in different tube length at 520 °C and 8 bar.

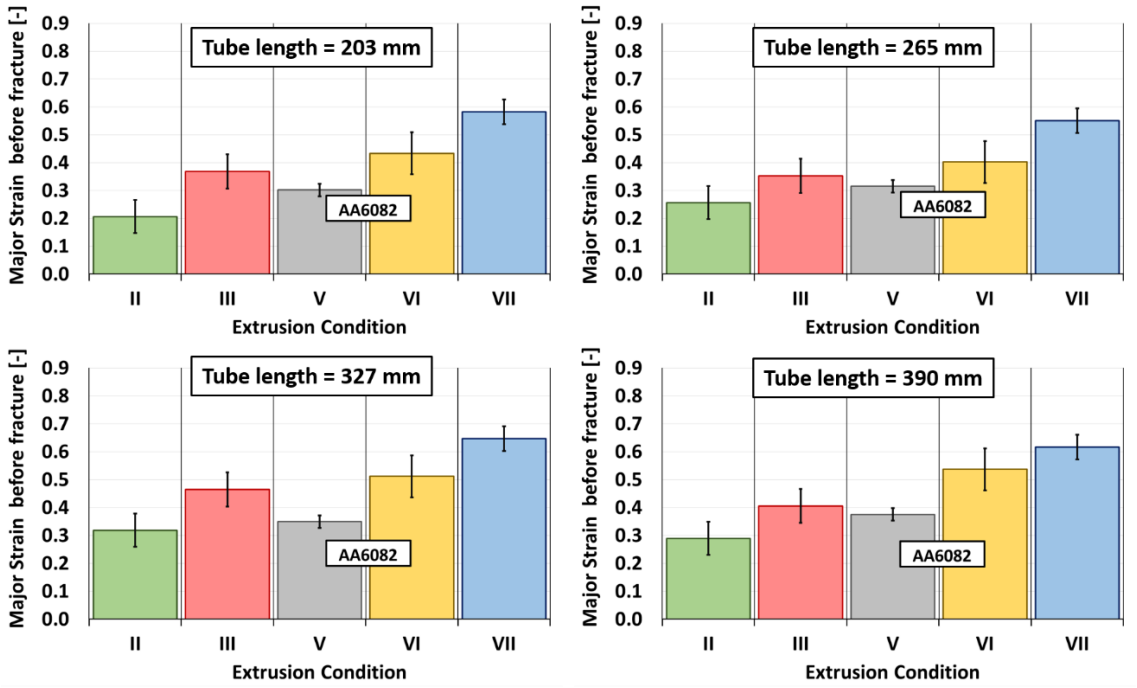

Figure 5.27: Major strain before fracture of AA6082 tubes extruded with different extrusion parameters and tested in different tube length at 520 °C and 8 bar.

As expected from the mechanical material properties, AA6060 has shown a higher value of true strain parameter before fracture, compared to the AA6082 for all tube lengths tested and in each extrusion condition.

Additionally, it is possible to observe that both materials present the same deformation trend considering the same extrusion condition, independently by the tube length. Therefore, tube dimension does not affect the amount of true strain before fracture parameter, proving that the heating device allows a concentrated rise temperature in the bulged area. Indeed, tubes length does not affect significantly the portion of the tube kept at constant temperature. In the case of the shortest tube, a constant thermal length located in the middle of the specimen of 40 mm was observed, while in the case of the longest tube an increase of 15 % (up to 46 mm) was found, as already measured during the thermal tests described in 5.1.3. The high differences in final deformation between the two alloys are also visible to the eye as reported in Figure 5.28 where, for the AA6060, a fracture appeared with ductile morphology creating a small crack and very thin sections around its edges, while, for the AA6082, a rupture was generated through an explosive long crack keeping its edges thick.

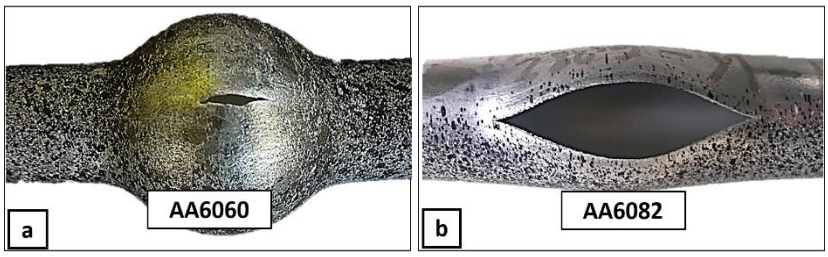

Figure 5.28: fracture morphology for AA6060 and AA6082 tube bulged at 520 °C with 8 bar.

Regarding the different extrusion conditions (shown in different colours and numbered from II to VII) the tubes extruded in the condition VII present the highest values of major strain for all tube lengths and in both aluminium alloys. On the other hand, tubes in the II extrusion condition show the lowest values of deformation for both alloys. The comparison between conditions II and VII, which differ only for the type of quenching as reported in Table 5.9, shows the impact of the heat treatment on the final material formability. On the contrary, in the case of the highest extrusion temperature at 460-510 °C for the AA6060 and 490-540 °C for the AA6082, no relevant differences were detected, as shown by the comparison of the cases III and VI.

Subsequently, as done for the rheological characterisation of aluminium metal sheets in section 4.4, the post-deformation properties, in terms of microstructure observation and micro hardness measurement, were analysed for the material with the best formability: AA6060.

In doing this, all the samples were mechanically polished and chemically etched with a solution made of 100 ml of H_2O, 4 g of K, 1 g of NaOH, for 15 seconds. Figure 5.29 shows the comparison between the sample microstructure in the non-deformed zone and in the area of maximum deformation. It was observed, that no static recrystallisation phenomena takes place after deformation, as shown by the irregular grain distribution and grain size in the thickness, shown by the bulged tube in comparison with the non-deformed one. This can be attributed due to tube cooling quickly by compressed air that prevents any microstructural change. As expected, only in the zone of the large deformations due to the tube bulging, the grains appeared stretched and distributed along a preferential direction.

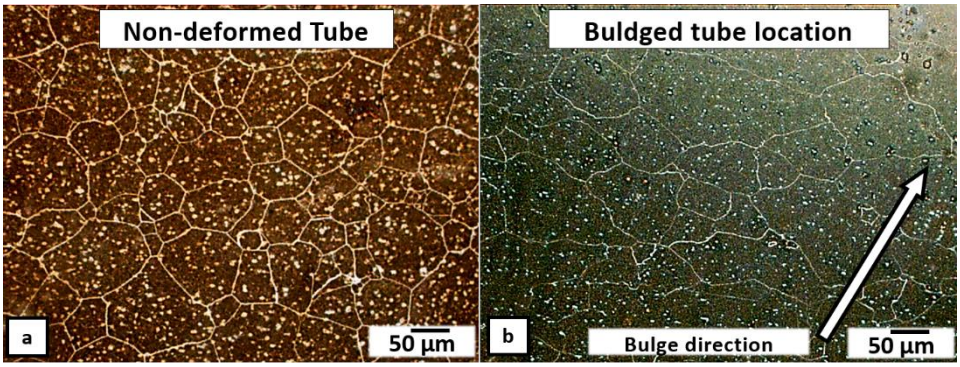

Figure 5.29: Microstructure of AA6060 non-deformed tube (a), and of bulged tube (b).

Finally, to evaluate the material mechanical properties after deformation, micro-hardness measurements were made on all tube extrusion conditions. Six measurements around the radial direction were performed on the tube thickness, both for non-deformed zone and for bulged zone near fracture location. Figure 5.30 shows the results for the five extrusion conditions with their standard deviation.

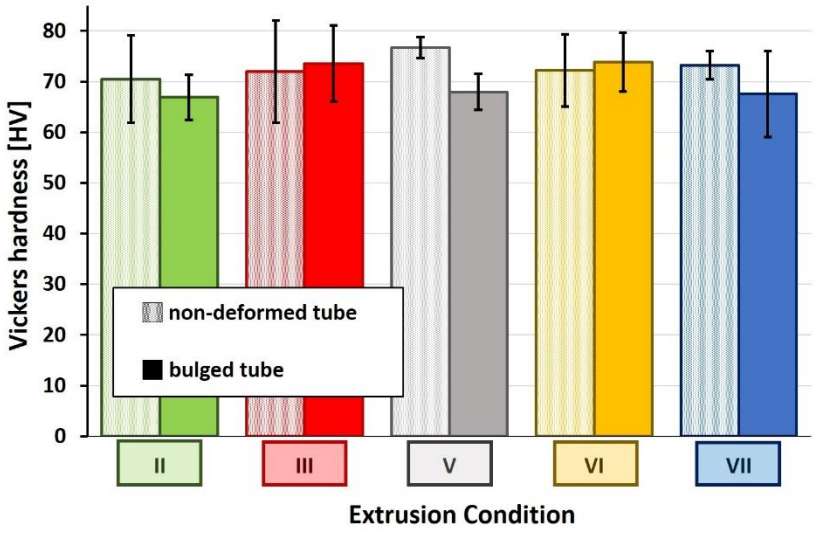

Figure 5.30: Micro-hardness measurement, bulged zone (dark bar), non-deformed tube (light bar), for AA6060 tubes.

The results show that there are not appreciable differences between the micro-hardness values of non-deformed and bulged tube, in all extrusion conditions. Therefore, even if the high temperature is sufficient to expand the AA6060 with an air pressure of 8 bar is in the range of solubilisation heat treatment temperature for this material, the low process time is not adequate to dissolve the precipitates in the aluminium matrix. In fact, even if micro-hardness were done four weeks after the bulge tests, the hardness does not show an increment, but rather it was maintained at the same level of non-deformed material. Moreover, it worth noting that not relevant differences of the micro-hardness values were found among the different extrusion conditions.

5.2.4 Tube formability conclusions

This section discussed the tests used to evaluate the formability of two different aluminium alloys 6xxx tubes, produced with five different extrusion parameters, through the Hot Metal Gas Forming process using a test temperature of 520 °C and cold air at 8 bar of pressure. Strain evaluation was performed using a CCD-camera measurement system to calculate the true strain at fracture, while microstructural analysis and micro-hardness measurements were used to investigate mechanical behaviour of the best formable material after the bulge tests. Between the two series studied, the AA6060 proved to be the best aluminium alloy in terms of formability assuring also, at high temperature, a ductile fracture morphology generating thin cracks at the appearance of fractures, without dangerous explosions. Post-forming analysis showed that non-appreciable differences were found among the different extrusion process parameters, in terms of microstructure. Moreover, micro-hardness measurement provided evidence that low process times for the bulge phase at 520 °C are not adequate to generate a solubilisation heating treatment.

Regarding the process, bulged tests in free air highlighted that tube length do not affect the amount of formability, but instead slightly increase the part in the tube middle at constant temperature. Moreover, a temperature of 520 °C proved a good compromise to reduce, as

much as possible, the pressure used for tube deformation without generating a solution heat treatment that could affect surface quality of the deformed part at high strain rate as found in 4.4.3. In addition, the fracture morphology without explosion generated by the AA6060 confirmed that it is more safer to regulate the air pressure with a successive inflation after reached tube target temperature, instead of using sealed air under pressure inside the tube before starting the heating, as done by Mori et al. in their studies, without any pressure control and thereby risking sudden explosion.

5.3. Square geometry shaping

In this section, starting from the results obtained in terms of formability found in the previous section 5.2, an evaluation is performed of the possibility to shape, through the HMGF technology, hollow components of AA6060 alloy inside a die. With this aim, an investigation into the influence of different die materials was performed, namely: mechanical properties, surface roughness and thermal properties, applied to produce an aluminium square component. Therefore, using a constant value of inflating cold air pressure and a constant tube temperature, the influence of different die temperatures on the final component, was analysed. In doing so, the filling level of the die corner, was measured with an optical measurement system that allowed measuring the thickness distribution and the corner radius of the final part. Subsequently, the mechanical properties of the shaped components were evaluated through micro-hardness measures.

A final analysis was attributed to the inflating time, measuring the amount of die filling by the tube expansion, reducing the time process and varying the die square geometry ratio.

5.3.1 Material

Tube dimension

The AA6060 tubes specimen utilised in this study, are cut from 6 m long tubes produced by hot direct extrusion using an homogenisation temperature in the range of 430-480 °C, a process feed rate of 8 m/sec and a final quick quenching in water; corresponding to the best extrusion condition found in section 5.2.3. All specimens exhibited an initial length of 500 mm, an inner radius of 27 mm, and an average thickness of 1.5 mm with a standard deviation of 0.22 mm obtained measuring each as-delivered tube in eight measurement points on the tube circumference at an angle of 45° as shown in Figure 5.31 (a). Furthermore, the microstructure of the as-delivered tube was evaluated to understand the grain geometry and distribution along the specimen thickness. The Figure 5.31 (b) suggests that a non-preferential orientation of the grain and rather uniform grain size, affected the material.

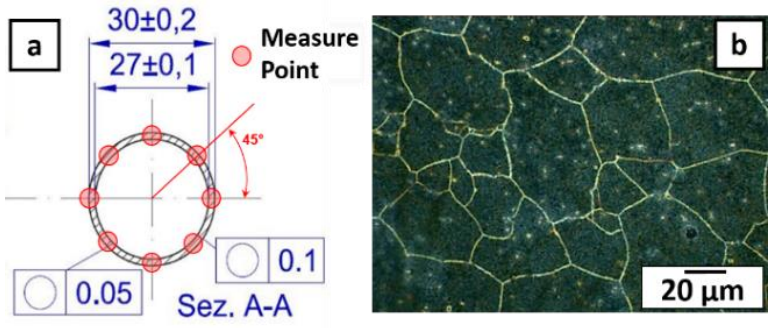

Figure 5.31: Measure points used to evaluate the average thickness (a) and microstructure distribution of the as-delivered tube.

Die material

The square die used to give the desired shape to the specimen was composed in non-magnetic AISI 304 steel, to allow the possibility to be used inside magnetic field. In fact, the tube crossed with high current presents the same behaviour as a wire; generating a magnetic field around it which is dependent on the current intensity. A magnetic steel matrix, under the influence of a magnetic field could be very dangerous for the process because its components can move attracted by other machine structural parts, compromising the final piece quality. As showed in Figure 5.32, the total die length is 200 mm with an inner square dimension, coupled with the insulator, of 40 mm in each side.

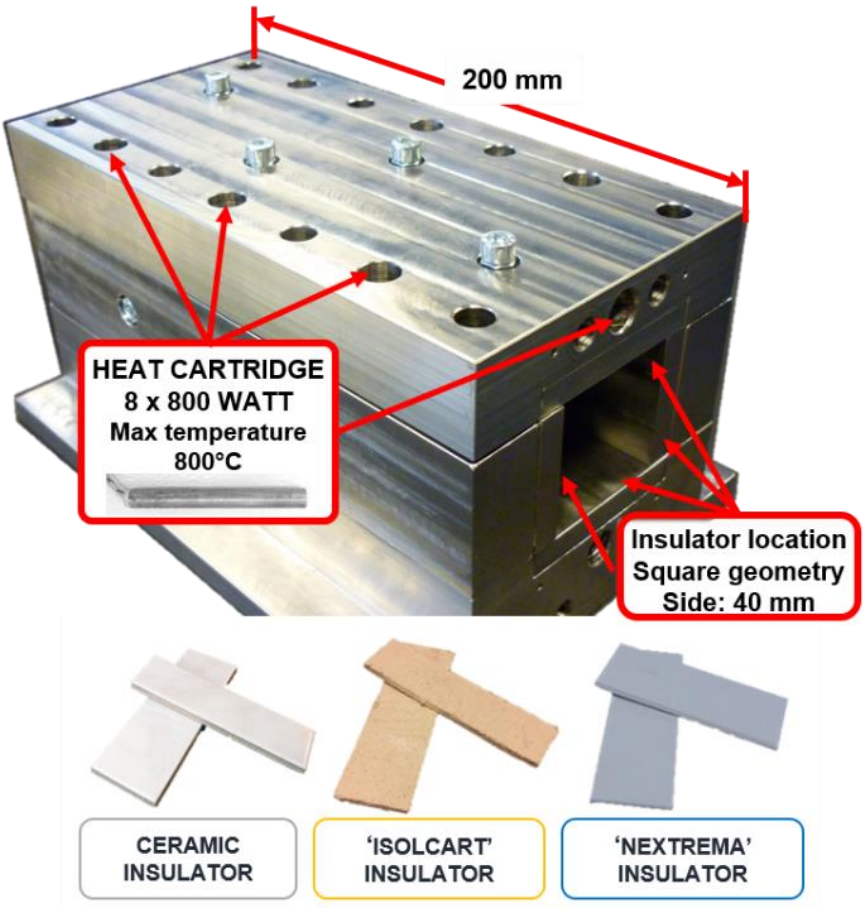

Figure 5.32: Square die with electrical insulator materials.

The die was divided in four part joined through eight M8 screws. During the experiments, eight holes in the die structure were used to insert six heating cartridges with 10 mm in diameter and 100 mm in length and two with 10 mm in diameter and 200 mm able to arrive at a surface temperature of 800 °C. An additional six dead holes with a diameter of 1.5 mm were used to evaluate the die temperature during the test through the insertion of K thermocouples inserted in different die locations.

Electrical insulator material

To avoid the electric current transfer, during the deformation, between tube specimen heated by the Joule effect, and the metal die, three kind of insulators were used, namely (i) double-fired common ceramic, (ii) glass-ceramic (Nextrema by Schott) and (iii) thermal insulator composed of inorganic mineral fibres and moderate quantities of organic binders (Isolcart K 85 B).

During the process the electric insulator is a fundamental characteristic because the high current value adopted can create local electric arcs that can damage the die surface through electroerosion Table 5.10, details the thermal, electric and mechanic properties of each insulator material, while Figure 5.33, shows their respective surface roughness.

Table 5.10: Insulator properties.

Properties	Double-fired ceramic	Glass-Ceramic (Nextrema by Schott)	Isolcart K 85 B
Thermal Conductivity (90 °C) [W/(m·K)]	0.8	1.7	0.1
Relative permeability ε_r (1MHz 25°C)	7	6.6	4
Thermal Shock (TSR) [°C]	500	700	/
Bending Strength σ_{bB} [MPa]	85	150	6.5
Hardness [Knoop]	560	600	35

Comparing the insulator properties, one can note that the glass-ceramic material exhibits thermal shock resistance and mechanical properties better than the other insulators. Moreover the roughness analysis indicates that the relevant difference between ceramics materials and Isolcart insulator does not present a fragile behaviour therefore is not subjected to possible breakage during the inflating step. The average values of surface roughness and topography surface images of each insulator material were measured by means of a Sensofar Plu-Neox™ digital profilometer considering seven scans for each different insulator piece. Regarding the electric insulation properties, all materials used showed low values of relative permeability sufficient to interrupt the electric flow from tube to die during the specimen shaping.

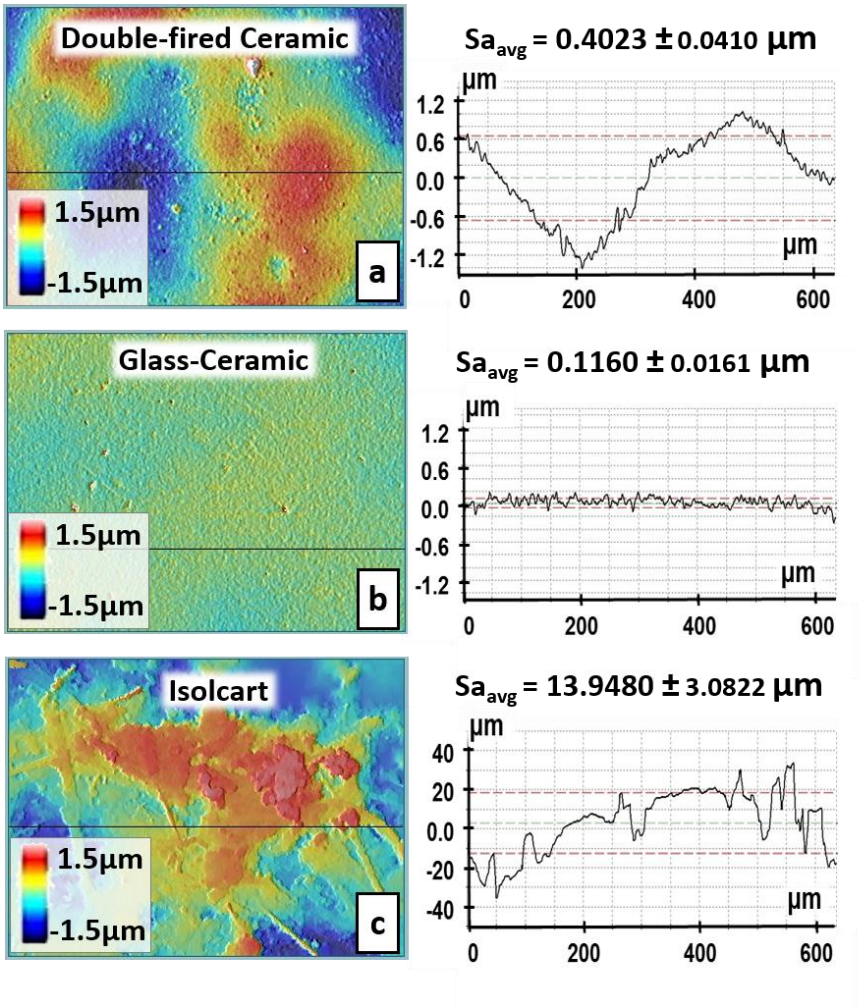

Figure 5.33: Surface roughness of insulator materials: double-fired ceramic (a), glass-ceramic (Nextrema) (b), Isolcart insulator (c).

5.3.2 Thermal calibration

In this type of test, which differs from that described in section 5.1.3 for the presence of a die, the tube temperature during the expansion was measured using two pyrometers pointed on the tube surface at the distance of 5 mm from each die edges. In this apparatus configuration, if one is to understand the exact temperature measured through the pyrometers at those points, a preventive calibration is necessary and so is performed through a thermo-camera. The correlation between temperature inside and outside the die, is measured using a drilled metal plate instead of one side of the die, allowing a spot temperature measurement every 20 mm along the tube, namely, where a 5 mm in diameter hole was drilled, as shown in Figure 5.

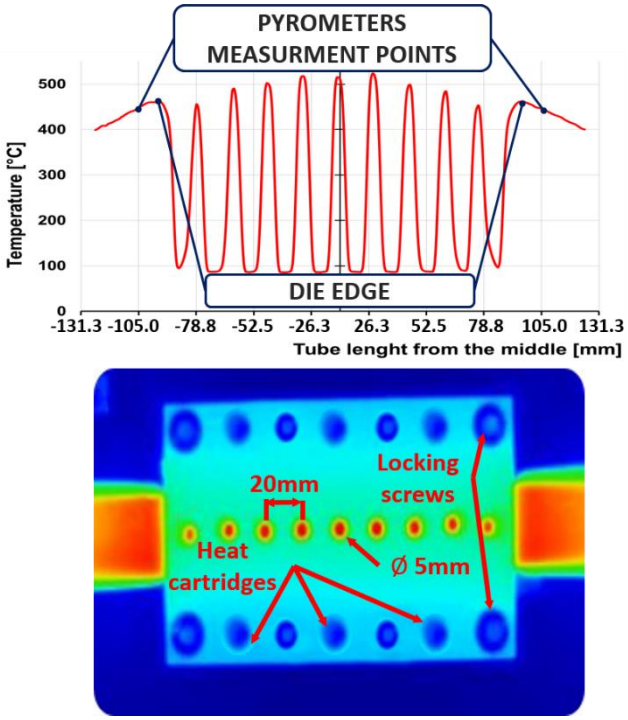

Figure 5.34 – Temperature measurement in die configuration experimental apparatus.

As shown in the figure, the tube temperature inside the die was maintained almost constant for a distance of about 80 mm highlighting a reduction of only 20 ° C compared to the target hottest point of 520 °C. Instead, the remaining part, until the end of the die, exhibited a tube temperature decrease up to the value of about 430 ° C to the outer edge and of 420 ° C at the point where the pyrometers were directed for the temperature measurement.

5.3.3 Experimental plan and process procedure:

To investigate different process parameters, the deformation tests were carried out for different values of die temperature and adopting different insulator materials. The experimental plan is given in Table 5.11. Each test was repeated three times. Moreover, tests without any insulator were performed for a comparison.

Table 5.11: Experimental plan

INSULATOR TYPE	Die Temperature [°C]	Number of test
Double-fired ceramic	20 ; 200 ; 400	3
Glass-Ceramic (Nextrema by Schott)		
Isolcart K 85 B		
No Insulator		

A square geometry die was used for its simplicity and, above all, for the difficulty of changing completely the geometric feature of the component.

Square geometry highlights critical aspects for the HMGF process. Indeed, in each forming process, the corners are very difficult to fill, due to the friction between tube and die walls. Moreover, inside a square die, corners are the points at the greatest distance from the tube. Therefore, a measurement of the amount of their fill based on different tube and die temperatures allows one to know which is the best process parameter to increase the formability. To evaluate the final component feasibility three inflating operations inside the die, each one of 30 seconds, were carried out for each component using an initial tube length of 500 mm and the operative process shown in Figure 5.35.

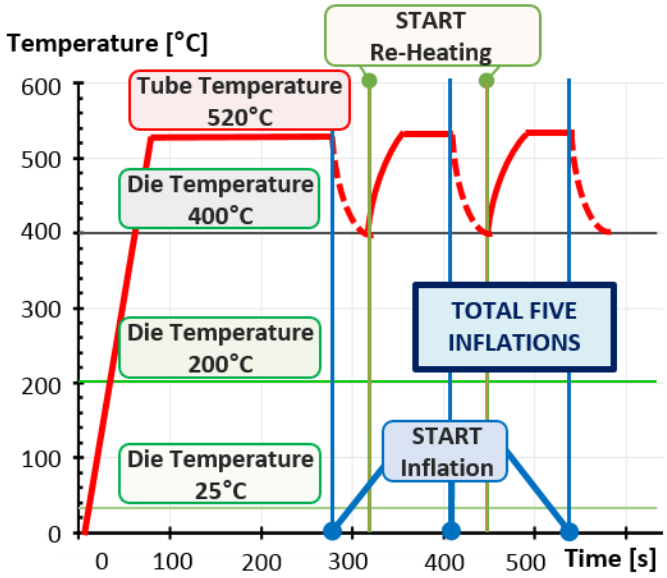

Figure 5.35: Scheme of the operative process use to shape a tube inside a square die with electric insulator through the HMGF process

Initially the die was heated up to test temperature using cylindrical resistance heaters and measuring the temperature through three K-type thermocouples located in three different points of the die. Simultaneously a remote control system was able to control the average die temperature allowing an accuracy of ±5 °C. Subsequently the tube specimen was heated up to the testing temperature, fixed at 520 °C, with a heating rate of 7.5 °C/s and held at this temperature for 200 s in order to guarantee the temperature distribution along tube length. During this step, two pyrometers and an analogic device control system connected to the electric generator, assured a temperature accuracy of ±0.5 °C, on the external tube surface, while a sealed K-type thermocouple measured the air temperature inside the tube. The aluminium reflection property, due to the problem with the emissivity setup, was avoided by covering the surface points monitored by the pyrometers with high resistance temperature black paint,. Additionally another two thermocouples were located inside each copper jaw electrode for measuring the temperature of the two cold sources responsible of temperature drop at tube extremities. This monitoring allows one to understand the possible non-uniform temperature distribution on tube surface and, better still, the possible asymmetry of the tube temperature. After the homogenisation step, an electro valve was used to open the high pressure circuit, blowing 8 bar of cold air inside tube specimen, inflating partially. During this

operation, an air temperature quick decrease was measured so, for this reason, another two inflating operations were performed on the same tube, reheating at target temperature with the same heating rate of the first step. Throughout the test duration, the die temperature was kept constant at the initial target temperature. Figure 5.36 shows the result given after three inflating operations using the double-fired ceramic electric insulator and a die temperature of 400 °C.

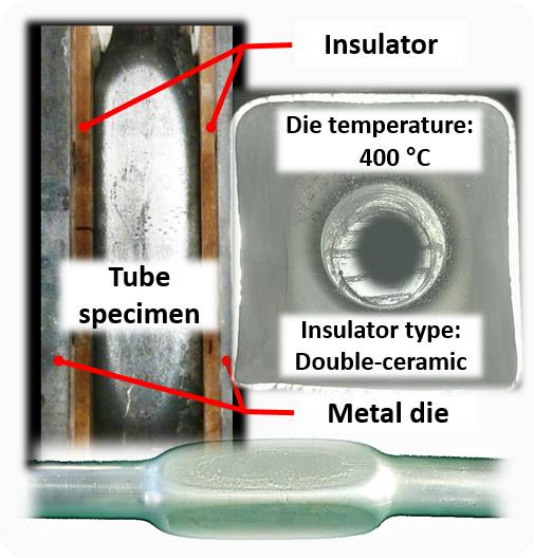

Figure 5.36 – Component shaped after bulge-up operation inside a square die.

5.3.4 Formability results

Table 5.12 reports the average qualitative results, in terms of die filling, obtained from all conditions test repeated three times. The possible results are: "complete shaping", "partial shaping" for results without an edge-completed filled, and "very low expansion" for when there is poor radial expansion or restricted bulge length. It worth noting that the results shown do not consider other important aspects of the final product, such as the surface roughness or give consideration to the process, such as due to insulator breakage. However the results in Table 5.12, demonstrate the high influence of die temperature on tube formability, as expected.

Table 5.12: Feasibility table of components obtained with different die temperatures and electric insulator.

Material insulator	Die temperature [°C]		
	20	200	400
Double-fired ceramic	X	≈	O
Glass-Ceramic (Nextrema by Schott)	≈	O	O
Isolcart K 85 B	≈	O	O
No Insulator	X	X	≈
X = very low expansion	≈ = partial shaping		O = complete shaping

The very low formability obtained in tests without insulation is due to the different procedure applied. Only a single inflation was used to avoid possible electrical conductive problems after the contact between the tube and die surfaces.

Therefore, results obtained from the formability test without die insulation are not comparable to those obtained with insulated die, but they highlight the large increase in formability obtained using several bulging steps on the same tube. Comparing instead results at the highest die temperature, all insulators produced a complete tube shaping. The glass-ceramic material assured an optimal surface roughness and a very high corner filled without any insulation fracture, even after many tests due to the high mechanical and thermal properties. Double-fired ceramic, even if has guaranteed a good surface roughness, appeared too fragile even to support the low pressure applied during the inflating. In fact, each test required a replacement, indicating that is not suitable for an industrial application. Different behaviour exhibited the Isolcart insulator that, even if not presents a fragile behaviour, compromised the surface roughness on the final parts, as expected after insulator texture observation shown in Figure 5.33. Moreover, due to the high temperature used, the Isolcart insulator deterioration led to the release of smoke, which is undesirable for the operator.

At the intermediate temperature of 200 °C, a good formability, even if lower than that obtained at 400 °C, was observed using glass-ceramic and Isolcart insulator. Also in this case the completely different surface roughness between the two parts created was considered as discriminating parameter.

To quantify the level of die filling after bulging operation, an optical measure system was developed using a small optical bench with a high resolution CCD camera sensor equipped with a telecentric lens. A high intensity red LED, was used to backlight the sample to be measured, creating an optimal thresholder image, therefore obtaining perfectly sharpened edges, as shown in Figure 5.37. Finally by using software developed in LabVIEW® environment, it was possible measure the thickness distribution and also the internal and external radius.

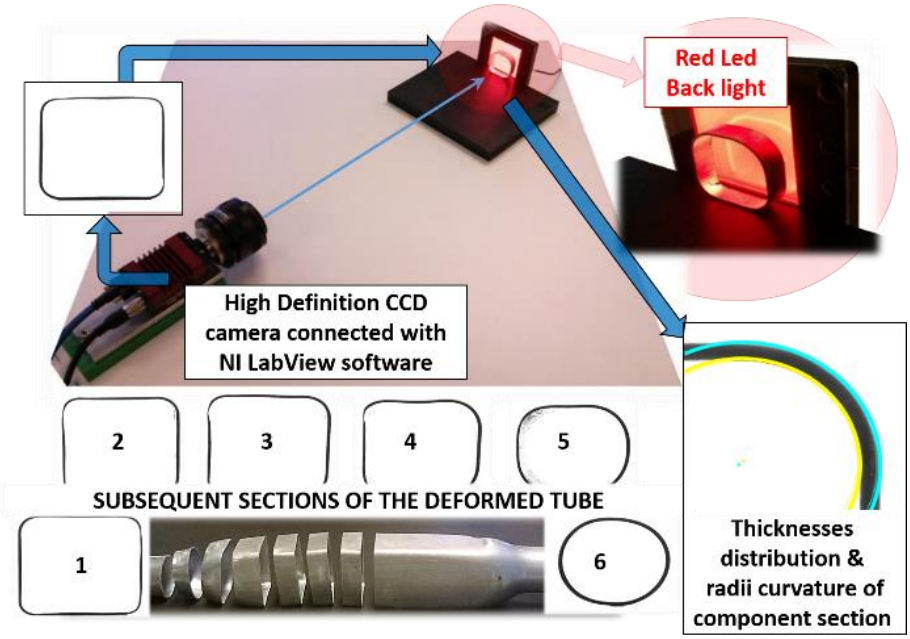

Figure 5.37: Optical measure system used to measure thickness distribution and the corner radius along tube length.

With this purpose, from each half tube specimen, six tube slices were obtained to evaluate the radius evolution along its length in order to understand the material behaviour during the shaping.

Figure 5.38 shows the results of the corner radius measurements for each insulator material. Through the radius drawing, for each one of the six tube slices, the material fills were evaluated as the die corner along tube length. Moreover, the analysing of the first tube slice highlights that the filling quantity reached is dependent of the die material used. Figure 5.38, shows that the material behaviour at the highest die temperature used of 400 °C. This case is representative of all die temperatures used. The results show, with the exception of the no-insulator condition, that, after 60 mm in length from the middle of tube, the tube bulging was inadequate to reach the die walls. Anyway, the Nextrema insulator case has demonstrated a good expansion considering the radius values measured after 60 mm.

Regarding the radius dimension in the middle of the die, and therefore in the middle of the tube (slice one), the Nextrema insulator attained the lowest radius of 3.54 mm very close to a sharp edge, remaining in the range from 4.88 mm to 3.54 mm considering 30 mm from the middle of the tube. Isolcart insulator and Ceramic insulator showed however, a good corner filling, reaching radius values around 6 mm for 30 mm in length from the middle of the tube.

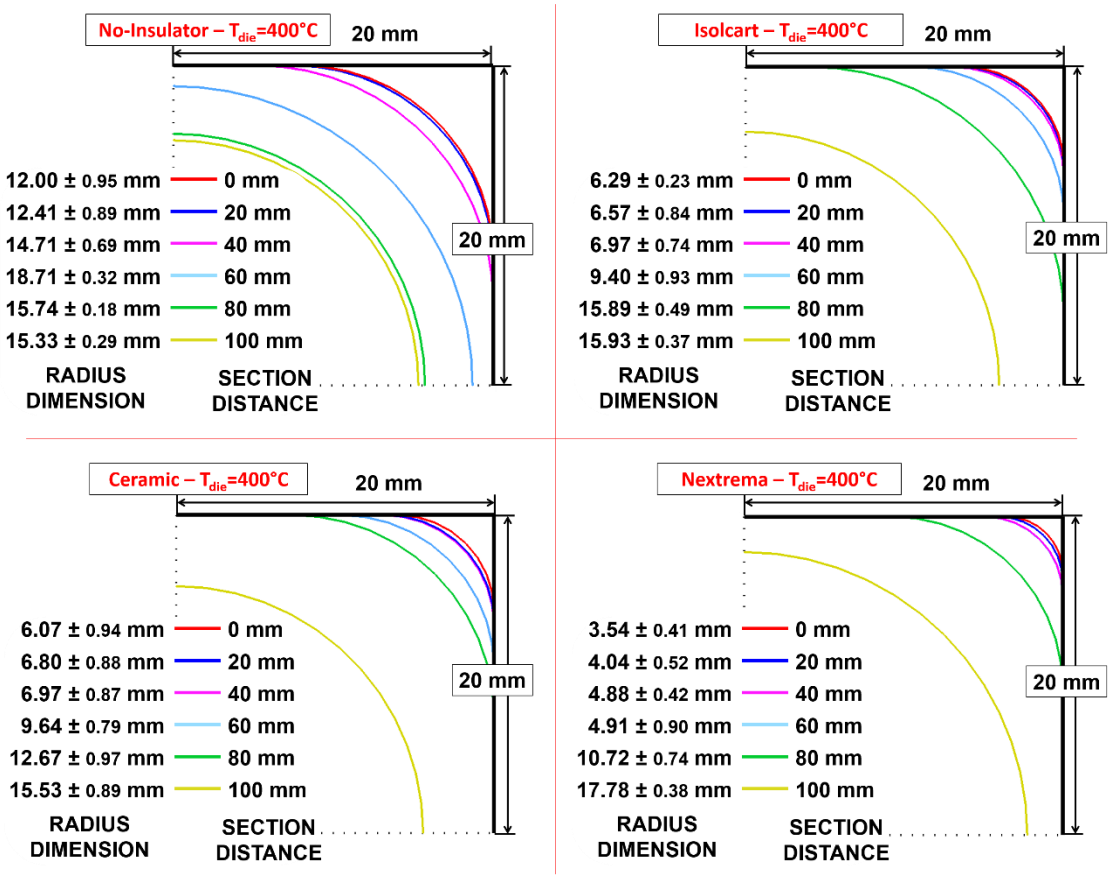

Figure 5.38: Corner radius filling for the 400°C die temperature and all insulator used.

The distributions of the thickness of the middle tube section after forming (slice one) are shown in Figure 5.39, which takes into account the different insulators used and all of the die

temperatures investigated. The results obtained from one side of the square were captured between the two corners. It was found that higher values of the extension in the section length axes lead to higher quantities of die filling. One should note the different behaviours of the thickness distribution for all of the insulators when changing the temperature. In particular, near the edges, the thickness decreases quickly up to values of 0.3 mm - 0.4 mm for ceramic and glass-ceramic insulator, increasing again, after the corner. Considering the initial tube thickness of 1.5 mm, the maximum thickness reduction was obtained at a die temperature of 400 °C and valuated in 80±2 % for Nextrema insulator, 73±2 % for Ceramic insulator, 47±2 % for Isolcart insulator and 0.36±2 % without any insulator.

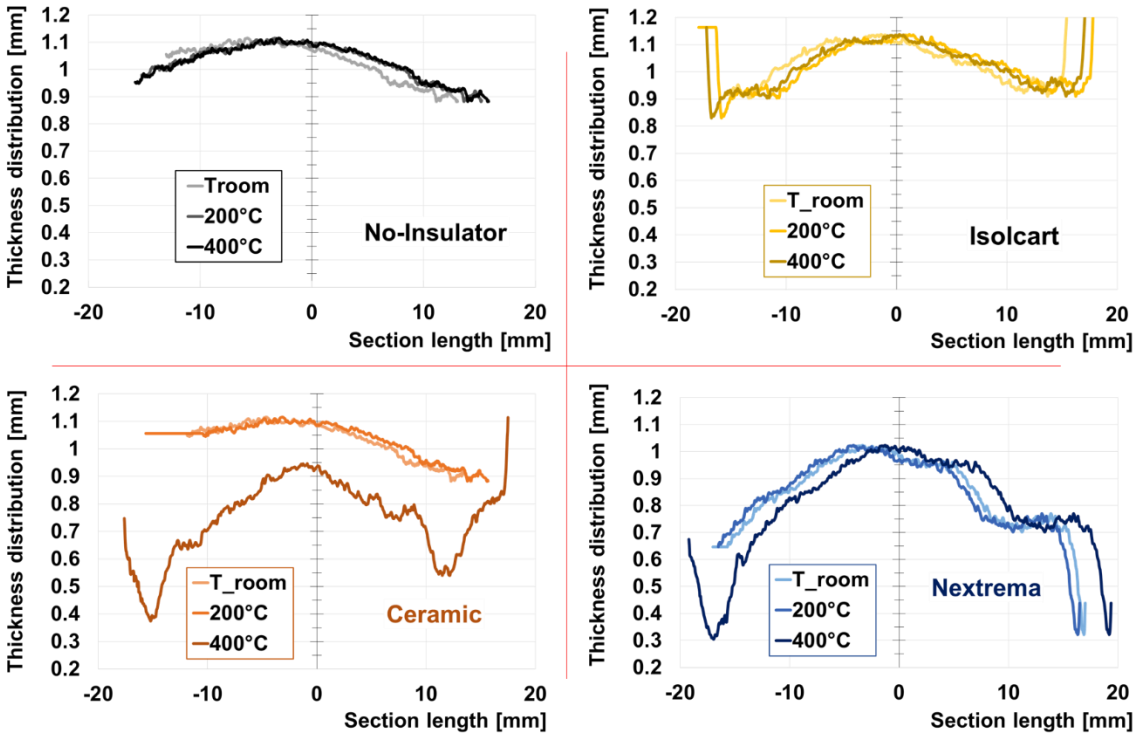

Figure 5.39: Thickness distribution for all insulators used and die temperatures.

Finally, mechanical properties of the shaped parts were investigated by measuring the micro-hardness values along the square part side and along the obtained corner parts, for of the all tested condition. The results, shown in Figure 5.40, show the average values after five points measured for each location and the respective standard deviations. Taken into account the error bars, it was found that the corner locations always exhibit strain-hardening phenomena even at the high temperatures. Conversely, no particularly difference in hardness values was found analysing the components obtained using different die temperatures. Moreover, similar values were obtained comparing tests performed using all insulator materials. The result of the comparison between micro-hardness of deformed tubes and non-deformed tubes (72.4 ± 3.2 HV) again showed that the low process time for the bulge phase at 520 °C is not adequate to generate a solubilisation heating treatment as found in section 5.2.3.

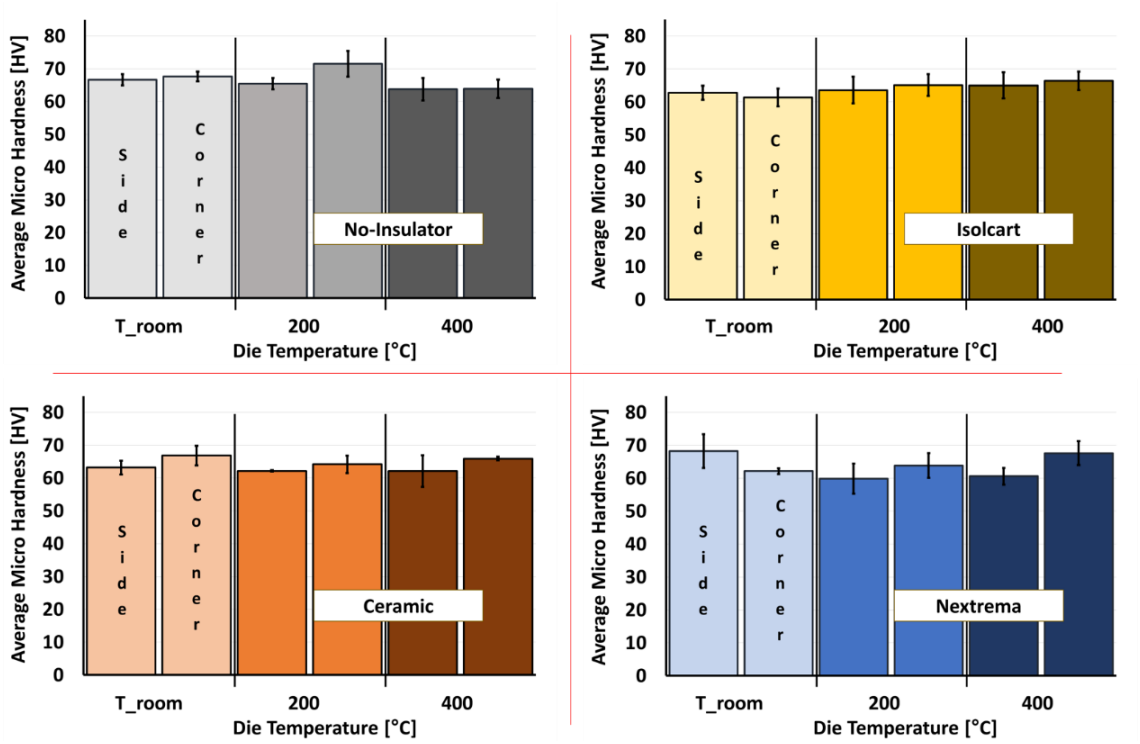

Figure 5.40: Micro-hardness values in the square side location and in the part corner location, for all test conditions.

5.3.5 Inflating time analysis

Taking into account the aims of the research; to reduce the process cycle time, to save energy and increase the productivity; a separate analysis was performed in order to observe the influence of the inflating time in creating a square component.

From the results, in terms of temperature and pressure obtained from previous analysis, it is clear that higher die temperatures lead to higher tube formability. For this reason, in this investigation AA6060 tubes were shaped into a square geometry at 520 °C using a high die temperature of 500 °C.

Bearing in mind the importance of the material die for the success of the final component and its surface quality, an alternative solution was developed to guarantee the electric insulation between tube and die as having an optimal surface roughness and an appropriate insulator life cycle. For these reasons, die inserts were machined in non-magnetic, high temperature resistant, stainless steel, AISI 310, and covered with a sprayed thin layer of boron nitride. This exhibits optimal electrical insulation properties, high working temperature (up to 900 °C) and good oxidation protection. Moreover, it exhibits an excellent lubricant property that could assist the material flow during the process. However, the rubbing between die and tube cause it to deteriorate from the surface and so it must be applied on die surfaces before each test.

Cold air with 8 bar of pressure was used to bulge-up the sample, in order to investigate the influence of different square ratios with the purpose of validating the process parameters found and for a qualitative evaluation of the influence of friction. The studied die geometries are represented by a square of 40 mm x 40 mm, a rectangle of 40 mm x 36 mm and another rectangle of 40 mm x 32 mm.

In Table 5.13, reports the process parameters used in the inflating time tests, which used process times for the bulging operation of 200, 100, 50, 25, 10 seconds respectively. Finally, for each test, the relation between die filling and die length, fixed at 200 mm was calculated as the formability parameter, (eq. 5.4).

Table 5.13: Process parameters used during the inflating time evaluation.

Tube temperature	520 °C
Die temperature	500 °C
Heating time	15 s
Inflating pressure	8 bar
Inflating time	200 s ; 100 s ; 50 s ; 25 s ; 10 s
Square ratio	40 mm x 40 mm ; 40 mm x 36 mm ; 40 mm x 32 mm

$$K_f = \frac{C_f}{Die\ length} \qquad \text{(eq. 5.4)}$$

K_f = Die filling ratio

C_f = Component die filled [mm]

Figure 5.41, shows the shaped tube comparison considering the different die square ratios; case a, b and c respectively of 40 mm x 40 mm, 40 mm x 36 mm and 40 mm x 32 mm; and the amount of inflation time which increases with arrow direction. It is worth noting that test performed with the square matrix are usually characterised by small breaks on plane surfaces this due to the too high tube deformation request to arrive at die surfaces. In fact, even if the maximum inserts distance was the same of the experimental test performed in section 5.3.3, the experiments differ in the heating time applied. In this test the heating time was 35 °C/s second, whilst it was previously 7.5 °C/s in addition to 200 seconds for temperature homogenisation.

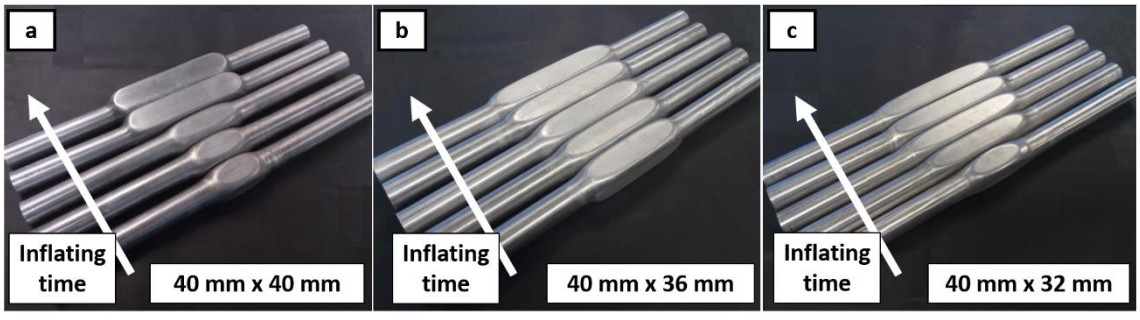

Figure 5.41: Square tube shaped changing the square ratio and using different inflating time.

From the results is clearly visible by eye inflating that the time has as key a role in the process as the square ratio. In fact, the comparison between case b and case c, where samples were always without failures, a relevant formability variation, especially at short inflating time appeared, showed that the lowest square perimeter involves more friction, because tube material reaches the contact with die surfaces more quickly.

Figure 5.42, shows the comparison among the K_f parameter calculated and reported in Table 5.14 considering the three square ratios investigated and the different inflating times used.

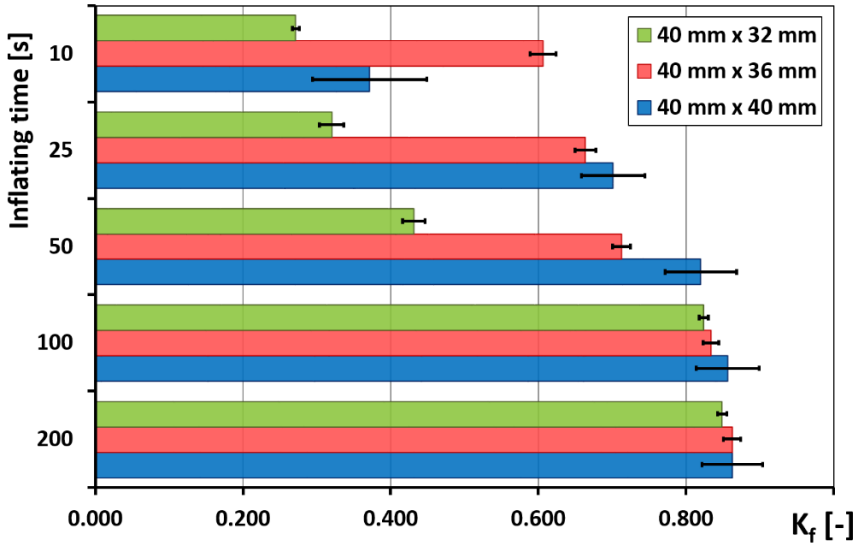

Figure 5.42: Comparison among the K_f coefficients using different square ratios and inflation times.

The figure shows that 100 s is sufficient, for each geometry, to shape the tube completely inside the die. Comparing the two strategies used with the material die, glass-ceramic and boron nitride, as shown in Table 5.15, and evaluating the amount of die filling, it is evident how the time step can be reduced whilst preserving the formability; i.e. by using boron nitride as electrical insulator thanks to its lubricant properties. Moreover, the trend is clear due to the friction influence, which, except for 40 mm x 40 mm test performed at 10 seconds, has reduced substantially material formability highlighting the importance of using lubricant during the process.

Table 5.14: Value of component die filled (C_f) and die filling ratio (K_f) measured using different square geometry ratio and inflating time.

Square die ratio: 40 mm x 40 mm					
Inflating time [s]	10	25	50	100	200
C_f = Component die filled [mm] (average)	74.25	140.25	164.00	171.25	172.50
K_f = Die filling ratio (average)	0.37	0.70	0.82	0.86	0.86
Square die ratio: 36 mm x 40 mm					
Inflating time [s]	10	25	50	100	200
C_f = Component die filled [mm] (average)	121.25	132.75	142.5	166.75	172.5
K_f = Die filling ratio (average)	0.61	0.66	0.71	0.83	0.86

Square die ratio: 32 mm x 40 mm					
Inflating time [s]	10	25	50	100	200
C_f = Component die filled [mm] (average)	54.25	64.00	86.25	164.75	169.75
K_f = Die filling ratio (average)	0.27	0.32	0.43	0.82	0.85

Table 5.15: Comparison between process parameters and amount of die filling using glass-ceramic and boron nitride as die material and insulator.

Die material	Glass-ceramic	Boron nitride
Tube temperature	520 °C	520 °C
Die temperature	400 °C	500 °C
Heating time	70 s	15 s
Temperature homogenisation time	200 s	-
Number of inflation	3	1
Inflation time	30 s	100 s
Die filling	75 %	80 %

5.3.6 Conclusions

In this section, the applicability of the HMGF process to shape aluminium AA6060 tubes inside a square die whist changing the geometry was investigated. Thanks to this approach, the investigation has shown the advantages of the new procedure applied to this technology, finding which are the best process parameters in terms of tube temperature, die temperature, heating time and inflating time. These can be used to increase the component formability in gas forming shaping operation. The effect of die temperature was evaluated by measuring the quality of the final component through the thickness distribution and radius curvature at the corners, proving high die temperatures lead to high tube formability. The same analysis was used to investigate the influence of different die materials, finding that the glass-ceramic material is the best candidate for its mechanical, electric insulator and surface roughness properties, but also for resistance to several production cycles. However, due its high cost and for the difficulties to obtain it in unconventional shapes and dimensions, the application of a thin layer of boron nitride was shown to be the optimal solution for the process from an industrial perspective. This guarantees the preservation of the die surface from electroerosion and also aids the material flow on die surfaces. The micro-hardness value of obtained parts was measured as index of the mechanical properties, confirming that, despite the high tube temperature applied to the process, the low process time for the bulging phase is not adequate to generate a solubilisation heating treatment, as shown in section 4.4.3, that leads to the low quality surface appearance when applied during the deformation step.

Finally, the influence of inflation time was tested in shaped square tube trying in order to reduce, as much as possible, the bulging process cycle. Tube and die temperature were chosen by considering previous results, which were 520 °C for the tube surface and 500 °C for the die, while boron nitride was used as an electric insulator and also as a lubricant. In this study, three different square ratios were investigated for process parameter validation and for a qualitative evaluation of friction influence. The results demonstrate the high influence of friction on material formability during the process and so the importance of lubrication during the inflating step. In doing this, boron nitride was shown to be the optimal solution because it guarantees both electrical insulation and lubricant properties. Moreover, the inflating analysis demonstrates that process time cycle can be reduced without compromise the shaped part, increasing drastically the heating rate and avoiding the temperature homogenisation time by applying gas in pressure directly after reached the target temperature and applying a lubricant layer between tube and die surfaces.

5.4. Case study

In this section, the innovative Hot Metal Gas Forming technology is applied in order to create a real industrial component in collaboration with an Italian company, Anodica Industries™. The industrial validation is an important testbed to understand possible flaws, and in which to study new mechanical or process solutions to improve the prototype.

Starting from the product specifications required by the company, relating to the material and the geometry dimensions, a new matrix was designed applying the knowledge acquired during the previous laboratory test. Several trials were performed with the aim to create the component without defects, with the purpose to reduce the length of the process cycle. An evaluation of the final product is given, which also considers feedback from the partner company.

5.4.1 Industrial request

The component object of this study is the main part of an aesthetic handle nowadays produced by the Anodica Industries™, through machining an aluminium AA6060 alloy rod. A 3D image of the final component and its geometrical characteristics is presented in Figure 5.43.

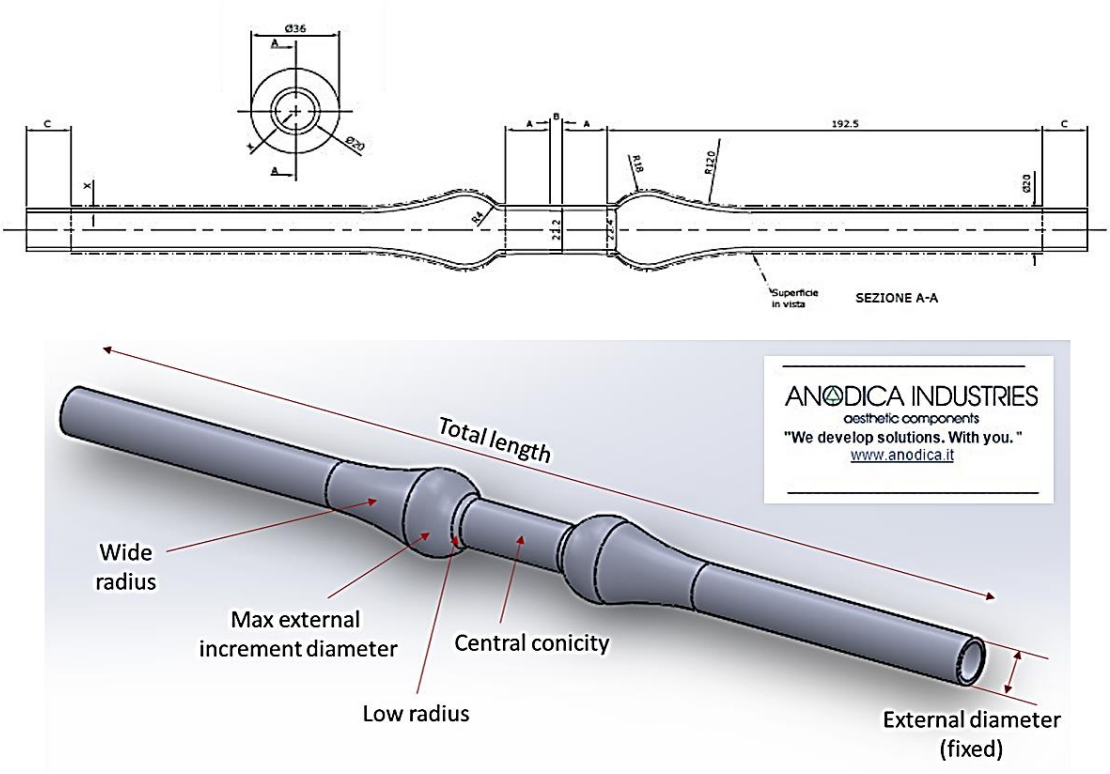

Figure 5.43: Three-dimensional picture and drawing geometries of the component requested; complete technical drawing is reported in appendix A.1.

For its geometrical dimensions and axial symmetry, the component presents characteristics that could be shaped through the HMGF technology and so through the designed prototype. Moreover, the required material is identical to that studied during the previous analysis, therefore allowing us to draw on this experience. This process, compared with the previous one used to produce the component, can reduce the process cycle whilst also saving raw material, especially when high production volumes are required.

The geometric characteristics of the final component are reported in Table 5.1 with reference to Figure 5.43:

Table 5.16: Geometric characteristics of the required final component.

Total length	500 mm
External diameter (fixed)	20 mm
Tube thickness	1.5 mm – 2 mm – 3 mm
Central conicity value	0.2 mm on diameter for 20 mm length
Wide radius	120 mm
Low radius	4 mm
Max external increment diameter	36 mm (80%)

For these reasons, commercial tubes of AA6060 in T5 condition were chosen with total length of 500 mm, an external diameter of 20 mm and in three different thicknesses; 1.5 mm, 2 mm and 3 mm.

Figure 5.43 shows that the shaped surfaces are concentrated in the middle part and are represented in sequence by a wide concave radius of 120 mm, a convex radius of 18 mm and a small radius of 4 mm. The middle part of the component presents a conicity of 0.2 mm on the diameter evolved in 20 mm of length, changing the external diameter from 22.4 mm to 22.2 mm in the middle. The remaining part is not subject to deformation and therefore exhibits an external diameter of 20 mm and an internal diameter which varies with the initial tube thickness.

5.4.2 Die design

To reproduce the component, a new die was designed and structured in two shells each one with the negative geometries of the part. Non-magnetic stainless steel AISI 310 was chosen as the die material for its high mechanical properties with temperature, and the possibility to be used within a magnetic field, as described in 5.3.1. AISI 310 presents a high percentage of Nichel and Crome (around 20 %) and so maintains its mechanical properties even at 800 °C. This means that the material is suitable to use in the HMGF process where an electric current is used to heat the sample to around 500 °C.

Considering the geometry to be shaped, the die structure was machined only for the tube length that is subjected to the deformation, keeping the component part without deformation in free air. Without the presence of the die at high temperature in those parts, a strong temperature drop in the tube would be expected, which would prevent bulging. The die was designed with a total length of 200 mm and a width of 100 mm to allow the screw seats, for die closing and also the heating cartridges seats, for die heating as shown in Figure 5.44.

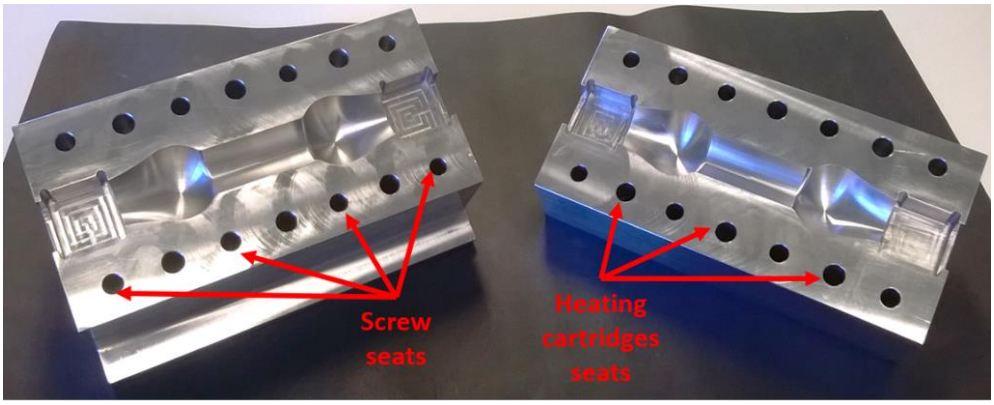

Figure 5.44: Two half parts of the AISI 310 die.

All die surfaces were machined with a roughness of 3.2 µm while, the negative part surfaces, presented a roughness of 0.4 µm, as shown in the technical drawing in appendix A.2, A.3.

Regarding the electric insulator, as shown in Figure 5.44, two square seats were machined at the die edges. This is to allow the insert of a different die material with the aim of avoiding the electric current transfer between tube and die. Indeed, at the edges, die surfaces are in contact with the tube during the heating step where high intensity current is used. Bearing this in mind, two different materials were used to create the electric insulator insert, based on the results reported in sections 5.3.4 and 5.3.5. The first material, a glass ceramic material with the

commercial name 'MACOR', is machinable with machine tools, as shown in Figure 5.45. The second material is AISI 310, which is the same material as the die but coated with a boron nitride layer.

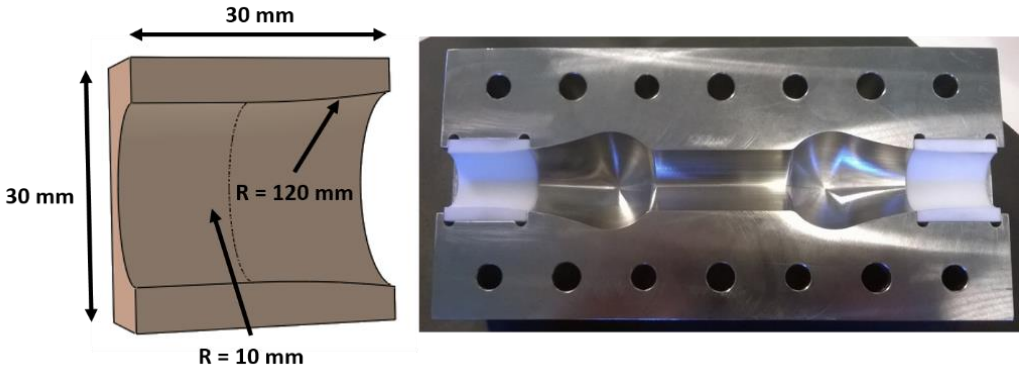

Figure 5.45: Electric insulator dimensions (a) and application of MACOR inserts on the die (b).

The main characteristics of the MACOR glass ceramics are detailed in Table 5.17.

Table 5.17: MACOR properties.

Density	$2.52 \cdot 10^3$ kg/m^3
Compressive strength	345 MPa
Hardness	400 HV
Max service temperature	1000 °C
Thermal expansion coefficient	13 μstrain/°C
Dielectric strength	41.6 MV/m

Die closing was guarantee through eight M8 screws with a resistance class 8.8, while, for a precise die localisation, a support was designed in order to arrange the assembled die quickly, even during high temperature operations. In doing so, a parallelepiped stainless steel block, with non-magnetic properties, was used as main support and fixed directly to the machine frame. Two plates with an "L" geometry fixed through four shoulder screws were used to centre the die in one direction, while support edges were used for centring in the other direction. Finally, to assure the electric and thermal insulation between the die and its support, plates of Thratermic MI700 material, with the properties detailed in Table 5.18, were used between the assembled components, as shown in and fixed through six M6 screws. All die support structures, were obtained using AISI 304 material.

Table 5.18: Thratermic MI700 properties.

Density	2.3·103 kg/m^3
Compressive strength	400 MPa
Thermal conductivity λ	0.2 W/m·K
Max service temperature	500 °C
Thermal expansion coefficient	13.2 μstrain/°C
Dielectric strength	41.6 MV/m

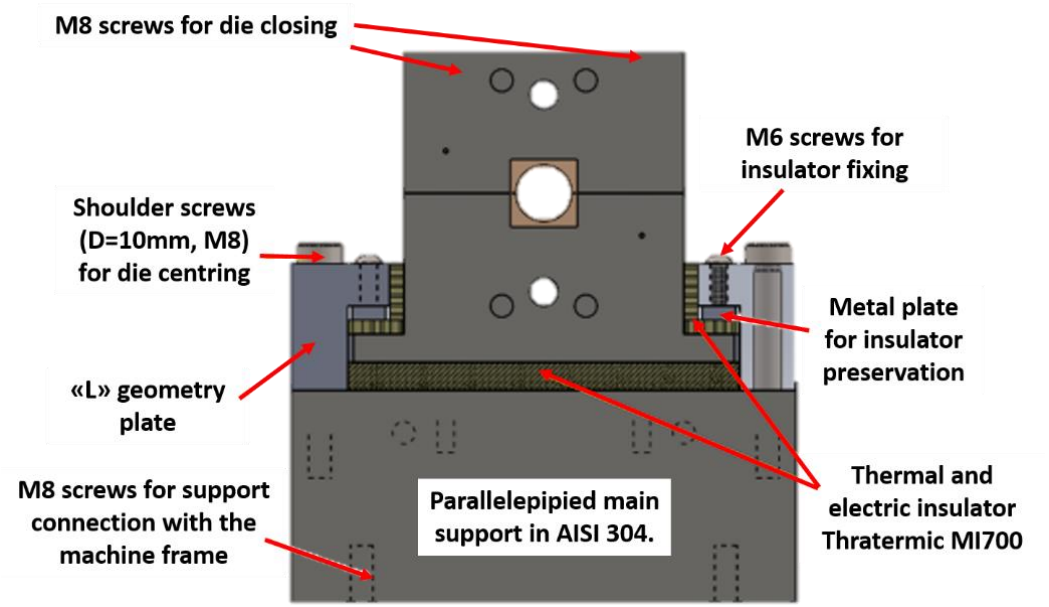

Figure 5.46: Die assemble to the support and principal components.

To assure a quickly die heating, as done for the square geometry test in section 5.3.1, six heating cartridges with a 10 mm diameter and 100 mm length, and a further two of 10 mm diameter and 200 mm length, which can be controlled manually or remotely through the developed software, were used to arrive at 500 °C in 20 minutes. Figure 5.47 shows an exploded view of all die and support components including of heating cartridges.

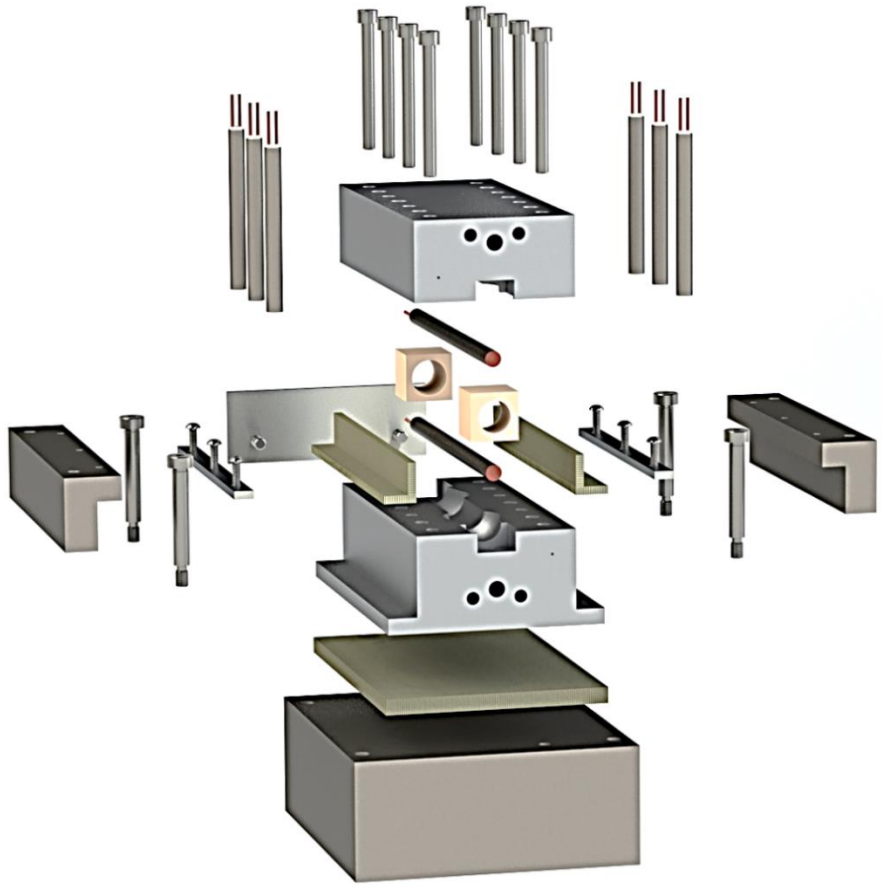

Figure 5.47: Exploded view of die and support components.

In order to perform tests on several tube thicknesses with smaller external diameter compared to the supplied tubes used to obtain the square geometry in section 5.3, different copper jaws with a seat of 20 mm in diameter were machined to assure the electric flow from the electric generator to the tube. Moreover, three cylindrical bushings in AISI 310 material, one for each tube internal diameter, were machined to support the sample and to guarantee a perfect tube sealing during the inflating operation.

Figure 5.48: Cylindrical bushings for the three tubes thickness studied.

5.4.3 Process procedure

Due to the small internal tube diameter and the low diameter to thickness ratio, tube bulging needs more than an air pressure of 8 bar, as instead done with 27 mm in inner diameter tube studied in section 5.3. Therefore, during all tests, the inflating air pressure was kept at the maximum available of 20 bar.

However, by performing deformation tests in free air, i.e. without the die, the importance of pressure ramp calibration becomes clear while working at high pressure. For example, by taking 1 second to ramp the pressure to 20 bar, the tube fracture morphology appeared as shown in Figure 5.49 (a), which is similar as found for the AA6082 aluminium tube in section 5.2.3. The fracture was generated as an explosive long crack with thick edges. By taking 5 seconds to arrive at the target pressure, the formability increased and the fracture morphology is typical of ductile fracture Figure 5.49 (b). This phenomenon is connected to the reduction of the strain rate parameter, as was expected given the studies on material rheological characterisation reported in section 4.3.4.

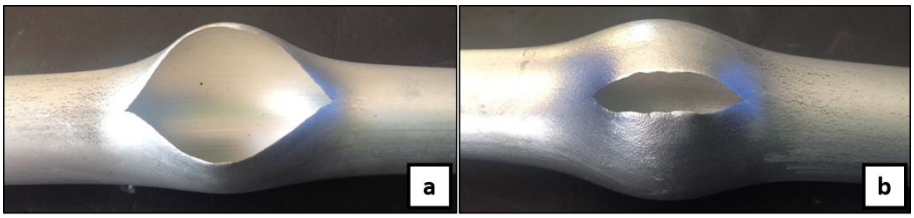

Figure 5.49: Fracture morphology due to different pressure ramp. 20 bar in 1 second (a), 20 bar in five seconds (b).

The heating time was always controlled remotely through the developed software and was fixed at 35 °C/s independently of the tube thickness, in order to reach the target of 520 °C in

15 seconds as used in tests performed in section 5.3.5. Moreover, using the results obtained in 5.3.5, , in order to reduce the process cycle, temperature homogenisation time was avoided, so inflation pressure air was applied immediately, as shown in, Figure 5.50. The amount of inflating time was instead changed for each test with the purpose of (i) obtaining the desired final part without defect and (ii) reducing the process time, as much as possible, without compromising the result

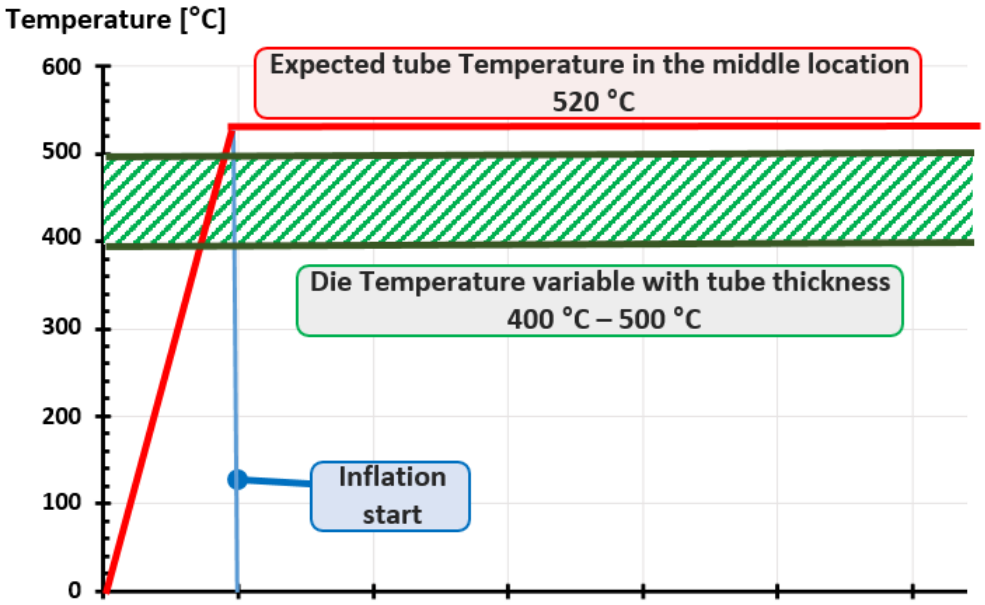

Figure 5.50: Thermal process cycle used to create the industrial component.

The same method of temperature measurement that was used for square die tests in section 5.3.3 was applied during the process. Therefore, three K-thermocouples located in three different locations was used to measure the die average temperature, while tube temperature was measured by means of two pyrometers pointed 5 mm outer from die edges, as shown in Figure 5.51 (a), and through a sealed K-thermocouple for the internal air temperature, as shown in Figure 5.51 (b). It is worth noting that in the pyrometer measurement location the tube surface was covered with black paint to avoid problems with reflection leading to an incorrect temperature reading. Temperature calibration was performed with the same procedure used in section 5.3.2, which differed for the no-contact between die and tube. Therefore, a temperature of 370 °C measured out of the die, was found to assure 520 °C in the tube middle point inside the matrix.

The die temperature was varied with the tube thickness that was tested. The temperature was however always kept over 400 °C because, as found in the previous study on square component in section 5.3.4 higher die temperatures lead to a higher tube formability, and moreover, high temperature differences between tube and die reduce the amount of deformation. However, the highest die temperature can overheat the tube through conduction (contact locations in the insert position), risking increasing the tube diameter during the bulge operation outside the matrix. Therefore, after thermal calibration, a delta temperature of 100 °C was imposed between die and tube, for highest temperature for the die, assuring in the middle of the sample a difference lower than 50 °C. A very high tube temperature concentrated

in the middle point, with a constant temperature length around 40 mm, allowed the starting of plastic deformation, while when material reached die surfaces, the tube, that exhibits lower mass compared to the die, is heated along all the matrix length reaching the die temperature. Successively the no-strain hardening behaviour of this material in a range from 450 °C and 500 °C allowed the deformation of the tube inside the die.

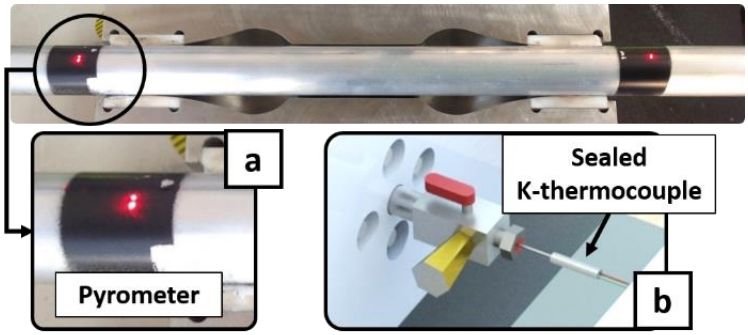

Figure 5.51: Temperature tube measurement through pyrometer (a) and sealed K-thermocouple (b).

During the test the electric insulation between die and tube was guaranteed by covering die surfaces with a layer of boron nitride, as shown in Figure 5.52. Due to the complex die shape, using a rigid insulator was not possible, while a spray insulator, as verified in section 5.3.5, is also good to assist the material flow inside matrix cavities.

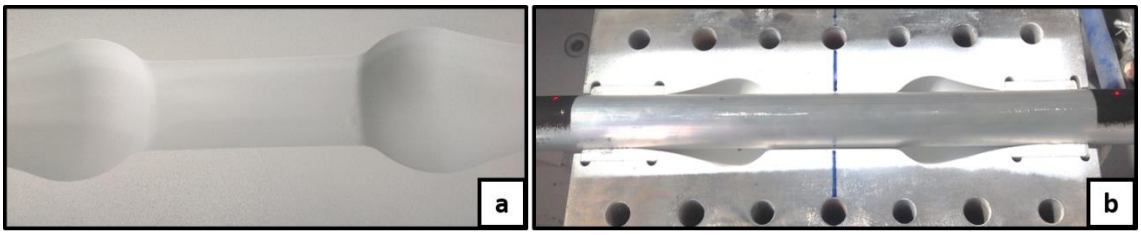

Figure 5.52: Die surfaces covered with boron nitride for electrical insulation and lubricant.

5.4.4 Results and observation

In this section the formability results are presented. They are divided into the three different tube thickness studied, starting from with 1.5 mm and concluding with 3 mm. Each test condition was repeated three times, to ensure the reproducibility of the results.

For each as-delivered tube, the best process parameter in term of temperature and inflating time is also indicated. Considerations of the component quality are reported, with respect to the aesthetic surface appearance before and after anodisation process.

Tube initial thickness 1.5 mm

The first trial was performed whilst maintaining a fixed inflating pressure of 20 bar given over 5 seconds and the heating rate of 35 °C/s and using an external tube temperature, measured with the pyrometers, of 370 °C, while an average die temperature was fixed at 470 °C. Figure 5.53, shows the tube breakage produced after 6 seconds from the inflating starting, due to high temperature used.

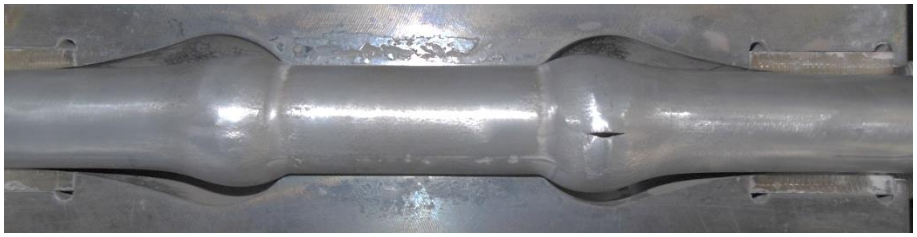

Figure 5.53: Tube with initial thickness of 1.5 mm inflated using a pressure of 20 bar, tube temperature of 370 °C and die temperature of 470 °C.

For this reason, a drastic reduction of the temperature used was applied. Specifically, a tube temperature of 320 °C was used, which corresponds to a centre temperature of 460 °C, in addition to using a die temperature of 420 °C. The result reported in Figure 5.54, indicates that no deformation appeared even after 300 seconds, meaning that the process temperatures used were too low for a tube plastic deformation.

Figure 5.54: Tube with initial thickness of 1.5 mm inflated using a pressure of 20 bar, tube temperature of 320 °C and die temperature of 420 °C.

Several test were performed in which the temperature parameter was increased as shown in Table 5.19, which summarises the experimental test plan.

Table 5.19: Experimental test plan with inflating pressure of 20 bar on tube thickness of 1.5 mm.

Test number	Tube temperature	Die temperature	Inflating pressure	Deformation results
1	370 °C	470 °C	20 bar	Break – 6 s
4	320 °C	420 °C	20 bar	undeformed
7	330 °C	430 °C	20 bar	Break – 92 s
10	340 °C	440 °C	20 bar	Break – 76 s
13	350 °C	450 °C	20 bar	Break – 53 s
16	360 °C	460 °C	20 bar	Break – 21 s

The results demonstrate that it is not possible to completely create the part without tube breakage. Regardless, test number 7 gave the maximum deformation reached, indicating that a tube and die temperature respectively of 330 °C and 430 °C as the best process parameters when a using cold air pressure of 20 bar.

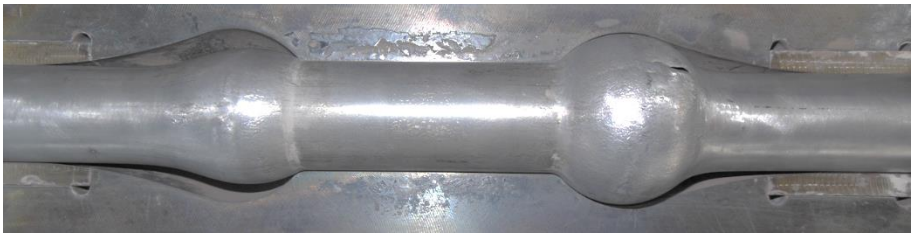

Figure 5.55: Tube with initial thickness of 1.5 mm inflated using a pressure of 20 bar, tube temperature of 330 °C and die temperature of 430 °C.

For this reason, a reduction of the inflating air pressure was attempted in order to deform the material with low load so decreasing the strain rate.

Initially a pressure of 10 bar was applied at the process parameters used in test 7 without obtaining deformation even after 300 seconds, showing that a pressure of 10 bar is not sufficient to bulge tubes with an internal diameter of 17 mm and a thickness of 1.5 mm. A pressure of 15 bar was then applied with the same test conditions, but even in this case, after 300 seconds the tube did not present any relevant deformation, as shown in Figure 5.56.

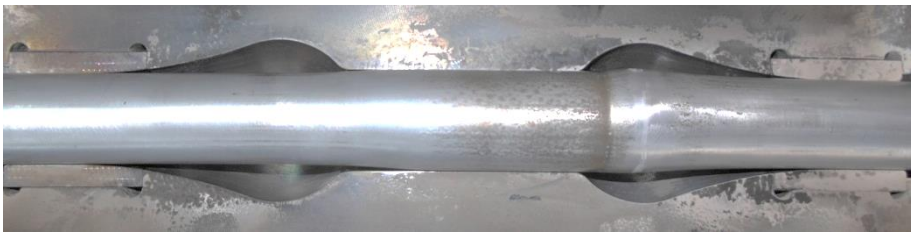

Figure 5.56: Tube with initial thickness of 1.5 mm inflated using a pressure of 15 bar, tube temperature of 330 °C and die temperature of 430 °C.

After several tests, it was found that only by increasing the tube temperature at 360 °C, with a respective die temperature of 460 °C, is it possible to deform the tube, which, ruptured after 170 seconds, as shown in Figure 5.57.

Figure 5.57: Tube with initial thickness of 1.5 mm inflated using a pressure of 15 bar, tube temperature of 360 °C and die temperature of 460 °C.

Finally, an additional test was performed by increasing the inflating pressure from 10 bar to 15 bar during the test, and then from 15 bar to 20 bar. Different pressure ramps were applied, using tube and die temperature as reported in Table 5.20. In test 34, 37 and 40, the first value of pressure was applied for 100 seconds and increased to the second pressure value during the next 100 seconds. Based on these results, test number 43 was performed applying the initial pressure for 500 seconds and then incrementing it successively to the final value using the next 500 seconds.

Table 5.20: Experimental test plan with variable inflating pressure on tube thickness of 1.5 mm.

Test number	Tube temperature	Die temperature	Inflating pressure	Deformation results
34	360 °C	460 °C	15 - 20 bar	Break – 85 s
37	330 °C	430 °C	15 - 20 bar	Break – 195 s
40	360 °C	460 °C	10 - 15 bar	Low deformation
43	360 °C	460 °C	10 - 15 bar	Break – 835 s

The results show that a pressure of 10 bar is not adequate to bulge the tube even at high temperature while, using a cold air pressure of 15 bar, the material starts to deform plastically but needs very long process time as showed for the case 43. Moreover, using the maximum pressure available of 20 bar, the tube reached the fracture with a time depending directly on the process temperature. The tube temperature of 320 °C measured at 5 mm from the die edges, which corresponds to a tube centre temperature inside the die of 470 °C, is not enough to start plastic deformation, which required at least 330 °C.

It is possible to conclude that if one starts with a thin tube thickness of 1.5 mm, it does not allow the external tube diameter to increase while shaping the component. In Table 5.21, reports the results for all of the test performed on these as-delivered tubes, inclusive of temperatures used and results obtained.

Table 5.21: Complete experimental test plan with initial tube thickness of 1.5 mm.

Test number	Tube temperature	Die temperature	Inflating pressure	Deformation results
1	370 °C	470 °C	20 bar	Break – 6 s
4	320 °C	420 °C	20 bar	undeformed
7	330 °C	430 °C	20 bar	Break – 92 s
10	340 °C	440 °C	20 bar	Break – 76 s
13	350 °C	450 °C	20 bar	Break – 53 s
16	360 °C	460 °C	20 bar	Break – 21 s
19	330 °C	430 °C	10 bar	undeformed
22	360 °C	460 °C	10 bar	undeformed
25	330 °C	430 °C	15 bar	Low deformation
28	350 °C	450 °C	15 bar	Low deformation
31	360 °C	460 °C	15 bar	Break – 170 s
34	360 °C	460 °C	15 - 20 bar	Break – 85 s
37	330 °C	430 °C	15 - 20 bar	Break – 195 s
40	360 °C	460 °C	10 - 15 bar	Low deformation
43	360 °C	460 °C	10 - 15 bar	Break – 835 s

Tube initial thickness 2 mm

These as-delivered tubes were all inflated with a cold air pressure of 20 bar, so these tests focus only on the temperatures and inflating time.

In the first test thermal parameters were used that were found as the best during the square geometry shaping analysis reported in 5.3.4. These correspond to a die temperature of 470 °C and a tube temperature measured at 105 mm from the centre of 370 °C. Air pressure was kept constant for 60 seconds, giving the results shown in Figure 5.58.

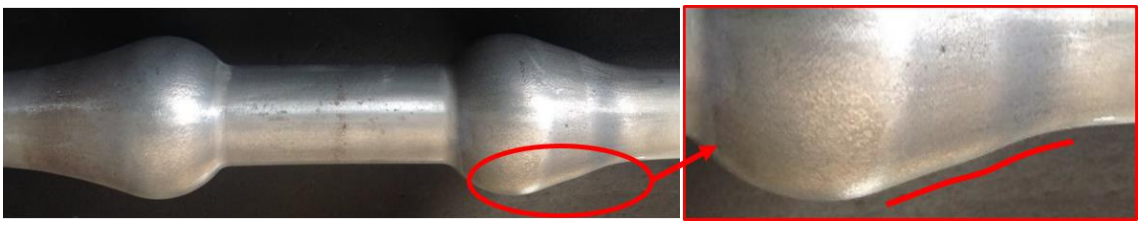

Figure 5.58: Tube with initial thickness of 2 mm inflated using a pressure of 20 bar for 60 seconds, tube temperature of 370 °C and die temperature of 470 °C.

From the image is possible to observe that the component appeared completely shaped, with the exception of the wide concave radius. For this reason another trial was performed increasing the tube temperature up to 390 °C, but the shaped component, shown in Figure 5.59 highlights an external tube diameter increment of 0.45 mm in the location enclosed within the die. Regardless, the part appeared completely shaped even reducing the inflation time from 60 to 30 seconds.

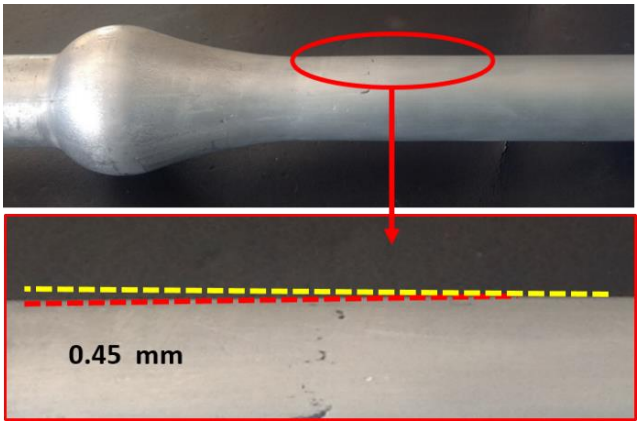

Figure 5.59: Tube with initial thickness of 2 mm inflated using a pressure of 20 bar for 30 seconds, tube temperature of 390 °C.

To avoid tube deformation in locations not bounded by the die, successive tests were done using the initial process temperatures applied, but with increased inflation time, initially at 100 seconds and ultimately obtaining a completely shaped component using only 70 seconds.

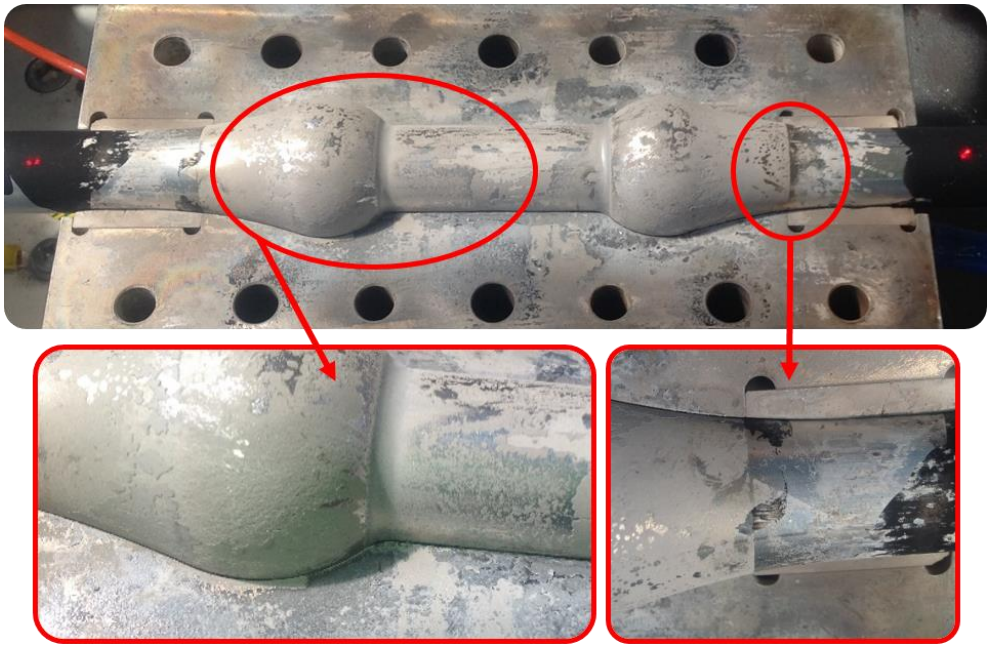

Figure 5.60: Tube with initial thickness of 2 mm inflated using a pressure of 20 bar for 70 seconds, tube temperature of 370 °C.

Figure 5.60, shows the shaped tube after the test, highlighting the perfect adhesion with die surfaces of the smallest radius of 4 mm and of wide radius of 120 mm. Moreover, picture shows the white boron nitride layer used as electric insulator and lubricant that covered tube and die surfaces. After sample cleaning through a mixture of water and ether, the component appears good without relevant aesthetics defects, as shown in Figure 5.61.

Figure 5.61: Tube with initial thickness of 2 mm completely shaped after cleaning.

Table 5.22, describes each of the all test that were performed on tubes with an initial thickness of 2 mm, inclusive of the temperatures used and results obtained.

Table 5.22: Complete experimental test plan with initial tube thickness of 2 mm.

Test number	Tube temperature	Die temperature	Inflating pressure	Deformation results
1	400 °C	500 °C	20 bar	Break – 2 s
4	350 °C	450 °C	20 bar	Low deformation after 60s
7	370 °C	470 °C	20 bar	Good deformation after 60s
10	390 °C	490 °C	20 bar	Deformation out of die
13	370 °C	470 °C	20 bar	Deformation ok after 100s
16	370 °C	470 °C	20 bar	Deformation ok after 80s
19	370 °C	470 °C	20 bar	Deformation ok after 70s

Tube initial thickness 3 mm

In the feasibility evaluation of shaping the desired component using aluminium tubes with an initial thickness of 3 mm, due to the small internal tube diameter where the air in pressure was applied it was not possible to use the same temperature parameters found in the previous studies. Higher tube and die temperatures, coupled to long process time, were necessary for plastic tube deformation. Table 5.23 shows the complete test plan for the 3 mm tube thickness, showing the temperatures and inflating time applied for each condition.

Table 5.23: Complete experimental test plan with initial tube thickness of 3 mm.

Test number	Tube temperature	Die temperature	Inflating pressure	Deformation results
1	370 °C	470 °C	20 bar	Undeformed after 100s
4	430 °C	500 °C	20 bar	Break – 43s
7	410 °C	500 °C	20 bar	Break – 64s
10	400 °C	500 °C	20 bar	Break – 110s
13	390 °C	500 °C	20 bar	Good deformation after 200s
16	390 °C	500 °C	20 bar	Deformation good after 250s
19	390 °C	500 °C	20 bar	Deformation ok after 300s

22	390 → 410 °C	500 °C	20 bar	Deformation ok after 250s

As shown by test 1, the temperatures used to completely shape the component with initial tube thickness of 2 mm were insufficient for a plastic deformation of the material. Instead very high temperatures were tried using the maximum die temperature available of 500 °C bounded by the maximum working temperature (500 °C) of the thermal insulator Thratermic MI700. As shown in Figure 5.62, material breakage in the location where high diameter increment was required, appeared using temperature value higher than 390 °C, as found from test 4, 8 10. In fact, considering a delta temperature of 150 °C between the centre of the tube inside the die and the value measured through the pyrometer at 5 mm outer the die edges, as shown in Figure 5.51, a centre tube temperature higher than 540 °C starts to be critical for the material tested.

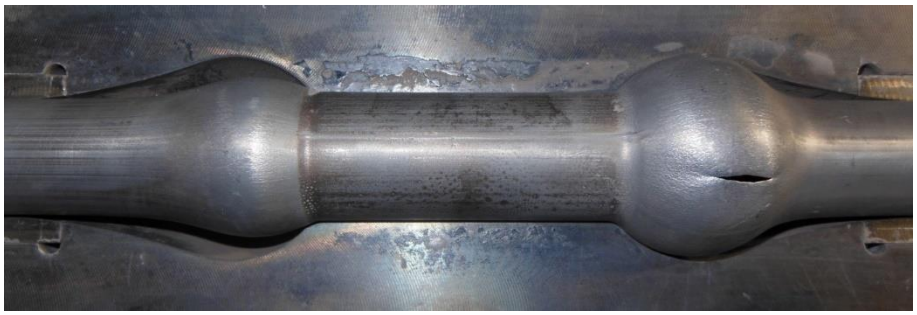

Figure 5.62: Tube with initial thickness of 3 mm inflated using a pressure of 20 bar, tube temperature of 410 °C and die temperature of 500 °C.

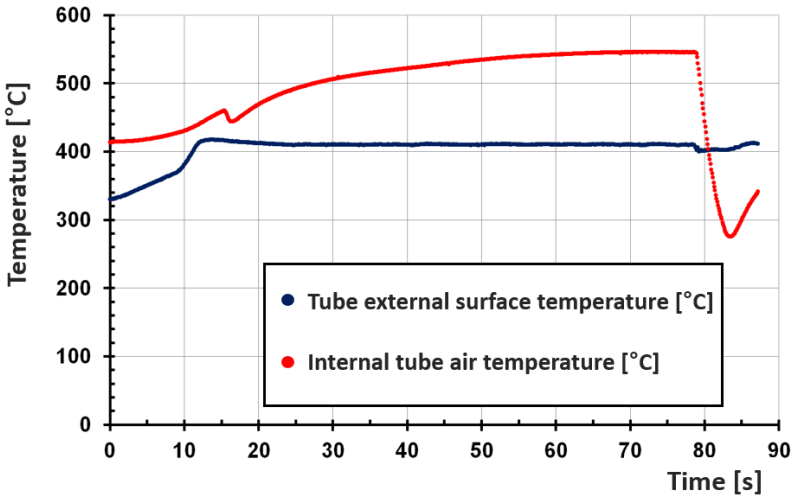

Figure 5.63: Temperature measurement during test number 7 using tube initial thickness of 3 mm.

Figure 5.63, shows temperature trend during the latter test. Blue dots represent the external tube surface temperature measured through the pyrometers while red dots represent the internal tube air temperature as illustrated in section 5.4.3. It worth noting that after 80 seconds, the internal air temperature becomes constant and representative of the tube external temperature in the middle, which is 150 °C higher inside the die. In addition it is possible to observe a first internal temperature drop due to air inflating start, and the second drop due to the tube breakage.

Test numbers 13, 16 and 19, which were conducted at 390 °C, allowed for tube plastic deformation with an amount of deformation dependent on the inflating time. A process time of 300 seconds was required to completely shape the component, as shown in Figure 5.64, while faster processes of 250 and 200 seconds, exhibited incomplete component development.

Figure 5.64: Tube with initial thickness of 3 mm inflated using a pressure of 20 bar for 300 seconds, tube temperature of 390 °C and die temperature of 500 °C.

The shaped component presented defects due to the high temperature that was involved. Moreover, the use of a greater thickness implies a greater mass which, at high temperature, increases its dimension through thermal expansion and thereby increasing the pressure on die surface. Figure 5.65 highlights the presence of the closing die line, which is visible even after tube cleaning.

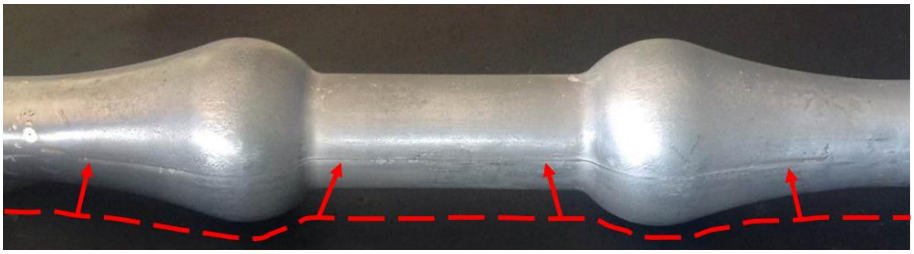

Figure 5.65: Closing die line visible on the 3 mm shaped component.

Considering Figure 5.66, where due to an imperfect contact between the copper jaw and the tube, the electric current was not symmetrically distributed along tube length.

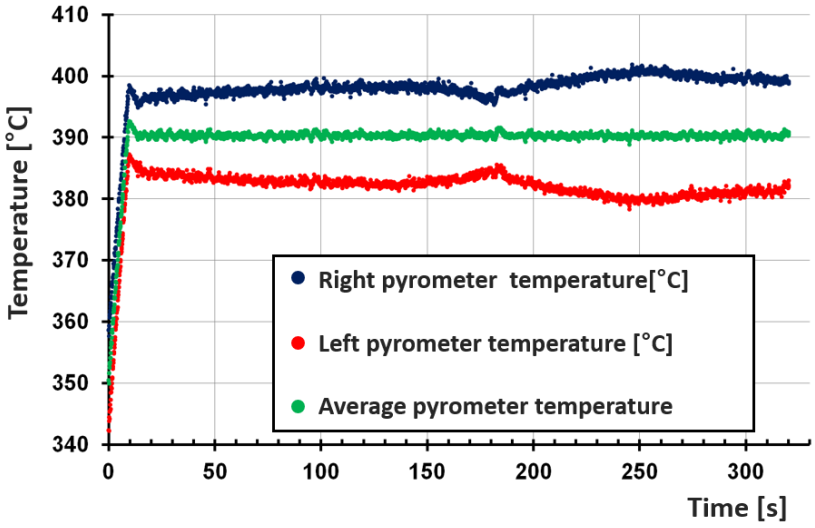

Figure 5.66: External tube temperature distribution on unconventional test.

Indeed, in this test, one pyrometer measured a temperature higher than the other, obtaining an average test temperature of 390 °C. Regardless of this, after 300 seconds the deformation on the sample appeared incomplete on the coolest side, while the other side was good, as shown in Figure 5.67.

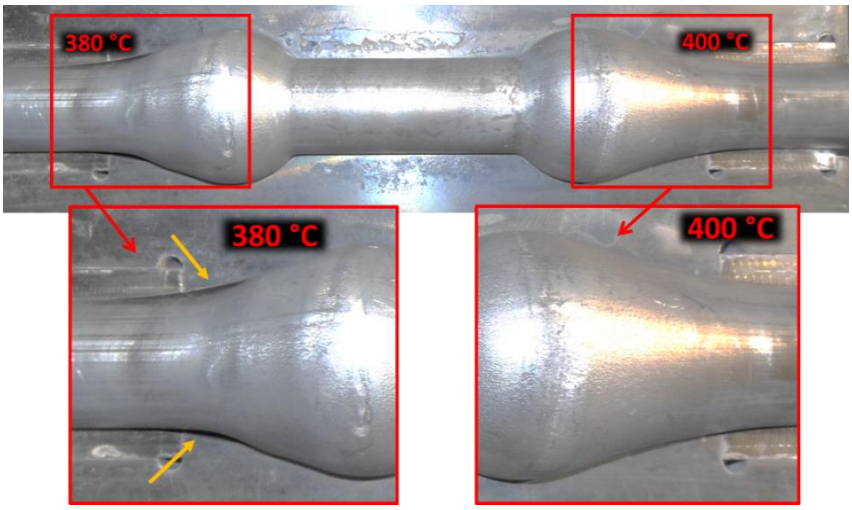

Figure 5.67: Deformation result using different temperature on the tube extremities.

Following this result, an additional test was conducted by increasing the tube temperature during the inflation time from 390 °C to 410 °C whilst decreasing the process cycle by 50 seconds.

Micro-hardness measurement

An evaluation of the mechanical properties after deformation was performed through micro-hardness measurements on final components with 2 mm and 3 mm in thickness, by considering five different locations. Starting from the undeformed part, the areas were investigated with the four geometries demonstrated in Figure 5.68, which also details the measured hardness values.

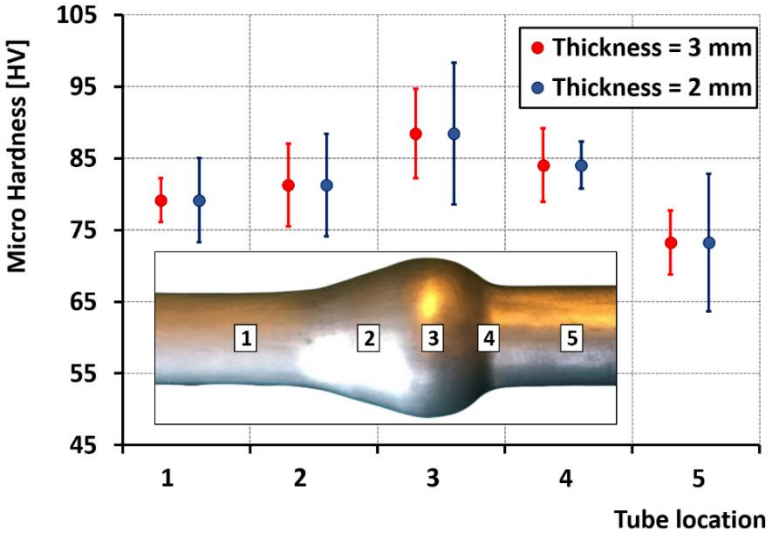

Figure 5.68: Micro hardness measurements for shaped component with 2 mm and 3 mm evaluated in the five locations highlight in the figure.

Even if the two components were produced from tubes with different thicknesses, the results exhibited the same hardness trend. The highest values were found in the locations where the highest deformations were required, as expected, whilst the lowest values were measured in tube centre due to the high temperature process used. Nevertheless, if one considers the error bars, the hardness values are found to be outside of the range exhibited by the undeformed part in location 1.

Aesthetic results:

The complete shaped components, created from tube with 2 mm and 3 mm in thickness, were subjected to anodisation chemical treatment by the partner company Anodica Industries™. The shaped tubes were first mechanically polished and then inserted in anodising bath in order to give different aesthetic finishing from gold, inox and chrome.

Results shown in Figure 5.69 (a) for the gold finishing and in Figure 5.69 (b) for the chrome finishing, exhibit opaque location along the tube where the anodisation treatment does not worked as expected.

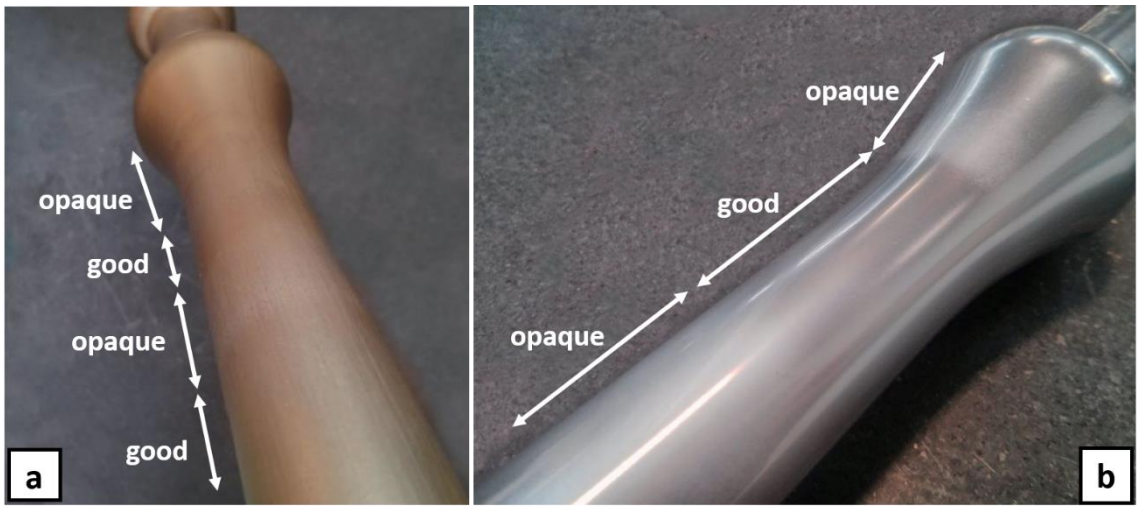

Figure 5.69: Anodisation surface treatment on final component. Gold colour (a), chrome colour (b).

Possible reasons can be attributed to grain morphology variation and residual stress generated inside the material after the deformation. For these reasons, microstructure evaluation was performed on the shaped tubes in three different locations, as shown in Figure 5.70, namely: undeformed location (a), maximum deformation location (b) in the dome apex, and low deformation location (c), in the middle of the tube.

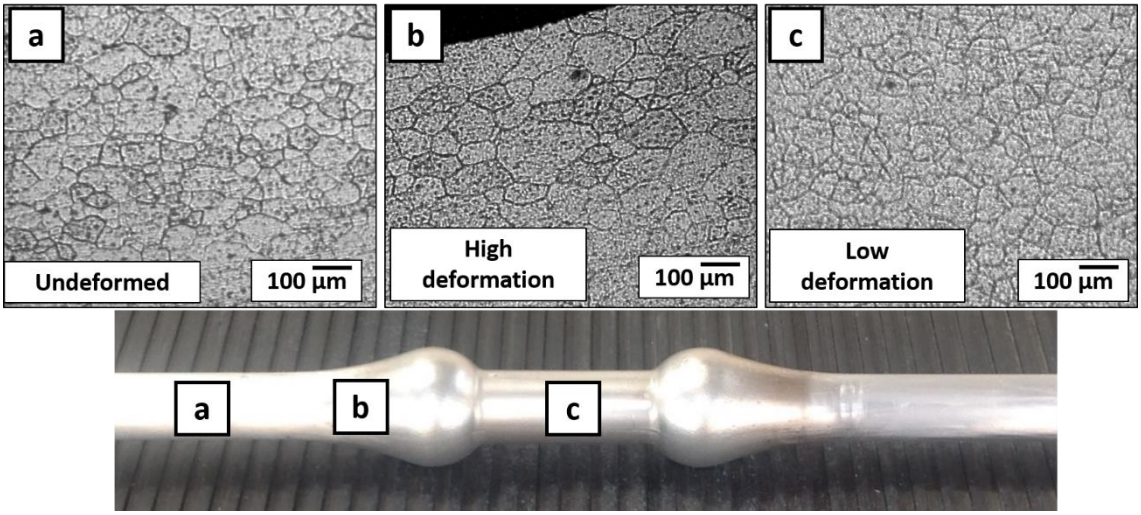

Figure 5.70: Microstructure evaluation of the shaped component.

The exhibited microstructure no significant changes in grain morphology but only a slightly grain coarsening, due to the different process temperatures used between the locations "a" and "c" where the amount of deformation is not relevant. Conversely, case "b" showed relevant grain coarsening, such that the grains were stretched along a preferential direction connected to tube deformation. Therefore, a complete homogenisation heat treatment was applied to the shaped part, keeping the sample in a furnace for 12 hours at 550 °C with a successive water quenching. Microstructure differences between the tube in the as-delivered condition and after heat treatment are shown in Figure 5.71, where grains appear slightly coarser but with a more homogenous size and morphology.

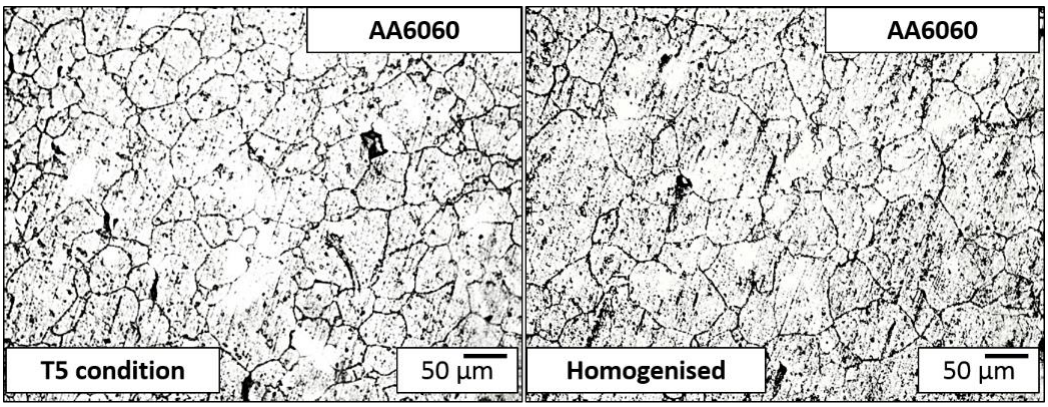

Figure 5.71: Shaped component microstructure before and after an homogenisation heat treatment.

After the tube homogenisation heat treatment, the anodisation process was repeated and the results did not present any aesthetic problems, indicating that a microstructure homogenisation on the final part was necessary for successive chemical surface treatments. Figure 5.72 (a) and Figure 5.72 (b), show the results of a chrome anodisation on the final component before and after the homogenisation heat treatment, while Figure 5.72 (c) exhibits a picture of the heat-treated component realised through the HMGF process, after gold anodisation.

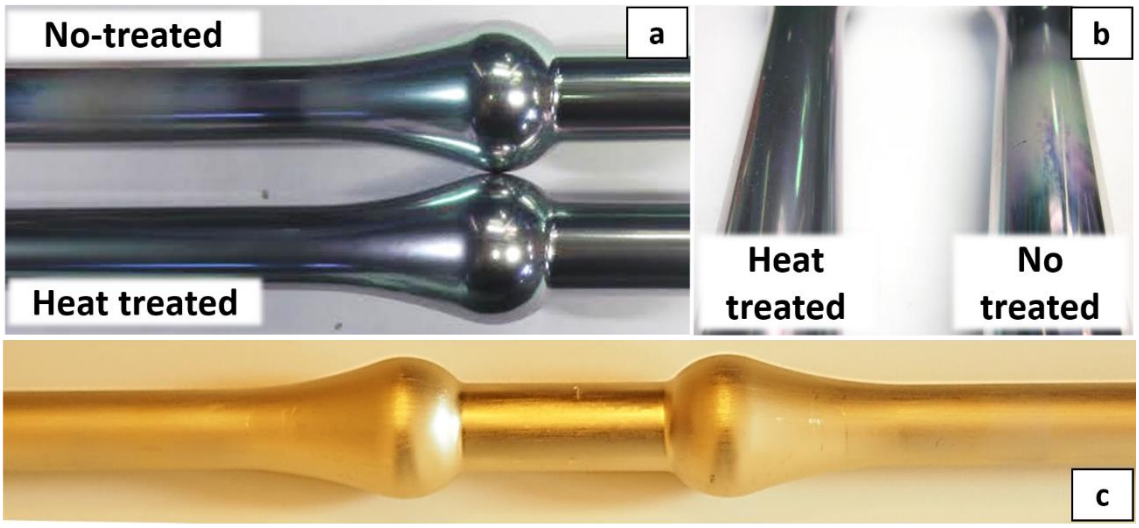

Figure 5.72: Anodised shaped component realised through the HMGF process; comparison between a chrome anodisation before and after homogenisation heat treatment (a) and (b), heat treated component after gold anodisation (c).

5.4.5 Conclusion

The industrial trials have confirmed the potential of the HMGF process and also the reliability of the prototype design In fact, even if the experimental apparatus is compact and with small dimension, compared to a hydroforming implant, after an adequate process setup the components released appeared good and without any defects.
Results have moreover proved that starting with tube with too low a thickness (1.5 mm) was insufficient to allow the external tube diameter to completely shaping the component, and that a pressure of 20 bar was excessive for the small thickness, causing a preventive fracture. Nevertheless, a tube with an initial thickness of 2 mm was shown to be the best initial solution. A die temperature of 470 °C and an external tube temperature of 370 °C were used to completely shape the component without defects in 70 seconds. Moreover, the longest die could be used to reduce the process time at 30 seconds, increasing the external tube temperature during the process at 390 °C.
The highest tube thickness of 3 mm required a very high temperature to completely shape the component, increasing the material thermal expansion leading to surface defects, such as the close die line due to the tube pressure on die surfaces. Furthermore, a long process time of 250 seconds is required to arrive at complete deformation, which is incompatible with the research aim to reduce the process cycle in comparison with modern processes used to shape hollow component.

During these tests, another aspect was confirmed regarding the electric insulator necessary between tube and die, due to the high current intensity used. Without electric protection, die surfaces can be damaged by electroerosion phenomena created through the generation of electric arcs, as shown in Figure 5.73. Boron nitride, was shown to be the best solution for its quick and easy applicability, and also for its cost no comparable with glass-ceramic material which presents also fragile behaviour especially when coupled with materials with different

thermal expansion values. Moreover, boron nitride presented optimal lubricant properties that can aid the material flow during the deformation.

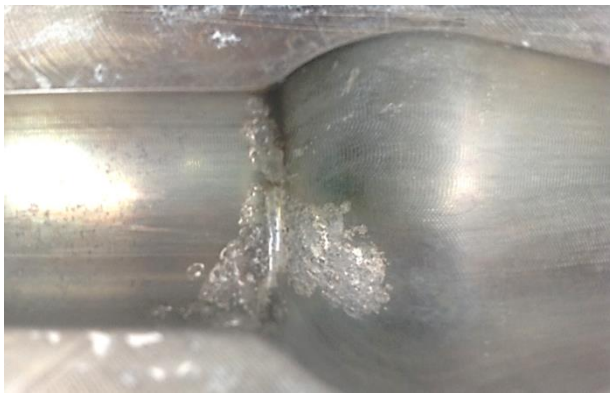

Figure 5.73: Electro erosion phenomenon due to the electric arc generation between tube and die surfaces.

An additional aspect that has been considered is the thermal symmetry, which is shown to be fundamental during tests with symmetrical die. Contact problems between tube and copper jaws can change the temperature distribution which compromises the process result. Therefore, monitoring the jaw temperature allows one to avoid potential defects on the final component. In Figure 5.74 (a),) shows a correct copper jaw temperature trend where the first temperature rise is due to the tube heating through the Joule effect, while the other minor trend slope is connected to tube inflating operation. Figure 5.74 (b) shows a problematic heating stage where different jaw temperatures, and therefore different tube extremity temperatures, compromise the process result.

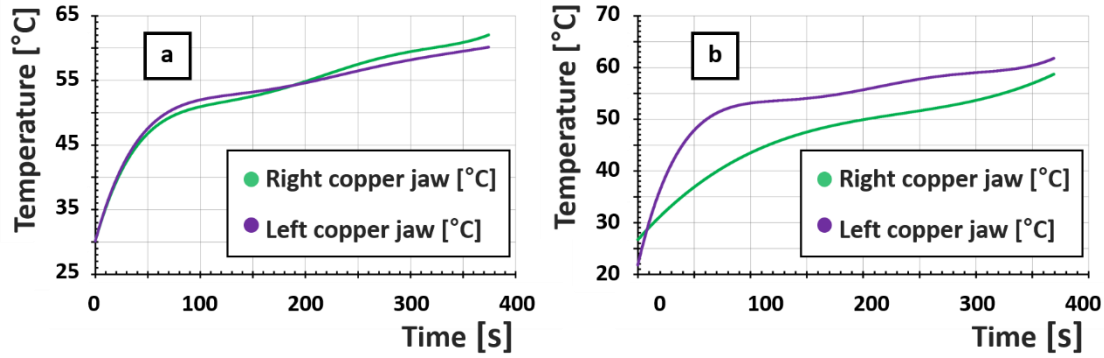

Figure 5.74: Copper jaw temperature trend: correct (a) and wrong (b).

5.5. Conclusions

The promising capabilities of the innovative Hot Metal Gas Forming process (HMGF), that allows forming parts with low pressures and high process temperatures increasing the formability, were investigated by designing a novel experimental hot gas forming apparatus. Initially the mechanic, electric and control software design were presented in detail. From the literature and research experience on metal sheets hot deformations, an electric current, and

therefore the Joule effect, was used as a heating device. Therefore an external electric current generator, providing 60 kW of power with a maximum current of 6000 A, was used and successively modified to be controlled through a real-time closed-loop based on the measured temperature, with an accuracy of ±1 A. Cold air under pressure was used for the deformation and was controlled with a manual pressure regulator in a range from 1 to 20 bar with an accuracy of ± 0.01 bar.

A thermal calibration, through a thermocamera, was realised in order to understand the temperature distribution along the tube during the high temperature process, and to understand the correlation between temperature and the electric current intensity provided. Subsequently, the prototype evaluation was performed on bulging aluminium AA6060 and AA6082 tubes, produced with 5 different extrusion parameters and cut in four different lengths. During the tube expansion, obtained at 520 °C with a low pressure of 8 bar, an optical measured system was used to measure the deformation by considering the major strain at fracture. These results have demonstrated the functionality of the experimental apparatus and also the relatively higher formability of the AA6060 tubes compared to the AA6082 alloy. The high percentage of manganese in the AA6082 decreases drastically the formability, even if the bulging process was at very high temperature (520 °C). Fractures in this alloy appeared with a large explosive crack. The fracture morphology of the AA6060 was completely different, where a thin breakage emerged. Moreover, formability results showed that tubes extruded with lowest temperature and that were subsequently quenched in water exhibited the highest formability for both the aluminium series. Micro-hardness measurements showed that even if at the high temperature process of 520 °C is compatible with a solubilisation heat treatment temperature range, for this aluminium alloy, a short process time is insufficient to activate the precipitates solution during the deformation which could compromise the surface appearance, as found in section 4.4.3.

Regarding the process, bulged tests in free air highlighted that tube length does not affect the amount of formability, but slightly increases the tube part at constant temperature. Moreover, a temperature of 520 °C proved to be a good compromise in order to reduce, as much as possible, the pressure used for tube deformation without generating a solution heat treatment that could affect the surface quality of the deformed part at high strain rate. Furthermore, the fracture morphology without explosion generated by the AA6060 confirmed that is safer to regulate the air pressure with a subsequent inflation after reaching the target temperature, as opposed to using sealed air under pressure inside the tube before starting the heating, which without any pressure control risks sudden explosion.

The results of the tests of tubes bulged in free air were used to evaluate the possibility of shaping tubes inside a square die, whilst also investigating additional parameters useful for process development. High values of current through the tube generate a magnetic field about the tube and so a non-magnetic steel was used as die material to avoid possible problems due to magnetic attraction that could move the die structure during the process. Therefore die temperatures, and the effect of different die materials aimed at avoiding electric contact between the tube and die, were analysed by considering the effect of the insulator surface roughness on the final component. In these tests, the tube was heated up to the testing temperature of 520 °C in 70 seconds and held at this temperature for 200 s in order to guarantee that the temperature was distributed along tube length. Subsequently, three 30-

second inflating operations were applied inside the die to avoid an air temperature drop during the inflation. Thanks to this approach the investigation has exhibited the advantages of the new procedure, finding which are the best process parameters in terms of tube temperature, die temperature, heating time and inflating time, which increase the component formability in gas forming shaping operation. Die temperature influences were evaluated by measuring the quality of the final component through the thickness distribution and the radius curvature at the corners, proving that high die temperatures lead to a higher the tube formability. Using the glass-ceramic material insulator, the highest value of die filling has been obtained with smallest corner radius value of 3.54 mm, extended for 40 mm and localised in the tube centre. Moreover, glass-ceramic was shown to be the best candidate for surface roughness properties, and also for resistance to several production cycles. However, for its very high cost and for the difficulties to obtain it in unconventional shapes and dimensions, the application of a thin layer of boron nitride was shown to be the best solution for the process from an industrial perspective. The very high thickness reduction of 80 % reached in components with the best die filling results have fixed the limit, for a tube with 1.5 mm in thickness and an internal diameter of 27 mm, to 40 mm for a square geometry without breaks. The influence of inflating time in shaped square tubes, characterised with three different square ratios, was investigated using only one inflation step applied immediately after reaching the target temperature, in order to minimise temperature homogenisation time, with the aim of reducing the process time cycle. Different square-ratios have also allowed the testing of the extendibility of process parameters found for the square die, to different die geometries, and to investigate qualitatively the effect of friction. The time dependence of formability, as expected, was verified by finding that 100 seconds were sufficient for completing the die shaping in each of the geometries. Furthermore, a significant trend with the influence of friction was observed, demonstrating a formability reduction on the geometry where tube arrives early in contact with die surfaces, and demonstrating that the use of boron nitride is an optimal process solution because it assures both electrical insulation and lubricant properties. In fact, a comparable value of die filling (80 %) can be reached using only 115 seconds thanks to the application of boron nitride compared to the 300 seconds needed using the glass-ceramic material.

Finally, using the results from the previous tests in free air and with the use of a square die, a real industrial HMGF application was applied, which confirmed several critical aspects of the process and validated the relevant choice of solutions. Specifically:

- The magnetic field generation produced with high current can compromise the process results which can be avoided using non-magnetic material for die and other die support;
- The electric insulation between the tube and die surfaces is guaranteed by applying a thin layer of boron nitride, which is suitable due to it's ease-of-application;
- The friction between the die and tube is reduced using boron nitride;
- A low time cycle is obtained by reducing the heating time to 15 seconds and by avoiding temperature homogenisation time without compromising the part shaping;

- The process safety without explosions, is guaranteed by applying air under pressure after reached tube target temperature, and through the pressure ramp regulation.

Therefore, in collaboration with an Italian company, the feasibility of creating an aesthetic part characterised by several radius dimension an other critical geometries, was investigated starting with tubes of AA6060-T5 with an external diameter of 20 mm and three different thicknesses, namely 1.5 mm, 2 mm and 3 mm. Due to the low diameter-to-thickness ratios, and the lower tube area where air under pressure could operate compared to the 27 mm inner diameter of previous studies, a pressure of 20 bar was used during each test. A die made from non-magnetic AISI 310 material was designed and assembled through mechanical fixed connections, while electrical insulation was guaranteed using a sprayed layer of boron nitride. The preventions of die surfaces from electric current transfer from tube to die proved to be fundamental. Electric arc generation during the process was found to cause severe damage to the die surfaces through electro erosion.

Several test with different parameters, in terms of tube temperature, die temperature and inflation time, showed that a tube thickness of 1.5 mm was insufficient to allow a complete part shaping due to a premature break. Furthermore, a pressure of 20 bar was excessive for the small thickness causing an instantaneous fracture. On the other hand, a tube with 3 mm in thickness can be completely shaped using very high temperature process and long process cycle, which is not consistent with the goal of the industrial trial. Moreover the high forming temperature coupled with high thickness of 3 mm tube and high thermal expansion generates surface defects on the final part such as a close die line, that could be avoided by using a controlled load press for die closing.

The tube with initial thickness of 2 mm was completely shaped without defects in only 70 seconds, showing also the possibility to reduce the productive cycle by 30 seconds, by increasing the process temperature and the die dimension to cover all tube surface, thereby preventing diameter expansion in undesired locations.

A symmetrical temperature distribution during the test showed to be essential for a homogeneous deformation distribution but also suggests the possibility of using dies with different temperatures for a better shaping of complicated parts.

Aesthetic analysis conducted on final components coupled with microstructure observation and hardness measurements demonstrated that a homogenisation heat treatment is necessary to guarantee a good applicability of an anodisation chemical treatment very used on aluminium aesthetic component. Results obtained with chrome and gold anodisation colours in parts without grains homogenisation have presented opaque spots that completely disappeared after heat treatment.

The complete study on the HMGF process, started with a literature review, continued with the design of an experimental apparatus, the bulging tests in free air and inside a die, and finished with the application of the knowledge acquired on an industrial case of study, confirms the potential of this technology and shows it to be a valid and concrete alternative to the modern processes for tube shaping.

Chapter 6

Conclusions

In recent years, the forming processes of aluminium alloys sheets and tubes at elevated temperature have gained a renewed interest for manufacturing parts of the car body-in-white and of the chassis, because of the more and more stringent requirements in terms of reducing cars weight, hence their fuel consumption on one hand, and increasing passengers' safety on the other.

The AA5xxx and AA6xxx series have proved to be the best candidates in replacing steels on passenger cars to save weight. Anyway, the common processes used nowadays for shaping aluminium alloys at high temperature aiming to enhance their poor formability at room temperature, are not efficient for a mass production because they involve long process times and they exhibit limited operating temperatures.

On this bases, the aim of this research was to investigate the formability of aluminium alloys to deform sheets and tubes at high temperatures and strain rates, by applying innovative forming technologies to overcome the limits of current industrial processes.

In the first part of this work, the applicability of Hot Stamping technology in sheet metal forming of aluminium alloys of the series 5083 and 6016 with different as-delivered conditions: commercial and superplastic for the 5xxx series and as built or solubilised for the 6xxx series, was investigated. As expected, for both the aluminium series, the material flow stress was influenced by the temperature and strain rate. The best formability window for hot stamping the AA5083 aluminium alloy was achieved by applying a forming temperature of 450 °C and a strain rate of 10^{-1} s^{-1}, while for the AA6016 aluminium alloy by applying a forming temperature ranging between 450 °C and 500 °C and a strain rate ranging from 10^{0} s^{-1} to 10^{-1} s^{-1}. Moreover, the formability window was enlarged by solubilising the AA6016 aluminium alloy that anyway exhibited a higher strain at fracture than the AA5083 even in its as built condition.

With regard to the superplastic treatment applied on the AA5083 alloy microstructure on the post-mechanical properties, hot stamping trials of real automotive components evidenced comparable results between superplastic and not superplastic alloy, thus is possible to conclude that it would be preferable and more sustainable to employ the aluminium alloy in its commercial grade rather than the superplastic grade, avoiding extra costs needed to obtain a specific microstructure.

On the other side, the solubilisation heat treatment strongly influenced the AA6016 aluminium alloy, inducing a very poor surface topography on deformed specimens, not suitable for subsequent finishing operations. In practise, although the solubilisation heat treatment could enhance the material formability, the rough and irregular surfaces even visible with eye, make this heat treatment not feasible for hot stamping applications. The followed approach consisting in both laboratory and industrial testing, allowed acquiring important knowledge regarding: (i) the material response during and after deformation at elevated temperatures, and (ii) the technical limits of hot stamping aluminium alloys in terms of FLDs. Based on the main findings of an extended experimental campaign, the optimal formability window could be individuated, when the maximum formability and desired mechanical properties were satisfied contemporarily. Furthermore, these results were validated on a real industrial case, in which automotive parts with complex geometries were hot stamped in a production plant. Excellent results in terms of formability where achieved, proving the robustness of the followed approach. Thanks to these tests, it was possible to conclude that under certain hot stamping process conditions, it is possible to shape aluminium alloy parts on cold dies when high temperatures and high strain rates are applied.

In parallel with this work, the potentiality of Hot Metal Gas Forming process to shape aluminium tubes was investigated: an experimental prototype was designed, developed and built, and then validated performing a wide experimental campaign.

The developed apparatus, used electrical current with a maximum power of 60 kW to heat the tube, while cold pressurised air ranging from 1 to 20 bar was employed to mechanically expand the aluminium tubes, mainly of the AA6xxx series. Aiming to accurately regulate the process parameters and to measure the variation of temperatures and pressure during the process, software was developed in LabVIEW®. The formability tests in free air were initially carried out to find out the best forming parameters, lately validated to shape the tubes constrained in a square die. Those latter tests, allowed investigating the effects of different die materials on the final tube surface roughness, on their electrical insulation capabilities and on their suitability in such forming process. Boron Nitride resulted the best choice among those tested, due to its high electrical insulation property and allowing a simple application even on complex die cavities. In fact, the tests conducted applying a high electrical current without an insulator mean, generated surface damages on the die cavities due to the formation of electric arcs between the tube and the die materials. The application of Boron Nitride facilitated also the material flow to fill the die cavity during the deformation phase thanks to its lubrication property, hence strongly reducing the friction forces arising within the die/tube interface. The tube forming tests, highlighted the necessity to employ no-magnetic die materials, in fact, because of the relevant magnetic field generated by applying electrical current at high intensity, all magnetic components present nearby the tube could be drifted compromising the outcome of the forming operation.

Finally, an industrial case study was simulated with the HMGF apparatus, consisting in shaping aluminium AA6060-T5 tubes supplied with different wall thicknesses, to produce complex parts characterized with several geometrical variations on the component final form. Short cycle times were tested ranging between 70 seconds for the first tests to a minimum of 30 seconds after some design improvements, with goal to validate the industrial feasibility of such technology. The case study, proved not only the technical feasibility of the apparatus and of the forming process to shape complex hollow parts in short cycle times, but also its capability to achieve excellent aesthetic aspects of the final part, preserving also the initial mechanical and microstructural properties of the aluminium alloy. Anodization surface treatments were also applied on the deformed parts, evidencing the necessity to perform a homogenization heat treatment after the forming process, in order to guarantee the desired aesthetic final result for an industrial application. Thanks to the industrial case study, the developed forming technology based on HMGF process foresaw a potential industrialization for the years to come.

APPENDIX

A.1. ANODICA COMPONENT TECHNICAL DRAWING

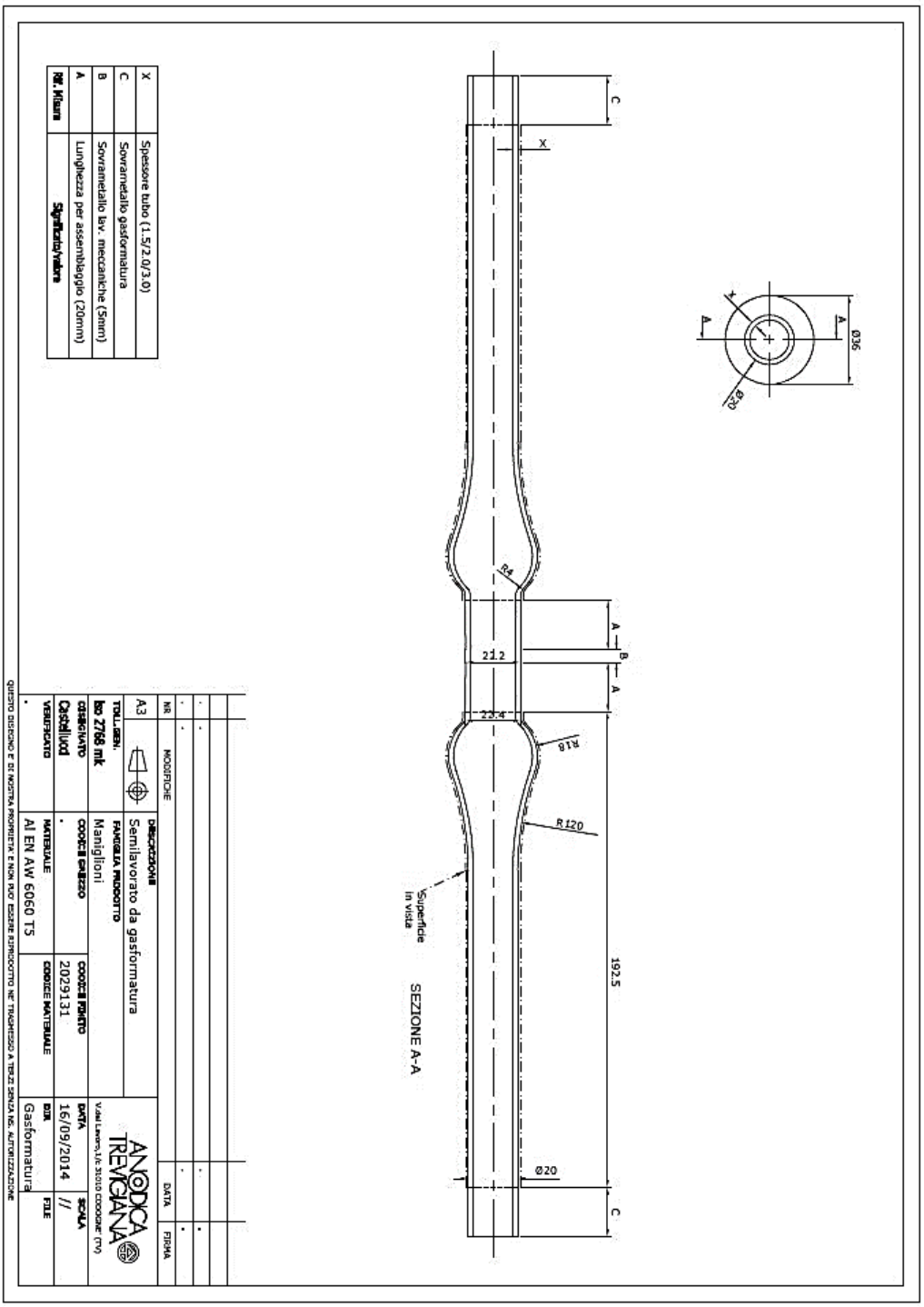

A.2. UPPER DIE TECHNICAL DRAWING

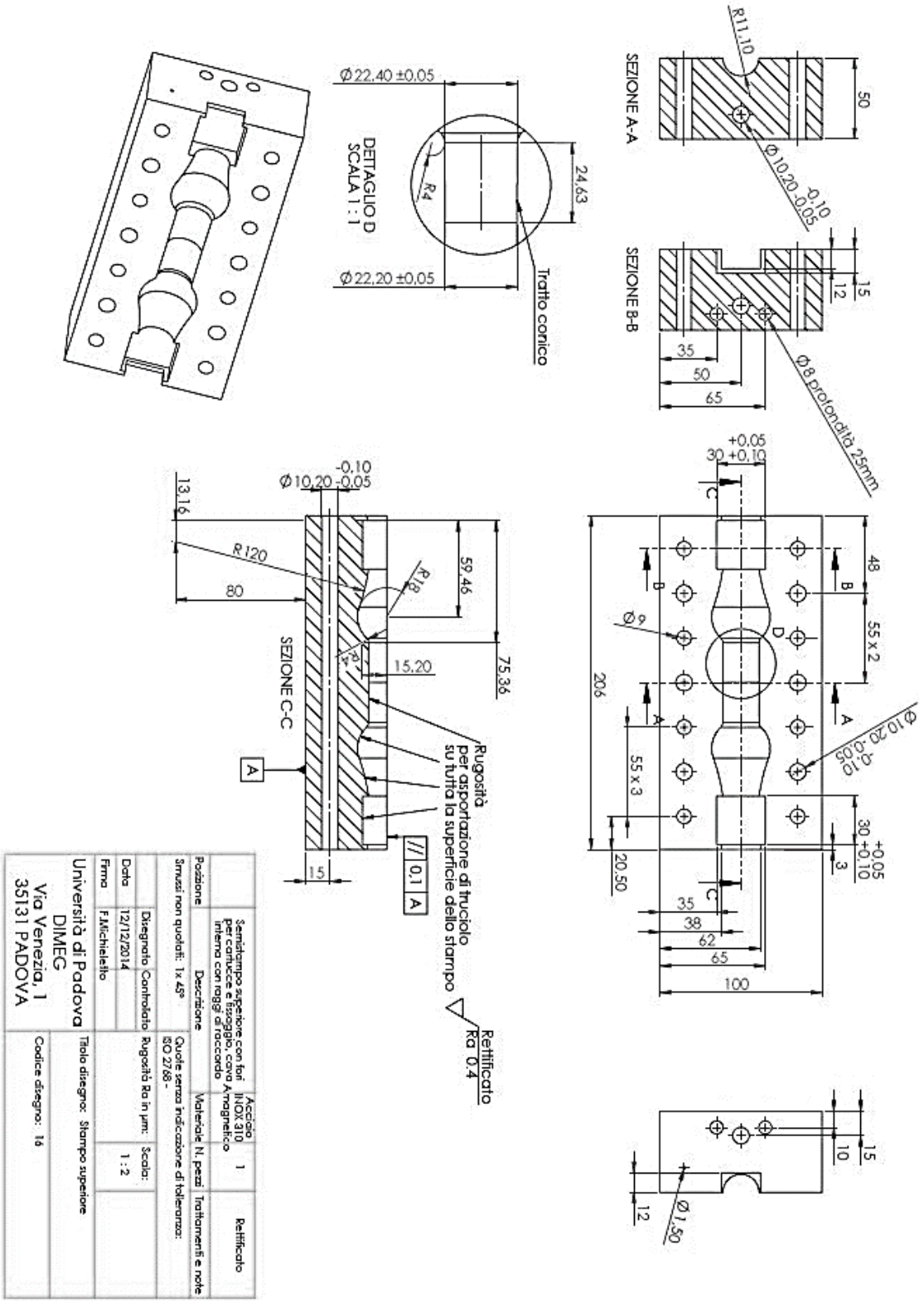

A.3. LOWER DIE TECHNICAL DRAWING

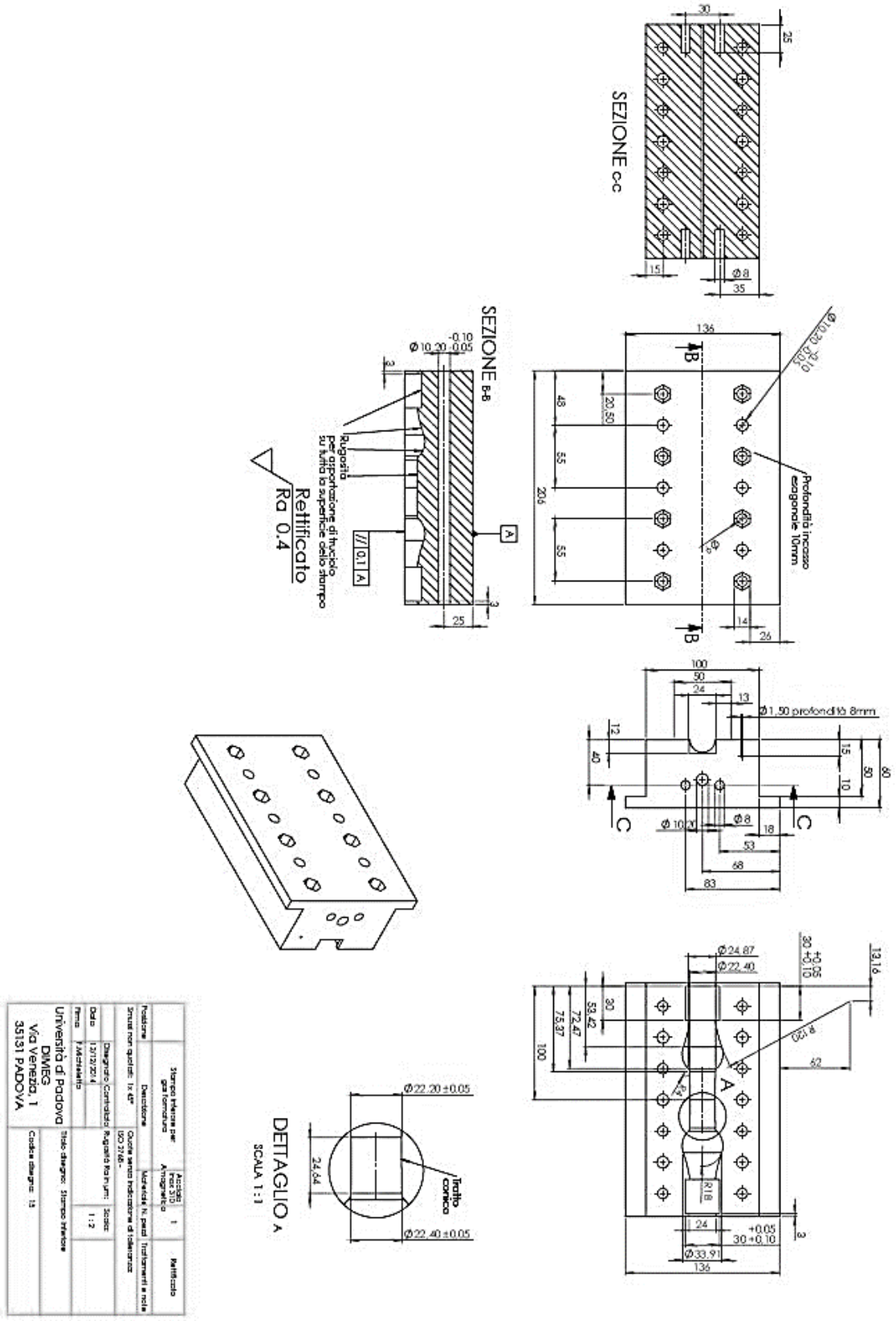

REFERENCES

[1] Unfccc, 1998, Kyoto Protocol To the United Nations Framework Kyoto Protocol To the United Nations Framework, Review of European Community and International Environmental Law, 7:214–217, DOI:10.1111/1467-9388.00150.

[2] SMMT Driving the Motor Industry, 95 CO2 g/km taget. .

[3] Ghiotti, A., Bruschi, S., 2011, Formability of aluminium alloy sheets at elevated temperatures, in *10th ICTP*.

[4] Schultz, R. A., 1999, Aluminum for Light Vehicles An Objective Look at the Next Ten to Twenty Years, in *14th International Aluminum Conference*.

[5] Carpenter J.A, 2AD, The Freedom CAR Challenge and Steel. pp. 96–111.

[6] Mildenberger, U., Khare, A., 2000, Planning for an environment-friendly car, Technovation, 20/4:205–214, DOI:10.1016/S0166-4972(99)00111-X.

[7] Canadian Industrial Machinery, Aston Martin Vanquish aluminium frame. [Online]. Available: http://www.cimindustry.com/article/formingfabricating/automotive-metal-stamping.

[8] Fisker Automotive, Fisker Karma aluminium space frame. [Online]. Available: http://autogreenmag.com/2010/03/01/geneva-preview-fisker-karmas-aluminum-space-frame-digitally-revealed/.

[9] Neugebauer, R., Altan, T., Geiger, M., Kleiner, M., Sterzing, A., 2006, Sheet metal forming at elevated temperatures, CIRP Annals - Manufacturing Technology, 55/2:793–816, DOI:10.1016/j.cirp.2006.10.008.

[10] Merklein, M., Hußnätter, W., Geiger, M., 2008, Characterization of yielding behavior of sheet metal under biaxial stress condition at elevated temperatures, CIRP Annals - Manufacturing Technology, 57/1:269–274, DOI:10.1016/j.cirp.2008.03.032.

[11] U.S. Department of Energy, 2010, Materials Technologies : Goals , Strategies , and Top Accomplishments, Vehicle Technologies program, DOI:DOE/GO-102010-3111.

[12] Materials, T., 2001, Properties and Selection: Nonferrous aloys and Special-purpose materials. .

[13] Conserva, M., Bonollo, F., Donzelli, G., 2004, Alluminio - Manuale degli impieghi. .

[14] Smith, W. F., 1995, Scienza E Tecnologia Dei Materiali. .

[15] Berglund, G., 2008, The history of hardening of boron steel in northern Sweden, in *1st international conference on Hot Sheet Metal Forming of High-Performance Steel*, pp. 175–177.

[16] Karbasian, H., Tekkaya, A. E., 2010, A review on hot stamping, Journal of Materials Processing Technology, 210/15:2103–2118, DOI:10.1016/j.jmatprotec.2010.07.019.

[17] Merklein, M., Lechler, J., 2006, Investigation of the thermo-mechanical properties of hot stamping steels, Journal of Materials Processing Technology, 177/1–/3:452–455, DOI:10.1016/j.jmatprotec.2006.03.233.

[18] Stöhr, T., Lechler, J., Merklein, M., 2009, Investigations on different strategies for influencing the microstructural properties with respect to partial hot stamping, in *2nd International Conference on Hot Sheet Metal Forming of High- Performance Steel*, pp. 273–281.

[19] R Kolleck, S Pfanner, E-P Warnke, 2007, Development of Cooled Tools for Press Hardening of Boron Steel Sheets, in *Proceedings of the 12th International Con-ference on Sheet Metal*, pp. 225–232.

[20] B. Casas, D. Latre, N. Rodriguez, I. Valls, 2007, Tailor Made Tool Materials for the Present and Upcoming Tooling Solutions, in *Hot Sheet Metal Forming. Proceed- ings of the 1st International Conference on Hot Sheet Metal Forming of High-performance Steel*, pp. 23–36.

[21] B-A. Behrens, S. Hu, M. Demir, 2008, Conductive Heating System for Hot Sheet Metal Forming, in *Proceedings of the 1st International Conference in Hot Sheet Metal Forming of High-performance Steel*, pp. 63–68.

[22] Mori, K., Maki, S., Tanaka, Y., 2005, Warm and Hot Stamping of Ultra High Tensile Strength Steel Sheets Using Resistance Heating, CIRP Annals - Manufacturing Technology, 54/1:209–212, DOI:10.1016/S0007-8506(07)60085-7.

[23] Kolleck, R., Veit, R., Merklein, M., Lechler, J., Geiger, M., 2009, Investigation on induction heating for hot stamping of boron alloyed steels, CIRP Annals - Manufacturing Technology, 58/1:275–278, DOI:10.1016/j.cirp.2009.03.090.

[24] Pellegrini, D., Study on thermal and rheological parameters of high strength steels in hot forming conditions, Padova.

[25] Lechler J., Merklein M., 2008, Hot stamping of ultra strength steels as a key technology for lightweight contruction, in *Materials Science and Technology*, pp. 1698–1709.

[26] I. Aranguren Mendieta, Telleria Arribas M., J.P. Drillet, J.P. Puerta Velasquez, Alsmann M., et al., Green Press Hardening Steel Grades (GPHS).

[27] Georgiadis, G., Tekkaya, A. E., Weigert, P., Weiher, J., Kurz, H., 2014, Investigations on the Manufacturability of Thin Press Hardened Steel Components, Procedia CIRP, 18:74–79, DOI:10.1016/j.procir.2014.06.110.

[28] Turetta, A., 2008, Investigation of thermal, mechanical and microstructural properties of quenchenable high strength steels in Hot Stamping operations, Padova.

[29] International, A., 2001, Forming and forging, p. 2110.

[30] Kulas, M.-A., Green, W. P., Taleff, E. M., Krajewski, P. E., McNelley, T. R., 2006, Deformation mechanisms in superplastic AA5083 materials, Metallurgical and Materials Transactions A, 37/3:645–655, DOI:10.1007/s11661-006-0036-8.

[31] Sotoudeh, K., Bate, P. S., 2010, Diffusion creep and superplasticity in aluminium alloys, Acta Materialia, 58/6:1909–1920, DOI:10.1016/j.actamat.2009.11.034.

[32] Cipoletti, D. E., Bower, A. F., Qi, Y., Krajewski, P. E., 2009, The influence of heterogeneity in grain boundary sliding resistance on the constitutive behavior of AA5083 during high-temperature deformation, Materials Science and Engineering: A, 504/1–/2:175–182, DOI:10.1016/j.msea.2008.10.037.

[33] Cao, W. D., Lu, X. P., Conrad, H., 1996, Whisker formation and the mechanism of superplastic deformation, Acta Materialia, 44/2:697–706, DOI:10.1016/1359-6454(95)00176-X.

[34] Zelin, M. G., 1997, On micro-superplasticity, Acta Materialia, 45/9:3533–3542, DOI:10.1016/S1359-6454(97)00065-7.

[35] Das, S., Riahi, A. R., Meng-Burany, X., Morales, A. T., Alpas, A. T., 2012, High temperature deformation and fracture of tribo-layers on the surface of AA5083 sheet aluminum–magnesium alloy, Materials Science and Engineering: A, 531:76–83, DOI:10.1016/j.msea.2011.10.033.

[36] Williams, R. S., 2007, The evolution of technology for electronic materials over the last 50 years, Jom, 59/2:58–62, DOI:10.1007/s11837-007-0023-6.

[37] Weetman, J., 1957, Steady-state creep of crystal, Journal of Applied Physics, 28:1185–1189.

[38] Stachurski, Z. H., 2009, Mechanical behavior of materials. .

[39] Green, W. P., Kulas, M.-A., Niazi, A., Taleff, E. M., Oishi, K., et al., 2006, Deformation and failure of a superplastic AA5083 aluminum material with a cu addition, Metallurgical and Materials Transactions A, 37/9:2727–2738, DOI:10.1007/BF02586106.

[40] McNelley, T. R., Oh-Ishi, K., Zhilyaev, A. P., Swaminathan, S., Krajewski, P. E., et al., 2008, Characteristics of the transition from grain-boundary sliding to solute drag creep in superplastic AA5083, Metallurgical and Materials Transactions A: Physical Metallurgy and Materials Science, 39:50–64, DOI:10.1007/s11661-007-9401-5.

[41] Kulas, M.-A., Green, W. P., Taleff, E. M., Krajewski, P. E., McNelley, T. R., 2006, Failure mechanisms in superplastic AA5083 materials, Metallurgical and Materials Transactions A, 37/3:645–655, DOI:10.1007/s11661-006-0036-8.

[42] Kulas, M.-A., Krajewski, P. E., Bradley, J. R., Taleff, E. M., 2007, Forming-Limit Diagrams for Hot-Forming of AA5083 Aluminum Sheet: Continuously Cast Material, Journal of Materials Engineering and Performance, 16/3:308–313, DOI:10.1007/s11665-007-9057-8.

[43] Luo, Y., Luckey, S. G., Friedman, P. A., Peng, Y., 2008, Development of an advanced superplastic forming process utilizing a mechanical pre-forming operation, International Journal of Machine Tools and Manufacture, 48/12–/13:1509–1518, DOI:10.1016/j.ijmachtools.2007.12.010.

[44] Y, L., SG, L., WB, C., PA, F., 2008, Comparison of advanced spf die technologies in the forming of a production panel, Journal of Materials Engineering and Performance, 17:142–152.

[45] P, M., K, K., KS, K., 2009, Influence of friction during forming processes: a study using a numerical simulation technique, International Journal of Advanced Manufacturing Technology, 40:1067–1076.

[46] D, P., P, Y., 2008, Effects of punch load for elliptical deep drawing product of automotive parts, International Journal of Advanced Manufacturing Technology, 35:814–820.

[47] Liu, J., Tan, M. J., Aue-U-Lan, Y., Jarfors, A. E. W., Fong, K. S., et al., 2011, Superplastic-like forming of non-superplastic AA5083 combined with mechanical pre-forming, International Journal of Advanced Manufacturing Technology, 52/1–/4:123–129, DOI:10.1007/s00170-010-2729-9.

[48] Garrett, R. P., Lin, J., Dean, T. A., Geiger, I., Duflou, J., et al., 2005, Solution Heat Treatment and Cold Die Quenching in Forming AA 6xxx Sheet Components: Feasibility Study, in *Trans Tech Publications Ltd*, Erlangen, pp. 673–680.

[49] Lin, J., Dean, T. A., Garrett, R. P., D., F. A., 2008, A process in forming high strength and complex-shaped Al-alloy sheet components, WO2008059242.

[50] Mrówka-Nowotnik, G., Sieniawski, J., 2005, Influence of heat treatment on the microstructure and mechanical properties of 6005 and 6082 aluminium alloys, Journal of Materials Processing Technology, 162–163:367–372, DOI:10.1016/j.jmatprotec.2005.02.115.

[51] Ma, W., Wang, B., Yang, L., Tang, X., Xiao, W., et al., 2015, Influence of solution heat treatment on mechanical response and fracture behaviour of aluminium alloy sheets: An experimental study, Materials & Design, 88:1119–1126, DOI:10.1016/j.matdes.2015.09.044.

[52] Mohamed, M. S., Foster, A. D., Lin, J., Balint, D. S., Dean, T. a., Feb 2012, Investigation of deformation and failure features in hot stamping of AA6082: Experimentation and modelling, *International Journal of Machine Tools and Manufacture*. pp. 27–38.

[53] Foster, A., Mohamed, M., Lin, J., T. Dean, 2008, An investigation of lubrication and heat transfer for a sheet aluminium heat, form-quench (HFQ) process, Steel Res. Int. 79-11-VII (2008) .

[54] Fan, X., He, Z., Yuan, S., Lin, P., 2013, Investigation on strengthening of 6A02 aluminum alloy sheet in hot forming-quenching integrated process with warm forming-dies, Materials Science and Engineering: A, 587:221–227, DOI:10.1016/j.msea.2013.08.059.

[55] Ji, K., Fakir, O. El, Gao, H., Wang, L., 2015, Determination of Heat Transfer Coefficient for Hot Stamping Process, Materials Today: Proceedings, 2:S434–S439, DOI:10.1016/j.matpr.2015.05.059.

[56] Fan, X., He, Z., Yuan, S., Zheng, K., 2013, Experimental investigation on hot forming–quenching integrated process of 6A02 aluminum alloy sheet, Materials Science and Engineering: A, 573:154–160, DOI:10.1016/j.msea..02.058.

[57] Wang, L., Strangwood, M., Balint, D., Lin, J., Dean, T. A., 2011, Formability and failure mechanisms of AA2024 under hot forming conditions, Materials Science and Engineering: A, 528/6:2648–2656, DOI:10.1016/j.msea.2010.11.084.

[58] Mohamed, M. S., Foster, A. D., Lin, J., Balint, D. S., Dean, T. a., 2012, Investigation of deformation and failure features in hot stamping of AA6082: Experimentation and modelling, International Journal of Machine Tools and Manufacture, 53/1:27–38, DOI:10.1016/j.ijmachtools.2011.07.005.

[59] Lang, L. H., Wang, Z. R., Kang, D. C., Yuan, S. J., Zhang, S. H., et al., 2004, Hydroforming highlights: sheet hydroforming and tube hydroforming, Journal of Materials Processing Technology, 151/1–/3:165–177, DOI:10.1016/j.jmatprotec.2004.04.032.

[60] Wang, Z. R., Wang, T., Kang, D. C., Zhang, S. H., Yi, F., 1989, The technology of the hydro-bulging of whole spherical vessels and experimental analysis, Journal of Mechanical Working Technology, 18/1:85–94, DOI:10.1016/0378-3804(89)90111-3.

[61] Zhang, S. H., Danckert, J., 1998, Development of hydro-mechanical deep drawing, Journal of Materials Processing Technology, 83/1–/3:14–25, DOI:10.1016/S0924-0136(98)00039-9.

[62] Kuvin, B. F., 2002, Hydroformer evolves into complete source for prototype and shortrun sheet, Metalforming, 12:26–29.

[63] Ahmetoglu, M., Sutter, K., Li, X. ., Altan, T., 2000, Tube hydroforming: current research, applications and need for training, Journal of Materials Processing Technology, 98/2:224–231, DOI:10.1016/S0924-0136(99)00203-4.

[64] HIRSCH, J., 2014, Recent development in aluminium for automotive applications, Transactions of Nonferrous Metals Society of China, 24/7:1995–2002, DOI:10.1016/S1003-6326(14)63305-7.

[65] Luke, H. U., Hartl, C., Abbey, T., 2001, Hydroforming, Jurnal Material Processes Technology, 115:87–91.

[66] L.H. Lang, 2001, Internal high pressure forming the numerical simulation of the forming process.

[67] Siegert, K., A survey of presses for hydroforming tubes, extrusions. [Online]. Available: http://www.thefabricator.com/article/hydroforming/.

[68] Choi, Y., Yeo, H. T., Park, J. H., Oh, G. H., Park, S. W., 2007, A study on press forming of automotive sub-frame parts using extruded aluminum profile, Journal of Materials Processing Technology, 187–188:85–88, DOI:10.1016/j.jmatprotec.2006.11.175.

[69] Hartl, C., 2005, Research and advances in fundamentals and industrial applications of hydroforming, Journal of Materials Processing Technology, 167/2–/3:383–392, DOI:10.1016/j.jmatprotec.2005.06.035.

[70] USS. [Online]. Available: http://ussautomotive.com/auto/steelvsal/alintensive.htm.

[71] M., O., N., M., 1995, Automotive bumper stay structure, 5441319.

[72] K., K., Kobe, 2002, Car body energy absorber and bumper stay, 6481690 B2.

[73] Sohn, S. M., Kim, B. J., Park, K. S., Moon, Y. H., 2007, Evaluation of the crash energy absorption of hydroformed bumper stays, Journal of Materials Processing Technology, 187–188:283–286, DOI:10.1016/j.jmatprotec.2006.11.184.

[74] Shirayori, A., Fuchizawa, S., Ishigure, H., Narazaki, M., 2003, Deformation behavior of tubes with thickness deviation in circumferential direction during hydraulic free bulging, Journal of Materials Processing Technology, 139/1–/3:58–63, DOI:10.1016/S0924-0136(03)00182-1.

[75] Fuchizawa, S., 1984, Influence of strain hardening exponent on the de- formation of thin-walled tube of finite length subjected to hydrostatic external pressure, in *First International Conference on Technology of Plasticity*, pp. 297–302.

[76] Fuchizawa, S., 1987, Influence of plastic anisotropy on deformation of thin walled tubes in bulging forming, in *Second International Conference on Technology of Plasticity*, pp. 727–732.

[77] D. Schmoeckel, Hielscher, C., Huber, R., Prier, M., 1997, Internal High Pressure Forming at PtU.

[78] M. Prier, Schmoeckel, D., 1999, Triobology of internal high pressure forming, in *International Conference on Hydroforming*.

[79] Vollertsen, F., Plancak, M., 2002, On possibilities for the determination of the coefficient of friction in hydroforming of tubes, Journal of Materials Processing Technology, 125–126:412–420, DOI:10.1016/S0924-0136(02)00292-3.

[80] Mori, K., Maeno, T., Maki, S., 2007, Mechanism of improvement of formability in pulsating hydroforming of tubes, International Journal of Machine Tools and Manufacture, 47/6:978–984, DOI:10.1016/j.ijmachtools.2006.07.006.

[81] Vollertsen, F., 2001, Hydroforming of aluminum alloys using heated oil, in *Ninth International Conference on Sheet Metal*, pp. 157–164.

[82] Groche, P., Huber, R., Dörr, J., Schmoeckel, D., 2002, Hydromechanical Deep-Drawing of Aluminium-Alloys at Elevated Temperatures, CIRP Annals - Manufacturing Technology, 51/1:215–218, DOI:10.1016/S0007-8506(07)61502-9.

[83] Novotny, S., Geiger, M., 2003, Process design for hydroforming of lightweight metal sheets at elevated temperatures, Journal of Materials Processing Technology, 138/1–/3:594–599, DOI:10.1016/S0924-0136(03)00042-6.

[84] Keigler, M., Bauer, H., Harrison, D., De Silva, a. K. M., 2005, Enhancing the formability of aluminium components via temperature controlled hydroforming, Journal of Materials Processing Technology, 167/2–/3:363–370, DOI:10.1016/j.jmatprotec.2005.06.024.

[85] Groche, P., Breitenbach, G., 2005, Tubular semi-finished product characterisation and optimisation for tube hydroforming, pp. 1–15.

[86] Yuan, S., Qi, J., He, Z., 2006, An experimental investigation into the formability of hydroforming 5A02 Al-tubes at elevated temperature, Journal of Materials Processing Technology, 177/1–/3:680–683, DOI:10.1016/j.jmatprotec.2006.04.044.

[87] Dykstra, ., Pfaffmann, G., Wu, X., 2001, Hot Metal Gas Forming – The Next Generation Process for Manufacturing Vehicle Structure Components, *Metalforming*. Metalforming.

[88] Fukuchi, F., Hayashi, N., Ogawa, T., Yokoyama, T., Hori, O., 2005, Development of aluminum automotive parts technologies for mass-production, Journal of Japan Institute of Light Metals.

[89] Wu, X., 2007, Non-Steady-State Creep Behavior in Tube Gas Forming, Journal of Materials Engineering and Performance, 16/4:418–431, DOI:10.1007/s11665-007-9077-4.

[90] Liu, Y., Wu, X., 2007, A Microstructure Study on an AZ31 Magnesium Alloy Tube after Hot Metal Gas Forming Process, Journal of Materials Engineering and Performance, 16/3:354–359, DOI:10.1007/s11665-007-9062-y.

[91] Wu, X., Hao, H., Liu, Y., Zhu, F., Jiang, J., et al., 2001, Elevated Temperature Formability of Some Engineering Metals for Gas Forming of Automotive Structures, Journal of Material Manufacture, 110:1045–1056.

[92] Maeno, T., Mori, K., Fujimoto, K., 2009, Development of the Hot Gas Bulging Process for Aluminium Alloy Tube Using Resistance Heating, Key Engineering Materials, 410–411:315–323, DOI:10.4028/www.scientific.net/KEM.410-411.315.

[93] Maeno, T., Mori, K., Unou, C., 2011, Optimisation of Condition in Hot Gas Bulging of

Aluminium Alloy Tube Using Resistance Heating Set into Dies, Key Engineering Materials, 473:69–74, DOI:10.4028/www.scientific.net/KEM.473.69.

[94] Maeno, T., Mori, K., Unou, C., 2011, Influence of initial wall thickness in Hot Gas Bulging of aluminium alloy tube using pressure of sealed air and resistance heating, in *Sheet Metal Forming*, pp. 423–428.

[95] Maeno, T., Mori, K., Unou, C., 2014, Improvement of Die Filling by Prevention of Temperature Drop in Gas Forming of Aluminium Alloy Tube Using Air Filled into Sealed Tube and Resistance Heating, Procedia Engineering, 81/October:2237–2242, DOI:10.1016/j.proeng.2014.10.314.

[96] He, Z. Bin, Fan, X. B., Shao, F., Zheng, K. L., Wang, Z. B., et al., 2012, Formability and microstructure of AA6061 Al alloy tube for hot metal gas forming at elevated temperature, Transactions of Nonferrous Metals Society of China (English Edition), 22/SUPPL.2:s364–s369, DOI:10.1016/S1003-6326(12)61732-4.

[97] He, Z. Bin, Teng, B. G., Che, C. Y., Wang, Z. B., Zheng, K. L., et al., 2012, Mechanical properties and formability of TA2 extruded tube for hot metal gas forming at elevated temperature, Transactions of Nonferrous Metals Society of China (English Edition), 22/SUPPL.2:s479–s484, DOI:10.1016/S1003-6326(12)61749-X.

[98] Maeno, T., Mori, K., Adachi, K., 2014, Gas forming of ultra-high strength steel hollow part using air filled into sealed tube and resistance heating, Journal of Materials Processing Technology, 214/1:97–105, DOI:10.1016/j.jmatprotec.2013.08.004.

[99] L. Vadillo I. Crelgo, 2007, Plasticity at high temperature for forming applications in the automotive industry — TUTEMP. .

[100] Vadillo, L., Pérez, I., Hori, I., Paar, U., 2010, Gas Forming of Boron Steel Tubes at Low Pressure - Applasting, STEEL RESEARCH INTERNATIONAL, 81/9:552–555.

[101] UNI Ente Nazionale Italiano di Unificazione, 2009, UNI EN ISO 12004-2. .